Aeration Control of Solidifying Lipid Matrices

Vom Promotionsausschuss der
Technischen Universität Hamburg
zur Erlangung des akademischen Grades

Doktor-Ingenieur (Dr.-Ing.)

genehmigte Dissertation

von

Linda Ehlermann

aus

Magdeburg

2020

Gutachter: 1. Prof. Dr.-Ing. Irina Smirnova,
2. Prof. Dr.-Ing. Stefan Heinrich

Tag der mündlichen Prüfung: 14.02.2020

Danksagung

An dieser Stelle möchte ich mich gerne bei allen Menschen bedanken, die mich bei dieser Arbeit maßgeblich unterstützt haben.
In erster Linie danke ich Frau Prof. Dr.-Ing. Irina Smirnova für die engagierte Betreuung meiner Doktorarbeit an Ihrem Institut auf fachlicher und zwischenmenschlicher Ebene. Danke, für die unzähligen Anregungen, Unterstützungen und erkenntnisreichen Gespräche.
Ich danke auch Herrn Prof. Dr.-Ing. Stefan Heinrich für die Arbeit als Zweit-Betreuer und Gutachter meiner Doktorarbeit. Danke für die Mitnutzung Ihrer Institutslabore und ihre zahlreichen fachlichen Hilfestellungen.
Mein Dank gilt auch der Firma Nestlé und ihren Mitarbeitern für das vielseitige und interessante Thema meiner Arbeit sowie dem Bereitstellen von internen Daten und vielseitigen Hilfestellungen.
Mein Dank gilt auch Prof. Dr. Michael Morlock für die flexible und umfangreiche Nutzung des Computertomographen.
Des weiteren bedanke ich mich bei allen Mitarbeitern des Instituts für thermische Verfahrenstechnik für die zahlreichen Anregungen und Hilfestellungen, den freundschaftlichen Austausch und die tolle Arbeitsatmosphäre. Mein besonderer Dank gilt dabei Frau Stefanie Meyer-Storckmann für die umfassende organisatorische Arbeit und alles Zwischenmenschliche.
Mein Dank gilt auch den damaligen Studenten: Nina Maria Heitz, Ilka Selmer, Jannik Sellin, Tobias Becke und Clarissa Lechtenberg, die mich während meiner Institutszeit tatkräftig unterstützt haben.
Abschließend möchte ich meiner Familie und meinen Freunden danken, die mich während dieser Arbeit ebenfalls unglaublich unterstützt haben.

Abstract

Many consumer products in the food industry are based on lipid matrices. Aerated chocolate is one important product for the confectionary industry and it is produced by bubble inclusion into the chocolate. The texture of aerated chocolate is a key driver for consumer preference and the need for differentiation through texture will gain even more importance in the future. The process of chocolate aeration is not yet fully understood and the control and prediction of the aeration process remaining difficult. Different processes can be used for chocolate aeration, either based on vacuum or high pressure. For the method used during this work, gas as foaming agent is dissolved and stirred into the chocolate at elevated pressures. Due to the decompression, the solution becomes supersaturated and this leads to bubble growth and the formation of a chocolate foam. The aim of this work was to understand the physical processes underlying gas solubility and bubble formation, as well as to determine the process conditions leading to optimal bubble formation during aeration of chocolate masses and to find the most suitable process control for various dimensions of consumer preference. In this work the high pressure aeration of chocolate was experimentally investigated with the aim to develop a kinetic model of bubble formation and coalescence. The influence of different process parameters and chocolate composition on the gas solubility and the final product foam structure was experimentally determined. Additionally an alternative method for the tempering of high pressure aerated chocolate was identified and evaluated. Finally a MATLAB Model for the prediction of three-dimensional bubble formation, bubble growth and coalescence was successfully developed and evaluated.

It was found, that the foam structure of aerated milk chocolate can be controlled through the gas composition used as the aerating agent. An increasing amount of carbon dioxide in the gas leads to bigger bubbles and higher porosities (with nitrogen the opposite behaviour is observed). Higher pressures promote the gas solubility and the chocolate foam porosity (until reaching a maximum porosity value of approximately 50 %). It was also shown that the foam porosity increases with increasing depressurisation rate and that temperature (process temperature and temperature reduction during depressuristion) and therefore the viscosity of the chocolate influences the foam structure. This results in the formation of foams with higher porosity and smaller bubbles at lower aeration temperatures. A statistical design of experiments was used to investigate the influence of every chocolate component on the gas solubility and foam structure. In conclusion it can be said that carbon dioxide is dissolved only in the cocoa butter and that no significant adsorption of the gas molecules on the particles takes places. It was found out that high cocoa powder amounts reduce the speed of gas dissolution due to trapping of cocoa butter within the porous and rough cocoa particle structure and that this leads to a diffusion limitation of the gas inside the fat. Additionally it was found out, that the diffusion limitation effect of cocoa particles on the foam structure of aerated milk chocolates is insignificant. It was shown that sugar leads to the generation of very small bubbles, milk

powder generates medium sized bubbles and cocoa powder big bubbles. Because of the strong influence of sugar on the foam structure, the detailed influence of sugar amount, particle size and particle shape was investigated. It was shown that the size of bubbles in aerated chocolates decreases with increasing sugar surface area, resulting from either increasing sugar particle sizes or increasing amounts with similar sugar size. It was shown that the dissolution of carbon dioxide in chocolate leads to a decrease in the melting point. Standard tempering methods are therefore not suitable for a high pressure aeration process of chocolate because the stable seeds crystals melt during aeration. In this work an alternative method with intense cooling for the tempering of high pressure aerated chocolate was identified. It was shown that the crystallisation temperature and time influences the crystal structure form of cocoa butter and milk chocolate. It can be concluded that the tempering of high pressure aerated chocolate can be realised with the subsequent cooling method at -20°C, where complete tempering of the cocoa butter takes place. The challenge of the melting point shifting due to carbon dioxide dissolution can therefore be overcome with this method.

In this work a MATLAB model for the prediction of bubble formation and bubble growth during depressurisation of carbon dioxide high pressure aerated cocoa butter was successfully developed. This model considers the spatial bubble formation, the coalescence, bubbles rising and the change of material properties during the process. The assumption of a constant volume during coalescence and the addition of a maximum bubble radius of 1 mm was identified to be optimal for the prediction of a realistic, homogenous foam. With these parameters, a final porosity and a final average bubble radius in good agreement with the experimental results of this work was achieved. It was shown that the depressurisation rate also influences the foam structure especially the predicted porosity in the same way as it was shown in the experiments of this work and in literature. In conclusion it can be said, that the bubble model developed can successfully predict the foam formation of aerated cocoa butter/chocolate during depressurisation.

In conclusion it can be said, that the differentiation through product texture can be realised by varying the chocolate composition or the process parameters. These findings could further enable a better control of the chocolate aeration process to obtain the production of various aerated chocolate products with different texture and foam characteristic.

List of Content

List of Symbols

symbol	definition	unit
A	projection surface of the particle	mm^2
c	concentration	$\mathrm{mol} \cdot \mathrm{m}^{-3}$
$\bar{c}$	average concentration	$\mathrm{mol} \cdot \mathrm{m}^{-3}$
coal	coalesced bubble	-
cooling	cooling tempering method	-
c_i, c_{ij}	model constants	-
c_R	concentration on the phase boundary of the bubble	$\mathrm{mol} \cdot \mathrm{m}^{-3}$
c_∞	dissolved gas concentration outside of the boundary layer	$\mathrm{mol} \cdot \mathrm{m}^{-3}$
c_p	isobar specific heat capacity	$\mathrm{kJ} \cdot \mathrm{kg}^{-1} \cdot \mathrm{K}^{-1}$
c_v	isochor specific heat capacity	$\mathrm{kJ} \cdot \mathrm{kg}^{-1} \cdot \mathrm{K}^{-1}$
c_0	initial concentration	$\mathrm{mol} \cdot \mathrm{m}^{-3}$
c_0	total mean value	-
$d_{equivalent}$	equivalent bubble diameter	mm
D	diffusion coefficient	$\mathrm{m}^2 \cdot \mathrm{s}^{-1}$
D	dispersion	-
F	„fitting“-parameter for the free energy barrier	-
f_i^α	fugacity of component I in phase α	bar
f_0	„fitting“-parameter of the Zeldovich faktor	-
g	gravity	$\mathrm{m} \cdot \mathrm{s}^{-2}$
g / gas	gas phase	-
$\bar{g}_i$	Gibbs energy of component i	kJ
$H_{1,2}$	henry constant	$\mathrm{mol}_{\mathrm{gas}} \cdot \mathrm{m}^{-3} \cdot \mathrm{Pa}^{-1}$
Δh_v	specific evaporation enthalpy	$\mathrm{kJ} \cdot \mathrm{kg}^{-1}$
Δh_S	specific melting enthalpy	$\mathrm{kJ} \cdot \mathrm{kg}^{-1}$
Δh_{Sub}	specific enthalpy of sublimation	$\mathrm{kJ} \cdot \mathrm{kg}^{-1}$
i	component	-
J	bubble nucleation rate	s^{-1}
$J_{threshold}$	threshold of the bubble nucleation rate	s^{-1}
k_B	Boltzmann constant	$\mathrm{J} \cdot K^{-1}$
l / liquid	liquid phase	-
m	mass	kg
M_W	molecular weight	$\mathrm{kg} \cdot \mathrm{mol}^{-1}$
n	number of measurements	-
n / $n_{bubbles}$	number of bubbles	-
N_A	Avogadro constant	mol^{-1}
p	pressure	bar
P	confidence interval	-
Q	thermal energy	kJ
r, R	radius	m

R^2	coefficient of determination	-
R_G	universal gas constant	$\mathrm{J \cdot mol^{-1} \cdot K^{-1}}$
R_{max}	„fitting“-parameter maximum bubble radius	m
s	standard deviation	-
s / *solid*	solid phase	-
standard	standard tempering method	-
$S_{specific}$	specific surface area of the foam	$\mathrm{1/mm}$
S_{total}	total foam surface	$\mathrm{mm^2}$
t	time	s
$t_{P,n}$	student t-factor	-
T	temperature	$\mathrm{°C}$
ΔT	temperature difference	$\mathrm{°C}$
Δt_N	time step size	s
v	speed, velocity	$\mathrm{m \cdot s^{-1}}$
V	volume	$\mathrm{m^3}$
V_{gas}	bubble volume /gas volume in the foam	$\mathrm{mm^3}$
V_{solid}	solidl volume of the foam	$\mathrm{mm^3}$
V_{total}	total volume of the foam	$\mathrm{mm^3}$
$\bar{x}$	average value	-
x_{Area}	coextensive spherical particle diameter	mm
x_i, y_i	mole fraction of component i	-
x_i	measurement values	-
x, y, z	coordinates	-
y	effect variable	-
0	initial conditions	-
0 / *pure*	pure substance	-
α	heating rate	$\mathrm{K \cdot min^{-1}}$
α, β, φ	phase	-
γ	activity coefficient	-
γ_i^*	activity coefficient of component I at infinite dilution	-
$\dot{\gamma}$	shear rate	$\mathrm{s^{-1}}$
δ	boundary layer size	m
η	dynamic viscosity	$\mathrm{Pa \cdot s}$
ε	residual error	-
μ_i	chemical potential of component i	$\mathrm{J{\cdot}mol^{-1}}$
ν	kinematic viscosity	$\mathrm{m^2 \cdot s^{-1}}$
$\Pi_{\infty,i}$	poynting correction factor	-
ρ	density	$\mathrm{kg \cdot m^{-3}}$
σ	surface tension	$\mathrm{N \cdot m^{-1}}$
τ	retention time	$\mathrm{s^{-1}}$
τ	shear stress	Pa
φ_i^G	fugacity coefficient of component I in phase G	-
ϕ	porosity	-
wt%	mass fraction	$\mathrm{kg \cdot kg^{-1}}$

List of Abbreviations

abbreviation	definition
A	arachidic acid
BD	bubble diameter
Ca	calcium
CB	cocoa butter
CBE	cocoa butter equivalents
CBS	cocoa butter substitutes
CFD	computational fluid dynamics
CM	chocolate mixtures
CO_2	carbon dioxide
CP	cocoa powder
DIN	Deutsche Industrie Norm
DSC	differential scanning calorimeter
FPDS	Fraction of Paired Design Space
GS	gas solubility
MC	milk chocolate
min	minutes
MP	milk powder
Na	natrium
N_2	nitrogen
K	potassium
Li	linoleic acid
O	oleic acid
P	palmitic acid
PLiSt	triglyceride with palmitic acid, linoleic acid and stearic acid
PLiP	triglyceride with palmitic acid, linoleic acid and palmatic acid
POO	triglyceride with palmitic acid, oleic acid and oleic acid
POP	triglyceride with palmitic acid, oleic acid and palmatic acid
POSt	triglyceride with palmitic acid, oleic acid and stearic acid
PO_4	phosphate
SP	sugar powder, icing sugar
St	stearic acid
StLiSt	triglyceride with stearic acid, linoleic acid and stearic acid
StOA	triglyceride with stearic acid, oleic acid and arachidic acid
StOSt	triglyceride with stearic acid, oleic acid and stearic acid
StOO	triglyceride with stearic acid, oleic acid and oleic acid

List of Figures

List of Tables

1 Introduction

Many consumer products in the food industry are based on lipid matrices. The appeal of these products can be improved through aeration, therefore delivering a point of differentiation. Aerated chocolate is one important product for the confectionary industry and it is produced by bubble inclusion into the chocolate [1]. It has become very popular since its first appearance in 1935 [1]. The texture of aerated chocolate products leads to an intense taste and creamy mouth feeling. Texture is a key driver for consumer preference of chocolate products. To respond to lighter eating trends, the need for differentiation through texture will gain even more importance in the future. Aeration of chocolate could further boost this product attribute and possibly compensate for a reduction in fat content. Used in different countries and different companies in many ways, the process of chocolate aeration is not yet fully understood, with control and prediction of the chocolate aeration process remaining difficult.

A large variety of different processes can be used for chocolate aeration, either based on vacuum or high pressure [1, 2]. For the method used during this work, gas as foaming agent is dissolved and stirred into the chocolate at elevated pressures [1]. After reaching thermodynamic equilibrium, the pressure is dropped to atmospheric conditions. Due to the decompression, the solution becomes supersaturated and the gas is released out of the solution. This leads to bubble growth and the formation of a chocolate foam. To stabilize the foam, it has to be crystallized [1].

The aim of this project is to understand the physical processes underlying gas solubility and bubble formation. To achieve this, experimental investigations are carried out with the aim to develop a kinetic model of bubble formation and coalescence for the high pressure aeration process. In this work the high pressure aeration process of chocolate is investigated experimentally and evaluated regarding gas solubility and final product characteristics like foam structure and porosity. The influence of different process parameters and of chocolate composition is experimentally determined. Additionally an alternative method for the tempering of high pressure aerated chocolate will be identified and evaluated. Finally a MATLAB Model for the prediction of three-dimensional bubble formation, bubble growth and coalescence is developed and evaluated for the high pressure aeration process. The final aim is to determine the process conditions leading to optimal bubble formation during aeration of chocolate masses and to find the most suitable process control for various dimensions of consumer preference.

2 Fundamentals and State of the Art

In this chapter the current research and fundamentals of chocolate and its ingredients as well as the industrial chocolate processing and different chocolate properties are presented. Afterwards the processing and properties of aerated chocolate will be discussed in detail. Finally the modelling of bubbles and foams is considered.

2.1 Composition of Chocolate

Chocolate is a mixture consisting of cocoa butter, cocoa mass, sugar, milk components, emulsifier and additives. In this chapter firstly the different compositions of chocolates will be shown. Furthermore the properties of each chocolate ingredient will be discussed in detail.

2.1.1 Chocolate Compositions

Chocolate in general is a mixture of different ingredients. The base component of chocolate is cocoa butter, which forms a suspension with the other main ingredients sugar, cocoa mass and milk powder. Additional chocolate components are emulsifiers for viscosity adjustment [3] and additives like flavours. Different fats can also be added with a maximum amount of 5 wt% [4], depending on local chocolate regulations. Due to this mix of different ingredient, chocolate is a mixture of carbohydrates, fats and proteins [1].

The quantitative composition of chocolates greatly dependents on the type of chocolate. The mixing ratio and also the ingredients variates for the three main types of chocolate: milk chocolate, dark chocolate and white chocolate. Even within one chocolate type a significant variation in recipe is possible. In Table 2-1 a standard composition with average values of different recipes is presented for the main chocolate types [3, 5].

Table 2-1: standard composition of different chocolates with average values of different recipes and one example recipe for white chocolate* [3, 5]

Components [wt%]	milk chocolate	dark chocolate	plain chocolate	white chocolate*
cocoa mass	11.8	39.6	60.7	-
sugar	48.7	48.1	36.3	45
cocoa butter (addition)	20.0	11.8	2.6	26
whole milk powder**	19.1	-	-	23.6
lecithin	0.35	0.35	0.3	0.4
vanillin	0.08	0.14	0.2	-
lactose	-	-	-	5
salt	-	0.06	-	-

** whole milk powder can be replaced by skimmed milk powder and clarified butter

Table 2-1 illustrates the varying composition for different types of chocolate. For example whole milk powder is used in milk (19.1 wt%) and white chocolate (45 wt%) but not in dark chocolates. Skimmed milk powder can also be used for the recipe. For the other main components there is also a huge variation in the quantity used. The different properties of the ingredients and their composition will be used to adjust the specific characteristics of each chocolate including taste, smell, texture or colour. In the following subchapter all chocolate components and their properties will be explained in detail.

2.1.2 Cocoa Butter

Cocoa butter (cacao oleum) originates from cocoa beans which contain around 50 to 58 wt% of this fat [3, 6]. Cocoa butter is a mixture of different triglycerides, which are esters of glycerine with three long-chained fatty acids [7], especially palmitic acid (P, 26 wt%), stearic acid (St, 34 wt%) and oleic acid (O, 35 wt%) [3, 8]. The main triglycerides that occur in cocoa butter are POP, StOSt and POSt [9]. In Figure 2-1 the structural formula of POSt is presented exemplary for a triglyceride.

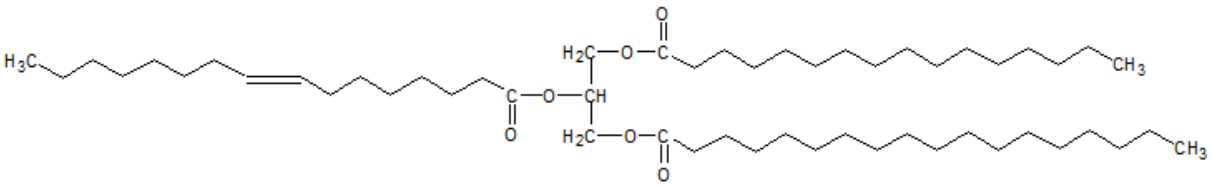

Figure 2-1: structural formula of the triglyceride POSt

The composition of coco butter differs and is influenced by the cultivation region, growth conditions, the age of the trees and also the manufacturing process used to extract the fat [2, 10, 11]. Table 2-2 show the amount of different triglycerides present in cocoa butter.

Table 2-2: minimum and maximum amount of different triglycerides in cocoa butter from 19 countries [10]

triglycerides	amount [wt%]
POSt	35.8 - 41.4
StOSt	22.8 - 31.3
POP	17.5 - 22.6
StOO	2.8 - 7.4
PLiSt	2.8 - 3.9
StLiSt	1.7 - 3.7
POO	0.9 - 4.3
PLiP	0.7 - 1.5
StOA	0.04 - 0.8

The triglycerides in cocoa butter are components with different individual melting points and properties. Due to this the cocoa butter has a characteristic melting range and no fixed melting point [12]. Cocoa butter can crystallises in different forms (polymorphism) which have different properties like hardness, stability, melting point, gloss and breakage behaviour [8]. Cocoa butter can crystallise in 6 different forms, which have been numbered from I to VI within the chocolate industry [12] or alternatively classified with α, β and γ in the oil industry [13]. In Table 2-3 different literature melting ranges of the 6 crystal structures [8, 12, 14] and an average melting range $\overline{T}$, calculated from the literature values is shown.

Table 2-3: literature [8, 12, 14] and calculated average melding points of the six crystal structures of cocoa butter

crystal form		melting range [°C]			
		BECKETT	CALVIGNAC et al.	WILLE et al.	$\overline{T}$
I	γ	16 - 18	12.95 - 17.45	17.3	15.4 - 17.6
II	α	22 - 24	17.65 - 19.75	23.3	21.0 - 22.4
III	β'_2	24 - 26	22.25 - 24.35	25.5	23.9 - 25.3
IV	β'_1	26 - 28	26.25 - 27.75	27.5	26.6 - 27.8
V	β_2	32 - 34	30.55 - 34.25	33.8	32.1 - 34.0
VI	β_1	34 - 36	33.65 - 33.95	36.3	34.7 - 35.4

The triglycerides in cocoa butter mostly have a chair shape structure with two fatty acids on position 1 and 3 and one fatty acid on position 2 in the opposite direction [15]. In each crystal form the triglyceride “chairs” pack in different orientations to each other resulting in density differences [15] as shown in Figure 2-2 [16].

Figure 2-2: double and triple chain length packing of cocoa butter triglycerides [16]

The thermodynamic stability of the crystal structures increase from form I to VI [2]. An arrangement in double chain length packing mostly occur for fatty acids with similar chemical properties and will build almost completely in unstable crystal structures I to IV. Triglycerides with dissimilar saturated

and unsaturated fatty acid tend to form triple chain length packing, which mostly occur in the stable crystal structure V or VI [16]. Packing of the formations to each other can occur at different angles which lead to a hexagonal, orthorhombic or triclinic form as shown in Figure 2-3 [17].

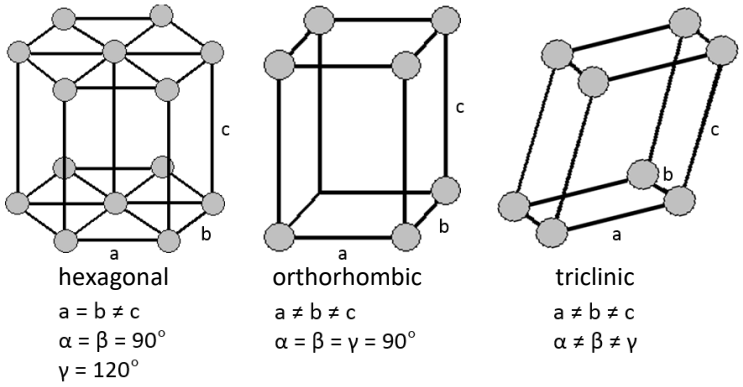

Figure 2-3: Different crystal lattices of cocoa butter triglycerides [17]

The hexagonal structure is the least stable formation and occurs in the crystal structure I and II (α form)[16]. The structure shows a high mobility which leads to a rapid transformation to a better chain packing like the orthorhombic crystal structure III and IV (β' form). The triclinic structure is the most stable one and occurs in the crystal form V and VI (β form) of cocoa butter [16].

Crystal structure I (γ form) is built when cocoa butter crystallises very quickly. Due to the very unstable structure it will turn to crystal form II rapidly and irreversibly [2, 12]. WILLE et al. found out that crystal structures turn from unstable to more stable forms during storage depending on temperature and time as shown in Table 2-4 [12].

Table 2-4: transformation time of solid cocoa butter crystals in the next higher forms at different storage temperatures [12]

T [°C]	crystal structure											
	I		II		III		IV		V		VI	
	start	end	start	end	start	end	start	end	start	end	start	end
-30	> 4 h											
0	15 s	15 min	5 h									
5			< 2 h	16 h	5 d		> 1 w					
10					1 d	3 d**						
16	2 s		1 h		< 4 h	4 h	2 d	2 w	> 14 w			
21							3 h	1 d	7 w	> 18 w		
26			melted*		melted*		< 1 h	1 h		3 w	stable	

* after 30 min crystallisation in form V, ** direct transition to form V

It is clear to see that crystallised cocoa butter structures transform to higher crystal forms during storage. Especially at higher storage temperatures the transformation is faster. Additionally turn the unstable structures change much more quickly to higher forms than the more stable structures [12]. For the chocolate industry it is important that chocolate exhibits a specific melting behavior as well as hardness, fracture and gloss properties.

The desired properties will be achieved with crystal structure V [12]. Final crystal structure can be adjusted with chocolate tempering during the processing (see chapter 2.2.3).

The addition of alternative fats to pure cocoa butter changes the melting and crystallisation behavior of the chocolate. These fats have different compositions and therefore generate other crystal forms than those found in pure cocoa butter. This disturbs the crystal structure of the cocoa butter and makes the structure of the fat mixture less stable and low-melting compared to pure cocoa butter [8]. To ensure final properties typical for chocolate, only a low amount of alternative fats, which exhibit similar crystallization behavior to pure cocoa butter can be added to the chocolate [8]. The European cocoa regulations define the maximum amount of vegetable foreign fats in chocolate as being 5 % [4]. Fats used to replace cocoa butter can be divided into two main groups known (CBE or CBS). CBE fats are equivalent to cocoa butter and have the same chemical and physical properties. They can be obtained from palm oil. CBS fats are substitute fats and they can be obtained from the oil of coconuts, nuts and seeds. The composition of CBS fats differs more from cocoa butter and results in a decrease in melting temperature and require more complex tempering profile [2].

2.1.3 Cocoa Mass and Cocoa Powder

The raw material for the production of cocoa mass and cocoa powder is the cocoa bean. Cocoa mass results from the grinding of cocoa beans [18]. During the grinding process the cocoa cells will be destroyed and the melted cocoa butter is released. Cocoa powder is the finely ground press cake remaining after extracting the majority of the cocoa butter from the cocoa mass [6, 19]. Cocoa butter as well as cocoa mass consists of cocoa cell tissue and different amounts of cocoa butter [20]. Cocoa mass should have a cocoa butter content of at least 53 wt%. There are two main cocoa powder types, highly de-fatted (10-11 wt% butter) and partially de-fatted (20-21 wt% butter) [6, 18]. The cocoa cell tissue consists mainly of cellulose, proteins and starch [21]. A detailed composition of partially de-fatted cocoa powder is given in Table 2-5.

Table 2-5: composition of cocoa powder [21]

component *	amount [wt%]
fat	21.0
proteins (albumin, globulin, prolamin, glutenin)	21.0
cellulose	16.5
starch	11.0
polyhydroxphenols	11.0
ash	4.8
water	4.0
acids	2.8
pentosans	2.8
purine (caffeine, theobromine)	2.5
sugars (glucose, fructose, sucrose, melibiose, raffinose, stachyose, manninotriose, planteose, verbascose, verbascotetraose	1.8

* vitamins and trace elements are not listed

Cocoa powder is mainly used for drinking chocolates and compound coatings (chocolate flavored products where the cocoa butter has been fully substituted for an alternative fat), cocoa mass for chocolate manufacturing [6, 18].

2.1.4 Sugar

For the production of chocolate a disaccharide consisting of glucose and fructose, known as sucrose ($C_{12}H_{22}O_{11}$) is used [22]. In Figure 2-4 the structural formula of sucrose is shown [23].

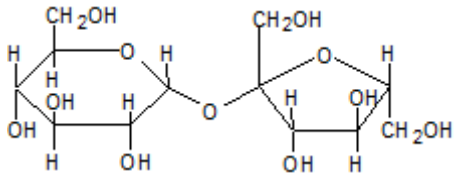

Figure 2-4: structural formula of sucrose [23]

Sucrose is produced from either sugar beet or cane. In the sugar industry sucrose is produced with a really high purity of more than 99.7 % and a particle size of 0.5 to 1.5 mm for chocolate production [22]. In the final chocolate product a desired particle size of 30 µm is achieved through roll refining of the mixed components (see chapter 2.2.2) [24]. In chocolate sucrose mostly occurs in its crystalline form but also a degree of amorphous sugar is present as a result of the refining process [25]. The amorphous sugar gives added value in terms of its ability to bind flavour components but due to moisture it recrystallizes with time [25]. Sometimes the sugar will be mixed with milk, the water evaporated from the mixture to dry it and then it will be milled. The resulting mass is called 'crumb' and delivers a slightly caramelised taste to the finished chocolate and can be used instead of pure sugar for chocolate production [24]. In addition to sucrose different sweeteners can also be used in chocolate. In Table 2-6 an overview of alternative sweeteners is given.

Table 2-6: overview of alternative sweeteners [25] (- - very low, - low, +/- constant, + high, + + very high)

chocolate sweetener	sweetener intensity (compared to sucrose)	suitable for diabetics	tooth friendly
glucose	-	-	-
fructose	+	+	-
lactose	- -	-	-
sorbitol	-	+	+
mannitol	-	+	+
xylitol	+/-	+	+ +
maltitol	-	+	+
isomalt	-	+	+
lactit	- -	+	+

Alternative sweeteners can be used separately or in combination to deliver a similar sweetness intensity as with sucrose [25]. Glucose and fructose must have a really low water content and should not contain water of crystallisation because the water will significantly increase the viscosity of the

chocolate during conching (see chapter 2.3.1). Additionally where using fructose it is important to regulate the conching temperature so that it is below 40°C because above this temperature fructose transforms his structure and negatively influence the taste of the chocolate product [22].

2.1.5 Milk Components

Milk components are also important ingredients in chocolate manufacture. Milk mainly consists of water, fats, proteins, lactose, vitamins and minerals. In Table 2-7 an average composition of cow's milk is given [26].

Table 2-7: average composition of cow's milk [26]

milk ingredients	amount	
	g / L_{milk}	dry mass [wt %]
water	870	-
lactose	47	36.6
fats	37	28.8
proteins	34	26.5
Minerals (Na, K, Ca, PO_4, citrate)	7.4	5.8
non-protein nitrogen	2.5	1.9
Vitamins (vitamin D,	< 0.5	< 0.4

The listed fats and proteins in the milk are in fact complex mixtures of different components. For example milk fat consists of 95% triglycerides and 5% diglycerides, monoglycerides, phospholipids, cerebrosids, gangliosides and fat-soluble vitamins [26]. The diglycerides, monoglycerides and phospholipids are surface-active substances and have similar properties to lecithin. The emulsifier lecithin is a phospholipid which strongly influences the chocolate viscosity (see chapter 2.3.1). Lecithin is added to the chocolate during the production but also a small amount of lecithin in contained in cow's milk [26]. The composition of milk fat influences the melting behaviour of chocolate because milk fat disrupts the regular structure of the cocoa butter. Due to this, less energy is required to melt chocolate containing milk fat [26]. The composition of the proteins in milk is given in Table 2-8 [26].

Table 2-8: composition of milk proteins [26]

milk protein components	amount [wt%]
caseins	75 - 85
whey proteins	18
fat globule membrane molecules	1
non-protein nitrogen components	5

Casein has a flexible and open-chain structure with hydrophilic and hydrophobic regions similar to surfactants. Due to this casein is an emulsifier which can bind water and fats. It forms high molecular surfactant-like aggregates [26]. Whey proteins have a spherical shape and they are less heat-resistant than casein. Whey proteins have a hydrophilic surface and they form helical structures with ionic bonds, hydrogen bonds and disulphide bridges. Due to the denaturation of whey proteins at higher

temperatures, it is important to treat the milk in standardised processes to get consistent properties and quality [26].

For the production of chocolate milk powder is used because water increases the viscosity of the chocolate too much (see chapter 2.3.1) [27]. For the production of milk powder the milk is heated up, vaporised and dried. The first heating step is for the pasteurisation of the milk and thus the killing of micro-organisms. Evaporation takes place in multi-stages at reduced pressure and temperatures of 55 to 75 °C. The drying of the milk is achieved with spray drying or drum drying [26]. During processing some milk fat is formed on the surface of the dried milk particles. Drum dried milk has 95% fat on the particle surface and spray dried milk under 10% fat. Drum drying is preferred for chocolate production because the high fat amount on the surface decreases the viscosity of the chocolate [26], although spray dried milk powder is often used due to its reduced cost. Drum drying is expensive and hygienically difficult, due to this spray dried milk powder in combination with clarified butter is often used [8]. During the evaporation and the drying of milk the Maillard reaction (non-enzymatic browning reaction) can take place. This generates a caramel-like flavour [26]. Sometimes milk is mixed with sugar, dried and milled to produce “crumb”. When this mass is used for chocolate manufacturing it reduces the conching time [24].

2.1.6 Emulsifier

Emulsifiers are surface-active substances which are required to decrease and adjust the viscosity of chocolate [27]. The most commonly used emulsifier, lecithin, is a surface-active phospholipid [2] and it can be obtained from soy plants [27], as well as sunflower. Soy Lecithin consists of phosphoglycerates and also 44 wt% soy oil [8]. It is estimated that the phosphatidylcholine molecules have the biggest influence on the chocolate viscosity [2]. Phosphatidylcholines consists of glycerine, fatty acids, phosphoric acid and choline as shown in Figure 2-5:

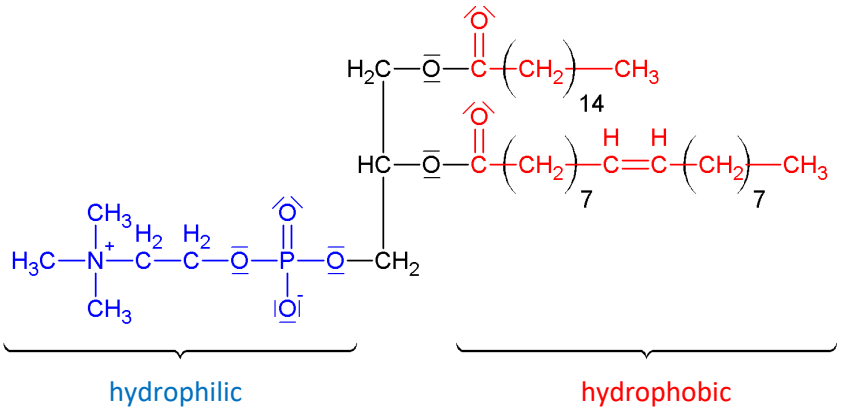

Figure 2-5: structural formula of a lecithin molecule (phosphatidylcholine with palmitic acid and oleic acid) [28]

Phosphatidylcholines have lipophilic tails (in this example oleic acid and palmitic acid) and a hydrophilic head region (choline and phosphate) [2]. In the chocolate a layer of lecithin is formed between the

hydrophilic sugar particles and the hydrophobic cocoa butter [28]. During this process the phospholipids cover sugar particles with the hydrophilic head group. The lipophilic tails orientate in the direction of the fat phase and generate a better flow-ability and lower viscosity of the chocolate [8]. Approximately 0.3 wt% lecithin is generally used in chocolate manufacture [5].

2.1.7 Additives.

The taste of chocolate can be influenced further by addition of flavours [3]. The use of additives in chocolate is strictly regulated and it is very important to ensure suitability and the safety of any added components [2]. Additional chocolate ingredients can be nuts ore flavours like vanilla, cinnamon or essential citrus oils. Natural or synthetic flavours can be used for the flavouring of chocolate [2]. The addition of alternative fats to cocoa butter have already been described in chapter 2.1.2.

2.2 Processing of Chocolate

In this chapter chocolate processing from the cocoa bean to the final product is described. The foundation of chocolate production is ensuring the correct processing of the different ingredients. This is important to deliver a chocolate with consumer favoured properties and taste [29]. In Figure 2-6 the flowsheet of the whole process of cocoa processing is shown [6]:

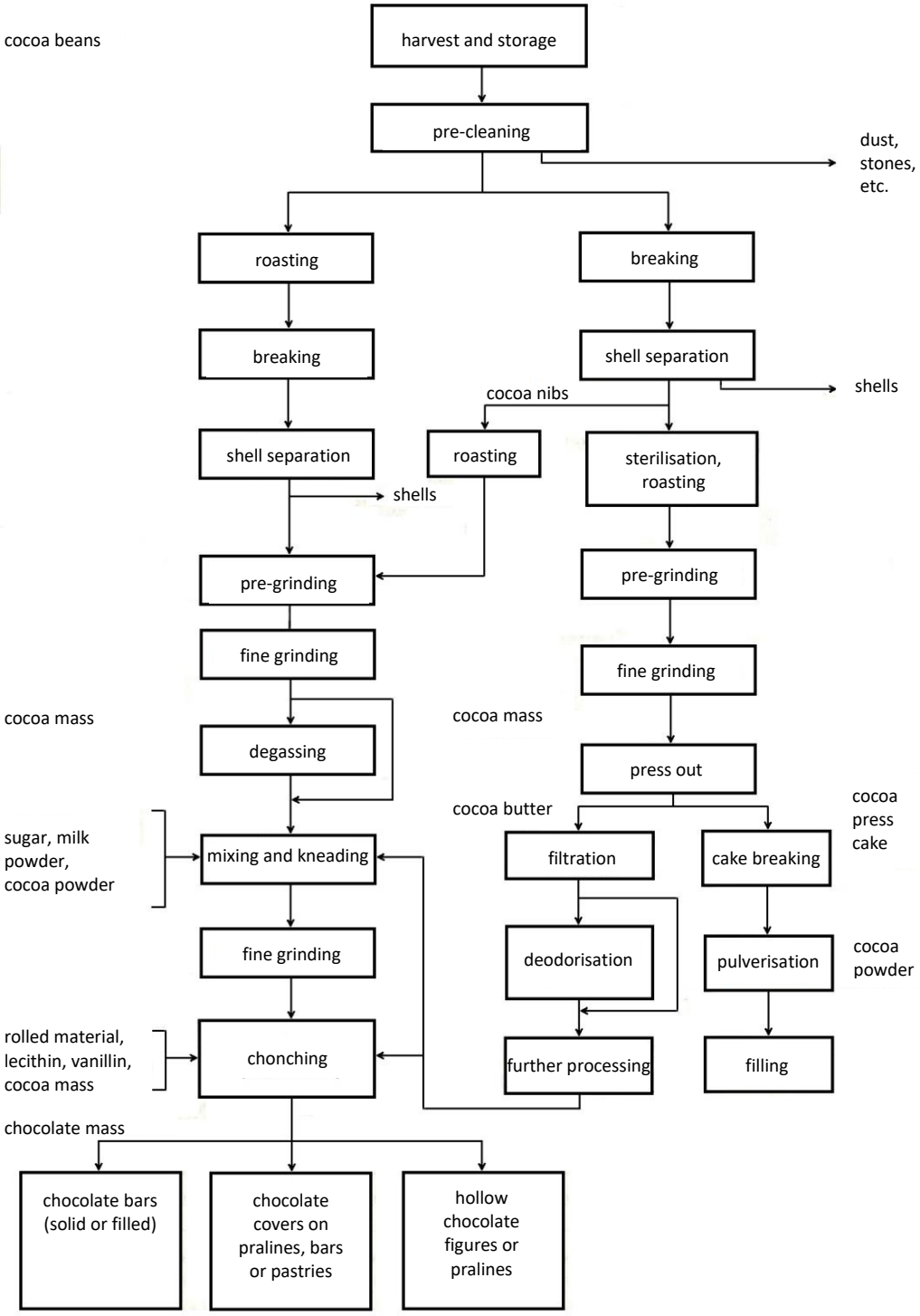

Figure 2-6: flowsheet of cocoa processing [6]

During the chocolate production it is important that desired flavours are allowed to develop and undesired flavours removed [29]. The taste of chocolate is mostly influenced by the flavours that are formed during the fermentation, drying and roasting of the cocoa beans [2]. Additionally it is required that the chocolate has unique textural properties. The product must be solid at room temperature and yet melt in the mouth. The favoured melting behaviour and other desired chocolate properties such

as gloss or hardness can only be achieved with a form V crystal structure as described in chapter 2.1.2 [29]. The grinding of the chocolate to a fine homogeneous mass and the conching process also significantly influence the texture of the final product [2]. Due to this the manufacturing of chocolate is a complex process with many different steps and the selection of process parameters is essential to produce a perfect product [8]. In Figure 2-7 the simplified flowsheet of chocolate production is shown.

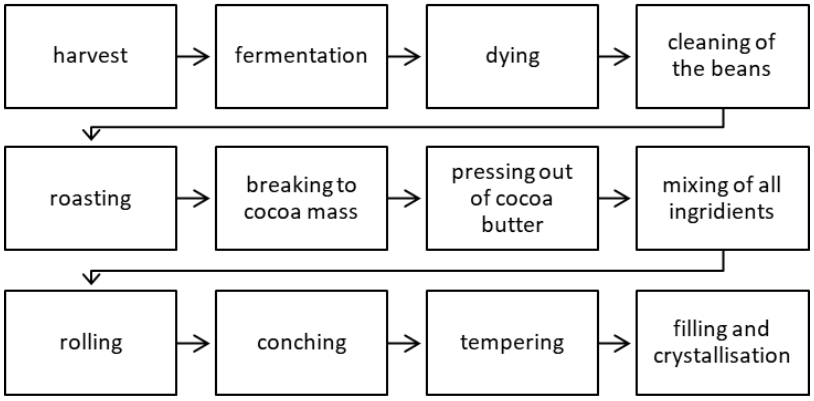

Figure 2-7: flowsheet of chocolate production

The different process steps in the chocolate production will be explained in more detail during the following chapters.

2.2.1 Treatment of Cocoa Beans

Harvest of Cocoa. The most important basic raw material of chocolate is the cocoa bean. The beans grow as seeds in the fruit of the cocoa tree (theobromacacao) [30]. The tree is cultivated in tropical rain forests [29] and yields fruits of 200g to 1kg in weight, each containing 30 to 45 cocoa beans inside the pulp. The mostly used cocoa beans in Germany are from the Ivory Coast, from Ghana, Nigeria, Ecuador and Papua New Guinea [31]. The cocoa pods are harvested after 6 month and the opening of the fruits is carried out by hand [30].

Fermentation. For this process the cocoa beans and the pulp are removed from the shells and placed in fermentation boxes or banana leafs [30]. The cocoa pulp includes the necessary bacteria and yeast cells for fermentation and also serves as a nutrient for the cells. They liquidate the pulp with the fermentation of the naturally present sugar to ethanol and acetic acid and cause it to flow off the cocoa beans [29]. The fermentation needs five to seven days and a large number of chemical and microbiological transformations take place during this time. During the fermentation of the beans precursors of chocolate flavours are formed. An overfermentation and the related risk of undesired flavour building in later process steps should be avoided [32]. Due to fermentation temperatures of up to 50°C and the formation of acetic acid, the beans are be killed and are no longer able to germinate [30].

Drying, Cleaning and Transport. After fermentation the beans will be dried to avoid formation of mould [30]. Additionally further formation of flavours takes place during the drying [29]. The traditional way is sun drying with regular turning of the beans. This method has good drying results, when the beans are covered at night and during periods of rain [2]. The standard drying time of the beans in the sun is one week [21]. Additionally drying units can be used in regions with high humidity and rainfall [2]. After fermentation the beans consists of 60 wt% water and they will be dried to a residual moisture content of 5 -7 wt% [21]. The fermented and dried beans are transported in jute bags to the consuming countries [6]. During transport adequate ventilation must be assured to avoid humidity, leading to condensation and therefore mould formation [30]. In the factories of the destination countries the beans will be cleaned to remove sand, dust, stones, wood and glass [21].

Roasting. After cleaning the cocoa beans from containments the beans will be roasted. The main purposes of roasting is dehumidification, removal of shells and formation of the typical chocolate flavour [6]. Before this process step the beans have a bitter, sour and only a chocolate related taste [29]. The precursors of chocolate aroma developed during fermentation will be transformed to the final flavours at this step [29]. During the roasting a non-enzymatic browning reaction between sugar and amino acids, also known as the Maillard reaction, takes place [32]. In addition to flavour development, any microorganisms present will be killed during the roasting process [30]. Roasting can be carried out with whole beans, cocoa nibs or liquid cocoa mass [33]. The original process is the roasting of whole beans, whereby the cocoa shells get brittle, break up easily ready for removal in a later sieving step. The disadvantage of this method is that the shells absorb a part of the cocoa butter reducing the amount of cocoa butter that can be extracted [33]. In addition, the roasting is an inconsistent process because of the temperature gradient between bean surface and core [6]. Because of this over- or under roasting effects may occur for small or big beans [19]. Due to this the roasting of whole beans is increasingly being replaced by the roasting of cocoa nibs or cocoa mass [6]. Before cocoa nib roasting the beans will be treated for example with hot air, steam or infrared radiation which leads to separation of the beans from the shells [19]. With this separation before the roasting no later absorption of cocoa butter in the shells can take place. During heating the cocoa beans break in pieces of different size (1-10 mm [19]), called nibs. The nibs will be subsequently further broken up (1-4 mm [19]) to achieve a consistent roasting [29]. Another possibility is the roasting of liquid cocoa mass following thermal pretreatment to remove the cocoa shells. The nibs are ground until a liquid suspension is formed. The advantage of this method is good process control due to the small particle size [34]. The type of procedure used depends on the quality of the beans and the desired properties of the final product. Beans of high quality will be roasted more gently to preserve the delicate flavours. On the other hand, sour and unsatisfactory fermented beans will be roasted to higher temperatures [21].The roasting temperature ranges between 90 and 220 °C depending on the method used [32, 33]. The roasting time is around 30 to 35 minutes for whole beans [21, 34], 12 minutes for cocoa nibs and just two minutes for cocoa mass [34]. During roasting the beans will be dried to a residual moisture content of 3 wt% [6].

2.2.2 Manufacture of Chocolate

Grinding. After the roasting process the cocoa beans are ground to produce cocoa mass. Firstly the beans are broken up in a bean crusher which leads to a separation of cocoa shells and cocoa nibs. The shells can be further removed using oscillating sieves. The separated cocoa nibs are then ground to cocoa mass in several steps. During grinding the cell walls rupture and the trapped cocoa butter is released [2]. The generated cocoa mass is a liquid above a temperature of 35 °C and can be used for the processing of chocolate, cocoa butter or cocoa powder [29].

The extraction of cocoa butter from cocoa mass takes place in hydraulic blocking machines at 90 °C and with pressures of up to 400 bar. The obtained cocoa butter contains small foreign particles which are subsequently filtered out. The cocoa butter can also be obtained directly from the whole bean without removing the shells. This process is critical to ensure food safety (shell can be contaminated with pesticides or excrement) [29]. Another process possibility is the solvent extraction of cocoa butter but this method is prohibited in Germany [21]. Deodorisation is a process that has become established over the last few years. This method is mostly used for white and milk chocolates because the intense flavour of cocoa butter can overpower the flavour of milk. During the deodorisation odorous and flavouring substance are removed with a special vacuum steam treatment [6].

Cocoa beans consist of 56 wt% cocoa butter which can be pressed out of the cocoa mass [6]. The mass will be pressed through a sieve to remove the cocoa butter and produce a press cake with up to 10-11 wt% fat (highly de-fatted) or 20-21 wt% fat (partially de-fatted) [6, 18]. The press cake is then ground, cooled and sieved to achieve cocoa powder [8, 33]. The cocoa powder can additionally be alkalised to make the taste milder and modify the colour [6]. This powder can be used for the further production of pudding powder, milk cocoa drinks or coating masses [29]. For the production of chocolate only cocoa mass and cocoa butter is used [19].

Mixing and Rolling. Chocolate is a suspension of different particles in cocoa butter. The mixing of the chocolate components cocoa mass, sugar, milk powder and cocoa butter is carried out in a mixer/kneader. Please see Table 2-1 in chapter 2.1.1 for the composition of the different chocolate recipes. The mixing time varies between 12 and 15 minutes [2]. For the production of milk chocolate sugar, milk powder and possibly clarified butter or alternatively crumb (see chapter 2.1.4 and 2.1.5) can be added to the cocoa mass and butter [6, 26]. The particles of the mixture are refined to a particle generally less than 40 µm so that they cannot be perceived as individual particles on the tongue [21, 29]. The grinding of the chocolate mass is done using rollers, typically five-roll refiners, with the gaps adjusted to deliver the desired particle size. During the refining process part of the crystalline sugar changes to the amorphous form [25]. Sugar with this structure has the property to adsorb flavour compounds from the cocoa mass and the milk powder. This influences the final taste of the chocolate positively. Due to humidity and high temperatures recrystallization of part of the amorphous sugar takes place [25].

Conching. During the refining process, agglomerates are formed in the chocolate mass [8]. Conching of the chocolate introduces shear stress to break them up [35]. Additionally conching removes unwanted aroma compounds, improves the flow characteristics of the chocolate for later filling and optimises the final product feeling on the tongue [31, 35]. During the conching process the water content decreases from 1.6 wt% to 0.6 wt% due to the temperature increase because of shear energy and additional heating with a water jacket. With the conche heating jackets a constant temperature is regulated throughout the process. Undesirable aroma compounds are removed through steam distillation caused by the chocolate humidity loss [35]. Additionally the Maillard reaction also takes place during conching because not all free amino acids are transformed during roasting [35]. The conching process consists of several steps. In the first stage the chocolate is stirred and kneaded for 6 to 10 hours at 65 °C (milk chocolate) or 75 °C (milk free chocolates) to remove humidity and unwanted volatile aroma substances, for example acetic acid [21]. Due to the risk of milk protein denaturation it is important that the temperature, especially for milk chocolate, does not exceed 75°C [21]. During the conching process particles are covered with fat which leads to a smoother chocolate texture and the humidity also corresponds to a decrease in viscosity [35]. In the second stage of the conching process cocoa butter will be added to the chocolate. This allows faster stirring and thus a quicker homogenisation. This step needs 6 to 40 hours. In the last conching step (2-3 hours) the viscosity and the flow characteristic of chocolate are adjusted through the addition of cocoa butter and lecithin [6]. The whole residence time of chocolate in the conche varies significantly. It depends on the construction type of the conche and the required quality of the chocolate [21]. Conching is the most energy consuming process step during the chocolate production. Due to this it has been optimised significantly over the last decades [6]. Through measures such as higher shear rates, the conching time can be reduced by several hours [6].

2.2.3 Tempering of Chocolate

Tempering, a thermal treatment of chocolate is done to achieve the desired stable and uniform crystal form V of cocoa butter [36]. The precise temperatures chosen for the cooling and heating of the chocolate are dependent on the tempering equipment used and chocolate type (dark, milk or white chocolate) [37]. In general temperature profiles similar to the ones shown in Figure 2-8 are used [1].

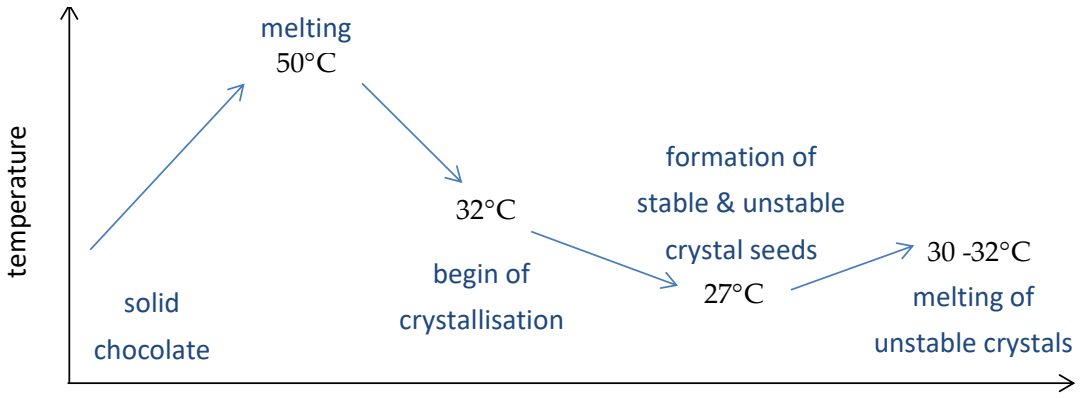

Figure 2-8: example temperature profile for chocolate tempering [1]

The solid chocolate is completely melted at around 50 °C and afterwards crystallisation begins at around 32 °C. With further cooling of the chocolate to around 27 °C, stable and unstable crystal seeds are formed. The chocolate is then heated up to around 31 °C to melt the unstable crystal forms leaving well tempered chocolate with structure of predominately form V crystals.

A wide range of tempering equipment is available on the market, for example those incorporating plate heat exchangers [37]. The Turbotemper® plate heat exchanger is produced by 'Sollich KG', one of the most major producers of tempering units and is shown schematically in Figure 2-9 [38].

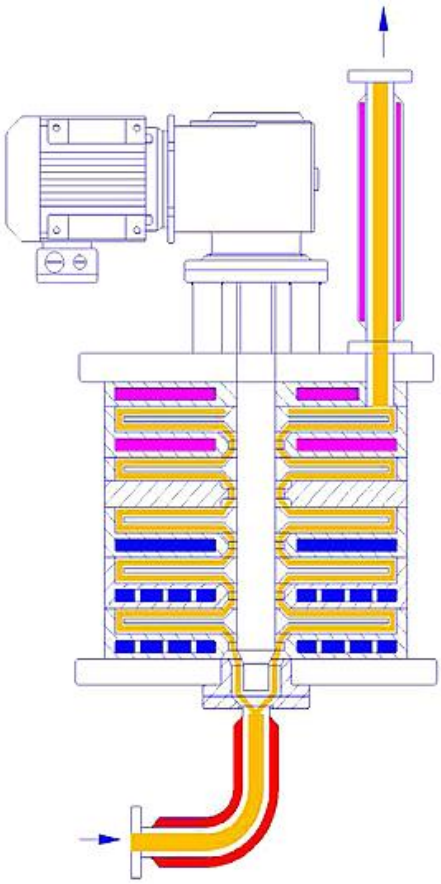

Figure 2-9: schematic illustration of the Turbotemper® plate heat exchanger (yellow = chocolate flow through the Turbotemper®) [38]

In the Turbotemper® several heat exchanging plates with one chocolate and one water chamber each are arranged on top of each other. The untempered liquid chocolate is transported by a pump from the storage tank upwards through the Turbotemper®. The chocolate enter the tempering unit at a temperature between 40 °C and 45 °C (red area in Figure 2-9). The blue zones are three cooling steps in which the chocolate is cooled down to around 29 °C. Afterwards the chocolate mass is heated up to around 32 °C (purple area) [38]. Mass flows from 100 to 18.000 kg/h can be realised [39]. The retention time τ of chocolate in the tempering unit can be calculated with the unit volume V_{unit}, chocolate density $\rho_{chocolate}$ and chocolate flow rate $\dot{V}_{chocolate}$:

$$\tau = \frac{\rho_{chocolate} \cdot 60 \cdot V_{unit}}{\dot{V}_{chocolate}} \quad (2\text{-}1)$$

The Nestlé Product Technology Centre York uses for example a three step tempering unit with the temperature profile shown in Table 2-9 [40].

Table 2-9: three step tempering profile of Nestlé PTC York (step 0 = inlet temperature) [40]

step	temperature [°C]
0	45 - 50
1	32 - 35
2	27 - 29
3	29 - 31

The higher temperatures are used for dark chocolates and the decreasing temperatures for chocolates with increasing milk fat amount. The retention time of chocolate in the tempering unit is 3 to 4 minutes independently of the unit size [40]. The average retention time of all available tempering units on the market is between 10 and 12 minutes for chocolate moulding and between 20 and 360 minutes for chocolate enrobing [37]. A faster crystallisation can be realised with increasing shearing [16].

Cooling following the tempering leads to a complete crystallisation of the chocolate (see Figure 2-7). The chocolate treatment in the tempering unit is thus a pre-crystallisation. The generated form V cocoa butter crystals act as seeds for the formation of further crystals of this structure [36]. An alternative to the tempering method is the addition of cocoa butter seeds of form V to the liquid chocolate. This inoculation leads also to the growth of more form V crystals. The cooling of chocolate is mostly realised in a cooling tunnel with different temperature zones. The chosen temperature also depends on the chocolate type and usage. Exemplary temperatures are given in Table 2-10 [2].

Table 2-10: cooling tunnel temperatures for chocolates [2]

step	entrance	center	outlet
chocolate	15 - 17 °C	10 - 12 °C	15 - 17 °C
chocolate coatings with other fats	10 - 12 °C	10 - 12 °C	15 - 17 °C

Nestlé uses an entrance temperature between 12°C and 14 °C for all chocolate types and usages (moulding, enrobing) [40]. Approximately 1/3 of the Nestlé tunnel is set at the lowest temperature but a minimum of 10°C. In the further 2/3 of the tunnel a temperature between 14°C and 16 °C is set to let the desired crystals grow. The higher temperatures are again used for dark chocolates and the lower temperatures for chocolates with increasing milk fat amount [40]. The retention time in the cooling tunnel should be 10 to 20 minutes for enrobing and between 20 and 45 minutes for moulding due to the higher chocolate volume [40]. In addition, it is important that the outlet temperature is chosen to be as high as possible to exceed the dew point temperature and avoid moisture on the product [37, 40].

2.3 Properties of Chocolate

In this chapter specific material properties will be discussed. The different properties of chocolate are important in various industrial process steps, for example the energy consumption during tempering. In this chapter the viscosity, specific heat capacity, specific enthalpy and the diffusion coefficient of chocolate will be discussed in detail. The melting temperature and the different crystal structures were already described in previous chapters.

2.3.1 Viscosity

Viscosity is a measure of the resistance of a fluid which is being deformed or get into flow by a force without changing the volume thus it is a measurement of fluid thickness [41]. The resistance leads to a flow velocity depending on the shear stress and the internal friction [42]. The viscosity is a temperature dependent property [43].

Viscosity can be differentiated further between dynamic viscosity η and kinematic viscosity ν, whereby the kinematic viscosity describes the density related dynamic viscosity ($\nu = \eta / \rho$) [42].

Flow behaviour can be used to distinguish Newtonian fluids and non-Newtonian fluids. Newtonian fluids show a linear correlation between shear rate $\dot{\gamma}$ and shear stress τ [42]. For this kind of fluid the viscosity is only depending on temperature and pressure and can be calculated as shown in equation (2-2) [42]:

$$\eta = \frac{\tau}{\dot{\gamma}} \tag{2-2}$$

Non-Newtonian fluids on the other hand show time-dependent and shear rate-dependent behaviour [42]. Shear rate-dependent behaviour can further distinguish between Bingham fluid, dilatant fluid (shear-thickening fluid), pseudo plastic fluid (shear thinning fluid) and Casson fluid. Time-dependent behaviour can be used to distinguish between thixotropy and rheopexy [42].

Binghan and Casson fluids have a yield value which must be overcome before the fluid starts to flow [42]. Afterwards Bingham fluids show a linear correlation between shear rate and shear stress. In contrast, Casson fluids have then a decreasing gradient of the shear stress with increasing shear rate [24, 27]. A comparison between the behaviour of a Newtonian fluids and a Non-Newtonian Casson fluid is exemplarily shown in Figure 2-10 [24].

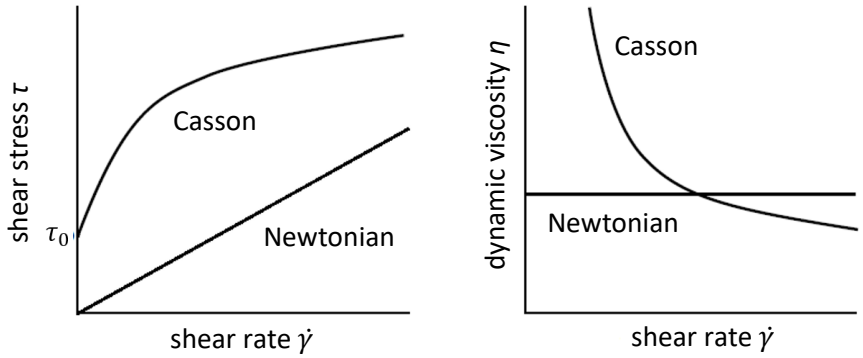

Figure 2-10: Influence of the shear rate on the shear stress and dynamic viscosity of a Newtonian fluids and a Casson fluid (τ_0 = yield point) [24]

Liquid cocoa butter is a Newtonian fluid and liquid chocolates are non-Newtonian Casson fluids because the continuous fat phase forms a suspension with solid particles [24]. For chocolate the yield value (minimum shear stress τ_0) must be overcome to realise a flowing of the suspension. During this the particles in the chocolate will be displaced and thus allowing the chocolate to flow as shown in Figure 2-11 [24].

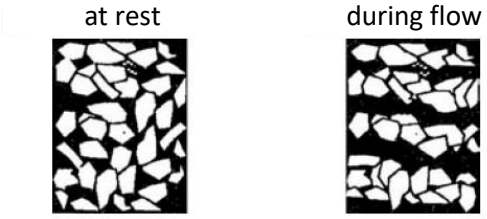

Figure 2-11: schematic diagram of particles within a suspension [24]

The viscosity of cocoa butter and chocolate is not so much temperature-dependent but highly influenced by the solid content of cocoa butter crystals *c*. The crystal content decreases during melting of the fat which leads to following empirical equation (2-3) [43]:

$$\eta_S = \eta_D \cdot \left[1 + \frac{ac}{(1-bc)^2}\right] \tag{2-3}$$

η_S is the viscosity of the solid dispersion, η_D is the viscosity of the liquid dispersion agent, *c* is the volume fraction of the solid crystal fat phase, a is half of the Einstein constant ($a = 1{,}25$) and *b* is a matter constant [43].

The viscosity of chocolate also depends on other parameters like particle size distribution of the solid particles, the amount of fat, lecithin and moisture in the chocolate as well as the conching time and the influence of thixotropy [24]:

1. **Particle size distribution**. Small particles have a higher specific surface area than bigger particles. Because of this for smaller particles more fat is necessary to coat them allowing the chocolate to flow. Additionally it is more likely that the smaller single particles interact with each other so that smaller particles increase the viscosity more than bigger ones [24].

2. **Amount of fat**. A high fat amount leads to low viscosities because of less interaction between the single particles. At lower fat amounts (ca. 25wt%) the viscosity reduction by adding fat is higher than at higher fat amounts (ca. 35wt%) [24].

3. **Amount of lecithin**. Adding of lecithin up to around 0.3wt% reduces the viscosity because of its surface active properties [24]. Lecithin covers the sugar particles with its hydrophilic head group. The lipophilic tails of lecithin orientate in the direction of the fat phase and thus generate a better flow-ability and lower viscosity of the chocolate (see chapter 2.1.6). In contrast to that, adding lecithin in the range from 0.3wt% to 0.5wt% leads to an increase of viscosity [24]. It is assumed that at these concentration, lecithin start to form micelles and a second lecithin layer accumulates around the sugar particles. The hydrophilic head group of the second lecithin layer orientates in the fat phase of the chocolate and this leads to a higher viscosity [24].

4. **Moisture content**. A moisture content in the chocolate above 1 wt% leads to interactions between the sugar particles, which adhere to each other and thus leads to an increase of viscosity. Below 1wt% moisture the effect of water can be buffered for example in the form of lactose crystal water [24].

5. **Conching time**. A longer conching time leads to a better covering of particles with fat and less particle agglomerates. The chocolate thus need less energy to flow. Additionally the moisture content decreases during conching below 1wt% and this also leads to a lower viscosity (see chapter 2.2.2) [24].

Thixotropy. Thixotropy is the time dependency of the viscosity. During the measurement time the particles arrange in a new way and this leads to a decrease of viscosity. Because of this the time for chocolate viscosity measurement should not exceed 7 minutes [24].

2.3.2 Specific Heat Capacity

The specific heat capacity *c* gives the amount of energy needed to rise the temperature of a fluid or a solid per unit mass [44]:

$$c = \frac{Q}{m \cdot \Delta T} \tag{2-4}$$

Q is the thermal energy, *m* the mass of the substance and ΔT the temperature difference between initial and final temperature. The isochor specific heat capacity c_v gives the relation of the applied heat

to the temperature difference for constant volume and the isobar specific heat capacity c_p for constant pressure [44]. In this work the isobar specific heat capacity c_p is considered and following named as specific heat capacity.

The specific heat capacity of white, milk and dark chocolate as well as cocoa butter at different temperatures are given in Table 2-11 for the solid state [45, 46] and in Table 2-12 for the liquid state [45–47]. The calculated values are determined with different equations and are explained in detail by ENGMANN et al., DEUERLING et al. and MORAD et al. [45–47]. The experimental values were determined with dynamic differential calorimetry (see chapter 4.5).

Table 2-11: calculated and measured specific heat capacities of different solid chocolates and cocoa butter [45, 46]

type	**Temperature [°C]**	**$c_{p,solid}$ [kJ/kg K]**		**reference**
		calculation	experiment	
white chocolate	5	2.51	2.10	[46]
milk chocolate	0	-	1.55	[45]
	5	2.44	2.10	[46]
	10	-	1.68	[45]
dark chocolate	0	-	1.30	[45]
	5	2.36	1.76	[46]
	10	-	1.34	[45]
cocoa butter	0	-	2.22	[45]
	10	-	2.38	[45]

Table 2-12: calculated and measured specific heat capacities of different liquid chocolates and cocoa butter [45–47]

type	**Temperature [°C]**	**$c_{p,liquid}$ [kJ/kg K]**		**reference**
		calculation	experiment	
white chocolate	45	2.12	1.76	[46]
milk chocolate	40	-	1.55	[45]
	45	2,26	1.84	[46]
dark chocolate	40	-	1.38	[45]
	45	1.83	1.84	[46]
cocoa butter	40	-	2.01	[45]
	60	2.13	2.12	[47]
	80	2.18	2.18	[47]
	100	2.23	2.24	[47]

The specific heat capacity of solid chocolates and cocoa butter is approximately constant in the considered temperature range. On the other hand the specific heat capacity of liquid chocolates and cocoa butter increases with temperature. Overall the specific heat capacities for the solid and liquid state show approximately similar values [45–47].

2.3.3 Specific Enthalpy

Specific enthalpy is the specific internal energy of a system. Δh_S is the specific melting energy that is required for the phase transition of a substance from solid to liquid state [44] and Δh_c the specific crystallisation enthalpy (transition from liquid to solid state). Both enthalpies have the same absolute values but reverse signs. Table 2-13 show the specific melting enthalpy of milk chocolate, dark chocolate and cocoa butter for the solid-liquid phase transition between 10°C and 40°C [45] at which all crystal structures are melted.

Table 2-13: specific melting enthalpy *Δhs* of chocolates and cocoa butter at temperatures between 10°C and 40°C [45]

type	Δh_S [kJ/kg]
milk chocolate	44.4
dark chocolate	46.5
cocoa butter	157

The chocolates have a significantly lower specific melting enthalpy than the cocoa butter because they have a lower amount of cocoa butter and thus less energy is required for melting. WILLE et al. [12] and CHAPMAN et al. [48] determined the specific melting enthalpies of each crystal form of cocoa butter with a calorimeter [12] and dynamic differential calorimetry [48]. The values are shown in Table 2-14:

Table 2-14: specific melting enthalpy *ΔhS* of all single cocoa butter crystal [12, 48]

crystal structure	Δh_S [kJ/kg]	
	WILLE et al.	CHAPMAN et al.
I	-	-
II	86.2	81.6
III	112.6	90.0
IV	117.6	103.8
V	136.9	117.6
VI	148.2	137.7

Equation (2-5) for the thermal energy *Q* to be removed can be transformed with equation (2-4) and the phase transition from solid to liquid for a mass *m* during the heating from T_{start} to T_{end}. Equation (2-5) applies only for one single crystal structure because it is calculated with the melting temperature of one crystal form and not with a melting range.

$$Q = mc_{p,solid}(T_s - T_{start}) + m\Delta h_s + mc_{p,liquid}(T_{end} - T_s) \quad (2\text{-}5)$$

2.3.4 Diffusion Coefficient

Diffusion is dependent of the molecular distance in a system. An increase of the free path length leads to a decrease of the diffusion resistance, for example because of less collision with other molecules. The diffusion coefficient *D* describes the mobility of molecules. Small diffusion coefficients have a big diffusion resistance and big coefficients have a small diffusion resistance [49]. In general *D* decreases with increasing pressures because of decreasing molecule path length. In contrast, the diffusion coefficient increases with increasing temperatures because of increasing molecular mobility [49]. The influence of temperature on *D* in liquids can be described with the Einstein-equation (2-6) [43]:

$$D = \frac{k_B \cdot T}{6 \cdot \pi \cdot \eta \cdot r} \tag{2-6}$$

k_B is the Bolzmann constant, T the temperature, η the viscosity and *r* the molecule radius of the diffusing material. WINDHAB [36] describes that the crystallisation of cocoa butter is controlled by diffusion. It was shown that low cooling temperatures lead to an increase of viscosity and thus to slow diffusion (small diffusion coefficient), that in turn leads to a slower crystallisation [36]. Decreasing of the diffusion coefficient with decreasing temperatures is also described by ZIEGLEDER [43] as shown inTable 2-15. In this example the diffusion coefficient of the triglyceride triolein in milk chocolate increases exponentially with increasing temperature.

Table 2-15: diffusion coefficient of triolein in milk chocolate for different temperatures [43]

temperature [°C]	*D* [cm²/s]
-30	$5.0 \cdot 10^{-13}$
10	$3.6 \cdot 10^{-11}$
26	$5.5 \cdot 10^{-9}$
35	$1.5 \cdot 10^{-8}$

2.4 Aerated Chocolate

Aerated chocolate is a type of chocolate with a porous structure because of the trapped bubbles (cavities) in the product [2]. In comparison with normal chocolate the bulk density of aerated chocolate is much lower [1] and thus the specific surface area much higher. This leads to a special mouth feeling and a more intense taste [1, 2].In 1935 the first aerated Aero® chocolate was produced by the Rowntree company, which belongs to Nestlé today [24]. Aerated chocolate is a popular product and for example sold as chocolate blocks or bars [2].

2.4.1 Processing of Aerated Chocolate

Aerated chocolate can be produced using four main processes, different gasses can also be used to impact the final structure. The different processes are explained below:

1. **Vacuum process.** Tempered liquid chocolate is stirred with or without gas addition (mostly carbon dioxide) so that gas will be introduced into the chocolate. Additionally the small gas bubbles in the chocolate grow during reduction of the pressure and thus decreasing of the gas solubility in the chocolate what leads to a chocolate foam. The foam is stabilised with a subsequent cooling and thus crystallisation of the aerated chocolate [2, 24].

2. **Pressure process.** Tempered liquid chocolate is pressurised and mixed with a gas (normally carbon dioxide or nitrogen). During this procedure the gas dissolves in the chocolate [2, 24]. Stirring is necessary for a faster solvation of the gas in the chocolate and avoids chocolate overheating and thus destroying the temper [1, 24]. A subsequent depressurisation to ambient pressure leads to a release of the dissolved gas because of the resulting gas solubility decrease and thus forming bubbles. For stabilisation the formed foam must be cooled until complete crystallisation takes place [2].

3. **Addition of emulsifiers under stirring**. Emulsifiers are added to liquid chocolate whilst stirring. Bubbles are formed in the chocolate during this powerful mixing. The bubbles are relatively stable and will not be destroyed during further processing of the chocolate [2]. It was found out that phospholipids, especially phosphatidylcholine are responsible for the foaming in cocoa butter [50]. It is assumed that the phosphatidylcholine build molecular layers out of liquid crystals on the gas/cocoa butter phase boundary which increase the surface tension and thus stabilise the bubbles [50].

4. **Gas injection during cooling**. Liquid chocolate is stirred, cooled and injected with gas (carbon dioxide, nitrogen or air). Due to the cooling the viscosity increases because of the formation of crystal seeds in the chocolate. Stirring prevents the complete crystallisation and leads to a uniform distribution of gas in the chocolate. Additionally the chocolate foam is further cooled and stabilised due to a complete crystallisation without stirring [51]. The fast cooling and crystallisation after gas injection are required to entrap and stabilise as many bubbles as possible in the chocolate [50].

KOLLER [52] developed a continuous high-pressure micro aeration process in a pilot plant twin-screw extruder for fat based confectionery enabling the production of micro-aerated foams with mean bubble sizes below 50µm [52]. The continuous extrusion process using an adjustable and controlled extrusion die, consisting of a serial arrangement of five sections comprising a high pressure build-up section, a gas dissolution section, a cooling and crystallization section, a foaming section and a moulding section [52]. The high-pressure foam extrusion process was combined with the injection of food-grade bubble nucleators (seeding) to produce high-porosity, micro-aerated, fat-continuous confectionery [52]. Milk and dark chocolate were micro-foamed with carbon dioxide and nitrogen reaching porosities between 10 - 40% [52]. KOLLER showed that the addition of micro fat crystals is highly effective as bubble and fat polymorph structure nucleating agent [52].

In the following chapters the pressure process in particular is taken into account. For chocolate aeration processes the selection of gas type is also important. In particular carbon dioxide and nitrogen are commonly used gases for the aeration of chocolate. HAEDELT and KOLLER [1, 52] found out that nitrogen leads to smaller bubbles than carbon dioxide [1, 52]. HAEDELT already investigated the aeration with other gases [1].

2.4.2 Gas Solubility

The gas solubility x_i is the amount of gas that can be dissolved in a liquid. The unit can be given in wt% or mol%. The gas solubility can be determined with the thermodynamic equilibrium between a gas and a liquid. A system is in a thermodynamic equilibrium when the pressure p, the temperature T and the chemical potential μ_i of each component *i* in the system is equal for all phases (α, β, φ) [53]:

$$p^{\alpha} = p^{\beta} = \cdots = p^{\varphi} \tag{2-7}$$

$$T^{\alpha} = T^{\beta} = \cdots = T^{\varphi} \tag{2-8}$$

$$\mu_i^{\alpha} = \mu_i^{\beta} = \cdots = \mu_i^{\varphi} \tag{2-9}$$

With the help of the Gibbs-Duhem equation it can be shown that the chemical potential μi is equal to the partial molar Gibbs energy $\overline{g_i}$ [53]:

$$\mu_i = \overline{g_i} \tag{2-10}$$

The partial molar Gibbs energy $\overline{gi}$ can be described with the fugacity f [53]:

$$\overline{g_i} = g_i^{pure}(T, p^0) + RTln\frac{f_i}{f_i^0(T, p^0)} \tag{2-11}$$

The values g_i^{pure} and $fi0$ describe the pure substances and only depending on the temperature and the pressure. Because of this they must be equal for all components at equilibria [53]. It therefore follows that not only the chemical potentials but also the fugacity of each component in all phases are equal at thermodynamic equilibria [53]:

$$f_i^{\alpha} = f_i^{\beta} = \cdots = f_i^{\varphi} \tag{2-12}$$

In the present case the gaseous phase *G* (for example carbon dioxide) is in equilibrium with the liquid fat phase *L* (cocoa butter or chocolate). A binary system with two components, for example carbon dioxide and cocoa butter, is considered (it is neglected that chocolate is a suspension of fat and particles):

$$f_i^L = f_i^G \tag{2-13}$$

The fugacity of the liquid phase for carbon dioxide (component 1) $f_1{}^L$ can be calculated with the mole fraction in the liquid phase x_1, the activity coefficient in the liquid phase at infinite dilution $\gamma_1{}^*$, the Henry coefficient $H_{1,2}$ and the poynting correction factor $\Pi_{\infty 1}$ (for pressure correction) [53]:

$$f_1^L = x_1 \gamma_1^* H_{1,2} \Pi_{\infty 1} \tag{2-14}$$

The fugacity of the gaseous phase for carbon dioxide (component 1) $f_1{}^G$ can be calculated with the mole fraction in the gaseous phase y_1, the fugacity coefficient $\varphi_1{}^G$ and the pressure p [53]:

$$f_1^G = y_1 \varphi_1^G p \tag{2-15}$$

With equation (2-13), (2-14) and (2-15) the main equation of the gas-liquid equilibria is obtained [53]:

$$x_1 \gamma_1^* H_{1,2} \Pi_{\infty 1} = y_1 \varphi_1^G p \tag{2-16}$$

The gas solubility can be approximately determined with Henry's law [53]. If is assumed that the gaseous phase behaves ideally, the fugacity coefficient $\varphi_1{}^G$ can be estimated with 1 [54]. Additionally it can be assumed that only a very small amount of gas dissolves in the liquid phase and thus the activity coefficient $\gamma_1{}^*$ can be estimated with 1 [54]. Furthermore at low pressures applied the Poynting correction factor $\Pi_{\infty 1}$ can also be assumed with 1 [54]. Thus obtained simplified equation for the gas-liquid equilibria is the Henry's law [54]:

$$x_1 H_{1,2} = y_1 p \tag{2-17}$$

The Henry coefficient is equal to the slope of the tangent applied at x_1 -> 0 (infinite dilution of gas in liquid) [54]. Henry's law defines, that the partial pressure p_i of a gas i ($p_i = p \cdot y_1$) is proportional to its mole fraction in the liquid x_1 [55]. The Henry coefficient $H_{1,2}$ depends on the type of gas and liquid and it increases with increasing temperature [56]. Because of this the gas solubility decreases with increasing temperature.

Investigations of gas solubilities in chocolate are not published but the solubility of carbon dioxide in liquid cocoa butter at thermodynamic equilibria was measured by CALVIGNAC [14], VENTER [11], KOKOT [57], SANTOS [58] and KOLLER [52]. Additionally the influence of pressure and temperature on the gas solubility was investigated. In Table 2-16 are given the different temperature and pressure conditions of the experiments [11, 14, 52, 57, 58].

Table 2-16: temperature and pressure conditions of the solubility measurements of carbon dioxide in liquid cocoa butter [11, 14, 52, 57, 58]

reference	temperature [°C]	pressure [bar]
CALVIGNAC	40, 80	up to 400
VENTER	40, 80, 100	20 - 350
KOKOT	30 - 80	up to 300
SANTOS	40, 50	30 - 200
KOLLER	30, 40	up to 60 bar

The listed measurements were all carried out in high pressure autoclaves. The experimental results of carbon dioxide solubility in liquid cocoa butter for all investigated pressures exemplarily at 40°C are given in Figure 2-12 [11, 14, 52, 57, 58].

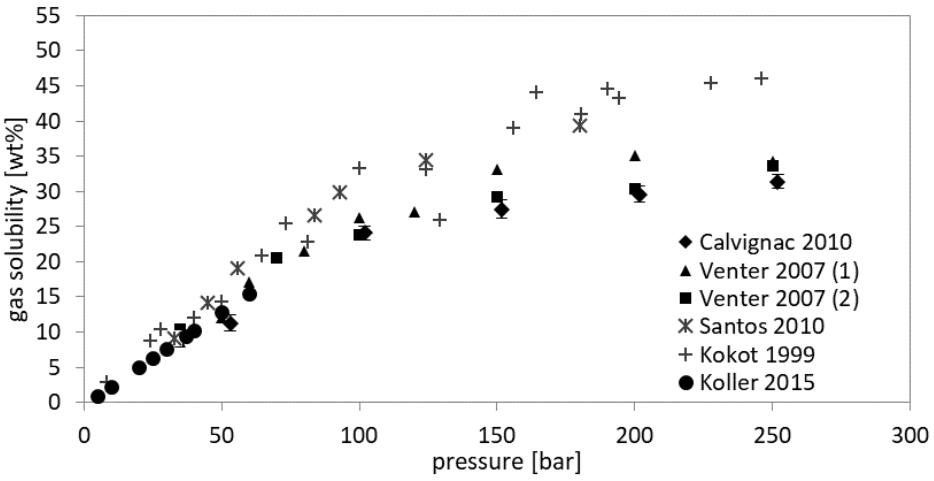

Figure 2-12: Influence of pressure on the carbon dioxide solubility in cocoa butter at 40 °C and thermodynamic equilibria [11, 14, 52, 57, 58]

Figure 2-12 shows the increasing of carbon dioxide solubility in cocoa butter with increasing pressure at 40 °C [11, 14, 52, 57, 58]. Measurements at other temperatures show equivalent behaviour [11, 14, 52, 57]. Additionally it was shown that a temperature decrease also leads to an increase of the carbon dioxide solubility in cocoa butter [11, 14, 52, 57, 58].

The different literature values at 40°C have a good agreement up to a pressure of around 100 bar. VENTER measures the solubility with two methods, one was sampling with a sample cell and subsequent depressurisation and the other was sampling without a sample cell and depressurisation directly on the autoclave [11]. The two measuring methods show very good agreement, also at higher pressures. The experimental values of SANTOS [58] and KOKOT [57] show at higher pressures (above 100 bar) higher deviations from the other authors [11, 14]. A reason could for example be the different triglyceride composition of the cocoa butters used. CALVIGNAC and VENTER [11, 14] investigated cocoa butter from the same manufacturer and KOKOT [57] used the butter from a different cultivation region.

KOLLER [52] also measured the solubility of nitrogen in liquid cocoa butter at pressures up to 250 bar. The nitrogen solubility in cocoa butter also increases with increasing pressure [52]. KOLLER found out that the solubility of nitrogen is much lower compared to carbon dioxide, at 250 bar approximately only 1 wt% of nitrogen is dissolved in the cocoa butter [52].

2.4.3 Properties of CO_2 Saturated Cocoa Butter

Gas, and especially carbon dioxide saturated cocoa butter at elevated pressure has different properties and show different behaviour in comparison with cocoa butter at ambient conditions [11, 14, 49, 57]. The pressure influenced parameter density, melting behaviour, viscosity, surface tension and diffusion will be discussed below.

Density. In general densities of solid and liquid substances are influenced by the temperature and densities of gaseous substances are influenced by the temperature and pressure [59]. The density of carbon dioxide aerated cocoa butter increases with decreasing temperature or increasing pressures [11, 14, 52]. The increase of density with increasing pressure is because of the rising hydrostatic pressure and the resulting compression effect [49]. CALVIGNAC [14] showed, that with increasing pressure the density of carbon dioxide saturated cocoa butter increases faster than of pure cocoa butter. The reason is the better solubility of carbon dioxide at higher pressures and thus the gas molecules fill the free spaces in the cocoa butter [14]. The influence of pressure on the density of carbon dioxide aerated cocoa butter at a saturation temperature of 40°C is given in Figure 2-13 [11, 14]. Both authors show a linear influence of the pressure on the density of carbon dioxide aerated cocoa butter and the same gradient of the curve [11, 14].

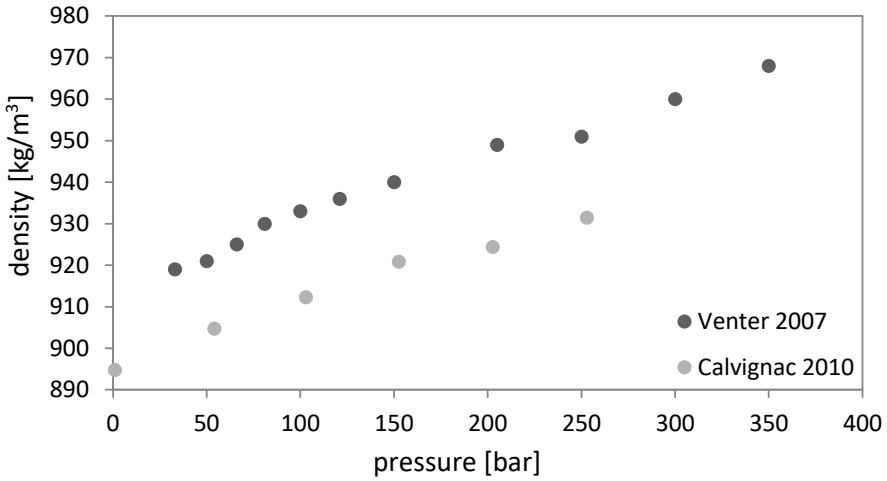

Figure 2-13: Influence of pressure on the density of carbon dioxide aerated cocoa butter at 40 °C [11, 14]

Melting behaviour. The influence of carbon dioxide saturation pressures on the melting point of cocoa butter was measured by VENTER [11],and KOKOT [57]:

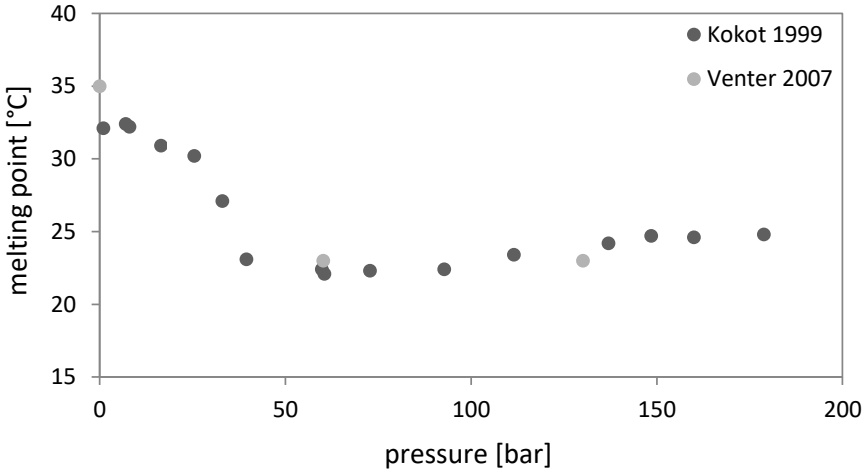

Figure 2-14: Influence of pressure on melting point of carbon dioxide aerated cocoa butter [11, 57]

The dissolution of carbon dioxide in cocoa butter decreases the melting point of the butter up to a pressure increase of around 50 bar [11, 57]. This effect was also described by KOLLER [52]. Pressures above 50 bar leads to a small increase in the melting point. This behaviour can be explained by two competing effects, on the one hand the increasing hydrostatic pressure results in a melting point increase and on the other hand there is the increase in dissolution of carbon dioxide [11]. The melting point reduction with dissolved CO_2 can be described with the colligative effect in mixtures [52]. Colligative properties are properties of solutions that depend on the ratio of the number of solute molecules to the number of solvent molecules in solution [52]. One such colligative property is the depression of the freezing point of a solution compared to the solvent caused by the reduction of the chemical potential [52, 60]. This effect results from the increased entropy or enhanced randomness which retards freezing [52, 60]. The dissolved gas molecules can interfere with the fat crystal structure and thus reduce the energy required for melting or breaking the intermolecular bonds [52, 57]. The carbon dioxide molecules disrupt the crystal structure of the cocoa butter and thus the melting point decreases. These two effects overlay each other and this results in a melting point decrease or increase depending on the pressure because the gas solubility gradient is higher at low pressure ranges and smaller at higher pressure ranges (see Figure 2-12).

Dynamic viscosity. The definition of the dynamic viscosity η was already given in chapter 2.3.1. The viscosity of carbon dioxide aerated and saturated cocoa butter decreases with increasing pressures [11, 14, 52]. The decreasing of the viscosity with increasing carbon dioxide saturation pressure is very fast up to 50 bar and with further pressure increases much lower [11]. This can be explained by the very steep increase of carbon dioxide solubility in cocoa butter up to 50 bar and followed by a lower increase with further pressurisation. The carbon dioxide molecules disturb the interactions between the cocoa butter triglycerides and thus facilitate the movement of the cocoa butter molecules. For

example at 40 °C the viscosity at ambient pressure is 0.042 Pas, at 50 bar carbon dioxide saturation pressure the viscosity is around 0.01 Pas and at 200 bar around 0.005 Pas [11, 14].

Surface tension. Liquids attempt to achieve the smallest possible surface areas. On the liquid surface only the minimum number of molecules required for surface stabilisation are present, subsequent creating the surface tension σ. The unnecessary molecules on the surface are moved into the inside of the liquid due to intermolecular forces [61]. The temperature and pressure dependence of the surface tension can be determined with fundamental equations in the form of the free energy and the free enthalpy. Additionally it must be assumed, that the phase boundary interface is an additional phase [49]. This shows that an increase of temperature leads to a decrease of surface tension because of the improved mobility of the molecules [49]. An increase in pressure also leads to a decrease in surface tension [49, 52]. The dependency of the surface tension from the pressure is approximately linear. Additionally it was shown, that bigger bubbles in aerated chocolate can be formed with higher surface tension [8].

Diffusion coefficient. The definition of the diffusion coefficient D is already given in chapter 2.3.4. In compressible liquids in general it will decrease with an increase in pressure because there is less space between the molecules. EGGERS [49] and LOCKEMANN [62] show that the diffusion coefficient remain stable or even rise due to the dissolution of carbon dioxide in a fat or oil phase. This behaviour can be explained with the decreasing viscosity because of gas solubility [49]. Up to now no investigations on the pressure dependence of the diffusion coefficient in carbon dioxide saturated cocoa butter have been performed. The diffusion coefficient greatly influences bubble growth (for example during the production of aerated chocolate) because the gas has to diffuse through the fat phase surrounding the bubbles [63].

Overall the changes associated with increasing pressure or rather carbon dioxide saturation pressure are higher for the melting temperature, the viscosity and the surface tension than for density. The change of the diffusion coefficient cannot be analysed quantitatively because of missing experimental values for the system carbon dioxide/cocoa butter.

2.4.4 Properties of Foams and Bubbles

The formation of a bubble or a foam results from the presence of gas in a for example liquid system. Foams can be produced in different ways for example with a high pressure process (see chapter 2.4.1). In this process bubbles are nucleated (“Cluster”), forming and growing during the depressurisation and corresponding gas release due to decreasing of gas solubility [64].

There are two different mechanisms for the formation of bubbles, homogenous and heterogeneous bubble formation [65]. For homogenous bubble formation a liquid does not need to be in contact with a gas phase and wet all contacting surfaces completely. Because of this the contact angle is 0°. If bubbles are formed, they will only be in the liquid. For heterogeneous bubble formation the bubbles are formed at the phase boundary interface between the liquid and another phase. For that the

contact angle must be bigger than 0° [65]. Heterogeneous bubble formation is favoured in comparison to homogenous bubble formation because less energy is consumed [66].

Single bubble. A stabile single bubble has to be in a balance of force with the surrounding liquid (Figure 2-15) [8]

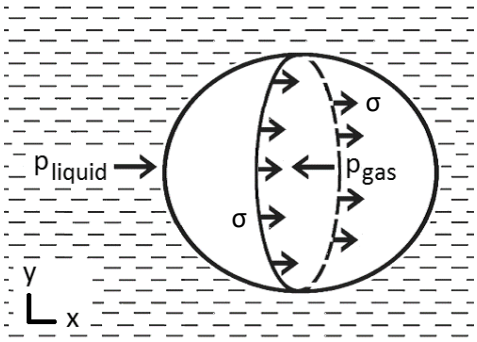

Figure 2-15: balance of force of a single bubble in a liquid [8]

The pressure is projected on the circular cross section (πr^2) with the bubble radius r. The surface tension σ is applied on the circumference of the circular cross section. The pressure inside the bubble p_{gas} on the circular cross section is equal to the pressure in the liquid p_{liquid} on the circular cross section and the surface tension σ [8]:

$$\pi r^2 p_{gas} = \pi r^2 p_{liquid} + 2\pi r\sigma \tag{2-18}$$

Foam. Foam is a liquid or solid material that has a high volume amount of dispersed gas inside. Aerated chocolate is a solid foam because the foam is produced with a liquid and afterwards solidified [67]. Processes like disproportionation, drainage and rising of bubbles, mutual deformation of the bubbles and coalescent take place in foams. This is because of concentration differences, weight force and interactions between the single bubbles [68]:

- **Disproportionation.** The disproportionation is also called Ostwald ripening and describes the gas transport from small bubbles to big bubbles through the liquid [68]. The pressure in the bubble p_{gas} can be calculated with simplification of equation (2-18):

  $$p_{gas} = p_{liquid} + 2\frac{\sigma}{r} \tag{2-19}$$

  Small bubbles have a higher inner pressure than bigger bubbles and thus a higher concentration of gas on the boundary surface. Diffusion of gas from a small to a big bubble takes place because of the concentration gradient [67].

- **Drainage and rising of bubbles.** Both these effects can be explained through the weight force and the different densities of the liquid and gas. The bubbles in the foam will rise up and the liquid will flow down the bubble, leading to a decrease of the liquid film between the bubbles [68]. The opposite movements can be slowed down or prevented by a viscosity increase of the liquid phase (for example due to temperature decrease). Drainage can also be reduced by surface active substances. The liquid is pushed together during drain off and this results in an opposite tangential tension [67]. The force balance on a spherical single bubble, neglecting the impact of drainage is given in Figure 2-16 [69].

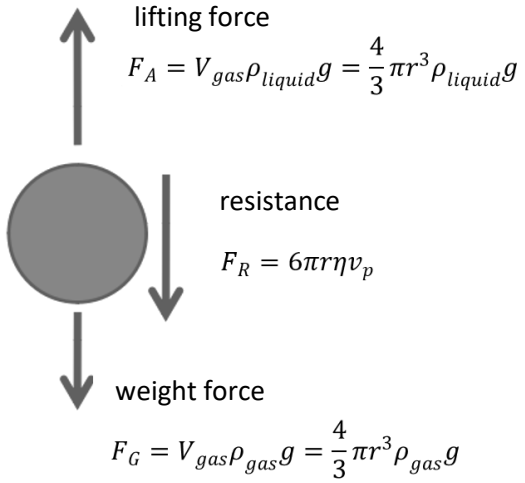

Figure 2-16: balance of force on a spherical single bubble [69]

The resistance of a spherical object F_R can be calculated according to Stokes with the radius r, ascend speed v_P and the viscosity of the surrounding liquid η [70]. The ascend speed v_P can be calculated with the density of the liquid ρ_{liquid}, density of the gas ρ_{gas} and the gravity g:

$$v_p = \frac{2r^2 g(\rho_{liquid} - \rho_{gas})}{9\eta} \quad (2\text{-}20)$$

- **Mutual deformation of the bubbles.** Foams can have volumetric gas amounts in a wide range up to 97%. The bubbles can form spherical bubbles inside the liquid at levels below 75% and high viscosities [67]. A deformation of bubbles is unavoidable when the volumetric gas amount exceeds a value of 75%. The densely packed bubbles exert forces on one another and deform each other [67].

- **Coalescence.** When the liquid film between two or more bubbles reaches a critical thickness it will rupture and the small bubbles form one new big bubble with a new radius and inner pressure [71]. This process is called coalescence. Other reasons for coalescence of bubbles could be solid hydrophobic particles in the liquid film or particles which are in contact with the

liquid film surface and decrease the surface tension [67]. Rising of bubbles and separation of bubbles on the upper part leads to a higher probability of coalescence because the gas amount in this area increases [72]. The radius of a newly created bubble R_{coal} can be calculated out of the radii of the coalesced bubbles (R_1, R_2) with assumption of a constant volume [73]:

$$R_{coal} = \sqrt[3]{R_1^3 + R_2^3} \tag{2-21}$$

The new bubble is initially not in equilibria with the environment and its radius will oscillate until the equilibria is reached [74]. The larger the initial bubbles, the longer is the oscillating time of the new bubble [74].

In summary, the size and form of single bubbles or bubbles in foams is influenced by different parameters including the pressure difference between the bubble and the surrounding liquid, the surface tension, the diffusion of the gas inside the liquid, the effect of surface active substances, the viscosity and the volumetric gas amount in the foam. For the high pressure aeration of chocolate process parameters can also influence the formation and growth of bubbles as follows [8]:

1. **Process pressure.** The pressure is an important parameter due to the pressure dependency of the gas solubility [1] (see chapter 2.4.2). The process pressure therefore has an impact on the available amount of gas for bubble formation and thus the foam structure [1].

2. **Type of gas.** The type of gas used for aeration is also important due to differences in gas solubility and thus for the foam structure of the final aerated chocolate product. HAEDELT showed that nitrogen and argon have much lower gas solubilities than carbon dioxide or nitrous oxide [1]. Because of this nitrogen and argon aerated chocolates exhibit very small bubbles (micro foam structure) and carbon dioxide or nitrous oxide aerated chocolate has bigger bubbles in the foam [1]. In the industry mostly carbon dioxide is used for the aeration of chocolate due to safety and economic reasons [8].

3. **Depressurisation rate.** The depressurisation speed can have influence on the foam structure of the pressure aerated chocolate [1]. At different speeds of depressurisation the gas is released at different times so that various foam structures can be formed [8]. High depressurisation rates and therefore also low depressurisation time leads to low time availability for gas diffusion and thus influences the disproportionation.

4. **Process temperature.** The process temperature is also relevant for the gas solubility (see chapter 2.4.2) and thus for the foam structure. Lower temperatures lead to higher gas solubility. The temperature also influences the diffusion coefficient because molecular movement increases with increasing temperature [75]. Because of this the gas can faster diffuse out of the chocolate and is no longer available for bubble formation in the chocolate foam. The disproportionation effect is also greater for higher temperatures resulting in faster diffusion [67].

5. **Crystallisation speed.** The crystallisation speed of the chocolate is also important for the foam structure because the bubbles are trapped in the chocolate due to this process of foam stabilisation [8]. At slow crystallisation times (for example due to high crystallisation temperatures) the bubbles have more time for rising or interactions between each other and more drainage occurs [67].

6. **Composition of chocolate.** The influence of the chocolate composition on the foam structure of the pressure aerated chocolate has not been investigated yet and is one element of this work.

In conclusion of this chapter it can be said, that already different properties of cocoa butter and chocolate as well as properties of gas saturated cocoa butter are investigated. The solubility of carbon dioxide in liquid cocoa butter as well as the influence of pressure and temperature on the gas solubility are also already investigated. Investigation of the properties of gas saturated chocolates as well as investigations of gas solubilities in chocolate are currently not published. A continuous high-pressure extruder micro aeration process for chocolate combined with the injection of food-grade bubble nucleators was already investigated. Extensive investigations of alternative the high pressure chocolate aeration processes without an extruder and bubble nucleator injection for example in an autoclave and with alternative tempering are missing. Especially the detailed influence of process parameters on the chocolate foam structure are not published. It was already described in literature, that the process pressure has an impact on the gas solubility and the foam structure. The influence of different gasses on the gas solubility and the chocolate foam bubble size is also discussed in literature. The effect of gas mixtures on the chocolate foam structure was currently not investigated. It was already shown, that the crystallisation speed of the chocolate is also important for the foam structure and that the depressurisation speed can have influence on the foam structure but detailed investigations with chocolate in the high pressure process are missing. In this chapter it was also shown, that the composition of chocolate is varying for diverse chocolate types and that all ingredients has different properties. The influence of each component and the chocolate composition on the gas solubility and especially the foam structure is currently not investigated extensively.

2.5 Modelling of Bubbles and Foams

Gas bubbles form and grow during aeration due to the dissolution of a gas in a liquid under pressure and subsequent depressurisation as described above. This process can be divided into four steps [63]:

1. Dissolving of gas in a liquid
2. Bubble formation in the gas oversaturated liquid due to depressurisation or temperature increase
3. Bubble growth
4. Foam stabilisation at temperatures below the melting point

For the description of bubble formation and bubble growth, different models with various complexity can be used. There are simple models for single bubbles, more detailed models for multi bubble systems and very complex models for foams [66]. The various models are described in the following chapters.

2.5.1 Single Bubble Models

Single bubble models are used for the simple definition of bubble formation and growth during depressurisation. These models are often developed for polymer melts [63, 64, 76–78] or lava [79, 80]. In these model types, a single spherical bubble is considered and the time dependent behaviour of the bubble radius *R* and the pressure in the bubble p_{gas} is described with differential equations. Figure 2-17 shows the growth model of a single bubble and an assumed concentration profile what will be explained later [63].

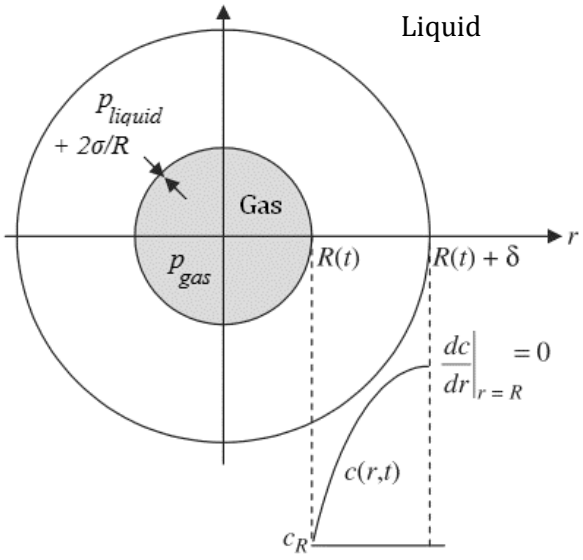

Figure 2-17: growth model of a single bubble [63] with the assumed concentration profile from HAN et al. [78]

With depressurisation and corresponding oversaturation of gas in the liquid, the gas molecules start to accumulate and form “Clusters”. These grow due to diffusion of gas through the liquid until they cannot be destroyed by thermodynamic fluctuations.

To calculate the growth process of the single bubble a number of assumptions have been made [63, 64, 77, 78]:

- The bubble is spherical at any point in time
- The pressure in the bubble at the formation $p_{gas,0}$ can be calculated depending on the concentration on the phase boundary of the bubble c_R by using Henry's law [63]:

$$\mathrm{p_{gas,0}} = \frac{c_R}{H_{1,2}} \tag{2-22}$$

- The diffusion coefficient, the Henry constant and the dynamic viscosity are constants independent from the concentration
- The liquid is a Newtonian fluid
- Gravitational effects can be neglected
- The gas is an ideal gas
- The depressurisation is isotherm
- The fluid is incompressible

The coordinate system for the growth process originates in the middle of the point symmetrical bubble to simply consider a radial velocity field. Tangential components will be neglected [77]. The bubble generates a radial velocity field in the liquid during growth. To describe the growth of the bubble with time, a simplified continuity equation for viscous and incompressible fluids (constant density) in polar coordinates is used. This equation describes the conservation of mass of a fluid in combination with its velocity field [77]:

$$\frac{\partial v}{\partial r} + \frac{2v}{r} = 0 \tag{2-23}$$

v is the velocity of the fluid in radial direction and *r* is the variable radius from the coordinate origin in the middle of the bubble in radial direction. The assumption is made, that on the phase boundary ($r{=}R$) the velocity of the liquid *v* is equal the modification speed of the radius $\dot{R}$ ($v = \dot{R}\big|_{r=R}$).The equation for the velocity field can then be integrated out of equation (2-23) [77]:

$$\mathrm{v}(r,t) = \frac{1}{r^2} R^2 \dot{R} \tag{2-24}$$

The velocity *v* is depending on the location of the radius *r* and the time *t*. The change of the bubble radius $\dot{R} = \frac{dR}{dt}$ can be determined with the radial stress tensors of the gas phase and the liquid phase [77]. Both stress tensors are equal at the phase boundary [77]. They describe the molecular momentum exchange due to shear and normal stress [81]. Due to the assumptions made only the radial stress tensors σ_{rr} for the radial velocity field is important [77, 82]. The radial stress tensor σ_{rr} for incompressible, viscous fluids in spherical coordinate systems is dependent on the viscosity η and

the pressure *p* in the velocity field at the actual place and can be calculated with insertion of equation (2-24) [82]:

$$\sigma_{rr} = -p + 2\eta\frac{\partial v}{\partial r} = -p - 4\eta\frac{R^2\dot{R}}{r^3} \tag{2-25}$$

To describe the tension on the phase boundary of the liquid, the surface tension σ must be included [77]. In the liquid phase the radial stress tensor makes a step of *2σ/R* because of the surface tension. This results in equation (2-26) for the liquid on the phase boundary [77]:

$$\sigma_{rr}(r = R) = -p_{liquid} - 4\eta\frac{\dot{R}}{R} - \frac{2\sigma}{R} \tag{2-26}$$

For the gas phase results, with the assumption that the viscosity and surface tension of the gas can be neglected and the simplification of equation (2-26) [77]:

$$\sigma_{rr} = -p_{gas} \tag{2-27}$$

The change of the bubble radius with time is achieved with equating and transforming the tensions on the phase boundary (equation (2-26) and (2-27)) [63, 77]:

$$\boxed{\frac{dR}{dt} = \frac{R}{4\eta}\left(p_{gas} - p_{liquid} - \frac{2\sigma}{R}\right)} \tag{2-28}$$

To derive the second necessary differential equation for the change of the bubble pressure p_{gas} with time the mass transfer in the bubble is considered. Fick's laws of diffusion can be used under the assumption that only diffusion takes place and every molecule that diffuses to the bubble will enter the bubble [63, 64, 77, 78]. The material flow over the phase boundary is calculated with Fick's laws on the place $r=R$ (right side of equation (2-29)) and contains the diffusion coefficient *D* and the change of the gas concentration in the liquid *c* along the variable radius *r*. For the description of the changing amount of substance in the bubble the ideal gas law is used (left side of equation (2-29)) [63, 64, 76, 78]:

$$\frac{d}{dt}\left(\frac{4\pi R^3 p_{gas}}{3R_G T}\right) = 4\pi R^2 D\left.\frac{\partial c}{\partial r}\right|_{r=R} \tag{2-29}$$

R_G is the general gas constant and the T temperature in kelvin. The concentration profile on the phase boundary ($\frac{\partial c}{\partial r}$) can be described with neglecting the convection. The diffusion of gas through the liquid in radial direction is given in the following equation [77]:

$$\frac{\partial c}{\partial t} = D\left[\frac{1}{r^2}\frac{\partial}{\partial r}\left(r^2\frac{\partial c}{\partial r}\right)\right] \tag{2-30}$$

For simplification of the model HAN & YOO, SHAFI & FLUMERFELT and TAKI assume in each case different simple concentration profiles for the diffusion of gas through the liquid [63, 64, 78] instead of equation (2-30). This concentration profiles is assumed in a thin layer around the bubble with the thickness δ) [63, 76, 77]. Figure 2-17 shows exemplarily the assumed concentration profile of HAN and YOO in the layer around the bubble [78]. TAKI [63] found out that this concentration profile has the best agreement with experimental values. The calculation of HAN and YOO's concentration profile is given in the following equation (2-31) [78]:

$$\frac{c_\infty - c}{c_\infty - c_R} = \left(1 - \frac{r - R}{\delta}\right)^2 \tag{2-31}$$

c_∞ is the concentration of the dissolved gas outside of the boundary layer size δ. The concentration profile of HAN and YOO (equation (2-31)) is inserted in equation (2-29). After integration and transformation the differential equation for the change of bubble pressure with time results [63]:

$$\frac{dp_{gas}}{dt} = \frac{6DR_GT(c_\infty - c_R)}{-R^2 + \left(R^4 + \frac{2R}{R_GT}\left(\frac{p_{gas}R^3 - p_{gas,0}R_0^3}{c_\infty - c_R}\right)\right)^{1/2}} - 3\frac{p_{gas}}{R}\frac{dR}{dt} \tag{2-32}$$

The starting conditions for the simulation of a bubble can be calculated with Henry's law for the starting bubble pressure $p_{gas,0}$ (equation (2-33)) and with the Young-Laplace equation for the starting bubble radius R_0 ((2-34) [63]:

$$p_{gas,0} = \frac{c_0}{H_{1,2}} \tag{2-33}$$

$$R_0 = \frac{2\sigma_0}{\frac{c_0}{H_{1,2}} - p_0} \tag{2-34}$$

The presented model can simulate the growth process of a single bubble but also models with more than one bubble can be based on it (see chapter 2.5.2). For the simulation of foams with different bubble interaction this model is not suitable.

2.5.2 Multi Bubble Models

The single bubble model from chapter 2.5.1 was extended and modified by TAKI [63]. The resulting model can simulate more bubbles in the same way as for a single bubble. The calculation was divided into time intervals Δt_N and in each interval there was the opportunity to form new bubbles. Because of this the bubble nucleation rate J was implemented for the probability calculation for the formation of a bubble seed [65].

(2-35)

$$J = f_0 \cdot \left(\frac{2\sigma}{\frac{\pi M_W}{N_A}} \right)^{\frac{1}{2}} \cdot \exp\left(- \frac{16\pi\sigma^3 F}{3k_B T \left(\frac{\bar{c}}{H} - P \right)^2} \right) \cdot N_A \cdot \bar{c}$$

f_0 and F are fitting parameters, M_W is the molecular weight of the gas, N_A is the Avogadro constant, k_B is the Boltzmann constant and $\bar{c}$ the average concentration of the gas in the liquid. TAKI [63] assumed a constant gas concentration in the liquid far away from the bubble. The resulting average gas concentration in the liquid can be calculated for every time step with subtraction the gas in the bubbles from the starting concentration c_0 [63]:

$$\bar{c} = c_0 - \frac{1}{V_{L,0}} \cdot \sum_{i=1}^{n} \frac{4\pi}{3} R_i^3 \frac{p_{gas,i}}{R_G T} \tag{2-36}$$

$V_{L,0}$ is the liquid volume before the depressurisation, n is the number of the formed bubbles and $p_{gas,i}$ is the pressure in the bubble i. The detailed calculation schema of the multi bubble model from TAKI [63] is given in Figure 2-18:

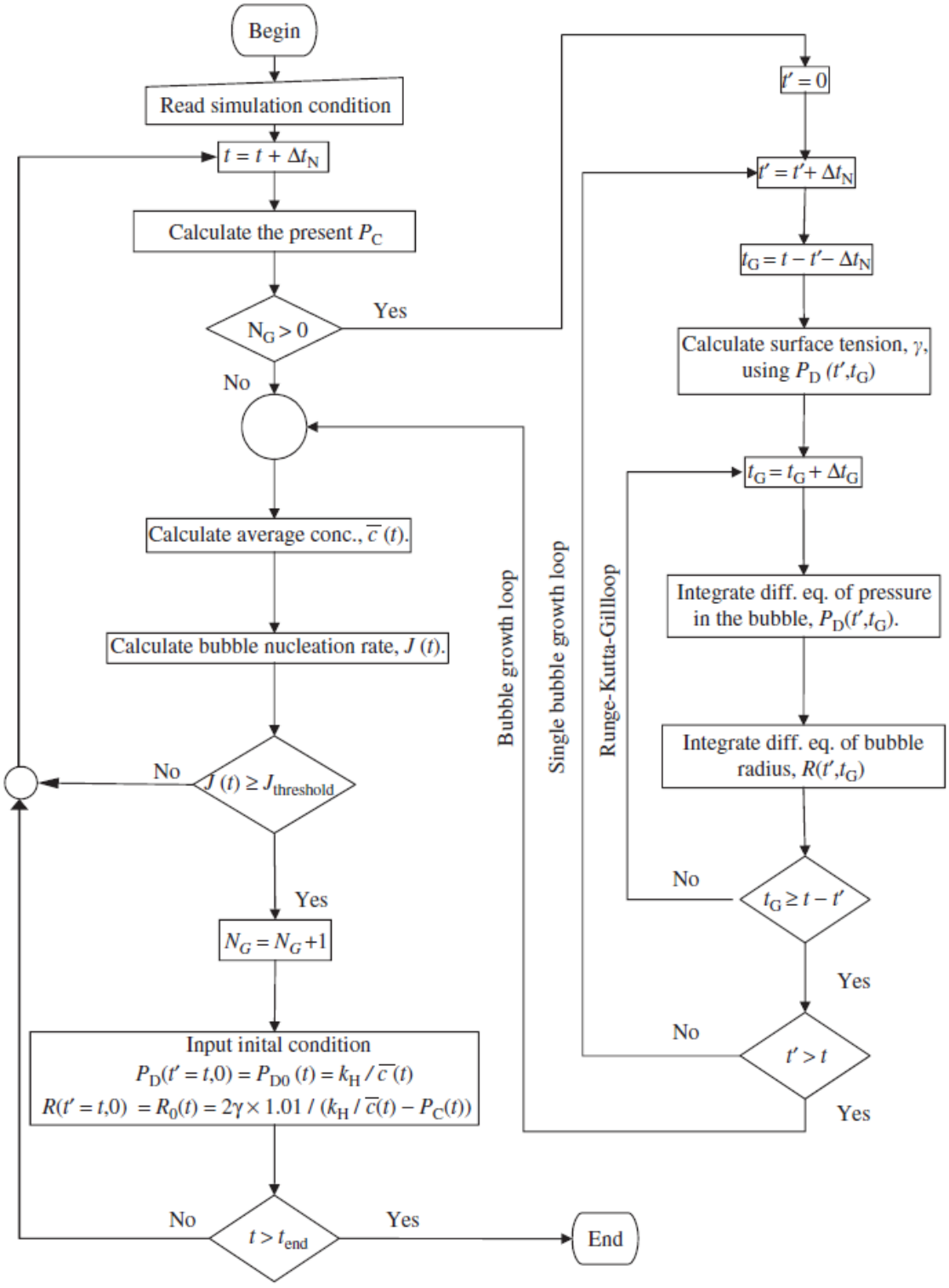

Figure 2-18: Simulation schema of the multi bubble model from TAKI [63]

Within one time interval, the growth of all existing bubbles was calculated with the differential equations (2-28) and (2-32) before a new bubble can be formed. For the newly formed bubble the starting pressure and starting radius are calculated with equation (2-33) (2-34) depending on the current values of the time interval ($\bar{c}$ and P) [63]. Also with this model no simulations of foams can be done because of the excluded interactions between the bubbles.

2.5.3 Foam Models

After explaining the modelling of a single bubble in this chapter the simulation of foams will be discussed. In literature some models for the calculation of polymer foams are known and summarised by THIES [66]. This models can be used for metal foams investigated by THIES [66] as well as aerated chocolate. The modelling approaches can be divided in three categories [66]: Modelling of equilibrium structures, modelling of drainage and modelling of foam expansion.

Modelling of equilibrium structures. Some models try to simulate the equilibrium structure of a foam under influence of bubble growth and rheology. The models belonging to this category describe the basic physical effects like gas diffusion and bubble wall movement in 2D or more complex in 3D [66, 83, 84]. KERMODE and WEAIRE [84] developed a two dimensional model for dry soap foams as shown in Figure 2-19:

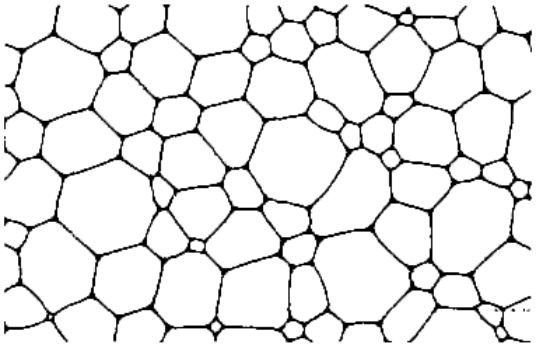

Figure 2-19: Simulation of a two dimensional foam structure by KERMODE and WEAIRE [84]

The structure showed in Figure 2-19 consists of non-overlapping polygons, called “cells” [85]. The contact points of the cells (cell corners) contain the whole liquid of the foam [86]. In the model from KERMODE and WEAIRE [84] for every cell corners a coordinate is determined as well as the pressure and the area of each cell. It is assumed, that every cell corner is like a circular arc that is depending on the inner pressure of the adjacent cells [84]. Furthermore only contact points of three cells are assumed as stabile [84]. BOLTON [86] assumed that gas diffusion occurs through the cell walls depending on the pressure difference of the cells. KERMODE and WEAIRE [84] develop the model further with the assumption that gas diffusion can also occur through the cell corners.

In addition equilibrium foam structures can be simulated with bubble-bubble-interaction models which include the interaction of a bubble with an adjacent bubble [66]. In this case the gas bubbles are calculated instead of the foam structure [87]. Every bubble has an equation of motion which contains the interaction between two bubbles as well as the influence of surface tension and viscosity [87].

Modelling of drainage. Another category of foam models regards the drainage in foams. Thereby the drainage of liquid in an existing foam for example due to weight force or capillary action is considered [66]. VERBIST et al. [85] developed a partial differential equation (“foam drainage equation”) which determines the liquid flow out of the cell corners due to weight force with the continuity equation and Darcy's Law.

BHAKTA and RUCKENSTEIN [88] developed a model for the drainage in standing foams in which the collapse and coalescence of bubbles in dependency of the liquid film radius is additionally included. The liquid film radius of a bubble will rupture and the bubble coalesce when the film is bigger than the maximum radius or smaller than the minimum radius [88]. It is assumed that the minimum radius increases with increasing number of coalesced bubbles and the maximum radius stays constant. Furthermore, liquid films with smaller radii show more drainage and rupture earlier [88].

Modelling of foam expansion. For this category of foam models it is assumed that the foam in the beginning of the calculation consists of spherical bubbles which are surrounded by a liquid layer with dissolved gas inside. This gas diffuses with time in the bubble and leads to expansion of the foam. The bubble growth can be considered as the being of different single bubbles because the interactions between the bubbles are neglected [66]. This kind of model will be often used for polymer foams and similar assumptions are made as for single bubble models [89, 90]. ORCUTT and CARPENTER [73] developed a model for bubble coalescence with constant volume (see equation (2-21) in chapter 2.4.4). ZÄHRINGER et al. [90] implemented the temperature and composition independent viscosity and diffusion. SCHWARTZ and ROY [91] described in detail the liquid film between the bubbles.

In addition to the mentioned models a foam can also be calculated with numerical flow simulation (CFD - Computational Fluid Dynamics) which are based on the continuity equation and the Navier-Stokes equations [66]. THIES [66] developed a model for the simulation of metal foams with propellant. He considers bubble growth, the liquid flow, drainage due to weight force and capillary action, surface tension effects, coalescence and collapse of bubbles and foam rheology. The model is based on diffusion, the ideal gas law and the Navier-Stokes equations and solved with the Lattice-Boltzmann method. Therefore the considered area is divided into grid cells and each cell is assigned to the gas phase, the liquid phase, the phase boundary between gas and liquid or the wall [66].

In conclusion it can be said, that in literature various foam and multi bubbles models for different systems are described. A foam model for the prediction of the high pressure aeration process of cocoa butter based systems including all important physical processes are not already existing.

3 Aims of the Work

The texture of aerated chocolate is a key driver for consumer preference and the need for differentiation through texture will gain even more importance in the future. The current state of the art is much too incomplete to allow a full understanding of the chocolate aeration process and due to this the control and prediction of the aeration process is difficult. This work should fill this gap. The aim of this project is to understand the physical processes underlying gas solubility and bubble formation, as well as to determine the process conditions leading to optimal bubble formation during aeration of chocolate masses and to find the most suitable process control for various dimensions of consumer preference. Therefore the high pressure aeration of chocolate is experimentally investigated with the aim to develop a kinetic model of bubble formation and coalescence.

To realise the investigation of a high pressure chocolate aeration process firstly it is necessary to create a suitable high pressure process plant enabling the aeration of chocolates at varying and adjustable process conditions like pressure, temperature, gas type, depressurisation rate, stirrer/mixing speed and crystallisation speed.

In chapter 2 (Fundamentals and State of the Art) it was shown that the composition of chocolate is varying for diverse chocolate types and that all ingredients have different properties. The influence of each component and the chocolate composition on the gas solubility and especially the foam structure of high pressure aerated chocolate (bubble size, bubble form and porosity) is currently not investigated extensively. One main element of this work is therefore the investigation of chocolate ingredient and composition effects on the gas solubility and foam structure.

The detailed determination of the influence of high pressure aeration process parameters, for example depressurisation speed or crystallisation speed, on the chocolate foam structure are also not yet investigated (see chapter 2). Also the effect of gas mixtures on the chocolate foam structure was currently not investigated. To reach the aims of this work therefore it is necessary to carry out all these experimental investigations of process parameters in the constructed high pressure process plant.

In literature various foam and multi bubbles models for different systems are described (see chapter 2). A foam model for the prediction of the high pressure aeration process of cocoa butter based systems including all important physical processes are not already existing. Due to this it is necessary to develop a new foam model for the prediction of bubble formation and growth especially for the

high pressure process with cocoa butter based systems and to determine the underlying physical properties. A sensitivity analysis as well as a validation of the model should also be carried oud.

In conclusion it can be said, that the influence of different process parameters and chocolate composition on the gas solubility and the final product foam structure should be determined experimentally for the high pressure aeration process. Additionally a model for the prediction of bubble formation and bubble growth for the high pressure aeration process should be developed and evaluated. These findings should further enable a better understanding and control of the chocolate aeration process to obtain the production of various aerated chocolate products with different texture and foam characteristic.

4 Materials and Experimental Methods

This chapter describes the materials and experimental methods used. The experimental setups, process plants and analytical instruments will be explained. The steps for the preparation of the materials, the manufacturing of the investigated chocolate samples will be discussed as well as the high pressure process for aeration. Additionally the analytical measurement of the samples and the error determination will be explained.

4.1 Materials

The materials used for this experimental investigations are listed in Table 4-1:

Table 4-1: Used materials for the experimental investigations

component	producer	specifications
milk chocolate	Nestlé Hamburg	see table Table 4-2
cocoa butter	ADM Cocoa B.V	
Icing sugar	Nordzucker	
cocoa powder, low de-oiled	Krüger GmbH & Co. KG	fat amount 22 wt%
cocoa powder, high de-oiled	Naturata	fat amount 10.66 wt%
milk powder	TSI GmbH & Co. KG	skim milk powder
lactose	Hafen-Mühlen-Werke GmbH	crystalline
lactose	TUHH – Institute of Solids Process Engineering and Particle Technology	spray dried
sucrose (saccharose)	TUHH – Institute of Solids Process Engineering and Particle Technology	spray dried
lecithin	Euro OTC Pharma GmbH	liquid
cocoa butter seeds		crystal structure V
carbon dioxide	Yara Deutschland	gaseous / solid (purity = 99.9 %) see Table 4-3
nitrogen	Westfalen	gaseous (purity = 99.999 %)

The composition of the used Nestlé produced milk chocolate is given in Table 4-2:

Table 4-2: Composition of the Nestlé milk chocolate (Nestlé factory Hamburg) with a listing of the fat content in the ingredients

material	amount [wt%]	amount of fat [wt%]
sugar	43.20	-
cocoa butter	21.03	21.03
cocoa liquor	15.88	8.41
skim milk powder	11.28	-
whey powder permeate	4.85	0.10
clarified butter	3.53	3.53
lecithin	0.43	0.42
vanilla flavour	0.02	
evaporation	-0.22	
total	100.00	33.47

Carbon dioxide was used in the gaseous and solid state (dry ice). Dry ice occurs on the sublimation point of carbon dioxide and has a temperature of -78.5 °C [92]. The most important substance data of carbon dioxide are given in Table 4-3 [93]:

Table 4-3: substance data of carbon dioxide [93]:

property	value
molar mass	$44.0098\ \mathrm{g \cdot mol^{-1}}$
density (20°C, 1bar)	$1.8152\ \mathrm{kg \cdot m^{-3}}$
density (40°C, 1bar)	$1.6975\ \mathrm{kg \cdot m^{-3}}$
density (20°C, 50bar)	$140.6\ \mathrm{kg \cdot m^{-3}}$
density (40°C, 50bar)	$113.1\ \mathrm{kg \cdot m^{-3}}$

4.2 High Pressure Autoclave

The aeration of cocoa butter and chocolate samples as well as the determination of the gas solubility (at equilibrium state) as well as the gas dissolution (not at equilibrium state) was done with the high pressure aeration process. Therefore a pressure resistant 1 litre reactor (autoclave) from the Hamburg University of Technology (Institute of thermal separation processes) was used. The schematic of the high pressure autoclave is given in Figure 4-1:

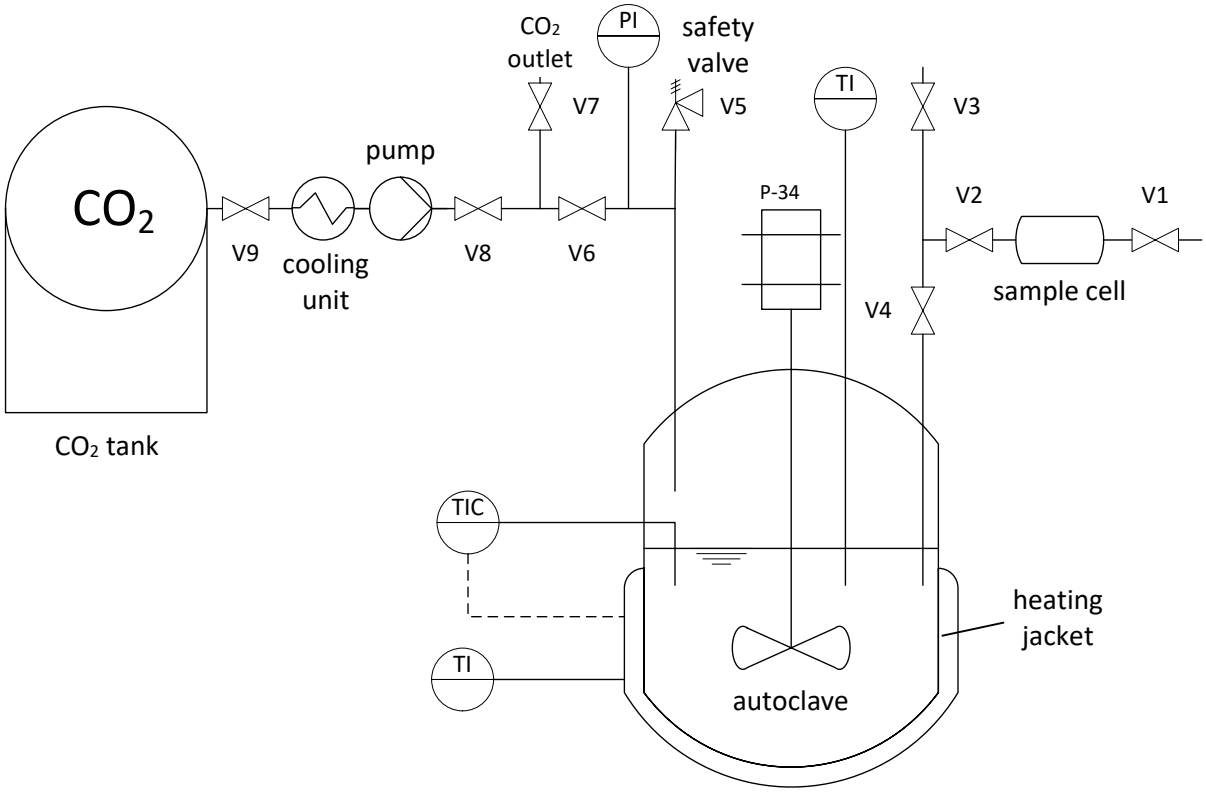

Figure 4-1: Schematic of the high pressure autoclave for the aeration of cocoa butter and chocolate mixtures and gas solubility measurements

The autoclave was manufactured by “Ernst Haage Apparatebau GmbH & Co. KG” and has a heating jacket with temperature regulation and a magnetically coupled stirrer for mixing. The temperature regulation was realised with a temperature sensor at the bottom of the autoclave and one temperature sensor in the sample inside the reactor. The reactor can be closed with a top cover in which the stirrer as well as inlet and outlet lines for the pressurisation and depressurisation are included.

The autoclave was filled with an approximately 500-750 ml sample (cocoa butter or chocolate mixtures), then the top cover was closed (the bolts tightened with a force of 100 Nm) and the desired process temperature was adjusted. All valves of the equipment were closed at that moment. After achieving the desired temperature the pressurisation takes place. Therefore valve V9, V8 and V6 were opened. The aeration with nitrogen was done with a gas cylinder connected with valve V9. For the aeration with carbon dioxide the gas out of the carbon dioxide tank with a pressure of around 55 bar was used. The gaseous carbon dioxide must be liquefied with a cooling unit so that the pump can compress the gas up to process pressures over 55 bar. For desired process pressures below 55 bar the valve V8 was used for reduction of the pressure. Valve V6 and V7 were used for releasing the gas and thus pressure regulation. With Valve V6, V8 and V9 the autoclave was separated from the gas supply

and valve V5 serves as a safety valve which automatically opens at 350 bar. The pressure in the autoclave was monitored with the pressure sensor PI.

The sampling of the high pressure aerated liquid phase was done through valve V3 (plus V4) or through valve V1 (plus V2 and V4). During the sampling the depressurisation takes place and the liquid phase forms a foam due to gas release (see chapter 2.4.1). The foam produced was stabilised by quick crystallisation in the freezer at -18 °C. The stabilised foam samples were analysed with micro-computer tomography to determine the foam structure (see chapter 4.4.4).

Besides regular sampling the depressurisation rate during the sampling was varied by controlling the outflow speed. Therefore the liquid phase was pressurised with carbon dioxide or nitrogen at 20 bar until equilibrium was reached. At these equilibrium conditions a regular sample was taken and the foam crystallised. Afterwards the process pressure was quickly increased to 50 bar and a sample of the liquid phase was quickly taken and crystallised. The higher pressure leads to a faster out flow speed of the liquid. No significant amount of additional gas is dissolved inside the liquid due to the very quick sampling after the pressure increase. The experiment was repeated with a fast pressure increase up to 75 bar, 100 bar, 125 bar and 150 bar.

For determination of the gas solubility (at equilibrium state) as well as the gas dissolution (not at equilibrium state) the sample cell with a volume of 20 ml was used. The sample cell was filled with the liquid phase at process conditions through valve V2 (plus V4). Afterwards V2 was closed to lock the sampling cell. The cell was detached from the equipment and gravimetrically analysed before and after depressurisation. In chapter 4.2.2 the gas solubility measuring method is explained in detail.

The high pressure aeration process was run at various temperatures between 30°C and 80°C but mostly at 40°C. The process pressures were adjusted from 20 bar up to 200 bar but mostly to 55 bar. Carbon dioxide, Nitrogen as well as a mixture of both gases was used for the aeration of the liquid phase. The composition and preparation of the different chocolate mixtures used for the aeration process will be explained in the following chapter.

4.2.1 Sample Preparation

This chapter is divided in three parts. At first the preparation of the raw materials is explained. Then the preparation of the chocolate mixtures for the aeration process is described and finally the different investigated mixtures are presented.

Raw material preparation. The chocolate raw materials milk powder, cocoa powder and sugar were treated in different ways to prepare them for chocolate production. The final chocolate mass could not be ground to reduce the particle size. Because of this the particle size of the solid components was reduced before mixing them with the cocoa butter. The maximum particle size of the particles for the production of the chocolate mixtures was adjusted to 63 µm. The particles were classified by sieving.

The skim milk powder was ground in an Ultra Centrifugal Mill from “Retsch”. Therefore the mill of the type ZM 200 with a cyclone, a rotation speed of 18000 revolutions per minute and a sieve with 0.12 mm trapezoidal perforations was used. The ground milk powder, collected with the cyclone was classified with a 63 µm sieve into coarse and fine particles. For the preparation of the chocolate only fine milk powder particles were used. Cocoa powder was also classified with a 63 µm sieve and only the fine particles were further processed to chocolate mixtures. Sieving of icing sugar was not possible due to agglomeration of the particles. Because of this the chocolate mixtures were produced with untreated icing sugar.

Additionally the icing sugar was classified using a air jet sieving process to investigate the influence of the sugar particle size on the aerated mixtures. A schematic of the air jet sieving process is shown in Figure 4-2:

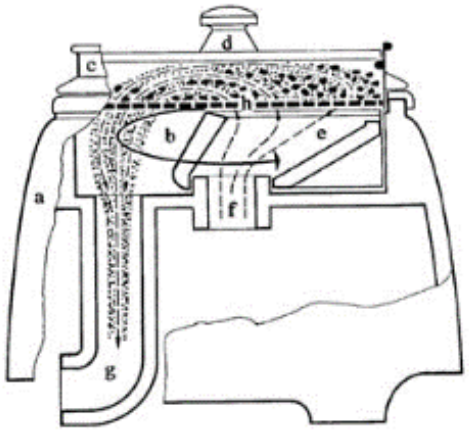

Figure 4-2: Scheme of the air jet sieving process [94]

The sieve (h) is perfused by a rotating air jet and the sieve chamber is protected by a top cover (d) [94]. A suction fan generates through the air outlet (g) a vacuum in the sieving chamber. Air is sucked in through the air intake (f) and guided on the sieve by the rotating nozzle (e). Swirling of the particles leads to a dispersion of the material and thus to a separation of agglomerated particles [94]. The fine material is leaded by the outgoing air jet to an attached cyclone and thus separated from the coarse material [94]. 25 µm and a 63 µm sieves are used to achieve two different sugar fractions: Particles with a diameter smaller than 25 µm and Particles with a diameter between 25 µm and 63 µm.

Chocolate mixture preparation. Solid cocoa butter was completely melted in a stove at 60°C for a minimum of 3 hours. Lecithin was added after weighing the required amount of cocoa butter. Afterwards the pre-treated particles (cocoa powder, milk powder and icing sugar) were weighed, mixed and added during stirring to the liquid cooled down to 40°C to prevent denaturation of the milk powder proteins. After adding the particles to the chocolate mixture, it was stirred for 20 minutes and heated to 40 °C to prevent crystallisation. Finally the chocolate mixture was stirred with a high speed stirrer for a better dispersion of the particles in the chocolate suspension. Some of the prepared chocolate samples were tempered before investigating them in the high pressure aeration process (for

details see below). The tempering was done to generate form V cocoa butter crystals (see chapter 2.2.3). Therefore the sample was melted during stirring and heated to 50°C. This leads to the destruction of all crystal seeds present. Afterwards the sample was cooled down in an iced water bath to 32°C whilst stirring. At this temperature the crystallisation of the cocoa butter in the sample begins. Then the sample was further cooled down until a temperature of 27°C was reached. Subsequently the sample was heated under stirring in a water bath up to 29 – 31 °C to melt the form III and IV crystals, leaving only form V. Finally the sample was completely cooled and crystallised in the fridge at 7°C or directly filled in the high pressure reactor for aeration.

Investigated Mixtures. For the determination of the influence of process pressure, process temperature, depressurisation rate as well as gas type, pure cocoa butter or a milk chocolate produced from the Nestlé factory Hamburg was used. The composition of this chocolate is given in Table 4-2 (chapter 4.1). This industrial produced chocolate consists of some other ingredients compared to those used for sample production at the Technical University Hamburg. For example Nestlé uses cocoa liquor compared to the cocoa powder / cocoa butter blend used by TUHH because no roll grinder was available for grinding the cocoa liquor. The Nestlé chocolate was conched and tempered which leads to different properties, in particular the final rheology and flavour profile.

In this work mixtures of cocoa butter and single particles as well as various chocolate mixtures were manufactured and investigated to determine the influence of the composition on foam structure and the gas solubility of the aerated chocolates. The following listed mixture compositions show the weight of the components taken (with the exception of Table 4-5). The cocoa powder used includes some cocoa butter as part of its structure and is therefore included as part of recipe calculation. When for example a cocoa butter amount of 27.8 wt% in the regular milk chocolate is targeted, it is necessary to weight only 26.3 wt% of pure cocoa butter because the low de-oiled cocoa powder includes the balance of this. The composition of the reference milk chocolate used for this study is given in Table 4-4. Three single particle mixtures were investigated to analyse the influence of each cocoa powder, sugar and milk powder on the foam structure and the gas solubility. Furthermore three chocolate types: milk chocolate, dark chocolate and white chocolate were produced, investigated and compared. The composition of the three investigated single particle mixtures as well as the composition of the three chocolate types is given in Table 4-4:

Table 4-4: Composition of the sugar, milk powder and cocoa powder rich mixture and the three chocolate types.*Using of low de-oiled cocoa powder with 22 wt% cocoa butter (net weight)

mixtures	cocoa butter [wt%]	sugar [wt%]	milk powder [wt%]	cocoa powder * [wt%]	Lecithin [wt%]
sugar rich	40.0	60.0	-	-	0.30
milk powder rich	40.0	-	60.0	-	0.30
cocoa powder rich	50.0	-	-	50.0	0.30
milk chocolate	26.3	47.9	18.5	7.0	0.30
dark chocolate	28.4	47.9	-	23.4	0.30
white chocolate	26.9	44.9	27.9	-	0.30

To investigate the influence of each chocolate component and the interactions between the components on the characteristic of high pressure aerated chocolate, a statistical design of experiments was used. With this model more than one parameter can be varied simultaneously [95] and thus the interactions between the different chocolate ingredients can be determined [95]. A detailed overview of the statistical design of experiment method used and evaluation of the results is given in chapter 5.1. The composition of the 25 chocolate mixtures calculated with statistical design of experiment is shown in Table 4-5:

Table 4-5: Composition of the 25 chocolate mixtures, calculated with the statistical design of experiments. Adjusted ranges: 50-100 wt% cocoa butter, 0-50 wt% sugar, 0-50 wt% milk powder, 0-50 wt% cocoa powder, 0-0.3 wt% lecithin. *Using of low de-oiled cocoa powder with 22 wt% cocoa butter, cocoa butter amount in the powder was added to the total cocoa butter amount in the mixture and subtracted from the total cocoa powder amount in the mixture

mixtures	cocoa butter* [wt%]	sugar [wt%]	milk powder [wt%]	cocoa powder (without cocoa butter)* [wt%]	lecithin [wt%]
1	64.4	8.9	11.9	14.8	-
2	83.9	0.8	3.7	11.5	0.13
3	50.3	-	3.1	46.5	0.10
4	50.3	2.5	13.3	33.8	0.07
5	64.3	18.2	0.1	17.1	0.30
6	86.4	7.2	6.5	-	-
7	67.0	0.2	-	32.9	-
8	50.9	41.6	5.5	1.7	0.30
9	98.8	1.0	-	-	0.17
10	69.6	-	30.1	-	0.31
11	85.6	0.4	2.6	11.0	0.30
12	50.0	-	26.1	23.7	0.22
13	50.2	-	37.3	12.2	0.30
14	50.0	-	49.7	-	0.30
15	52.2	-	47.8	-	-
16	64.3	18.2	0.1	17.1	0.30
17	50.0	20.8	28.4	0.7	0.15
18	50.0	22.3	-	27.4	0.30
19	74.4	14.2	5.6	5.8	-
20	59.9	30.8	-	9.3	0.03
21	83.9	0.8	3.7	11.5	0.13
22	50.3	-	3.1	46.5	0.10
23	59.9	30.8	-	9.3	0.02
24	50.9	47.1	2.1	-	-
25	50.0	20.8	28.4	0.7	0.15

This 25 mixtures was tempered before investigating them in the high pressure aeration process. Additionally to the investigated mixtures showed above, the influence of sugar on high pressure aerated chocolate was investigated in detail. Therefore at first three milk chocolates with different sugar amounts were produced and aerated. The compositions are given in Table 4-6:

Table 4-6: Composition of the milk chocolates with low, regular and high sugar amounts.*Using of low de-oiled cocoa powder with 22 wt% cocoa butter (net weight)

mixtures	cocoa butter [wt%]	sugar [wt%]	milk powder [wt%]	cocoa powder * [wt%]	Lecithin [wt%]
low sugar milk chocolate	30.5	35.7	24.3	9.2	0.30
regular milk chocolate	26.3	47.9	18.5	7.0	0.30
high sugar milk chocolate	30.9	54.3	10.5	4.0	0.30

Afterwards the influence of sugar particle size and form was investigated. Therefore the regular milk chocolate (Table 4-6) was produced using two sugar particles fractions classified with the air jet sieving process (explained above). The three milk chocolates were prepared with icing sugar, sugar particles with a diameter smaller than 25 µm and sugar particles with a diameter between 25 µm and 63 µm. These were then investigated and compared. Additionally spray dried sugar was used for the investigation of spherical sugar particles. The sugar was spray dried at the Institute of Solids Process Engineering and Particle Technology (SPE) at the Technical University Hamburg. The particles with a spherical particle shape were mixed with 50wt% cocoa butter and compared with regular milk chocolate prepared with crystalline sugar (Table 4-6) and a mixture of 40wt% cocoa butter and 60wt% crystalline sugar.

In addition to sugar the effect of cocoa powder was investigated. Therefore a regular milk chocolate (Table 4-6) was produced with highly de-fatted cocoa powder (10.66 wt% cocoa butter, see Table 4-1) and compared with regular milk chocolate mixed with weakly de-fatted cocoa powder. Furthermore a single particle mixture of 50 wt% cocoa butter, 50 wt% highly de-oiled cocoa powder and 0.3 wt% lecithin was compared with the weekly de-oiled cocoa powder mixture (see Table 4-4).

4.2.2 Gas Solubility

The gas solubility (at equilibrium state) as well as the gas dissolution (not at equilibrium state) in the fat based liquids was gravimetrically determined assuming the thermodynamic equilibria (see chapter 2.4.2). Therefore a sample cell consisting of a pipe and two valves was used (V1 and V2 in Figure 4-1). The stirrer in the autoclave was switched off for 5 minutes before sampling so that only liquid with dissolved gas and no mixture of gas and liquid enters the sample cell. The valves V1, V2 and V4 (see Figure 4-1) were carefully opened for a short time to purge the sample cell. After closing the valves V1, V2 and V4, the sample cell was removed from the autoclave. Therefore the valve V3 was first opened to depressurise the pipe between valve V2, V3 and V4, so that the sample cell with valve V1 and V2 can be screwed off. During sampling, the sample cell, pipes and valves are heated to prevent crystallisation of the cocoa butter. A flexible hose is added on one valve (V1 or V2) of the demounted sampling cell to collect the sample during expansion. Additionally the sample cell (with V1, V2 and hose) including the sample was weighed. Afterwards the valve on the hose was slowly opened to depressurise the sample. Then the cell was put in an oven at 80°C for around 30 - 150 minutes for liquefaction and outgassing of the sample. During this time the cell including the outgassing sample was weighed several times until the weight does not further decrease due to a completion of

outgassing. The amount of dissolved gas in the cocoa butter based sample can be determined with the measured weight of the sample cell before $m_{cell,sample}$ and after the completed depressurisation or rather outgassing $m_{cell,outgased}$. Therefore it is necessary to know the weight of the empty sample cell with the valves V1 and V2 and the attached hose $m_{cell,0}$. The gas solubility and gas dissolution was calculated with the following equations (4-1), (4-2) and (4-3):

$$gas\ solubility\ [wt\%] = \frac{m_{gas}}{m_{sample}} * 100 \quad = \frac{m_{gas}}{m_{liquid} + m_{gas}} * 100 \tag{4-1}$$

$$m_{gas} = m_{cell,sample} - m_{cell,outgased} \tag{4-2}$$

$$m_{sample} = m_{cell,sample} - m_{cell,0} \tag{4-3}$$

4.3 High Pressure Viewing Cell

In addition to the high pressure aeration process explained in chapter 4.2, a high pressure viewing cell was used for the aeration of low amounts of cocoa butter and Nestlé milk chocolate (Table 4-2). The influence of process pressure and depressurisation rate on the foam structure of aerated milk chocolate and cocoa butter was additionally investigated with this equipment. The high pressure viewing cell was also used for the optical determination of the melting range in a pressurised carbon dioxide atmosphere. Another method used for the melting range determination of cocoa butter based mixtures was the differential scanning calorimetry explained in chapter 4.5.2. The scheme of the high pressure viewing cell is given in Figure 4-3:

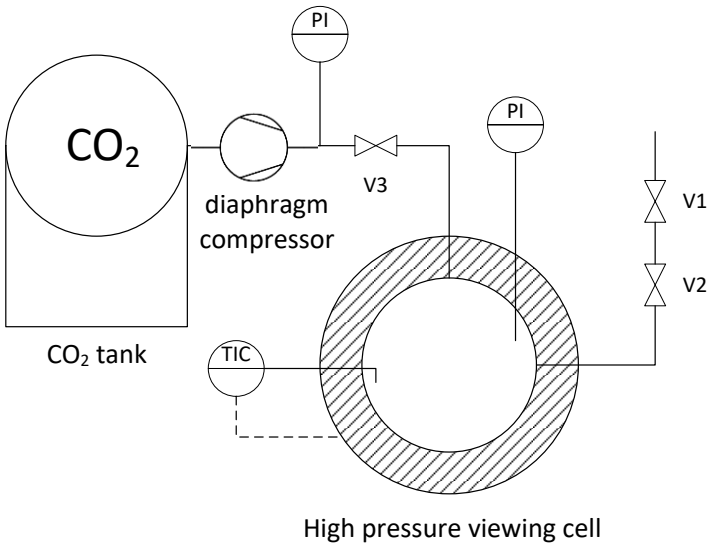

Figure 4-3: Schematic of the high pressure viewing cell

The viewing cell has a volume of 250 ml and two viewing windows for internal inspection. The temperature in the viewing cell can be adjusted with a heating jacket and a graphite ring was used for sealing. The investigated samples were melted and filled in a plastic cup (around 1 ml) and were placed in the tempered viewing cell. The autoclave was closed and the carbon dioxide was introduced into the viewing cell if necessary by using the diaphragm compressor until the desired pressure was reached. It was assumed that the gas was completely dissolved in the liquid or rather thermodynamic equilibrium was reached after 24 hours of constant pressure and temperature. After this time optical evaluation of melting was done or the samples were depressurised. Therefore the opening of valves V1 and V2 were varied opened to release the gas at different speeds. A hot air blower was used to heat the valves and prevent them from blockages due to dry ice formation. The aerated foam samples were additionally stabilised in a freezer.

4.4 Analysis

In this chapter the analytically methods for investigation of the particles, investigation of the foam structure of the aerated samples as well as measuring of other material properties such as viscosity are explained.

4.4.1 Particle Size Distribution

The size of the suspended particles is very important for chocolate production. Small particles (smaller than 40 µm) are necessary for a pleasant smooth mouth feeling so that the consumer cannot feel the single particles with their tongue [21]. The goal was to produce chocolates with similar properties to industrially produced chocolate. Therefore the particles of cocoa powder, sugar and milk powder used were ground and sieved to achieve smaller particle sizes (see chapter 4.2.1). For these treated particle fractions the particle size distribution was measured and compared with the industrially achieved particle size.

The measuring of the particle size distribution was done in a “Camsizer” from Retsch at the Institute of Solids Process Engineering and Particle Technology (SPE) of the Technical University Hamburg. The measurement was performed by means of compressed air (3 bar) to separate the particles. The sample volume of a maximum weight of 1g was transported by a feeding tray in the measuring field. Thereby compressed air atomizes the particles so that every individual particle can optically recorded by two digital cameras. The software of the measuring program calculates the particle size distribution from the camera pictures. Speed adjustments of the particles were made before measuring for prevention of particle overlap in the pictures.

Table 4-7: Adjusted parameter settings for the particle size distribution measurement of milk powder, cocoa powder and sugar with the Camsizer

parameter	adjusted settings
measuring range	1-300 µm
particle size classes	amount: 30, linear division, unit = µm
transport in the feeding tray	dispersion pressure = 50 , gap width = 4 mm
basis camera	ignores particles bigger than 100 mm
zoom camera	ignores particles bigger than 16 mm
both cameras	frame rate = 100%, step size for displaying = 50
end of measurement	after 150 blank fields
picture storage	rate = 1/200, minimum surface density = 0.2%
particle shape analysis	x_{Area}

The particle shape analysis parameter x_{Area} describes the diameter of a circle with the same surface like the measured projection surface of the particle A [96, 97]:

$$x_{Area} = \sqrt{\frac{4A}{\pi}} \tag{4-4}$$

The particle size distribution measurement of the air jet sieved sugar particles (see chapter 4.2.1) was done with a “Beckman Coulter Laser Diffraction Particle Size Analyser” also at the Institute of Solids Process Engineering and Particle Technology (SPE) of the Technical University Hamburg. The measurement was done in isopropanol to prevent dissolution in water.

4.4.2 Particle Structure

To investigate the shape and structure of cocoa powder, milk powder and sugar particles the scanning electron microscope Leo Gemini 1530 of the Technical University Hamburg was used. Therefore some particles of the sample were applied on the microscope object carrier. Afterwards the sample was coated with gold vapour to make it conductive and then measured in the microscope.

4.4.3 Moisture and Lipid Content

The determination of the lipid content of cocoa powder and milk powder as well as the measurement of the moisture content of cocoa powder, milk powder and sugar was carried out by the central lab of the Technical University Hamburg. The moisture was determined gravimetrically by means of drying and the lipid content with Soxhlet extraction.

4.4.4 Foam Structure

The bubble structure of the aerated foam samples was measured by using x-ray micro-computer tomography (µCT). The µCT 35 from Scanco Medical with a line-detector from the Institute of Biomechanics (Hamburg University of Technology) was used. A µCT is based on density measurements and it can visualise the density differences between the fat phase and the gas bubbles of the aerated

samples in a two- or three-dimensional range. With this method it is also possible to measure the porosity, specific surface area and the equivalent bubble diameter of the samples.

The foam samples were taken from the high pressure aeration process and stabilised in the freezer at -18°C (see chapter 4.2). Afterwards the sample was cut in a 1 cm^3 cube (approximately 1cmx1cmx1cm) to fit in the µCT measurement tube with a diameter of 20.5 mm and placed in the computer tomograph. The µCT was run with a voltage of 70 kVp, an amperage of 114 µA and an integration time of 300 ms or 459 ms. With the help of a first quick scan, a vertical two dimensional image of the sample was produced for the adjustment of a round measuring area in the middle of the sample. By doing this, the edges of the cube sample were ignored to exclude edge effects like cut bubbles, coalescence and bubbles rising. Additionally the threshold between the measured densities (gas phase and cocoa butter based phase) were adjusted between 19 and 40 depending on the measured sample. The µCT measurement of the sample was done in different slices with a thickness of 10 µm. Approximately 700 slices of the sample (2-D images) with a total height of 7 mm were joined by the software to generate a 3-D structure of the foam. In this calculation process the porosity, specific surface area and the total volume of the sample was also determined. The porosity ϕ is the ratio of the cavity volume V_{gas} (bubble volume = gas volume) to the total volume of the foam V_{total} [94]:

$$\phi = \frac{V_{gas}}{V_{total}} \tag{4-5}$$

The specific surface of the foam $S_{specific}$ is the relation of the total foam surface S_{total} to the total volume of the foam V_{total} [94]:

$$S_{specific} = \frac{S_{total}}{V_{total}} \tag{4-6}$$

The determination of the bubble size was carried out using different methods. One method was the implementation of an equivalent bubble diameter $d_{equivalent}$. Therefore the assumption was made that all bubbles has the same size and were spherical. The volume of the bubbles in the foam V_{gas} was calculated with the following equation (4-7):

$$V_{gas} = V_{total} - V_{solid} = \frac{1}{6}\pi d_{equivalent}^3 n_{bubbles} \tag{4-7}$$

The number of bubbles in the foam $n_{bubbles}$ was calculated with the total foam surface S_{total} :

$$S_{total} = \pi d_{equivalent}^2 n_{bubbles} \tag{4-8}$$

Through the combination of equations (4-7) and (4-8) the equivalent bubble diameter $d_{equivalent}$ can be calculated with the following equation (4-9) and the µCT measured parameter porosity, specific surface area and the total volume of the sample:

$$d_{equivalent} = \frac{6(V_{total} - V_{solid})}{S_{total}} \quad (4\text{-}9)$$

The equivalent bubble diameter is only an initial estimation and gives no information about the bubble size distribution because only a mean bubble diameter is determined. To obtain a bubble size distribution for the detailed evaluation of the foam structure a further analysis script of the µCT software was used. This script calculates makes a pore size analysis of the measured sample and out of it the bubble size distribution of the foam samples can be determined.

4.4.5 Viscosity

The measurement of the viscosity was done in the rotational viscometer "Kinexus Pro" from Malvern. The viscometer measures the viscosity of the liquid samples depending on the shear rate. Therefore the sample was sheared between a plate and a rotating cone. The cone was adjusted with a gap of 0.15 mm between the bottom plate and the cone. The dynamic viscosity was determined at constant rotation speed through measuring the resistance [42]. The measurement was carried out at atmospheric pressure and a temperature of 40 °C. The viscosity was determined for shear rates from 0.1 to 100 1/s.

4.5 Differential Scanning Calorimetry

This chapter explains the general functionality of the BT2.15 Differential Scanning Calorimeter (DSC). Afterwards the sample preparation, experimental procedure, settings for the determination of the melting range and the specific heat capacity as well as the experimental setup for measuring the heat transfer from the environment in the sample, is explained.

Heat is exchanged during all chemical reactions or physical material conversions (for example melting or vaporisation). Calorimetry is the measurement of the heat amount and can therefore be used for the description of reactions or material conversion [98].

Differential Scanning Calorimetry is a method for measuring the heat uptake or release of a sample compared to a reference. The reference sample is heated simultaneously as the sample under analysis with a constant heating rate α [98]. Phase transitions of the sample can be determined with the measured endothermic and exothermic reactions through measurement of temperature and time [99]. An endothermic reaction like melting or evaporation shows a high heat consumption of the sample compared to the reference and leads to a negative heat flow (Figure 4-4). In contrast, exothermic reactions, like crystallisation, exhibit a positive heat flow.

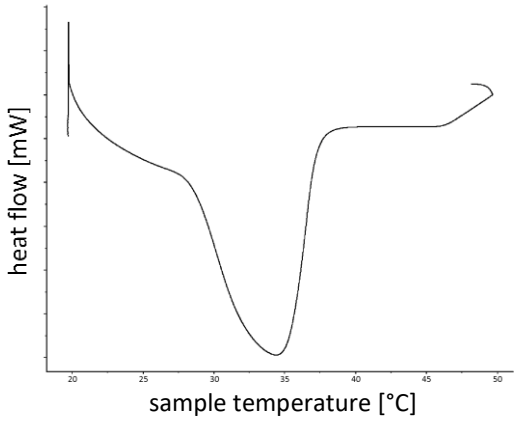

Figure 4-4: exemplarily DSC measured heat flow of a melting process

A blank measurement can be carried out before measuring the sample to determine the heat capacity by comparing both heat flows. For the Differential Scanning Calorimetry two DIN norms exist (DIN 51007 and DIN ISO EN 11357). In the standards the equipment and the calibration are detailed [100–103].

The equipment used during this study was the BT2.15 Differential Scanning Calorimeter from "SETARAM Instrumentation", which is a micro calorimeter for small sample amounts and low temperatures. Operating temperatures of -196°C up to 200°C can be reached with the help of liquid nitrogen or an electrical heating system [104]. Condensation can appear at low temperatures and distort the measurement. To prevent this, the calorimeter measurement block is placed in a cylindrical vacuum-sealed chamber with a controlled gaseous atmosphere (isolation chamber) [105]. The construction of the BT2.15 DSC used is given in Figure 4-5:

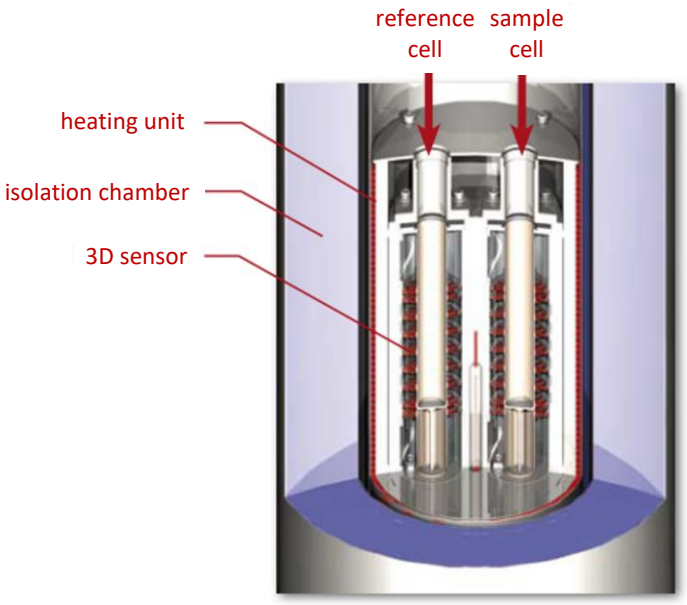

Figure 4-5: structure of the BT2.15 Differential Scanning Calorimeter [104]

The DSC used is a Tian-Calvet type calorimeter with two 3D Tian-Calvet sensors. A Tian-Calvet sensors is a thermopile that consists of a high amount of thermal elements (around 480 [106]) connected in series [107]. Each thermal element is in contact with the outside of the sample or reference [107]. A 3D sensor surrounds the whole sample or reference in the calorimeter block and this allows to measure the total heat including radiation, convection and heat conduction [108]. In contrast to this a 2D sensor measures only one layer of the sample. Due to the measurement using a 3D sensor, the results are independent of sample weight, form and structure (for example powder or liquid) as well as from the measuring cell type. The standard measuring cell of the DSC has a volume of 12.5 cm^3, a diameter of 1.5 cm and a height of 7 cm. This cell is constructed for temperatures of up to 220 °C and pressures up to 5 bar. The high pressure cell has a smaller volume of 3.6 cm^3 and allows temperatures up to 500 °C and pressures up to 600 bar. After calibration, the heat flow can be determined with the temperature difference between the sample (or reference) and the calorimeter block.

4.5.1 Sample Preparation

Cocoa butter as well as the Nestlé milk chocolate reference (see Table 4-2) were analysed using the DSC. Each sample was melted for 2 hours in a heating oven to destroy all crystal structures. Cocoa butter was melted at 85 °C and milk chocolate at 60 °C to prevent the denaturation of milk powder. BETZ [109] found that beta-lactoglobulin, a whey protein, denatures at temperatures above 60 °C. Afterwards the liquid sample was crystallised directly in the measuring cell of the DSC at different cooling temperatures and for different cooling times. In addition cocoa butter was measured without melting first and after tempering (see chapter 4.2.1). Furthermore some real chocolate samples and a high pressure aerated chocolate (see chapter 4.2) were analysed in the DSC to determine the melting range.

Both the standard cell and the high pressure cells were used for the DSC measurements. The standard cell was filled with 10g liquid cocoa butter, 7g solid cocoa butter powder or 15 g of liquid Nestlé milk chocolate. The low volume high pressure cell was filled with 1g liquid cocoa butter or milk chocolate. With the DSC the melting range of each sample was measured.

4.5.2 Melting Range

The DSC measures the heat flow of a sample (cocoa butter or chocolate) in comparison to the reference (air) during gradual heating. During heating and melting of cocoa butter or chocolate more energy is required compared to air due to different melting enthalpies. The melting range of the sample can be determined by plotting the necessary heat flow against the sample temperature.

A starting temperature (setting point) of around 20 °C on the DSC was adjusted with liquid nitrogen. The weight and the molar mass of the sample was entered in the software (850 g/mol for cocoa butter and chocolate). For determination of the melting range the sample was heated from 20°C to 50°C. The sample was melted during this heating process. The DSC heating rate α was varied between 0.01 K/min and 30 K/min. Before heating the temperature was kept constant for 3 hours at 20°C and after heating

the temperature was kept constant for 3 hours at 50°C. Afterwards the sample was cooled down to room temperature.

To investigate the influence of crystallisation temperature and time on the crystal structure of cocoa butter and chocolate, different cooling conditions of the liquid samples were used before analysis in the DSC. The cooling temperature was varied between -78.5°C and 6°C and the cooling time was varied between 30 minutes and 24 hours. Dry ice was used for cooling the sample down to -78.5°C. For cooling temperatures between -40°C and -20°C the liquid sample was crystallised in a freezer and for temperatures between -15°C and -5°C in a cryostat. A cooling temperature of 6°C was achieved by crystallisation in a fridge. Additionally a high pressure process aerated Nestlé milk chocolate (see chapter 4.2) was measured with the DSC to determine the melting range and the crystal structure. Therefore the chocolate was aerated with carbon dioxide at 20 bar and 130 bar and crystallised at -20°C for 24 hours before measuring in the DSC. The measurement of the heat transfer during the cooling is explained in chapter 4.5.4.

Additionally the change of melting range by pressurisation with carbon dioxide or nitrogen up to 80 bar was investigated. Therefore the high pressure DSC cell was used and pressurised with a pump. The measurement was started after a minimum dissolving time of 1 hour.

4.5.3 Specific Heat Capacity

For the determination of the specific heat capacity with the DSC a control measurement was carried out. This measurement was done with air in the reference cell as well in the sample cell. The following heat capacity measurement was done by heating cocoa butter or chocolate from 0°C up to 60°C. This allows the determination of the heat capacity for the solid and for the liquid sample phase. Before and after the heating process the temperature was again kept constant for 3 hours (at 0°C or rather 60°C). A heating rate of 0.1 K/min was used.

4.5.4 Heat Transfer in the DSC Sample Cell

The heat transfer from the environment to the sample is important for the determination of cooling temperature and cooling time on crystallisation (see chapter 4.5.2). This was done in a separate measurement setup. The DSC measurement cell was filled with liquid cocoa butter or chocolate (melted in an oven) like explained in chapter 4.5.1. Afterwards the sample was cooled with air at -39°C, -21.5°C or 4.5°C. A thermal element was placed in in the middle of the sample inside the cell to measure the temperature decrease during cooling. Therefore temperature loggers “OM-EL-USB-TC-LCD” from Omega Engineering Inc. were used. The measurements were done in triplicate to allow error estimation (see chapter 4.6). The experimental setup of the heat transfer measurement is given in Figure 4-6:

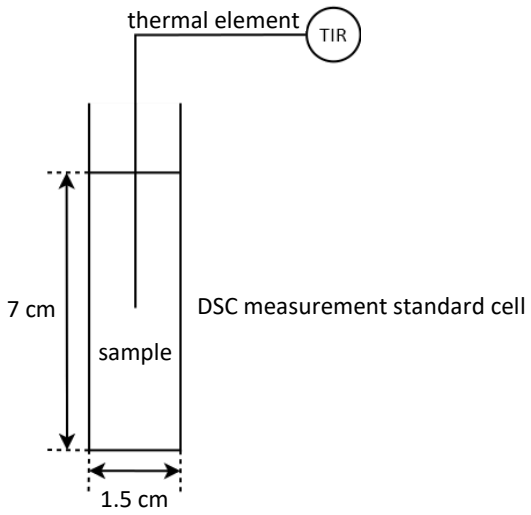

Figure 4-6: experimental setup of the heat transfer measurement in the DSC cell

4.6 Error calculation

The error calculation based on measurements repeated several times. The measurement of gas solubility, bubble structure and viscosity was done in duplicate to determine the error. Some viscosity measurements were repeated 10 times. The error was also determined for DSC measurements, for the tempering method due to cooling, the gas influence on the melting point as well as for the heat transfer and the specific heat capacity.

The average value $\bar{x}$ of the measurement values x_i for a number of n measurements was calculated with the following equation:

$$\bar{x} = \frac{1}{n}\sum_{i=1}^{n} x_i \tag{4-10}$$

The standard deviation s was calculated with the following equation:

$$s = \sqrt{\frac{\sum_{i=1}^{n}(x_i - \bar{x})^2}{n-1}} \tag{4-11}$$

The determination of the absolute error was done with Student t-distribution. This method gives a good estimation of the error for a small number of repetitions. The absolute error of the Student t-distribution was calculated with the Student t-factor $t_{P,n}$, the confidence interval P, the standard deviation s and the number n of repeated measurements:

$$absolute\ error = t_{P,n} * \frac{s}{\sqrt{n}} \tag{4-12}$$

For the calculation a confidence interval of P = 68.26% was used and this results in a Student t-factor of $t_{P,n} = t_{68.26\%,n=2} = 1.84$. For the viscosity measurements repeated 10 times a Student t-factor of $t_{P,n} = t_{68.26\%,n=10} = 1.06$ results. The error calculation of the model based experiments (statistical design of experiments) is explained in the following chapter.

5 Modelling Methods

In this chapter the statistical design of experiments used for the study and evaluation of results is explained. This model was used for the investigation into the influence of chocolate composition on the foam structure of aerated chocolate. The second part of this chapter explains the developed MATLAB foam model. This model predicts bubble formation and bubble growth during depressurisation of high pressure aerated cocoa butter considering spatial bubble formation, coalescence, bubble rising and change of material properties.

5.1 Statistical Design of Experiment

Experiments are often very complex especially if multiple parameters are investigated. A statistical experimental design model enables a more efficient design and evaluation of an experimental series. A statistical design of experiments was used for the investigation of high pressure aerated chocolate ingredients and composition on the foam structure, carbon dioxide solubility and other properties (see chapter 4.2.1). The experimental design and statistical evaluation was done with the program "Stat-Ease Design-Expert® 8.0.7.1". With this model more parameters can be varied simultaneously per experiment and therefore less experiments are necessary and the interactions between the single parameters can be investigated [95]. The single chocolate ingredients form a cocoa butter based mixture with different compositions depending on the type of chocolate. Due to this, the mixture design "IV-optimal" was used for modelling of the experimental design [95, 110]. To ensure acceptable processing properties of the mixtures a maximum particle content of 50% in the chocolates was set. The chosen limitations of each component amount in the calculated mixtures are given in Table 5-1. The sum of all components must be equal 100 wt%.

Table 5-1: Adjusted limits for each ingredient in the chocolate recipes used to generate the statistical design of experiments

ingredient	component amounts [wt%]
cocoa butter	50 - 100
icing sugar	0 - 50
milk powder	0 - 50
cocoa powder	0 - 50
lecithin	0 - 0.03

With this specifications an experimental plan including 25 different compositions was calculated (see Table 4-5). 15 calculated mixtures are necessary for the determination of the description model, 5 mixtures are necessary for the calculation of deviations due to adjustments of the experimental data on the model ("lack of fit") and 5 mixtures are duplicate measurements for the determination of the experimental error ("pure error") [110]. The sum of both errors (lack of fit and pure error) is called residual and it describes the deviation of the measured experimental data from the model [110]. All three errors were calculated with the summed quadratic differences of each data point to the mean value [95]. It was specified that the calculated cocoa butter amount includes the 22wt% cocoa butter amount of the weakly de-fatted cocoa powder and thus the calculations show the fat free cocoa powder amount.

Preliminary studies. Preliminary experiments at different pressure and temperature conditions were done to verify the feasibility of the experiments and to determine a suitable process temperature and pressure. For the first aeration tests mixtures of 66wt% sugar or rather milk powder with cocoa butter (0.2wt% lecithin) were used to estimate the effect of high viscosity and low gas solubility. Additionally a comparison of aerated mixtures with the aerated Nestlé chocolate was done to determine the transferability of the results to industrially produced chocolates.

Effect variables. The 25 different mixtures were aerated at constant pressure and temperature of 50 bar and 30°C. Effect variables for the modelling were chosen as follows: carbon dioxide solubility, foam porosity, equivalent bubble diameter of the foam, foam structure, specific surface of the foam, viscosity of the mixture and time until the equilibria is reached in the high pressure aeration process.

Statistical evaluation. The statistical evaluation is based on the regression of the measured experimental values and calculates an empirical description model [95]. For a linear model the model constants c_i und c_{ij} were fitted to the experimental data [95]:

$$y = c_0 + \sum_{i=1}^{n} c_i x_i + \sum_{i=1}^{n-1} \sum_{j=i+1}^{n} c_{ij} x_i x_j + \varepsilon \qquad (5\text{-}1)$$

The effect variable y was calculated with the total mean value c_0, the changeable parameters x_i and x_j ("factors") [95] and the residual error ε [111]. Equation (5-1) can be extended with quadratic terms and further interaction terms to achieve a quadratic model.

Performance indicators. A description model can be used when the model is significant (F-value < 0.0001) and the experimental data show a good agreement with the model (lack of fit is not significant, probability value > 0.1). Additionally it is necessary, that the scattering of adjusted data around the model mean value is similar to the predicted scattering (adjusted R-Squared similar to predicted R-Squared) and when the ratio of measured values to dispersion of measured values is big enough (Precision > 4) [110]. These performance indicators are calculated during the modelling to be verified by the user.

Accuracy of the model. An estimation of the model accuracy for mixture designs is only possible with a “Fraction of Paired Design Space (FPDS)” because there is a strong dependency between the single components [110]. Figure 5-1 shows the FPDS plot of the used linear and quadratic mixture models. The relative average error is the prediction accuracy deviation of pairwise data points and it is plotted against the factor space. The smallest error occurs in the middle of the investigated factor space (factor space = 0) and the highest error occurs at the limits of the measurement range (factor space = 1)

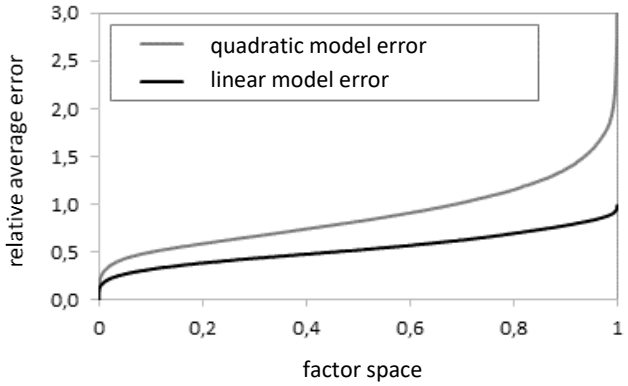

Figure 5-1: FPDS plot for the linear and quadratic mixture model

Figure 5-1 shows that the accuracy of the linear model is higher than of the quadratic model because the relative error is smaller. Furthermore it is clear to see that the prediction is much better in the middle of the factor space. For the calculation of the FPDS plot it was assumed, that the experimental standard deviation was 1 (confidential interval = 68.27, accepted measured values dispersion = 5%). The relative average error can be also plotted against the factor space by using a ternary triangle plot to show the interactions between three of five components. The amount of the not presented components in the diagram is constant. Figure 5-2 shows an exemplarily ternary triangle plots of the relative average error for the used linear and quadratic mixture model.

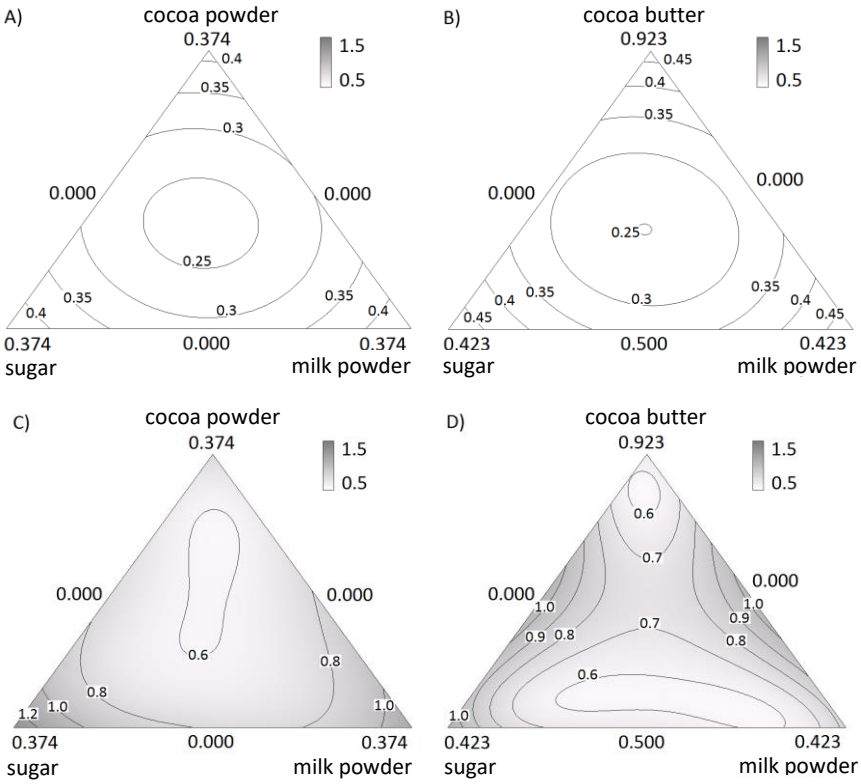

Figure 5-2: ternary triangle plot of the relative average error for the linear (A and B) and quadratic (C and D) mixture model; A and C: cocoa butter = 0.625wt%, lecithin = 0.001wt%; B and D: cocoa powder = 0.076wt%, lecithin = 0.001wt%

With these diagrams it is also clear to see that both model predictions are less accurate on the limits of the measurement range and much better in the middle of the factor space. Additionally it can be seen that the linear model is more precise than the quadratic one.

Control procedure. Control methods are necessary to ensure that the model is significant and can differentiate between measured value dispersion and real component effects [95]. To examine that the residual errors (deviation of the measured values from the predicted values) are independent of experiment order or rather time, they were plotted against the run order. No trend should be identifiable [95]. For the adjustment of the measured values to the model it is assumed, that the residuals are normal distributed. This was checked with the “Normal Plot of Residuals” (Figure 5-3 A). In this the measured values should lie on a straight line if the residuals are normally distributed [95, 110]. Additionally it is assumed, that all data point groups have the same variances (dispersion of the measured values). This was checked by plotting of residuals against predicted values (Figure 5-3 B). Again no trend should be identifiable [110]. Outliers of the data points can be determined with plotting the externally studentised residuals against the run order (Figure 5-3 C) [110]. The Box-Cox-Plot (Figure 5-3 D) shows whether a different model should be used for the prediction [95]. No model transformation is necessary if the calculated Lambda lies near the minimum of the plot and inside the confidence interval of 95% [110].

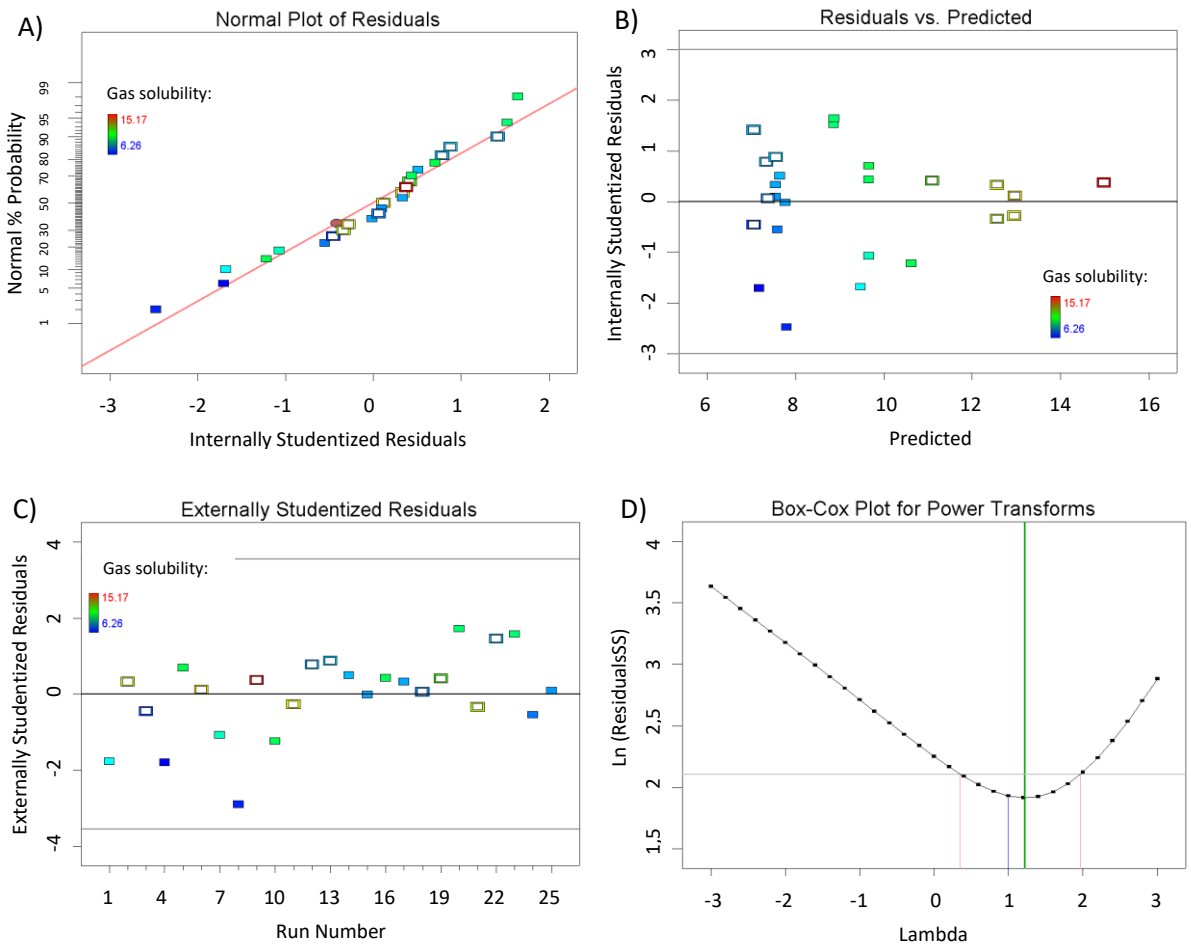

Figure 5-3: Exemplarily control plots for determination of the prediction accuracy of the used model, A) Normal Plot of Residuals, B) Residuals vs. Predicted, C) Externally Studentised Residual-Run Number Plot, D)Box-Cox Plot

5.2 Modelling of Foam Formation

In this work a model for the prediction of bubble formation and bubble growth during depressurisation was developed for high pressure aerated cocoa butter. This model considers the spatial bubble formation, the coalescence, bubbles rising and the change of material properties during the process. A simplification of the developed simulation is given in Figure 5-4 a schematic:

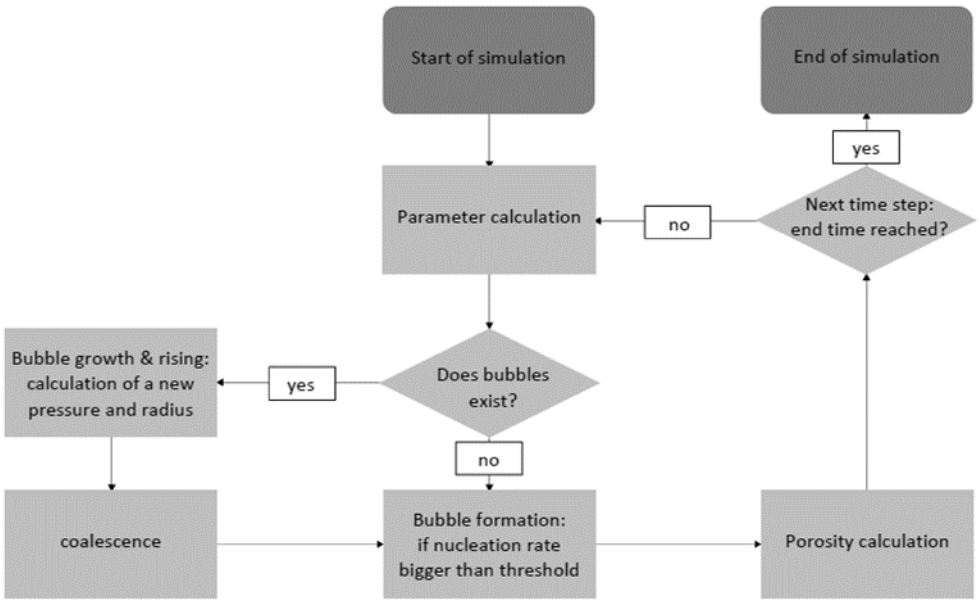

Figure 5-4: simplified signal flow diagram of the developed foam model

The simulation is divided in small time steps Δt_N for which in each case the conditions at that time were calculated. If no bubbles are existing they were formed if the nucleation rate was bigger than its threshold. Per time step, a maximum 10 new bubbles can be formed. For already existing bubbles the growth, rising and coalescence were calculated afterwards. Finally the foam porosity ϕ was determined for this time step. When the simulation end was not reached a new simulation cycle for the next time step starts over. The foam model was developed in MATLAB from MathWorks. The detailed signal flow diagram of the developed foam model is shown in Figure 8-6 in the appendix and a list of all used variables is given in Table 8-1 in the appendix.

5.2.1 Starting Conditions / Parameters

Before beginning the simulation the total simulation time t_{end} and the starting equilibria pressure p_0 at which the gas was dissolved was specified. The simulation time was varied from 1s to 20s and the starting pressure from 50bar to 70bar. The most commonly used standard modelling parameters were 2s simulation time and 58bar starting pressure. The time step size Δt_N was set at 0.005s in all simulations. The pressure after depressurisation p_{end} was fixed at 1bar ambient pressure and the saturation temperature T_0 *was* always set on 40°C.

The following assumptions described in chapter 2.5.1 were made for the modelling of the foam:

- The bubble is spherical at any time
- The bubble pressure at formation $p_{gas,0}$ can be calculated depending on average concentration $\bar{c}$ by using Henry's law (see equation (2-22))
- The diffusion coefficient *D* and the Henry constant *H* are constants
- The liquid is pure cocoa butter and a Newtonian fluid
- The gas behaves like an ideal gas

The single bubble model of Taki (chapter 2.5.1) [63] was extended by including different property changes during the foam formation. The change of viscosity was included, the weight force was take into account, the temperature change during depressurisation was included and the fluid was not defined as incompressible. Key material properties and process parameter necessary for the simulation are explained as follows:

1. **Density.** The density of cocoa butter saturated with dissolved carbon dioxide was used for determination of the initial carbon dioxide concentration in cocoa butter and for determination of the bubble ascend speed. The measured linear pressure influence on the density of carbon dioxide saturated cocoa butter by VENTER [11] (see Figure 2-13) was used for the simulation:

$$\rho_{CB,CO2} = 0{,}1491 \cdot p + 916{,}15 \tag{5-2}$$

The pressure *p* was used with the unit bar and the density $\rho_{CB,CO2}$ was received with the unit $\mathrm{kg \cdot m^{-3}}$. The bubble ascend speed was calculated with the help of the carbon dioxide density. Therefore equation (5-3) from the VDI Heat Atlas [93] usable for pressures up to 90 bar was used for a temperature of 40°C. The pressure *p* was again used with the unit bar and the density was received with the unit $\mathrm{kg \cdot m^{-3}}$:

$$\rho_{CO2} = 2 \cdot 10^{-8} p^6 - 3 \cdot 10^{-6} p^5 + 0{,}0003 p^4 - 0{,}0107 p^3 + 0{,}193 p^2 + 0{,}5 p + 1{,}5413 \tag{5-3}$$

2. **Gas solubility.** The gas solubility was also used for the determination of the initial carbon dioxide concentration in cocoa butter. The pressure influence on the carbon dioxide solubility in cocoa butter was experimentally determined in this work and used in this model:

$$x_{CO_2} = -0{,}0007 \cdot p^2 + 0{,}2696 \cdot p \tag{5-4}$$

The pressure *p* was used with the unit bar and the gas solubility x_{CO_2} was received with the unit wt%.

3. **Concentration.** For the calculation of the initial concentration c_0 $[\mathrm{mol \cdot m^{-3}}]$ a new equation was developed. Therefore equation (5-2) and (5-4) was used to include the influence of the initial pressure p_0:

$$c_0 = \frac{x_{CO_2} \cdot \rho_{KB,CO2}}{100 \cdot M_{CO2}} = \frac{-1{,}0437 \cdot 10^{-4} \cdot p^3 - 0{,}6011 \cdot p^2 + 246{,}994 \cdot p}{100 \cdot M_{CO2}} \tag{5-5}$$

The molecular weight of carbon dioxide M_{CO2} is 0.044 $\mathrm{kg \cdot mol^{-1}}$. The average concentration of carbon dioxide in cocoa butter $\bar{c}$ was calculated with equation (2-36).

4. **Surface tension.** The surface tension σ influences the initial bubble properties and the bubble growth. KOLLER [112] measured the influence of pressure on the surface tension of carbon dioxide saturated cocoa butter at 40°C. These results was used for the linear surface tension equation applied in the foam model:

$$\sigma = -2{,}693 \cdot 10^{-4} \cdot p + 2{,}854 \cdot 10^{-2} \tag{5-6}$$

The pressure p was again used with the unit bar and the surface tension was received with the unit $\mathrm{N} \cdot \mathrm{m}^{-1}$.

5. **Temperature.** The system temperature T_C was used for the nucleation rate calculation (equation (2-35)). The Temperature decreases during the depressurisation due to the Joule-Thomson effect. For the simulation an end temperature T_{end} of -5°C was assumed and a linear temperature decrease over simulation time t was estimated:

$$T_C = T_0 - \frac{T_0 - T_{end}}{t_{end}} t \tag{5-7}$$

6. **Dynamic viscosity.** The cocoa butter viscosity influences the bubble growth and the bubble ascend speed. The dynamic viscosity increases with decreasing temperatures (see chapter 2.3.1). VENTER [11] shows that there is an approximately linear dependency between viscosity and pressure up to 70 bar at 40°C (see chapter 2.4.3). With these results the initial cocoa butter viscosity η_0 for the simulation can be assumed with:

$$\eta_0 = -0{,}0005 \cdot p_0 + 0{,}0412 \tag{5-8}$$

The viscosity η_0 can be assumed as being constantly at 0.005 Pas for pressures above 70 bar [11].The dynamic viscosity for the end time of the simulation η_{end} at -5°C and 1 bar was estimated as 0.4 Pas using the experimental results from DHONSI [113]. The influence of simulation time t on the viscosity was assumed as linear, even though the temperature viscosity depends on temperature due to crystal formation:

$$\eta_C = \frac{\eta_{end} - \eta_0}{t_{end}} t + \eta_0 \tag{5-9}$$

7. **Diffusion coefficient.** The diffusion coefficient is important for bubble growth because this process is limited by diffusion. In the literature no data for the diffusion of carbon dioxide in cocoa butter is available. Due to this the diffusion coefficient for the simulated system was estimated as $D = 10^{-9} \frac{\mathrm{m}^2}{s}$ using the experimental data for carbon dioxide in rapeseed oil [114]. The diffusion coefficient was assumed to be constant because also the diffusion coefficient of the system carbon dioxide/ rapeseed oil does not significantly change with pressure ($D_{170bar} = 0.75 * 10^{-9} \frac{m^2}{s}$).

8. **Pressure.** The current system pressure p_C influences the surface tension, the nucleation rate and the bubble rising as well as the starting conditions of new formed bubbles (see chapter 5.2.2). For the depressurisation it was assumed, that the pressure firstly decreases by 2/3 of the initial pressure within the half of the simulation time. The remaining 1/3 overpressure falls linearly within the second half of simulation time. This was assumed regarding the experimental results of this work.

5.2.2 Spatial Bubble Nucleation

The bubble nucleation rate *J* was calculated for every simulation time step with equation (2-35). The needed fitting parameters was taken over from TAKI [63] and set to $f_0 = 3.5 \cdot 10^{-25}$ and $F = 0.5 \cdot 0.014085$. If the nucleation rate was bigger than the threshold $J_{threshold} = 0.01\ \mathrm{s}^{-1}$ [63] a maximum of 10 new bubbles were formed. The bubble formation time was stored in a variable and the starting bubble pressure $p_{gas,0}$ was calculated with the present average concentration $\bar{c}$ using Henry's law (equation (2-22)):

$$p_{gas,0} = \frac{\bar{c}}{H_{1,2}} \tag{5-10}$$

The Henry coefficient $H_{1,2}$ = 0.0005091 $\frac{mol}{Pa \cdot m^3}$ was determined by using the experimental carbon dioxide/cocoa butter solubility measurements at 40°C for this work (see chapter 6.2). Additionally an initial bubble radius R_0 was calculated for all newly formed bubbles with the Young - Laplace equation (equation (2-34)) by using the present average concentration $\bar{c}$, the present system pressure p_C and a factor of 1.5 to ensure numerical stability regarding the balance of forces:

$$R_0 = 1{,}5 \frac{2\sigma}{\frac{\bar{c}}{H_{1,2}} - p_C} \tag{5-11}$$

For the simulation a fixed cubic area with a volume of 1 cm³ was defined. In this considered space the spatial bubble formation was implemented. Therefore all new formed bubbles receive a random x-, y- and z-coordinate within the cubic volume:

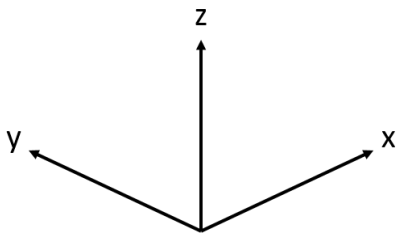

Figure 5-5: Defined coordinate system used for the spatial simulation of bubbles

This 3D coordinate system and the calculated radius of each bubble allows a spatial presentation of the foam at every simulation time step by using the "sphere function" in MATLAB.

5.2.3 Bubble Size Distribution

A calculation of the bubble size distribution and a corresponding plotting of the gas volume against the bubble radius was implemented in the simulation for every time step. Therefore the bubble radii was divided into 0.025 mm steps and the gas volume of all bubbles with the same radius classification was summed. Out of this a bar diagram for the bubble size distribution was plotted:

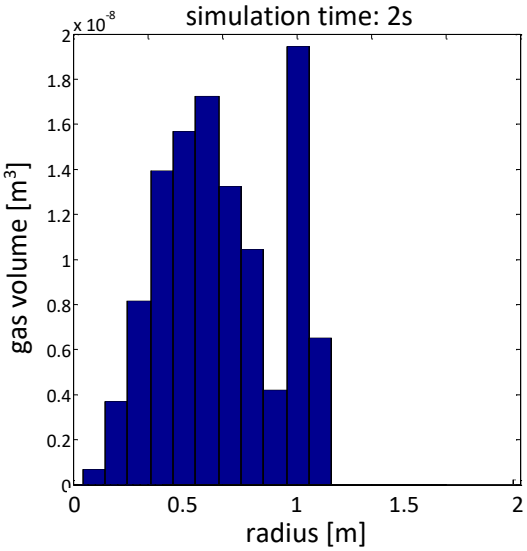

Figure 5-6: Exemplarily bar diagram for the bubble size distribution in the simulated foam

5.2.4 Bubble Rising

Taking into account the experiments of this work it was assumed that the bubbles rise and leak from the considered cubic simulation space until cocoa butter is in the liquid state. The bubble rising was calculated with Stokes law (equation (2-20)) (see chapter 2.4.4). The used liquid density ρ_{liquid} was the density of carbon dioxide saturated cocoa butter $\rho_{CB,CO2}$ (equation (5-2)) and the used gas density ρ_{gas} was the carbon dioxide density ρ_{CO2} calculated with equation (5-3). For the simulation necessary viscosity was determined with equation (5-9). The simulated bubble ascent happened only in the z-direction. Therefore each bubble gets a new z-coordinate depending on its ascent speed in every simulation time step. The outgassing of the bubbles from the simulated system was also only considered in the z-direction. A bubble was declared as “outgassed” if the bubble plus the half of its radius was located outside of the considered simulation space. The outgassed bubble volume was not considered in further simulation steps for example for calculation of foam porosity.

5.2.5 Coalescence

The coalescence of bubbles was also implemented in the foam model. The distances between the bubbles was determined pairwise by using the bubble coordinates. Coalescence was assumed for distances smaller than the sum of both bubble radii plus a boundary layer size δ of $2 \cdot 10^{-5}\mathrm{m}$. The value was freely selected. These boundary layers represent the coalescence resistance of the bubbles which

needs to be overcome. Due to this it is not enough that the bubbles touch each other, they must overlap to allow coalescence in the simulation.

The newly coalesced bubble has a new bubble pressure and radius. For the simulation of these parameters different methods were tested. Only one parameters must be calculated and the other one was concluded by using the ideal gas law:

$$R_{coal} = \frac{p_{gas,1}R_1^3 + p_{gas,2}R_2^3}{p_{gas,coal}} \tag{5-12}$$

$$p_{gas,coal} = \frac{p_{gas,1}R_1^3 + p_{gas,2}R_2^3}{R_{coal}} \tag{5-13}$$

The indices 1 and 2 represent both coalesced bubbles. The different coalescence calculation methods used are explained below:

Method 1: Bubble pressure as in the case of bubble formation

In this method the bubble pressure of the newly formed bubble due to coalescence was calculated using Henry's law (equation (5-10)). The corresponding bubble radius was calculated with equation (5-12).

Method 2: Implementation of a growth rate

In this method the growth per time step of both coalescing bubbles was determined and rated by the gas mole content. Therefore the mole content was calculated for both bubbles *i* with the ideal gas law:

$$n_i = \frac{\frac{4}{3}\pi \cdot R_i^3 \cdot p_{gas,i}}{R_G \cdot T_0} \tag{5-14}$$

Therefore the simulation starting temperature was used. Otherwise a gas mole change in the bubble takes place only due to temperature change. The growth rate for the newly formed bubble was calculated with the radii of both coalesced bubbles in the previous time step $R_{old,i}$:

$$grad = \sum_{i=1}^{2} \frac{R_i - R_{old,i}}{\Delta t_N} \cdot \frac{n_i}{n_1 + n_2} \tag{5-15}$$

The new bubble pressure was then calculated with equation (2-28) by assuming $\frac{dR}{dt} = grad$ and neglecting any further radius dependency:

$$p_{gas,koal} = 4\eta \cdot grad + p_C + 2\sigma \tag{5-16}$$

The corresponding bubble radius was again calculated with equation (5-12).

Method 3: Bubble pressure equal to environmental pressure

In this method the pressure of the new formed bubble was put on a level with the present system pressure p_c. The corresponding bubble radius was again calculated with equation (5-12).

Method 4: Assumption of a constant volume

With the assumption of a constant gas volume during coalescence the new bubble radius can be calculated with equation (2-21). The new bubble pressure was calculated with equation (2-32) depending on the new bubble radius.

- **Additional option: Maximum bubble radius**
  Additionally to the 4 presented methods a maximal bubble radius R_{max} was implemented for the simulation of coalescence. From this radius R_{max} the bubble could only rise and outgas but it was not allowed to coalesce or grow further. This additional option was tested in the foam simulation with the coalescence method 4.

The source code of the foam model is given in the appendix. The code includes all 4 presented methods and the additional option for method 4. They are marked in the code. Furthermore the allocation of the MATLAB code variables to the variables used in the test with the corresponding values or calculation equation is given in the appendix.

6 Results and Discussion

The aim of this work is to understand the physical processes underlying gas solubility and bubble formation, as well as to determine the process conditions leading to optimal bubble formation during aeration of chocolate masses and to find the most suitable process control for various dimensions of consumer preference. Therefore the high pressure aeration of chocolate is experimentally investigated with the aim to develop a kinetic model of bubble formation and coalescence. In this chapter the results of the experimental work and the model prediction are presented and discussed.

In chapter 2 it was shown that the composition of chocolate is varying for diverse chocolate types and that all ingredients has different properties. The influence of each component and the chocolate composition on the gas solubility and especially the foam structure of high pressure aerated chocolate is currently not investigated extensively. One main element of this work is therefore the investigation of chocolate ingredient and composition effects on the gas solubility and foam structure. At first the characterisation of the used ingredients is given in this chapter (chapter 6.1). To realise the investigation of a high pressure chocolate aeration process firstly it was necessary to create a suitable high pressure process plant enabling the aeration of chocolates at varying and adjustable process conditions. This high pressure aeration process of chocolate was experimentally investigated in detail. Therefore the influence of different process parameters (chapter 6.2) and the influence of chocolate composition (6.3) on the gas solubility and the final product foam structure are experimentally determined for the high pressure aeration process. Additionally an alternative method for the tempering of high pressure aerated chocolate is identified and evaluated (chapter 6.4).

In literature various foam and multi bubbles models for different systems are described (see chapter 2). A foam model for the prediction of the high pressure aeration process of cocoa butter based systems including all important physical processes are not already existing. Due to this it was necessary to develop a new foam model for the prediction of bubble formation and growth especially for the high pressure process with cocoa butter based systems and to determine the underlying physical properties. The developed MATLAB Model for the prediction of bubble formation and bubble growth for the high pressure aeration process is presented and evaluated in chapter 6.5.

6.1 Characterisation of the Ingredients

In the following chapters the measured size, structure and properties of the chocolate ingredients used will be discussed. The particle size distribution (chapter 6.1.1) was measured for the solid substances and their particle structure was evaluated with an electron microscope (chapter 6.1.2). Finally the moisture and lipid content of the particles (chapter 6.1.3) is discussed.

6.1.1 Particle Size Distribution

The particle size distribution was measured for the chocolate ingredients used, as described in chapter 4.4.1. This was done to determine if the chocolate produced during this work (see chapter 4.2.1) is comparable with that manufactured industrially. It was therefore necessary that the majority of suspended particles should have a particle size below 40 µm to ensure the right mouth feeling of the chocolate [24]. The particle size distribution was measured for both untreated, sieved or ground and sieved particles. Figure 6-1 shows the particle size distribution for milk powder (A) and cocoa powder (B) in the untreated and treated form (milled and sieved or only sieved):

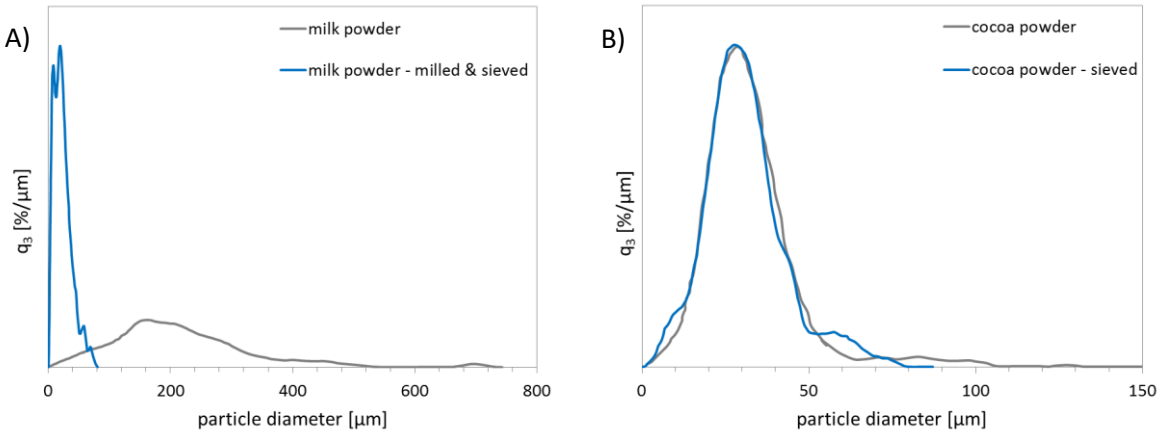

Figure 6-1: Particle size distribution of A) untreated and treated milk powder and B) untreated and treated cocoa powder

In Figure 6-1 it is clear to see that milling and sieving of the large milk powder particles (up to 700 µm) leads to a very significant particle size reduction to below 80 µm. The largest proportion of untreated cocoa powder particles was smaller than 50 µm. The additional sieving of cocoa powder with a 63 µm mesh leads to a reduction in the number of bigger particles above 50 µm. Figure 6-1 shows that the sieved cocoa powder consists of particles smaller than 80 µm. In conclusion, the treatments of both powders has a positive effect in terms of overall particle size distribution. Figure 6-2 shows the cumulative particle size distribution (A) and the particle size distribution (B) for sugar powder, treated milk powder (ground and sieved) and treated cocoa powder (sieved):

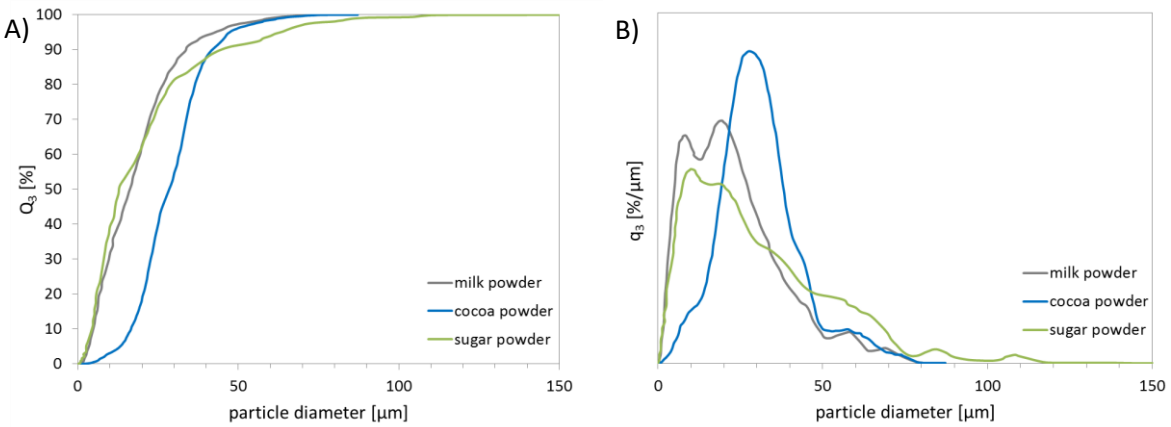

Figure 6-2: Comparison of sugar powder, treated milk powder and treated cocoa powder; A) cumulative particle size distribution; B) particle size distribution

Table 6-1 shows three characteristic values from the cumulative particle size distribution curve ($x_{Q3=10\%}$, $x_{Q3=50\%}$, $x_{Q3=90\%}$) measured for icing sugar, treated cocoa powder and treated milk powder. These values provide information on the biggest particle size diameter of the of the smallest 10%, 50% or 90% particles.

Table 6-1: Particle sizes of sugar powder, treated milk powder and treated cocoa powder (error calculation with triple measurements)

particle diameter x_{Q3} [µm]	milk powder	cocoa powder	sugar powder
$x_{Q3=10\%}$	6.27 ± 0.12	17.4 ± 0.1	7.08 ± 0.08
$x_{Q3=50\%}$	20.1 ± 0.3	29.4 ± 0.2	27.0 ± 0.6
$x_{Q3=90\%}$	43.1 ± 1.1	46.1 ± 0.5	73.4 ± 5.7

In Figure 6-2 and Table 6-1 it is clear to see, that icing sugar (sugar powder) has almost the desired particle size distribution. Treatment of sugar using regular sieving was not possible due to agglomeration. Due to this icing sugar was used in the untreated form for further chocolate manufacturing. Additionally it was shown, that the half of the particles were smaller than the maximum 30 µm and 90% of the particles were smaller than 46 µm (respectively 74 µm for sugar). Figure 6-3 shows the particle size distribution of the particles compared to that of industrially produced chocolate [33]:

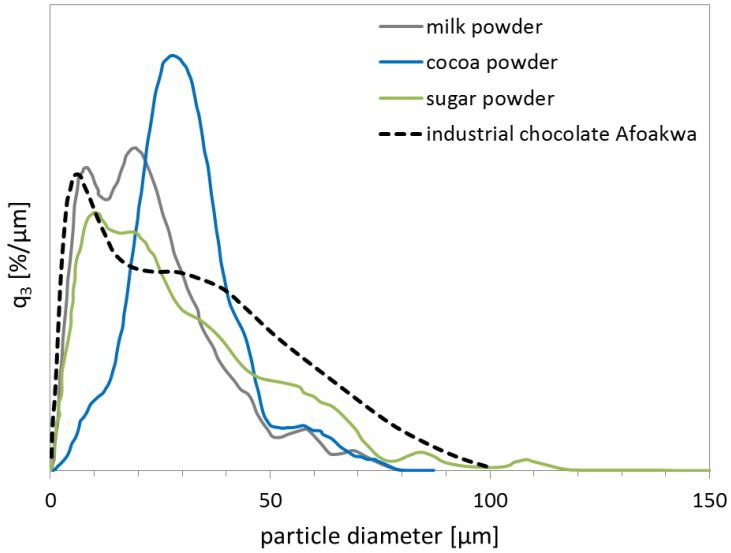

Figure 6-3: Comparison of particle size distribution for sugar powder, treated milk powder, treated cocoa powder and industrial produced chocolate [33]

It can be noted that treated milk powder, treated cocoa powder and untreated icing sugar can be used for chocolate manufacture because the particles sizes are very similar to those obtained during industrial production of chocolate.

Additionally the icing sugar was sieved using an air jet sieving process (chapter 4.2.1) to obtain two different sugar fractions with particle diameters of d<25µm and 25µm<d<63µm. This was done for the investigation of the influence of particle size on the foam structure of aerated chocolate. The efficiency of separation is shown in Figure 6-4 with the particle size distribution comparisons of untreated sugar with received air jet sieved sugar fractions.

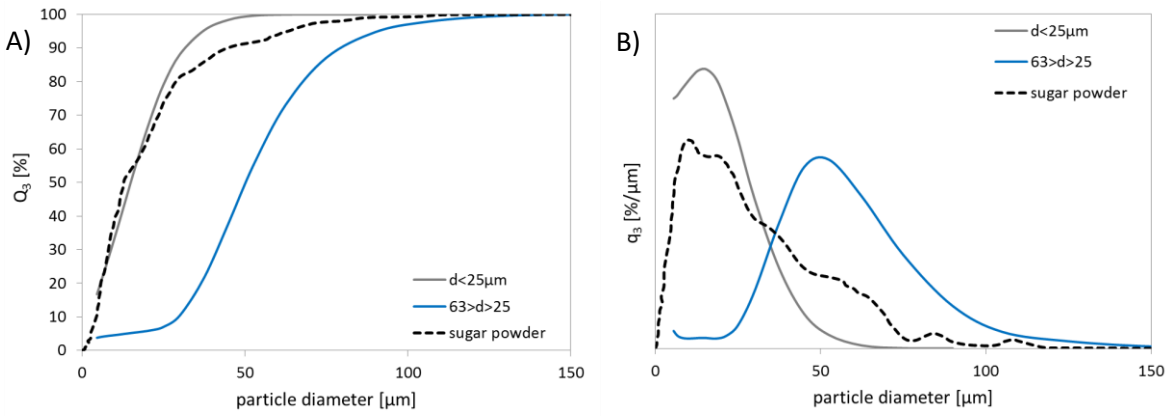

Figure 6-4: Comparison of untreated sugar powder with air jet sieved sugar powder (d<25µm and 63µm>d>25µm); A) cumulative particle size distribution; B) particle size distribution

The air jet sieved sugar particles show good separation of both fractions. The untreated icing sugar has a wider range of particle sizes. Table 6-2 shows the $x_{Q3=10\%}$, $x_{Q3=50\%}$ and $x_{Q3=90\%}$ values for icing sugar and both sieved fractions.

Table 6-2: Particle sizes of untreated sugar powder with air jet sieved sugar powder (d<25µm and 63µm>d>25µm); error calculation with double measurements

particle diameter x_{Q3} [µm]	d < 25 µm	63µm > d > 25µm	sugar powder
$x_{Q3=10\%}$	2.43 ± 0.17	29.5 ± 0.3	7.08 ± 0.08
$x_{Q3=50\%}$	14.9 ± 1.1	50.3 ± 0.3	27.0 ± 0.6
$x_{Q3=90\%}$	31.5 ± 1.3	79.2 ± 0.5	73.4 ± 5.7

Figure 6-4 and Table 6-2 show that the air jet sieved sugar fraction also has some bigger and smaller particles in addition to the adjusted fraction. The reason for this could be for example agglomeration. The d<25µm fraction corresponds to 75% of particles being smaller than 25µm and the 25µm<d<63µm fraction consists of 65% of particles with the adjusted size. In conclusion the fractionation of icing sugar with air jet sieving was considered successful for further investigations. Finally the particle size distribution of spray dried sugar (sucrose) was compared with the particle size distribution of regular sugar powder (crystalline sucrose) as shown in Figure 6-5 and Table 6-3:

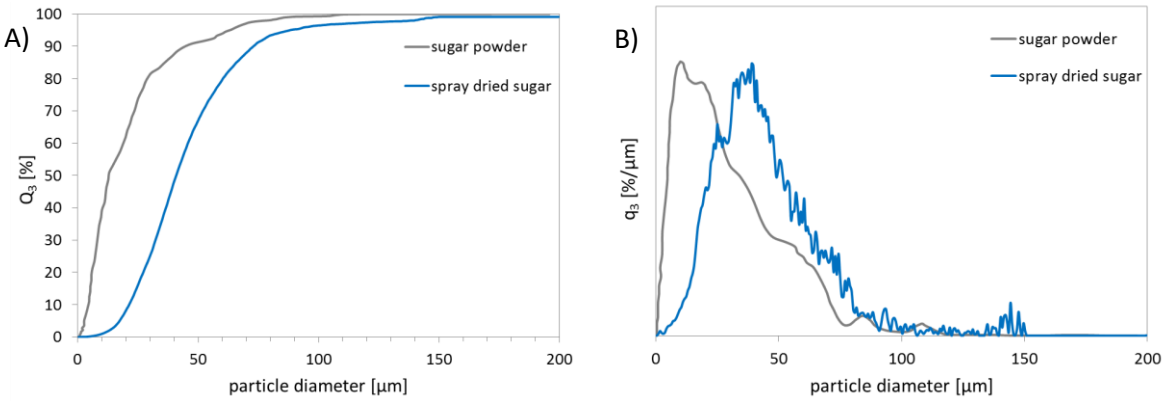

Figure 6-5: Comparison of crystalline sucrose sugar powder and spray dried sucrose sugar powder; A) cumulative particle size distribution; B) particle size distribution

Table 6-3: Particle sizes of crystalline sucrose sugar powder and spray dried sucrose sugar; error calculation with fourfold measurements

particle diameter x_{Q3} [µm]	spray dried sugar	sugar powder
$x_{Q3=10\%}$	21.6 ± 0.2	7.08 ± 0.08
$x_{Q3=50\%}$	41.2 ± 0.3	27.0 ± 0.6
$x_{Q3=90\%}$	73.4 ± 0.3	73.4 ± 5.7

The spray dried sugar has slightly more small ($x_{Q3=10\%}$) and medium ($x_{Q3=50\%}$) sized particles compared to the crystalline sample. But 90% of both sugar sample particles are smaller than around 74 µm and therefore in a good range for the production of chocolate.

6.1.2 Particle Structure

In this chapter the particle structure of cocoa powder, milk powder and icing sugar is discussed. The different particles were measured with electron microscopy (see chapter 4.4.2). Figure 6-6 shows the electron microscopy pictures of treated and untreated particles used.

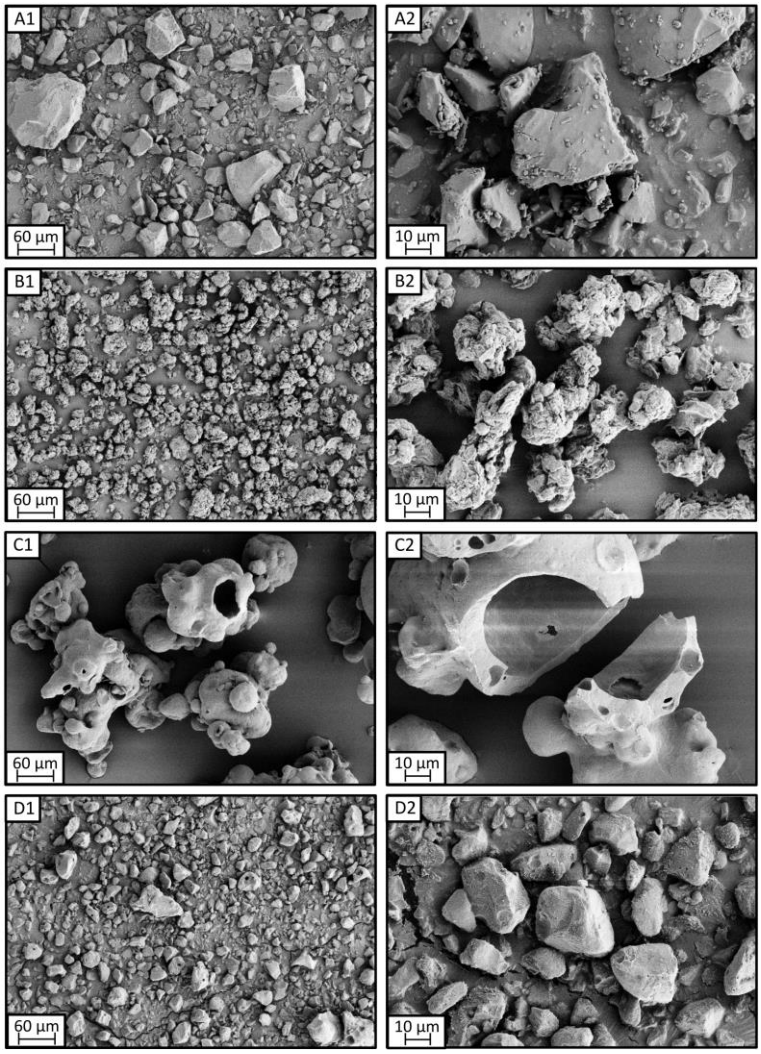

Figure 6-6: Particle structure of (A) sugar powder, (B) sieved cocoa powder, (C) milk powder, (D) milled and sieved milk powder; (1) 500x magnification, (2) 2000 x magnification

In Figure 6-6 (A) it is clear to see, that the particles of the icing sugar used has sharp edges and flat surfaces. It is also interesting to note the wider range of particle sizes present compared to the other measured particles resulting from the fact that no pre-treatment (sieving) was carried out. Cocoa powder has an irregular porous or rather sponge like structure (Figure 6-6 B). The untreated spray dried milk powder particles show a ball-like structure of different sizes which are partially hollow inside and adhere together (Figure 6-6 C). The milling of milk powders breaks up the agglomerates as well as the ball structure itself (Figure 6-6 D). The broken edges of the milk powder are relatively smooth and it is clear to see that small gas bubbles are trapped inside the milk powder particles. Additionally the air jet sieved sugar particles (chapter 4.2.1, $d<25\mu m$ and $25\mu m<d<63\mu m$) were measured using the electron microscope. The pictures obtained are shown in Figure 6-7:

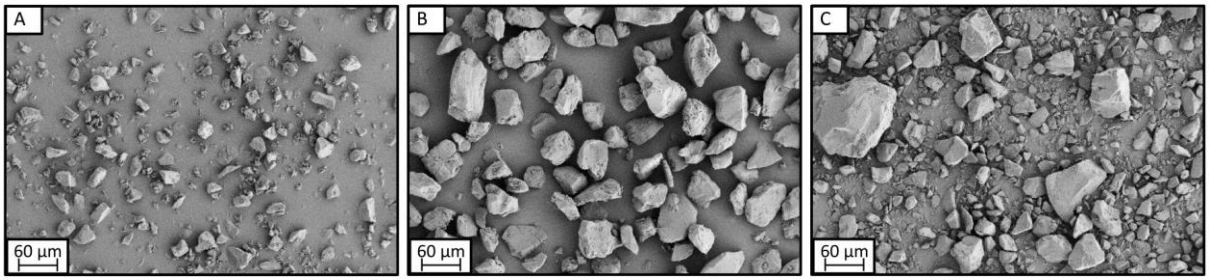

Figure 6-7: Particle structure of sugar powder (C) and sieved sugar powder, (A) particle diameter < 25 µm, (B) 25 µm < particle diameter < 63 µm; 500x magnification

It is clear to see, that particle fractionation with the air jet sieving process was sucessful. The different sugar particle fractions are well seperated. In adition cocoa powder with different cocoa butter amounts was measured with the electron microscope to determine the structural differences of highly, weakly and totally de-oiled cocoa particles. The totally de-oiled cocoa powder was obtained through Soxhlet extraction (carried out for the fat amount determination of highly de-oiled cocoa powder). The electron microscope pictures are given in Figure 6-8:

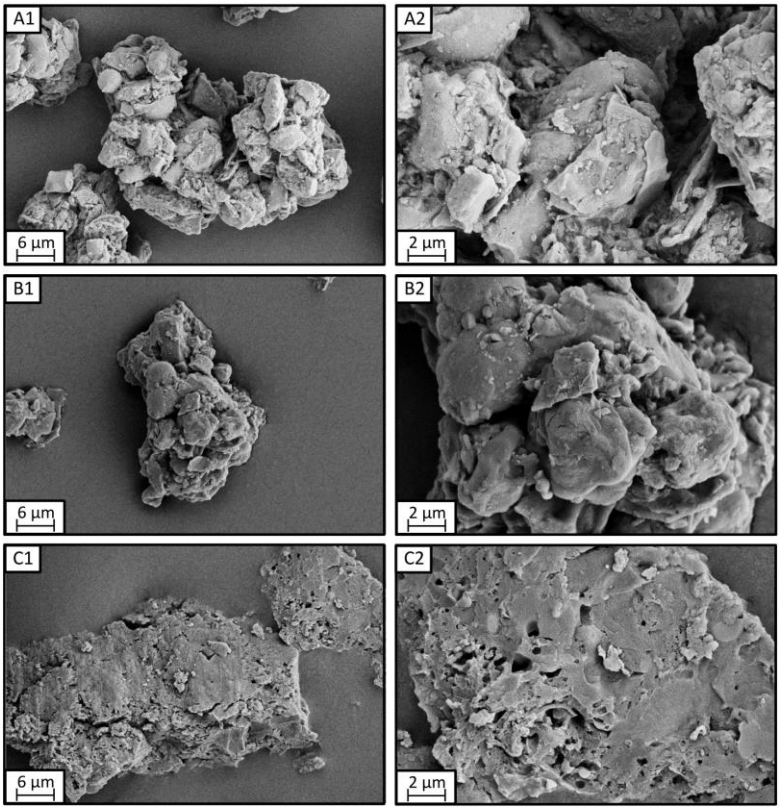

Figure 6-8: Particle structure of cocoa powder, (A) low de-oiled , (B) high de-oiled, (C) totally de-oiled; (1) 5000x magnification, (2) 15000x magnification

It can be seen, that the surface of highly and weekly de-oiled cocoa particles is covered with a layer, likely to be cocoa butter. Totally de-oiled cocoa powder consists of sharped edged particles without a layer covering them and a porous surface. The cocoa butter was probably bound in the irregular surface but it should be noted that the extraction could have had influence on the particle structure.

Finally the particle structure of spray dried sugar (sucrose) was compared with the structure of regular crystalline sucrose (icing sugar):

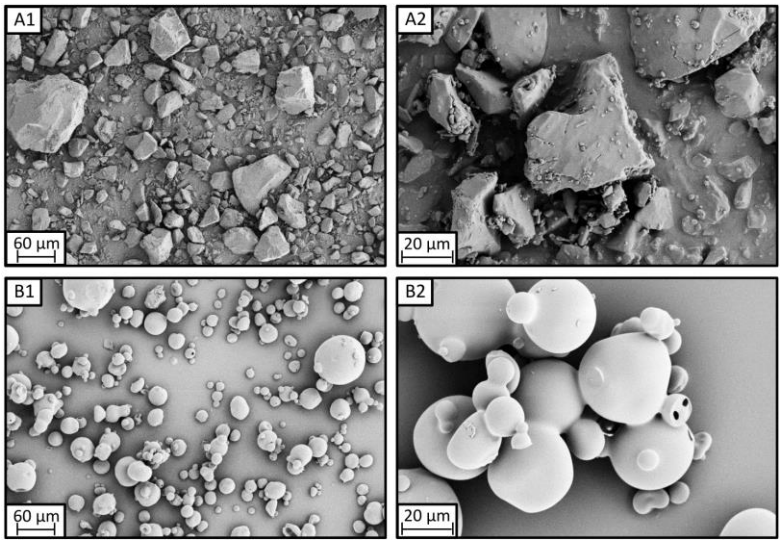

Figure 6-9: Particle structure of (A) cristallin sucrose (saccarose) and (B) spray dried sucrose; (1) 500x magnification, (2) 2000x magnification

The spray dried sucrose particle has a round smooth surface compared to the sharp edged structure of crystalline icing sugar. The particle size varies for both samples but they are in the same size range.

6.1.3 Moisture and Lipid Content

The moisture and lipid content of the solid chocolate ingredients used: icing sugar, cocoa powder and milk powder was measured (chapter 4.4.3) and the results are given in Table 6-4 and Table 6-5.

Table 6-4: Moisture content of chocolate ingredients

material	moisture content [wt%]
sugar powder	< 0.1
cocoa powder (low de-oiled)	4.7
milk powder	6.4
milk powder (milled and sieved)	6.8

It can be seen, that the sugar powder contains almost no water in comparison with cocoa powder (4.7 wt% water). The grinding and sieving of milk powder leads to a minimal moisture increase from 6.4 wt% up to 6.8 wt%.

Table 6-5: Lipid content of chocolate ingredients

material	lipid content [wt%]
cocoa powder (low de-oiled)	22
cocoa powder (high de-oiled)	10.66
cocoa mass	56.5
milk powder	< 0.1

The lipid amount of the skimmed milk powder can be neglected (below 0.1 wt%) as done for the statistical design of experiments (see chapter 5.1).

In chapter 2 it was shown that the composition of chocolate is varying for diverse chocolate types and that all ingredients has different properties. One main element of this work is the investigation of chocolate ingredient and composition effects on the gas solubility and foam structure in the high pressure aeration process. Therefore the characterisation of the used ingredients, given in this chapter is very important for a deep understanding of the chocolate composition and ingredient effects on the foam structure (see chapter 6.3).

6.2 High Pressure Aeration - Influence of Process Parameters

In this chapter the influence of process parameters on the gas solubility (at equilibrium state) as well as the gas dissolution (not at equilibrium state) in the fat phase and the foam structure of milk chocolate is discussed for the high pressure aeration process. The effect of pressure, gas type, stirrer speed, process temperature, crystallisation temperature and depressurisation rate is described.

6.2.1 Effect of Gas Type and Pressure

The influence of gas type used for aeration as well as the influence of aeration pressure on the gas dissolution and equilibrium solubility as well as foam structure of the samples is described in this chapter. Cocoa butter and milk chocolate were aerated with carbon dioxide, nitrogen and an equivalent mixture of both gases at 40°C and different pressures up to 250 bar. In Figure 6-10 the influence of pressure on the CO_2 equilibrium solubility in aerated cocoa butter at 40 °C is presented and compared to literature values [11, 14, 52, 57, 58] for validation of the measuring method.

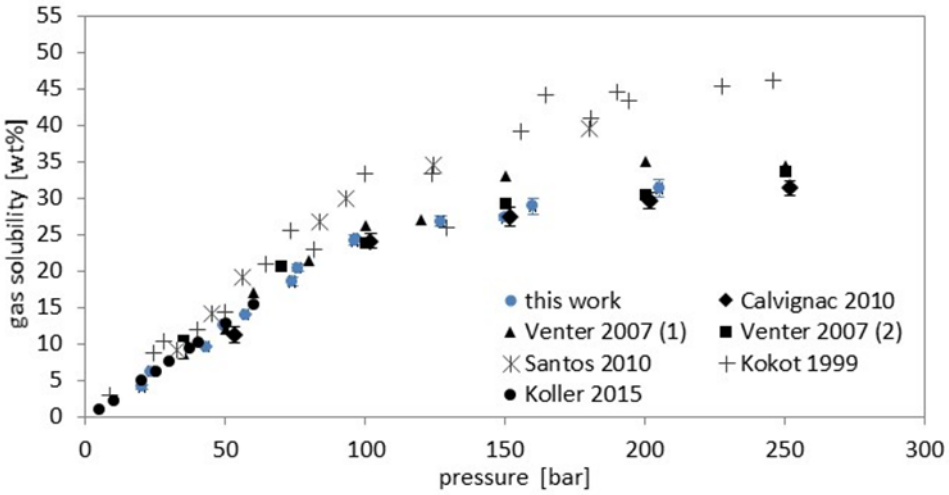

Figure 6-10: Influence of pressure on CO_2 solubility in aerated cocoa butter at 40 °C and equilibrium. Comparrison of literature values (black symbols) and values of this work (blue symbols)

The determined experimental values are in good agreement to the literature at pressures up to 100 bar [11, 14, 52, 57, 58]. At higher pressures above 100 bar the results from SANTOS [58] and KOKOT [57] deviate from the results from VENTER [11], CALVIGNAC [14] and this work. The reason for this could be different compositions of cocoa butter, which as a natural product, varies depending on the growing region. Nevertheless it can be concluded that the applied procedure is a reliable method for the determination of accurate gas solubility data. As can be seen from Figure 6-10, the gas solubility is strongly influenced by the pressure. At pressures up to 100 bar the solubility of carbon dioxide in cocoa butter increases linearly with rising pressure. Above 100 bar the solubility increase is less steep. The influence of pressure on the gas solubility in cocoa butter was also investigated for nitrogen, as shown in Figure 6-11.

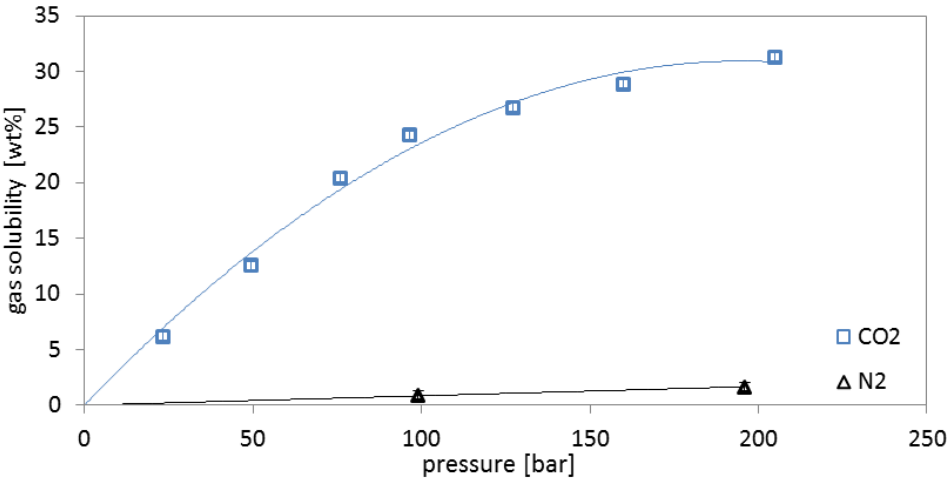

Figure 6-11: Influence of pressure on CO_2 and N_2 solubility in aerated cocoa butter at 40 °C (**Δ** N_2, □ CO_2)

Figure 6-11 illustrates, that nitrogen has much lower gas solubility in cocoa butter than carbon dioxide and is even less influenced by increasing pressure. The measurements were made at the equilibrium state of the lipid/gas system for each pressure. KOLLER also measured similar nitrogen solubilities in

cocoa butter for pressures up to 250 bar (approximately 1wt% at 250 bar) [52] . To show the influence of the dissolution time on the gas dissolution, milk chocolate was aerated with carbon dioxide at 20 bar, 55 bar and 130 bar. In Figure 6-12, the time dependent dissolution of carbon dioxide is presented.

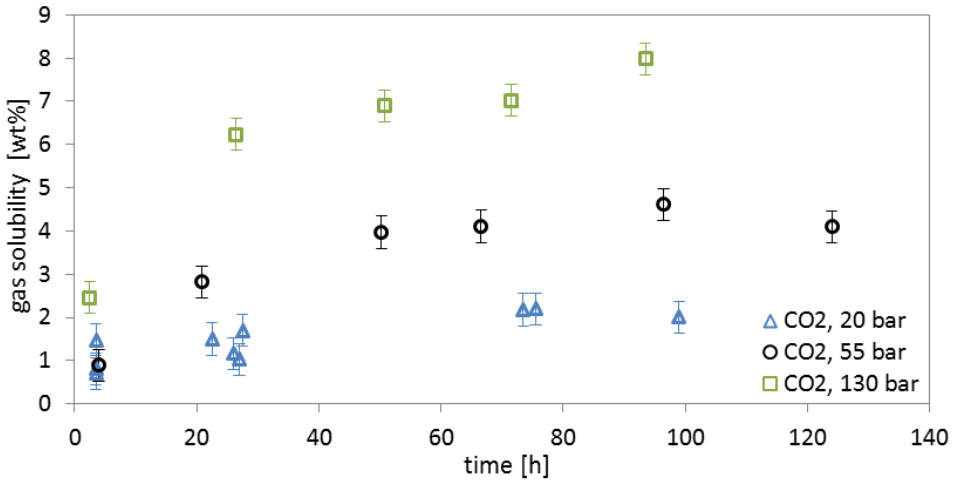

Figure 6-12: Influence of pressure on CO_2 dissolution in aerated milk chocolate at 40 °C as function of the dissolution time (Δ 20 bar, ○ 55 bar, □ 130 bar)

In Figure 6-12, it can be seen, that increasing pressure leads to an increase in carbon dioxide solubility for milk chocolate, just like fore pure cocoa butter. As shown before, the pressure influence is bigger for the lower pressure range. It can be seen that the dissolution at all pressures investigated increases rapidly at the beginning of the process. After around 50 hours the system reaches equilibrium and therefore constant gas solubilities for all pressures are observed. At higher pressure the increase of the gas dissolution in the first 50 hours is much greater because of the higher equilibrium gas solubility.

In addition to the influence of time and pressure on the gas dissolution, also the influence on the foam structure is interesting. Therefore the carbon dioxide/milk chocolate foam structure was determined by measuring the milk chocolate samples in the microcomputer tomograph. The Influence of the dissolution time on the carbon dioxide/milk chocolate foam is shown in Figure 6-13 for the three investigated pressures.

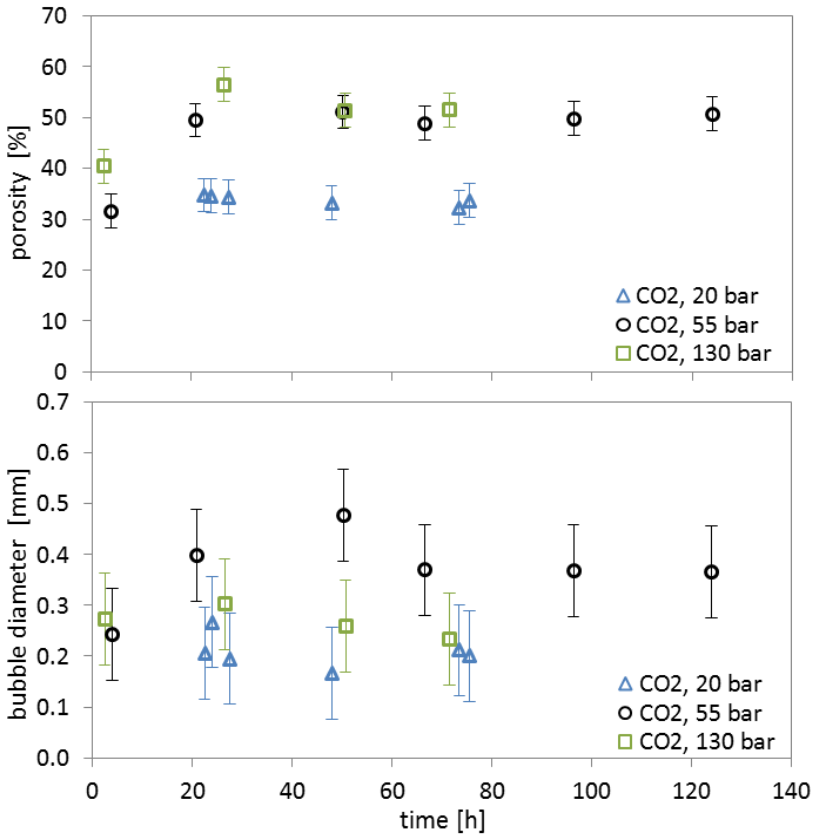

Figure 6-13: Influence of pressure on the porosity and the bubble diameter of CO_2 aerated milk chocolate at 40 °C as function of the dissolution time (Δ 20 bar, ○ 55 bar, □ 130 bar)

It was found that both pressure and dissolution time influences the final foam structure of carbon dioxide aerated milk chocolate. At the beginning of the aeration process, a porosity increase is shown with increasing dissolution time (Figure 6-13). After around 20 hours aeration the porosities remain constant at all investigated pressures. For pressures of 20 bar the equilibrium porosity is around 30 % and for pressures of 55 bar and 130 bar the equilibrium porosity is around 50 %. This result leads to the conclusion that the porosity of the carbon dioxide aerated milk chocolate rises with increasing pressure and reaches a maximum limit porosity value of 50 % with further pressure increase. The lowest pressure produces also the smallest mean bubble diameters in the foam. In contrast to these findings, it is shown that the mean bubble diameters are bigger at the 55 bar aeration compared to the 130 bar aeration. It is necessary to take the high error rate of the bubble diameter determination into account. Because of this it is difficult to define clearly the influence of pressure and dissolution time on the bubble diameter of the chocolate foam. Figure 6-14 compares the foam structure micro CT pictures of the carbon dioxide aerated milk chocolates at three different pressures.

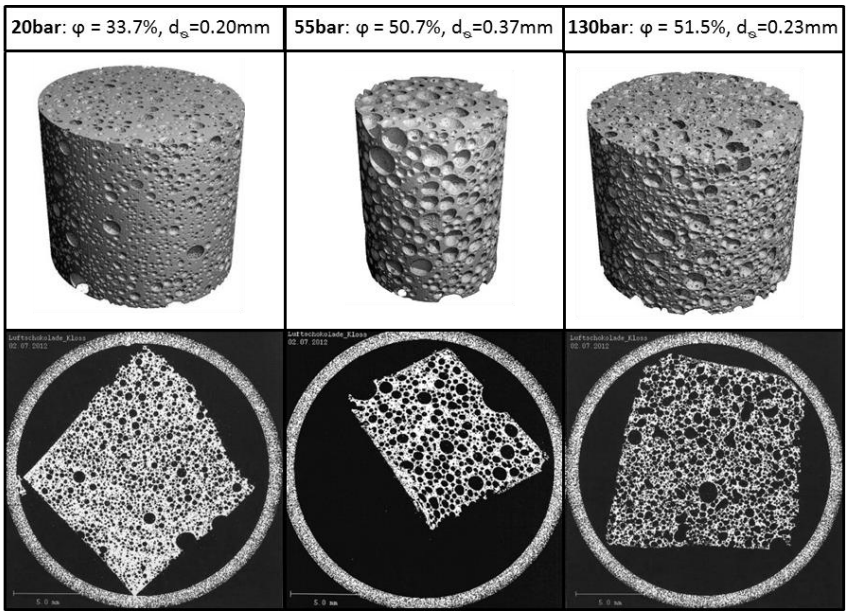

Figure 6-14: Influence of pressure (20bar, 55bar, 130bar) on the foam structure of CO_2 aerated milk chocolate at 40°C and equilibrium (φ = porosity, d_{32} = equivalent bubble diameter)

Looking at Figure 6-14 it is apparent that bubbles in the foam at 20 bar are smaller compared to those formed at higher pressures and that these fact of lower gas volume leads to an apparent lower porosity. At higher pressures the influence on foam structure does not seem to be significant. To validate the pressure influence, milk chocolate was also aerated with nitrogen. In Figure 8-1 (see appendix) the time dependent gas dissolution, porosity and mean bubble diameter for nitrogen aerated milk chocolate at 20 bar, 55 bar and 150 bar is presented. The gas solubility of nitrogen in milk chocolate is also much lower than the solubility of carbon dioxide, as shown before for cocoa butter (Figure 6-11). The lower solubility of nitrogen compared to carbon dioxide in chocolate was also referred to by Headelt [1] at 30 °C and 2.5 bar. During the process, the gas dissolution in this system increases with time from 0.5 to 1.2 wt%. The influence of pressure on nitrogen solubility is not significant and in the range of measurement error. The pressure and the dissolution time show no significant influence on the foam structure of nitrogen aerated milk chocolate (porosity and the mean bubble diameter). Figure 6-15 compares the foam structure of nitrogen aerated milk chocolates at 20, 55 and 150 bar.

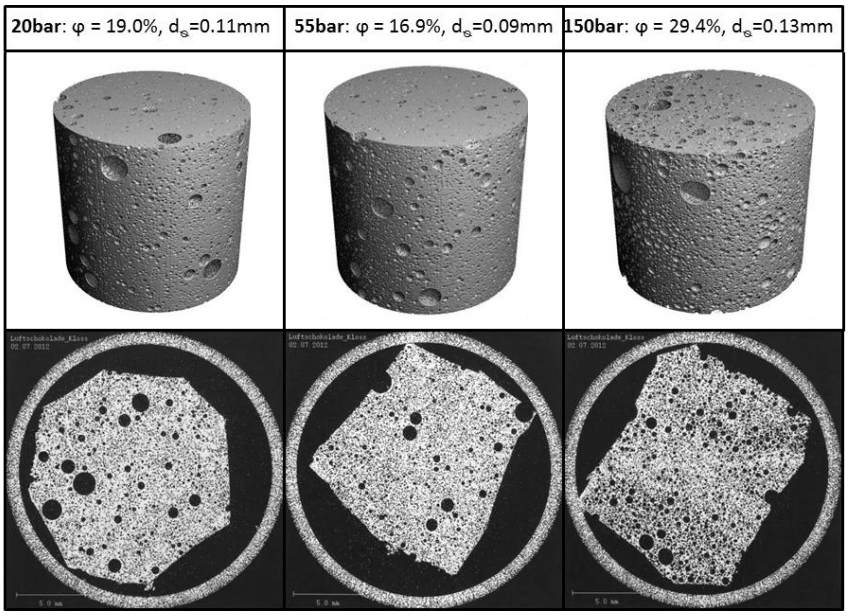

Figure 6-15: Influence of pressure (20bar, 55bar, 150bar) on the foam structure of N_2 aerated milk chocolate at 40°C and equilibrium (φ = porosity, $d_{⌀}$ = equivalent bubble diameter)

The micro CT pictures show no significant difference between milk chococlate foams aerated with nitrogen at 20 bar, 50 bar or 150 bar. The changes in the solubility with pressure are very small because of the very low nitrogen solubility and thus the difference in the foam structure is also very slight. In conclusion it can be said, that both the porosity and the mean bubble diameter of the nitrogen aerated milk chocolate are much lower than the values for the carbon dioxide aerated milk chocolate. Because of the low nitrogen solubility in milk chocolate only a little gas volume is available to form bubbles. The formed bubbles therefore stay small and the porosity remains low. The fact that carbon dioxide leads to a higher porosity and bigger bubbles can be explained with the high gas solubility. It has been demonstrated that the pressure influence on the gas solubility and foam structure is very strong for carbon dioxide and not significant for nitrogen aerated milk chcocolate.

In a further step it was decided to investigate the effect of a gas mixture. Milk chocolate was aerated with an equal mixture of carbon dioxide and nitrogen and the results were compared with samples previously produced with unmixed gas. In Figure 6-16 the time dependent gas dissolution of the investigated gases in milk chocolate is shown for a pressure of 55 bar and a temperature of 40 °C.

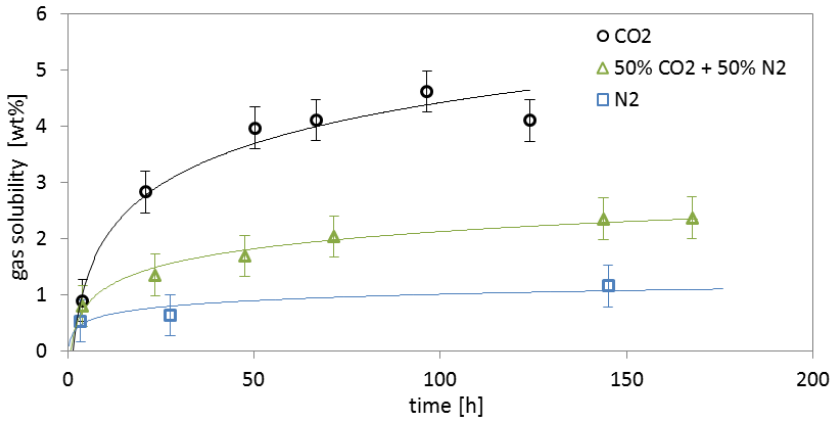

Figure 6-16: Influence of gas composition on the gas dissolution in aerated milk chocolate at 55 bar and 40 °C as function of the dissolution time (○ CO2, Δ 50%CO2 + 50% N2 , □ N2)

It can be seen that as before, the dissolutions of all investigated gases increase rapidly at the beginning of the process. After around 50 hours all systems reach equilibrium and thus constant gas solubilities. After reaching the equilibria state the solubility of carbon dioxide is around 4 times higher than the nitrogen solubility at the investigated constant pressure and temperature. The gas dissolution and solubility of the mixed gas in milk chocolate leads to values between the pure gas values. In conclusion the gas dissolution and equilibrium solubility in milk chocolate increases with an increasing amount of carbon dioxide and thus decreases with an increasing amount of nitrogen. The milk chocolate samples aerated with the different gases were measured using the micro computer tomograph. In Figure 6-17 the time dependent porosity and mean bubble diameter of the foam is shown for a pressure of 55 bar and a temperature of 40 °C.

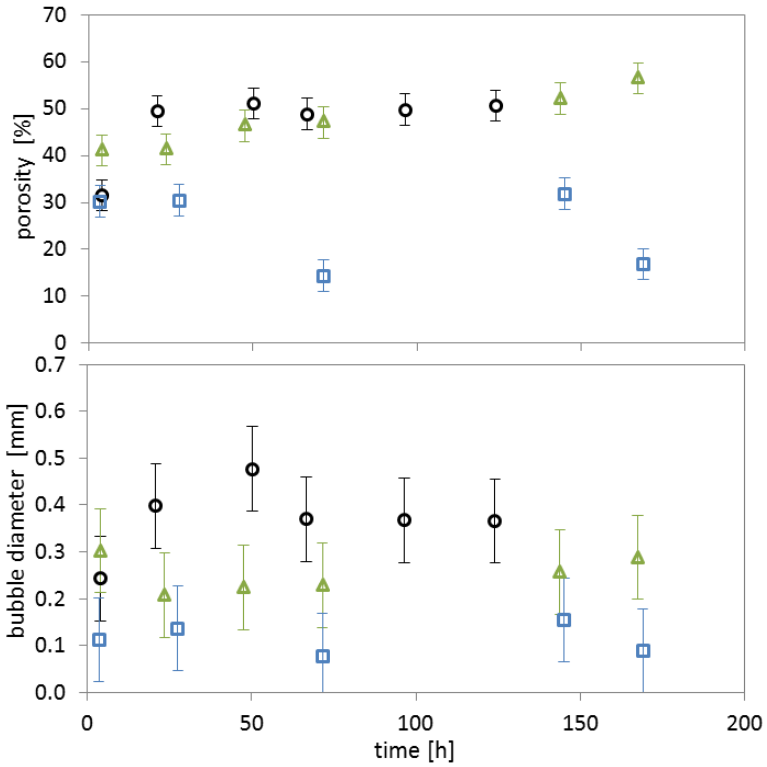

Figure 6-17: Influence of gas composition on the porosity and the mean bubble diameter of aerated milk chocolate at 55 bar and 40 °C as function of the dissolution time (○ CO2, Δ 50%CO2 + 50% N2 , □ N2)

For the gas mixture it was found that the mean bubble diameter values are in between the pure gas values. That means that an increase in the ratio of carbon dioxide in the mixture leads to an increasing bubble diameter in the chocolate foam. The porosity of the milk chocolate aerated with the gas mixture is in the range of pure carbon dioxide. This implies that when the dissolved gas volume increases the porosity in the chocolate increases till they reach a limited maximum porosity of around 50%. The influence of the gas phase composition on the foam structure of aerated milk chocolate is demonstrated in Figure 6-18. In the appendix in Figure 8-5, the foam structures of aerated milk chocolate at 55 bar and 40°C is given for different dissolution times using nitrogen, carbon dioxide or a 50% nitrogen/50% carbon dioxide mixture as foaming agent.

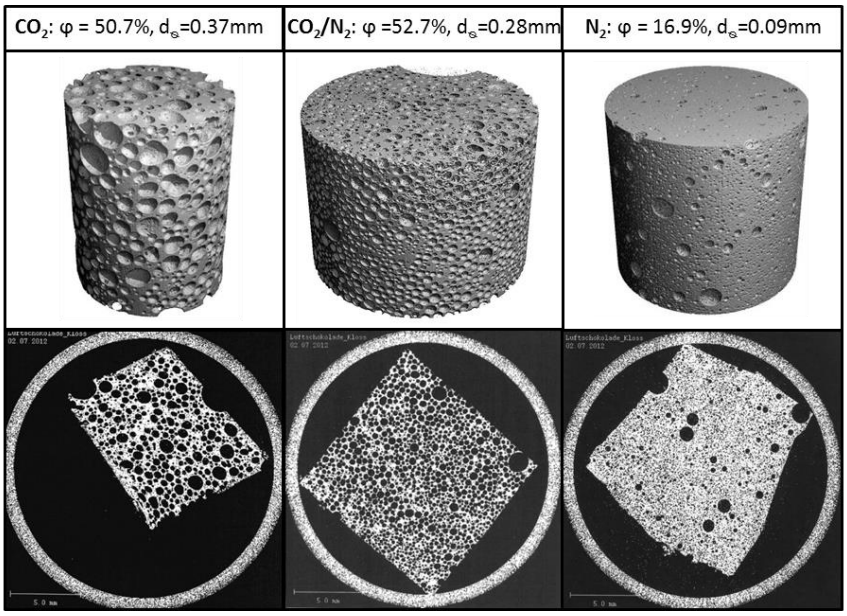

Figure 6-18: Influence of gas phase composition (N_2, CO_2, 50% CO_2 + 50% N_2) on the foam structure of aerated milk chocolate at 55 bar, 40°C and equilibrium (φ = porosity, $d_ø$ = equivalent bubble diameter)

In Figure 6-18 the significant impact of the aerating agent is clearly seen. Increasing amounts of carbon dioxide leads to bigger bubbles in the chocolate foam because of the higher gas solubility. HAEDELT [1] classified aerated chocolate in two categories: micro and macro foams. In micro foams less coalescence takes place and the gas release is low. In macro foams the gas release is much higher and this results in coalescence of the bubbles before crystallisation of the chocolate occurs. A carbon dioxide aerated chocolate was classified by HAEDELT as macro foam and nitrogen aerated chocolate as micro foam [1]. In consideration of gas mixtures it can be concluded that the ratio of carbon dioxide to nitrogen is key value, a high amount of carbon dioxide leads to macro foams and a high amount of nitrogen to micro foams.

In conclusion it can be said that the foam structure of aerated milk chocolate can be controlled through the gas composition used as the aerating agent. An increasing amount of carbon dioxide in the gas leads to bigger bubbles and high porosities until equilibrium porosity is reached. With nitrogen the opposite behaviour is observed. Additionally it can be said that higher pressures promote the solubility of gases in cocoa butter and chocolate. Due to the increased solubility, the porosity of carbon dioxide

aerated milk chocolate also rises with increasing pressure, reaching a maximum porosity value of approximately 50 % (above any further pressure increase has no impact).

6.2.2 Effect of Stirrer Speed

In previous chapters it has been shown that time significantly influences the amount of gas that can be dissolved and therefore also the foam structure produced. The open question is if the dissolution time can be influenced and therefore the aeration process can be accelerated through process parameters such as stirrer speed. In order to answer this question, milk chocolate was aerated at two different stirrer speeds with carbon dioxide at 40°C and 55 bar. In Figure 6-19 the influence of stirrer speed on CO_2 dissolution and the resulting change in foam structure over time is presented.

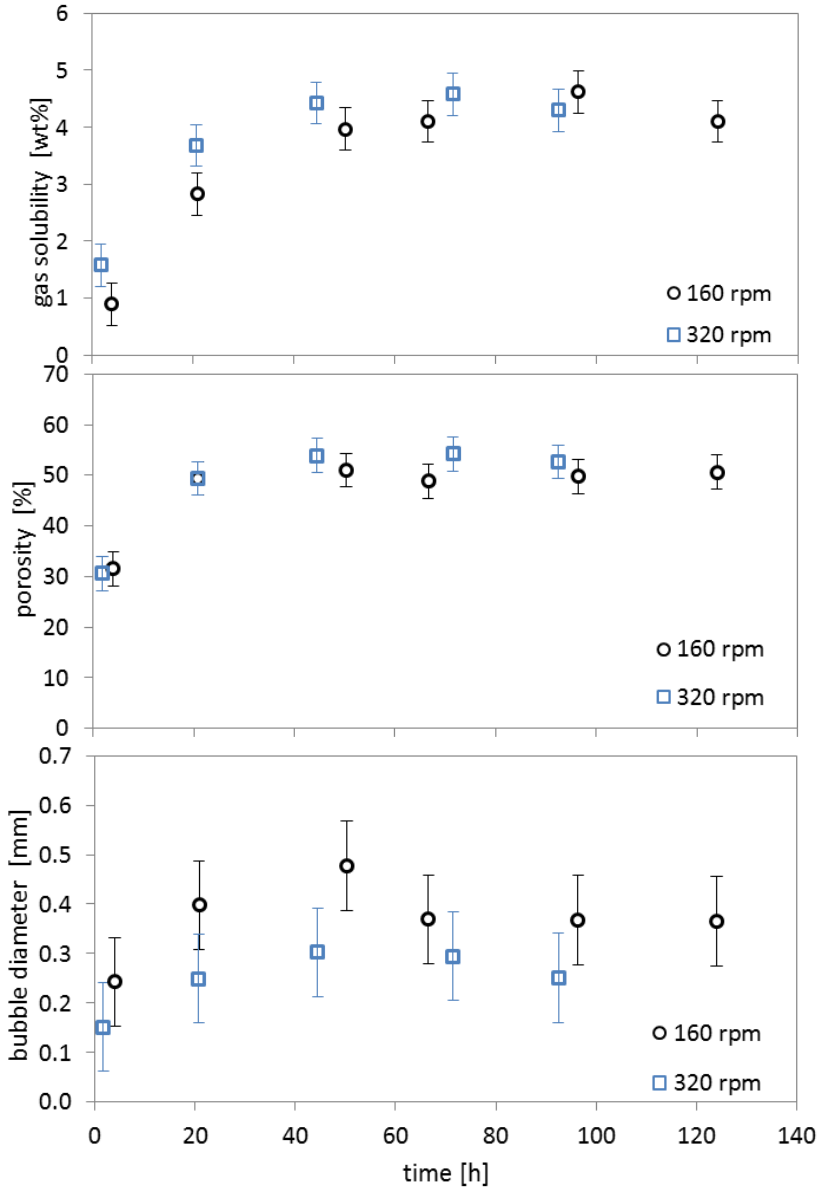

Figure 6-19: Influence of stirrer speed on the gas dissolution, porosity and the bubble diameter of CO_2 aerated milk chocolate at 55 bar and 40 °C as function of the dissolution time (○ 160 rpm, Δ 320 rpm)

The results show, that the gas dissolution increases a little bit more quickly at higher stirrer speed and thus reaches equilibrium earlier. This means that with an increase of stirrer speed the gas dissolution increases faster and the maximum equilibrium solubility is reached earlier. In contrast to this, the stirrer speeds do not significantly influence the porosity of the aerated chocolate as shown in Figure 6-19. The maximum limited porosity of 50% is reached in both cases of stirrer speed after around 20 hours. The reason could be that the porosity reacts much less sensitive on the stirrer speed compared to the gas dissolution or there are not enough data points to present the influence of stirrer speed on gas dissolution. Due to the influence of stirrer speed on the gas dissolution there should also be an impact on porosity (as described before). As well at the lower stirrer speed enough gas will be solubilized in the chocolate after 20 hours to generate the maximum porosity and there are not enough data points in the beginning to determine the definite porosity increase. In Figure 6-19, it can be seen, that a higher stirrer speed seems to lead to lower mean bubble sizes, however because of the big error of this measurement no clear statement can be made. The reason could be the better dispersion of the gas in the chocolate because of faster stirring and thus the formation of more, smaller bubbles during depressurisation.

In conclusion it can be said, that the stirrer speed accelerated the gas dissolution in chocolate. On the contrary, the influence on the foam structure is very little at least in the investigated range.

6.2.3 Effect of Temperature

The influence of the aeration process temperature is discussed in this chapter. Pure cocoa butter and milk chocolate were aerated at different pressures with carbon dioxide and nitrogen at 30°C, 40°C and 80°C. In Figure 6-20 CO_2 solubility in cocoa butter and milk chocolate is presented for different temperatures and plotted against the pressure or the density of CO_2 in the gas phase.

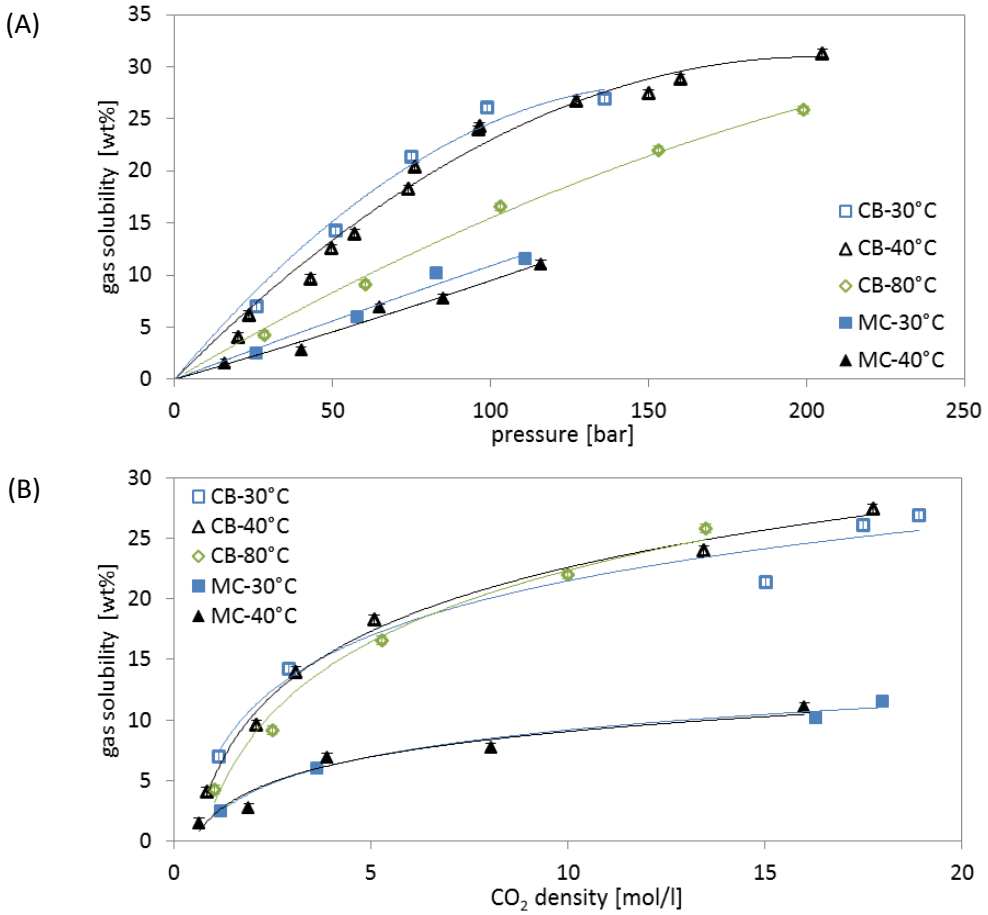

Figure 6-20: Influence of (A) pressure and (B) density of CO_2 on the CO_2 solubility in aerated cocoa butter and milk chocolate at 30°C, 40 °C and 80°C (□ cocoa butter 30°C, Δ cocoa butter 40°C, ◊ cocoa butter 80°C, ▪ milk chocolate 30°C, ▲milk chocolate 40°C)

For cocoa butter and milk chocolate it is clear to see that the CO_2 solubility decreases with increasing temperature at constant pressure. Therefore the solubility at 30°C is higher than the solubility at 40°C and 80°C in both investigated lipid systems. In literature a decrease of gas solubility with increasing temperature was also referred to for a cocoa butter/CO_2 system [11, 14, 57]. The reason for this is the density change of gasses at different temperatures. In Figure 6-20 (B) it can be seen, that gas solubility is almost the same at constant carbon dioxide density for all investigated temperatures. The same temperature influence on gas solubility is also evident for the nitrogen/cocoa butter system. In Figure 8-2 (see appendix), the influence of pressure on the CO_2 and N_2 equilibrium solubility in aerated cocoa butter is presented for 40 °C and 80°C.

In the next step the influence of temperature on the gas dissolution and the foam structure was investigated. Therefore the pressure was kept as constant. The gas dissolution, porosity and mean bubble diameter were measured at 30 °C and 40°C for carbon dioxide aerated milk chocolate at 55 bar. The dissolution time dependent results are shown in Figure 6-21.

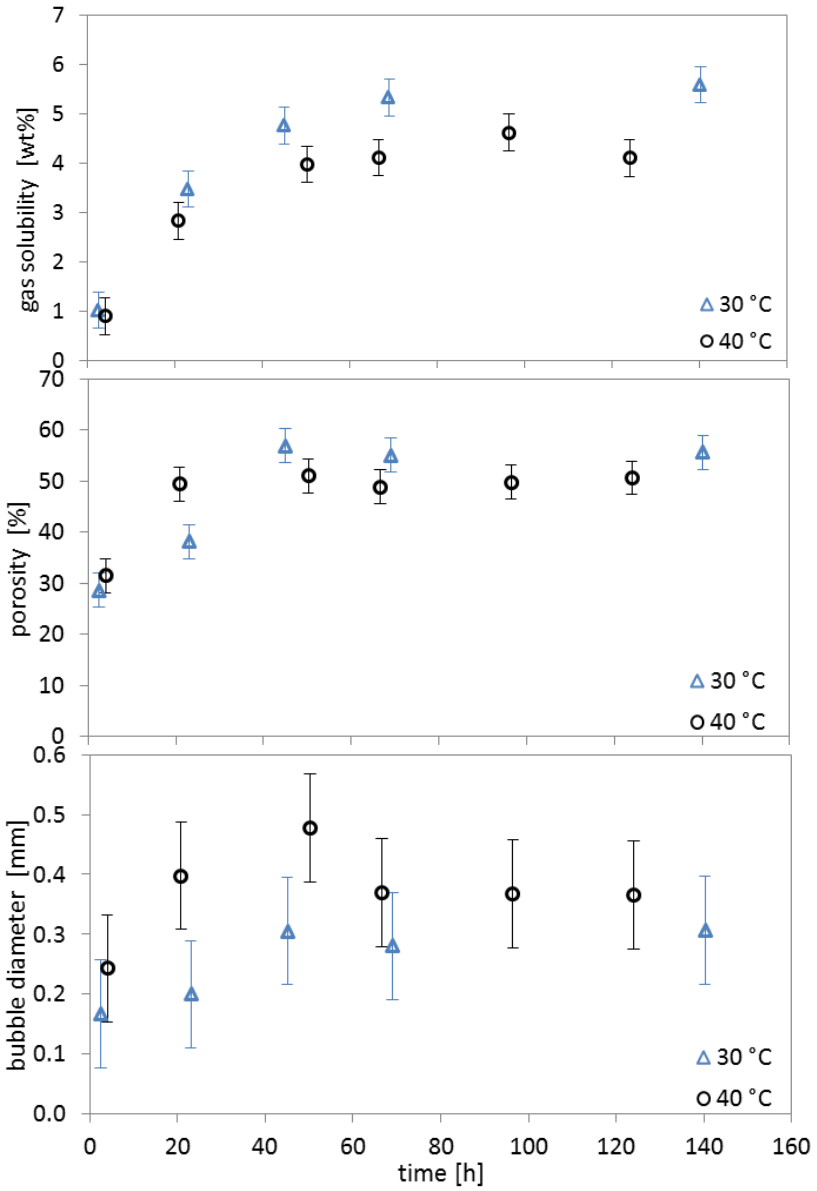

Figure 6-21: Influence of temperature on gas dissolution, porosity and the bubble diameter of CO_2 aerated milk chocolate at 55 bar as function of the dissolution time (Δ 30°C, ○ 40°C)

In Figure 6-21 it is apparent, that the speed of gas dissolution is not significantly influenced by temperature in the investigated range. Only the equilibria solubilities at different temperatures differ from each other as shown before. Both, the porosity increase during aeration and the maximum porosity were not strongly influenced by the temperature, only a little increase in porosity with decreasing temperature is apparent. The reason is the faster dissolution at lower temperatures and thus more trapping of gas in the foam. The impact of temperature on the mean bubble diameter is also obvious. In Figure 6-21 it is shown, that a 30°C process temperature leads to smaller bubbles over

the whole aeration time in comparison to 40 °C. For a better illustration of the temperature effect on the bubble diameter, the foam pictures of the 30°C and 40°C aerated milk chocolate are shown in Figure 6-22.

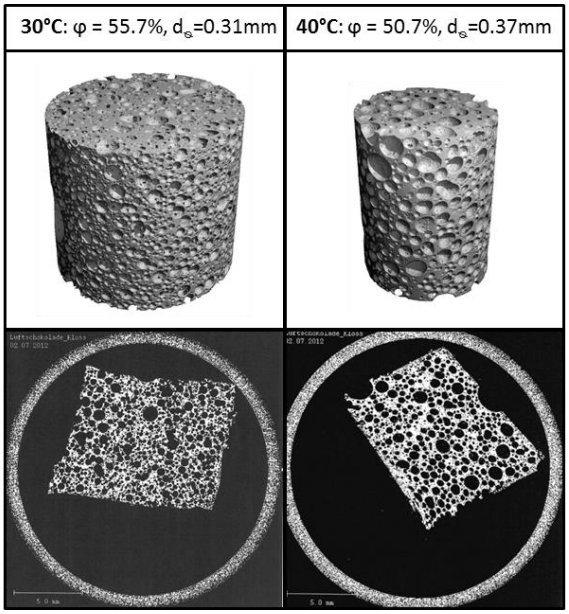

Figure 6-22: Influence of temperature (30°C, 40°C) on the foam structure of CO_2 aerated milk chocolate at 55 bar and equilibrium (φ = porosity, d_{32} = equivalent bubble diameter)

In Figure 6-22 it is also clear to see, that the bubbles in the milk chocolate foam are smaller for the 30 °C aerated chocolate than for the 40°C aerated one. This is also because of the faster crystallisation of the lower temperature aerated foam. At 40°C there are more time for coalescence of the bubbles and thus results in foam with bigger bubbles.

In conclusion it can be said, that temperature influences the density of the gas which leads to an increase of the gas solubility with decreasing temperature at constant pressure. Due to the density change of gasses with temperatures it can be seen, that gas solubility is almost the same at constant gas density for all investigated temperatures. Additionally the aeration temperature affects the crystallisation speed and thus the time for outgassing, coalescence and bubbles size. This results in the formation of foams with higher porosity and smaller bubbles at lower aeration temperatures.

6.2.4 Effect of Depressurisation Rate

In chapter 6.2.3 it was shown, that the aeration temperature influences the crystallisation speed, coalescence and bubble size. During the depressurisation the chocolate cools down because of the Joule-Thomson effect. The Joule-Thomson effect describes the cooling of gases during an adiabatic expansion from a higher to a lower pressure [53]. Because of this, the speed of depressurisation can influence the temperature of chocolate foam and thus the foam structure. To realise the experimental investigation of the depressurisation rate, milk chocolate at a temperature of 40 °C was aerated with carbon dioxide or nitrogen at 20 bar and then shortly pressurised to higher pressures up to 150 bar before depressurisation. The reason for this procedure was, that higher system pressures leads to

higher depressurisation speeds. In chapter 6.2.1 the kinetic of gas solubility (gas dissolution) was investigated and it was shown that the dissolution of gas in chocolate is a very slow process with a necessary time of 50 hours to reach the equilibrium. For this reason this experiment was based on the assumption that no significant dissolution of gas in chocolate takes place in this short time of pressurisation without stirring. In Figure 6-23 the influence of depressurisation rate on the porosity and the bubble diameter of CO_2 and N_2 aerated milk chocolate is shown. The depressurisation rate is presented as pressure gradient between shortly adjusted process pressure and ambient pressure at the end of the process.

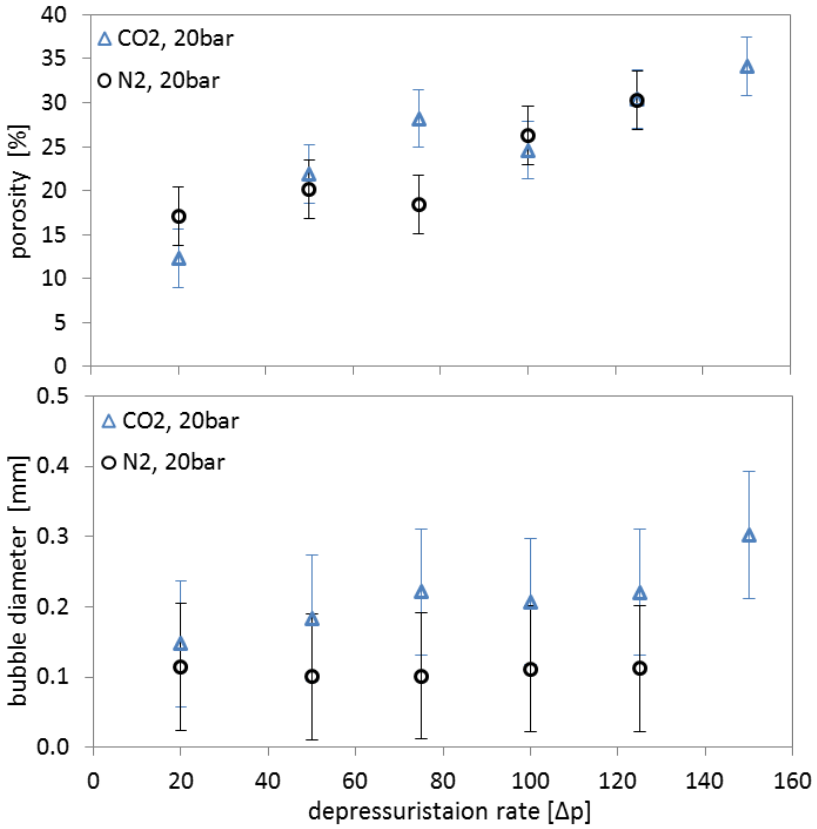

Figure 6-23: Influence of the depressurisation rate as pressure gradient on the porosity and the bubble diameter of CO_2 and N_2 aerated milk chocolate at 20 bar and 40 °C as function of the dissolution time (Δ CO_2, ○ N_2)

In Figure 6-23 can be seen, that the depressurisation rate influences the porosity of the milk chocolate for both CO_2 and N_2. The explanation is, that at higher pressure gradients and thus at faster depressurisation rates the temperature of the chocolate decreases more quickly than for slower depressurisation rates, because of the Joule-Thomson effect. As shown in chapter 6.2.3 a decrease of temperature leads to an increase of porosity and decrease of bubble size because of the faster crystallisation. In contrast to these findings the depressurisation rate does not influences the mean bubble diameter of the foam. Still, a reason could be the big error of the measurement method. Figure 6-24 shows the foam structures of CO_2 aerated milk chocolates depressurised at three different rates. In Figure 8-3 in appendix the same illustration for the nitrogen aeration is given.

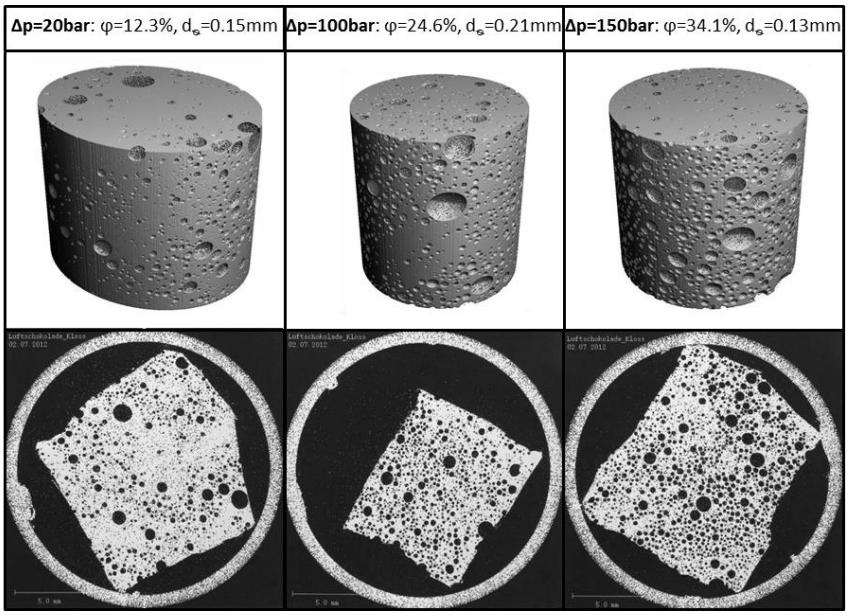

Figure 6-24: Influence of the depressurisation rate (Δp = 20bar, 100bar, 150bar) on the foam structure of CO_2 aerated milk chocolate at 20 bar, 40°C and equilibrium (φ =porosity, d_{32}=equivalent bubble diameter)

In Figure 6-24 it is clear to see, that the porosity and the number of bubbles in the foam increase with increasing depressurisation rate. This means that more bubbles are formed at faster depressurisation and that less coalescence takes place because of the faster crystallisation. The same behavior was visible for the nitrogen aerated chocolate presented in Figure 8-3 (see appendix). The aeration and subsequent depressurisation of milk chocolate in the viewing cell (see chapter 4.3) has also shown, that the porosity increases with increasing depressurisation speed and that the depressurisation rate do not significantly influence the mean bubble diameter. The measurements were done at different equilibrium pressure (24 - 148 bar) and at constant equilibrium temperature of 40°C with small milk chocolate amounts of around 1 g. The depressurisation takes place directly in the viewing cell. The achieved milk chocolate foam porosities for different depressurisation rates are shown in Figure 6-25.

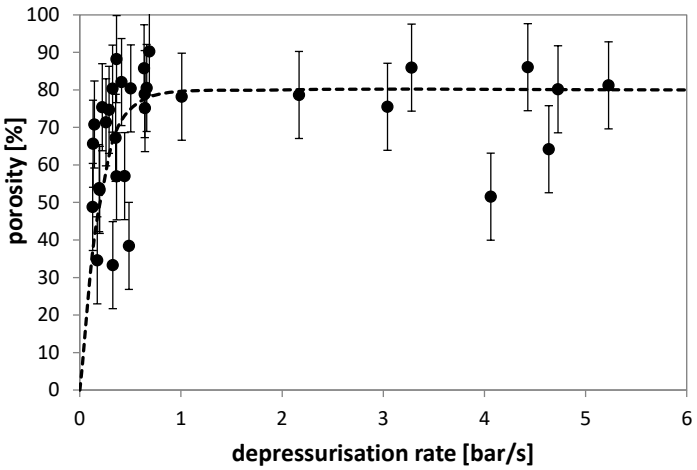

Figure 6-25: Influence of the viewing cell depressurisation rate on porosity of CO_2 aerated milk chocolate at equilibria conditions of 40 °C and different equilibrium pressures from 24 bar up to 148 bar

The porosity firstly increases fast up to around 80% with increasing depressurisation rate. From a depressurisation rate of around 0.8 bar/s the chocolate porosity remains almost constant. The achieved porosity value however are not comparable with the porosities of regular autoclave aerated milk chocolate in this work because of process differences. In the viewing cell a very low sample amounts was taken and the depressurisation takes place directly in the autoclave. However the influence of depressurisation rate on the chocolate foam porosity was also confirmed with this different process. In the viewing cell experiments it was also shown, that the depressurisation rate does not significantly influences the bubble size of the milk chocolate foam.

KOLLER [52] also investigated the effect of depressurisation rates (5bar/min and 30 bar/min) in carbon dioxide or nitrogen/cocoa butter systems with a visual method [52]. KOLLER described that higher bubble number density and faster coalescence were observed at higher depressurisation rate and that the main formation of small bubbles took place when ambient pressure was just reached [52]. TAKI et al. [115] described that an increased pressure release rate lead to an increase in bubble nucleation and growth rate for carbon dioxide saturated polymers [115]. PARK et al. [116] described that faster pressure drop leads to a higher nucleation rate by investigating the influence of nozzle geometries and depressurization rates on bubble nucleation [116]. These findings described in literature [52, 115, 116] confirm the results of this work suggesting that porosity increases with increasing depressurisation speed.

In conclusion it can be said, that porosity increases with increasing depressurisation speed and that the depressurisation rate do not significantly influence the mean bubble diameter for both CO_2 and N_2 aerated milk chocolate. The reason is that a higher pressure gradients and thus a faster depressurisation leads to a more quickly temperature decrease due to the Joule-Thomson effect. This leads to a faster crystallisation of the foam with a higher trapped gas amount up to a maximum porosity level.

6.2.5 Effect of Crystallisation Rate

For a better validation of the temperature effect on the foam structure the influence of the crystallisation temperature was investigated. Therefore nitrogen or carbon dioxide aerated milk chocolate foams were crystallised at temperatures from -78.5 °C to 20 °C. At higher crystallisation temperatures the chocolate crystallise more slowly. At -78.5 °C the chocolate is completely solidified after around 6 minutes and at 20 °C after around 30 minutes but a statement about the completeness of crystallisation at this times can not be made. The influence of the crystallisation temperature on the foam structure is presented in Figure 6-26.

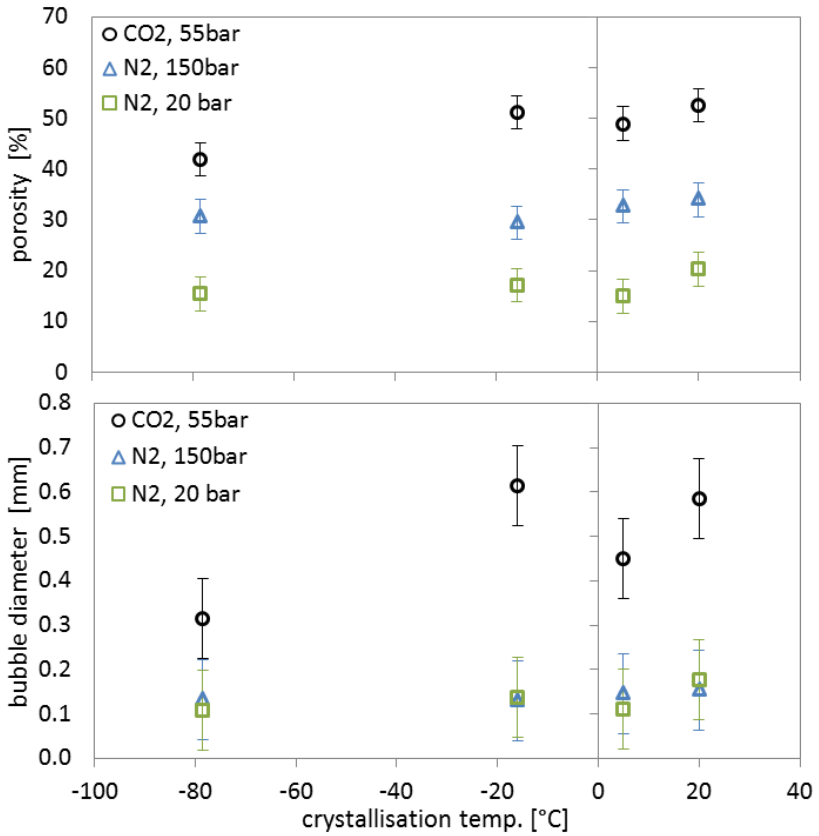

Figure 6-26: Influence of the crystallisation temperature on the porosity and the bubble diameter of CO_2 and N_2 aerated milk chocolate at 40 °C and equilibrium (○ CO_2-55 bar, Δ N2-150 bar, □ N_2-20 bar)

In contrast to the findings of previous chapters, the crystallisation temperature does not significantly influence the foam structure of the aerated chocolates. The porosities in particular are quite constant over the whole temperature range. Only the CO_2 aerated, -78.5 °C crystallised chocolate has a slightly lower porosity and bubble diameter. To illustrate these findings, the pictures of aerated chocolates crystallised at different temperatures are presented in Figure 6-27.

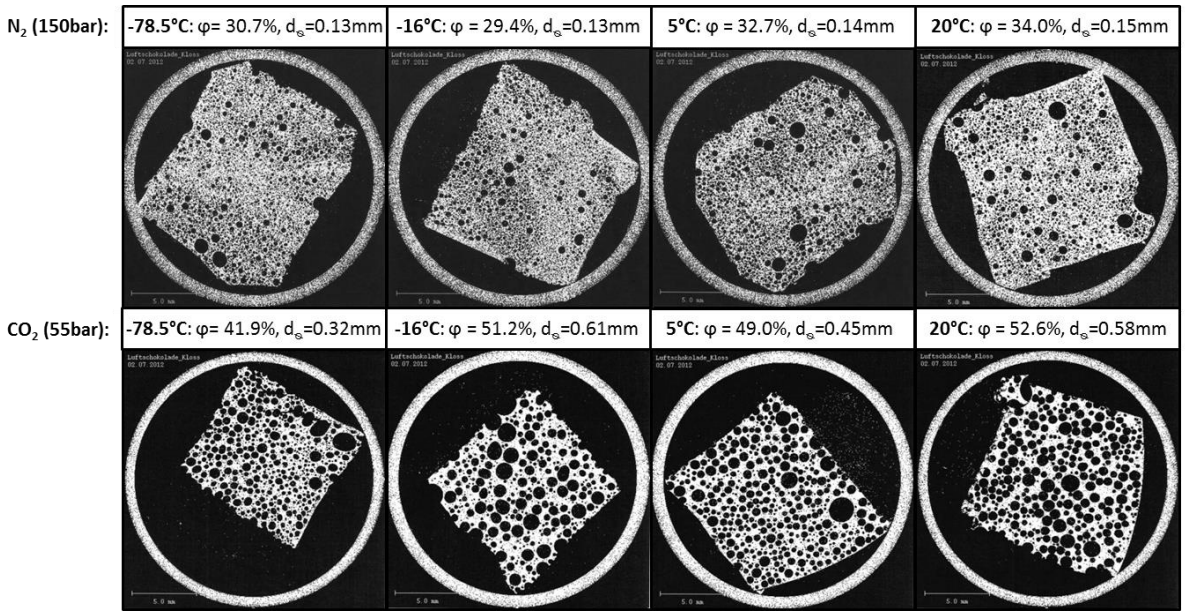

Figure 6-27: Influence of the crystallisation temperature on the foam structure of CO_2 (55 bar) and N_2 (150 bar) aerated milk chocolate at 40 °C and equilibrium (φ =porosity, d_S=equivalent bubble diameter)

Figure 6-27 also illustrates that crystallisation temperature does not significantly impact the foam structure of aerated milk chocolate. Only at the lowest temperature (-78.5°C) the CO_2 aerated chocolate shows slightly smaller bubbles and a lower porosity. The reason could be the very early stabilisation of the foam during depressurisation. As shown in chapter 6.2.4, depressurisation leads to cooling of the chocolate because of the Joule-Thomson effect and thus to an increasing in viscosity. The result is a pretty stable foam which is not crystallised completely. In consideration of the crystallisation temperature results it means, that the foam structure is mostly formed during depressurisation and not during crystallisation. Only very low crystallisation temperatures and therefore very fast crystallisation lead to a slight decrease of bubble size and porosity. It seems like only directly after the depressurisation the relatively stable foam structure changes slightly, due to outgassing and coalescence. After a few minutes the foam structure becomes totally stable, even without complete crystallisation. This means that beyond a certain viscosity of the cooled chocolate the bubbles are fixed in the foam and have no possibility to move, coalesce or grow.

In conclusion, temperature and therefore the viscosity of the chocolate influence the foam structure. The biggest influence is from the aeration process temperature and the reduction in temperature during depressurisation. The influence of crystallisation temperature on the foam structure is secondary. It was shown, that only very fast crystallisation at very low temperatures of around -80°C can influence the foam structure but generally the foam structure is stable after depressurisation even without complete crystallisation.

6.3 High Pressure Aeration - Influence of Chocolate Composition

In this chapter the influence of chocolate composition on the gas solubility, gas dissolution time and the foam structure is discussed for the high pressure aeration process. In particular the effect of sugar and cocoa powder particles was investigated.

6.3.1 Effect of Chocolate Composition on the Gas Solubility

A statistical design of experiments (see chapter 5.1) was used to investigate the influence of every chocolate component on the gas solubility and gas dissolution speed. With this technique 25 mixed compositions were calculated. The mixtures contained the five main ingredients of chocolate: cocoa butter, sugar, cocoa powder, milk powder and lecithin. The detailed composition of every mixture is given in Table 4-5 in chapter 4.2.1. After preparation each mixture was aerated with carbon dioxide at constant conditions of 55 bar and 30°C. In Figure 6-28 the scaled carbon dioxide dissolutions in different mixtures and cocoa butter are given for a time range of 100 hours.

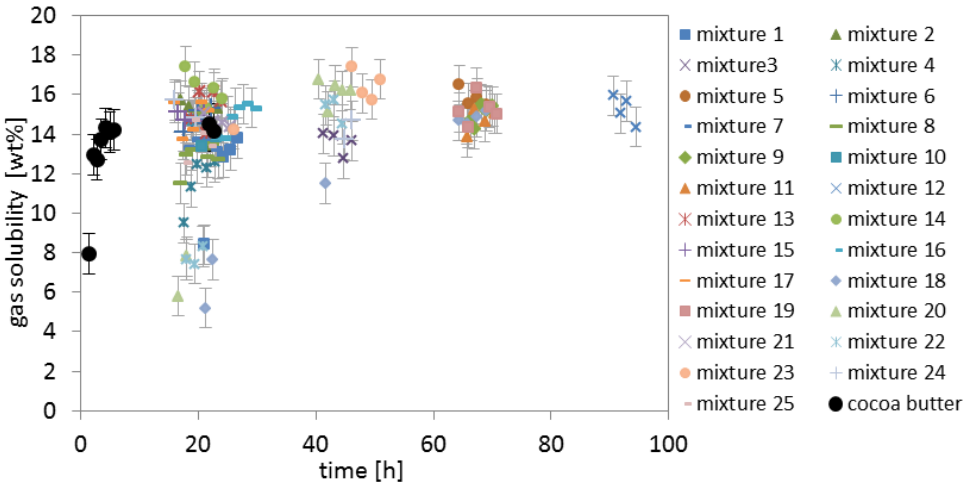

Figure 6-28: Influence of dissolution time on the CO_2 dissolution in CO_2 aerated cocoa butter and different chocolate mixtures scaled on 100wt% cocoa butter at 55 bar and 30°C (black symbols = cocoa butter, coloured symbols = chocolate mixtures)

Figure 6-28 shows, that pure cocoa butter reaches the equilibrium much earlier than the mixtures containing the chocolate particles (sugar, cocoa powder, milk powder). For cocoa butter it needs less than five hours to reach equilibria and after 20 hours the equilibria is not even reached for all of the mixtures. The different cocoa butter amounts in the mixtures (50-100 wt%) makes the gas dissolution difficult to compare. Due to this all presented gas dissolution are re-scaled for 100 % cocoa butter amount in the mixtures, because of this the values are better comparable. It seems like all the mixtures and pure cocoa butter have nearly similar scaled equilibria solubilities. The comparison of the equilibria gas solubilities in the mixtures compared with the gas solubility in cocoa butter is given in Figure 6-29.

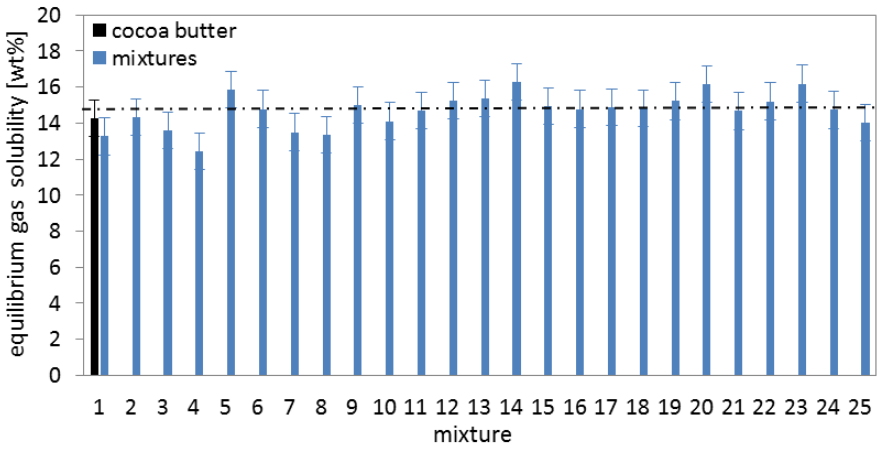

Figure 6-29: Comparison of the equilibrium CO_2 solubilities in cocoa butter and different chocolate mixtures scaled on 100wt% cocoa butter at 55 bar and 30°C. (black bar = cocoa butter, blue bars = chocolate mixtures, the black dotted line represents the mean value)

Figure 6-29 verifies the conclusion that the scaled equilibria gas solubilities of the all mixtures are nearly similar and in the same range like the solubility in pure cocoa butter. The medial equilibrium carbon dioxide solubility in the mixtures scaled on 100% cocoa butter is around 15 wt%. To identify the influence of each component, the gas solubility is plotted against the amount of each chocolate component in the mixtures (Figure 6-30).

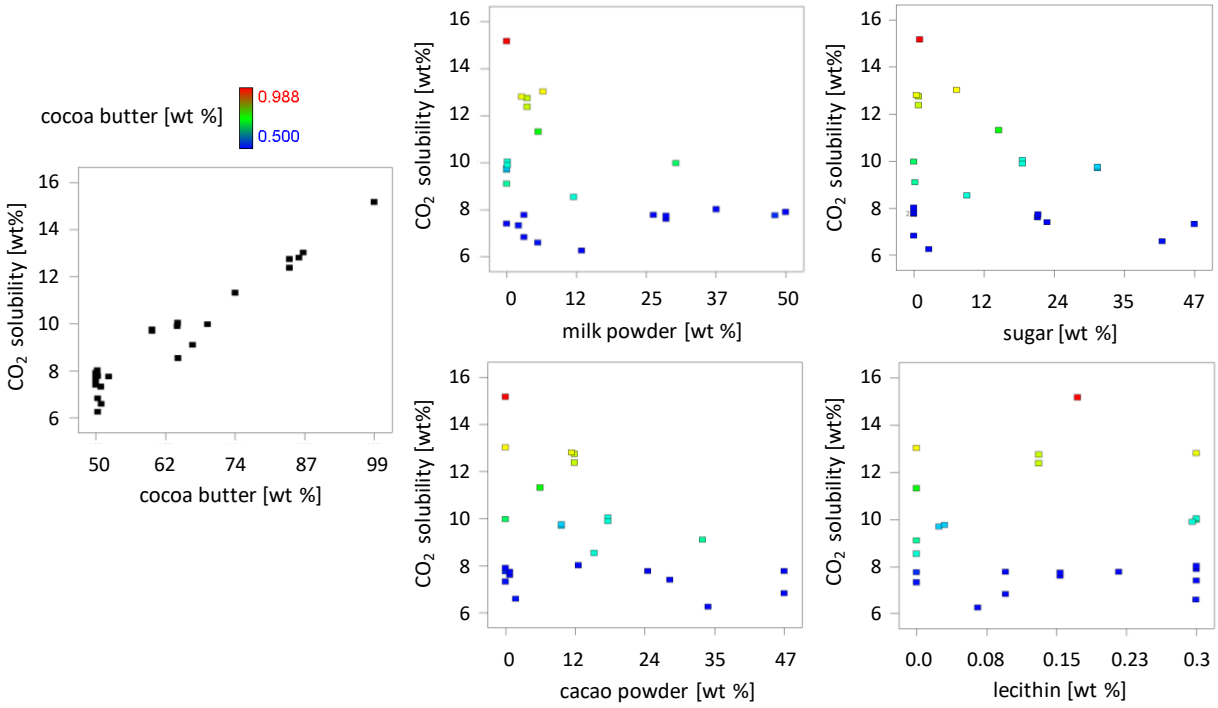

Figure 6-30: Influence of the single chocolate component amounts in the chocolate mixtures on the CO_2 solubility in the chocolate mixtures at 50 bar, 30°C and equilibrium

The carbon dioxide solubility increases linearly with increasing amount of cocoa butter in the mixture. An increasing amount of each chocolate particle in the mixtures leads to a decrease of gas solubility in consideration of an overall increasing amount of particles. Lecithin does not have an influence on the gas solubility in the investigated range. The gas solubility correlation for each component and the

interactions can be calculated with statistical design of experiments and plotted in a three component diagram. In order to do this, 2 components must be kept constant. In Figure 6-31 the three component diagrams show the influence of the three main particles in chocolate on carbon dioxide solubility (left hand diagram) and also the influence of cocoa butter, sugar and milk powder on the carbon dioxide solubility (right hand diagram).

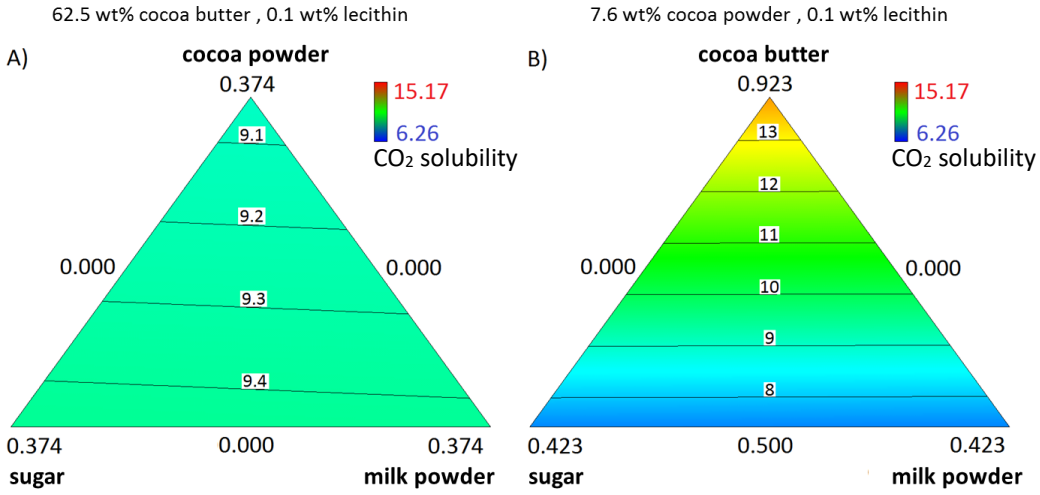

Figure 6-31: Influence of the chocolate components on the CO_2 solubility at 50 bar, 30°C and equilibrium. A) relationship between the influence of cocoa powder, sugar and milk powder B) relationship between the influence of cocoa butter, sugar and milk powder

In Figure 6-31 A) it is clear to see, that the particles in the mixtures do not influence the carbon dioxide solubility. Figure 6-31 B) show the strong influence of the cocoa butter amount, an increasing cocoa butter amount leads to strong increase of the solubility. The used linear model has a very good deviation value of R^2 = 0.989. It can be concluded that the carbon dioxide is soluble only in the fat phase, the cocoa butter. No significant adsorption of the gas molecules on the particles takes places. Because of this the gas solubility in the mixtures increases linearly with the amount of cocoa butter, due to the fact that there is more material for the dissolution of the gas. It is also interesting to understand the influence of different chocolate ingredients on the time until the equilibrium solubility is reached (equilibrium dissolution time). The equilibrium dissolution time was therefore categorised as shown in Table 6-6, because the exact equilibrium time cannot be identified by taking a sample every few hours.

Table 6-6: Categorisation of the necessary process time until equilibrium solubility is achieved for the system CO_2/chocolate mixtures at 55 bar and 30 °C

category	time till equilibria [hours]
1	less than 21
2	21 - 40
3	40 - 45
4	more than 45

Please see Figure 8-4 in appendix for plots of the equilibrium dissolution time against the amount of each chocolate component in the mixtures. Figure 6-32 shows the three component diagrams which illustrates the influence of the different particles on the time until equilibrium solubility is reached.

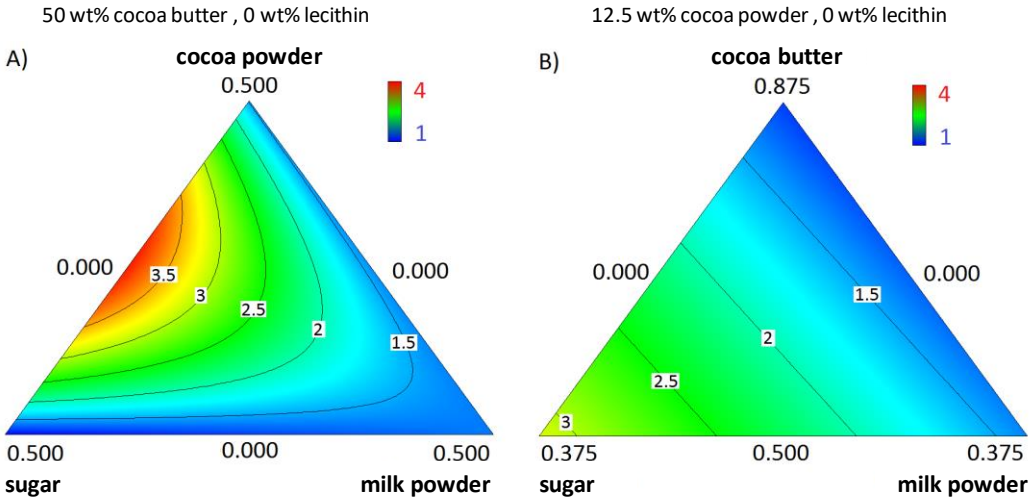

Figure 6-32: Influence of the chocolate components on the CO_2 equilibrium dissolution time at 50 bar, 30°C and equilibrium. A) relationship between the influence of cocoa powder, sugar and milk powder B) relationship between the influence of cocoa butter, sugar and milk powder

The triangle plot shows that the time till the equilibrium solubility is reached is influenced by the composition of the chocolate. For the calculation of the interactions of all components a quadratic model was used, which leads to a deviation of $R^2 = 0.677$. Especially in the boundary area of the triangle diagrams the error of the quadratic model is very high. Because of this only first trends of the component influence on the equilibrium dissolution time can be identified. In Figure 6-32 A) it is illustrated that high amounts of cocoa powder in interaction with sugar leads to long equilibrium dissolution times. The long equilibrium dissolution times with increasing sugar amount, shown in Figure 6-32 B), mirror the interactions with cocoa powder which was kept constant at 12.5 wt% in this illustrated triangle diagram. To identify the component influence the three chocolate particles were each mixed with cocoa butter and investigated in the high pressure process with carbon dioxide at 55 bar and 40°C. In Figure 6-33 scaled carbon dioxide dissolutions in the three different particle/cocoa butter mixtures are given for a time range up to 180 hours. The amount of particles in the cocoa butter is the maximum possible, whilst still maintaining a processable viscosity (including 0.3wt% lecithin).

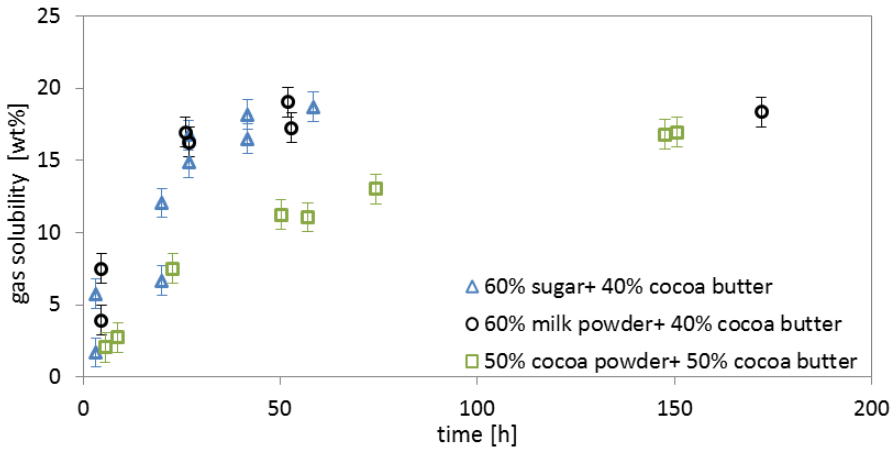

Figure 6-33: Influence of the single particles in cocoa butter on the CO_2 dissolution in CO_2 aerated mixtures, scaled on 100wt% cocoa butter, at 55 bar and 40°C as function of the dissolution time (Δ 60wt% sugar powder + 40wt% CB, ○ 60wt% milk powder + 40wt% CB, □ 50wt% cocoa powder + 50wt% CB)

In comparison with pure cocoa butter, the dissolution speed decreases when particles are added to the cocoa butter, as illustrated before in Figure 6-28. The results show, that the mixture of cocoa butter with sugar or milk powder reaches equilibria earlier after around 50 hours compared to the cocoa powder/cocoa butter mixture with 150 hours. It can be concluded that cocoa powder reduces the speed of gas dissolution in the cocoa butter more than sugar or milk powder. The time dependent dissolution in sugar/cocoa butter and milk powder/cocoa butter systems show no significant differences. The reason for the reduced gas dissolution speed resulting from adding cocoa powder could be due to the cocoa butter trapped inside the cocoa powder particles. For the experiment a low defatted cocoa powder containing 22 wt% cocoa butter was used. This cocoa butter is trapped inside the cocoa powder particles and not easily available like the free additional added cocoa butter in the mixture. It appears that the carbon dioxide starts to solute in the free cocoa butter and then into the particles. Diffusion limitation could therefore be a reason for the reducing gas dissolution speed. Another reason could be the structure difference between the three chocolate particles. Figure 6-34 show the particle structures of sugar, cocoa powder and milk powder.

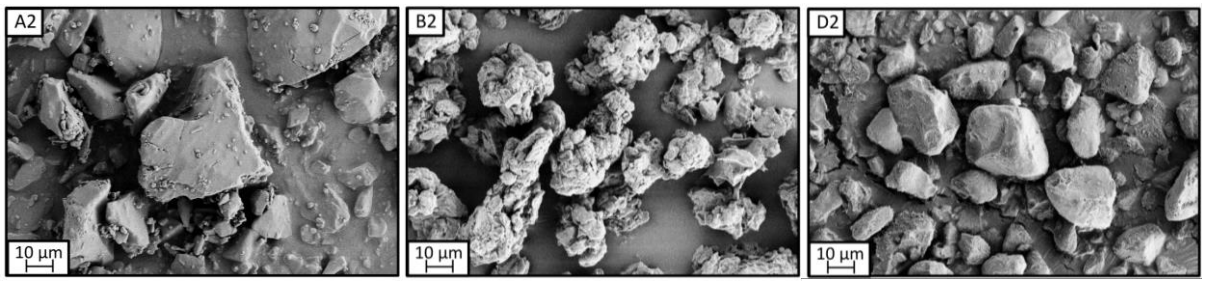

Figure 6-34: electron microscope pictures of the used (A2) sugar powder, (B2) sieved cocoa powder, and (D2) milled and sieved milk powder; 2000x magnification

The structure of both the sugar and milk powder particles is very dense and flat. Cocoa particles have a more porous and rough structure. Due to this irregular structure it could be possible that the free cocoa butter infiltrates inside the cocoa particles and this leads to a diffusion limitation of the gas inside the fat as described before. A further explanation for the slower increase of the gas dissolution

could also be the viscosity of the different mixtures. In Table 6-7 the shear viscosities of the three single particle/cocoa butter mixtures and pure cocoa butter are given for a constant shear rate.

Table 6-7: shear viscosity of the particle/cocoa butter mixtures at a shear rate of 0.1 1/s and 40 °C

	shear viscosity [Pa s]
cocoa butter	0.064 ± 0.005
60 wt% sugar + 40 wt% cocoa butter	20.5 ± 2.7
60 wt% milk powder + 40 wt% cocoa butter	17.2 ± 14.0
50 wt% cocoa powder + 40 wt% cocoa butter	55.3± 19.0

The results show some differences in the viscosities. Cocoa butter has the lowest viscosity compared to the mixtures of cocoa butter with single chocolate particles. Mixing of cocoa butter with milk powder or sugar leads to lower viscosities than with cocoa powder, as a result of the higher surface area of cocoa particles. The increase of viscosity leads in the same range to a decrease of the dissolution speed. The equilibria are reached after around 4 hours for the system CO_2/cocoa butter and after around 50 hours for the systems CO_2/sugar or milk powder mixture and after around 150 hours for the system CO_2/cocoa powder mixture. The higher viscosity of the cocoa powder mixture could therefore also be a reason for the slower gas solubility kinetic compared to the sugar and milk powder mixture. Three real chocolates mixtures were aerated to identify effects of multi component chocolate mixture on the gas dissolution speed. In Figure 6-35 the change in CO_2 dissolution with time in dark, milk and white chocolate is shown.

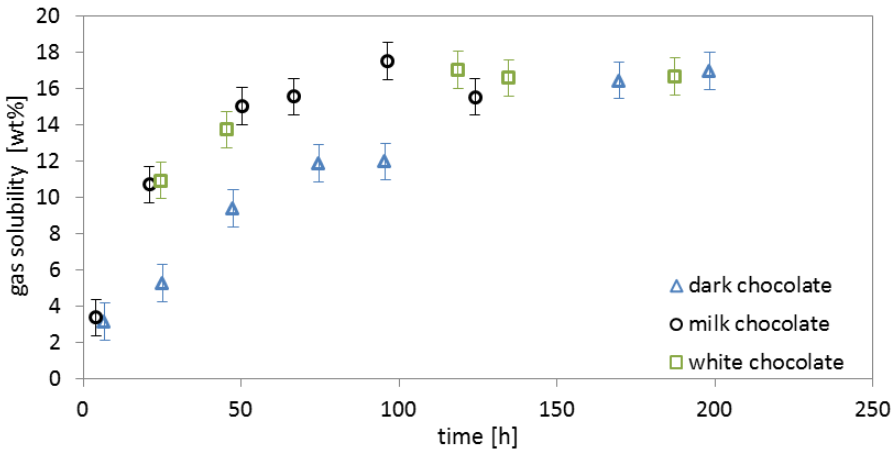

Figure 6-35: Influence of different chocolate compositions on the CO_2 dissolution in CO_2 aerated chocolates, scaled on 100wt% cocoa butter, at 55 bar and 40°C as function of the dissolution time (Δ dark chocolate, ○ milk chocolate, □ white chocolate)

Carbon dioxide shows a slower increase in dissolution for dark chocolate compared to milk and white chocolate. In dark chocolate equilibrium is reached after around 170 hours and in milk or white chocolate after around 50 hours. The cocoa powder amount is 23.4 wt% in the dark chocolate and 7% in milk chocolate (Table 4-4). Again it can be concluded that the high cocoa powder amount in the dark chocolate reduces the speed of gas dissolution. The reason again could be a diffusion limitation due to the fat which is hidden in the pores of the irregular particles and the 20wt% of cocoa butter trapped

in the cocoa powder particles which are not easily available like the free additional added cocoa butter in the mixture. Carbon dioxide starts to solute in the free cocoa butter and then into the particles. Diffusion limitation could therefore be a reason for the reducing gas dissolution speed. White chocolate does not contain cocoa powder and the amount in milk chocolate is very low, meaning there was no measurable difference between the CO_2 dissolution speed in milk and white chocolate. Viscosity differences of the chocolates could also impact the gas dissolution speed. In Table 6-8 the shear viscosities of the three chocolates are given for a constant shear rate.

Table 6-8: shear viscosity of the three chocolates at a shear rate of 0.1 1/s and 40 °C

	shear viscosity [Pa s]
dark chocolate	64.2 ± 3.1
milk chocolate	68.5 ± 3.6
white chocolate	78.4 ± 10.1

The viscosities of the three chocolates are higher than the viscosities of pure cocoa butter and also of the single particle mixtures (Table 6-7). Dark and milk chocolate show similar viscosities, which are lower than the viscosity of white chocolate. Therefore the gas dissolution speed is in contrast to these findings. For real chocolates it can be said, that the viscosity of the lipid phase does not significantly influence the carbon dioxide dissolution speed.

In conclusion it can be said, that carbon dioxide is dissolved only in the cocoa butter and that no significant adsorption of the gas molecules on the particles takes places. Because of this the gas solubility in the mixtures increases linearly with the amount of cocoa butter. Additionally it can be concluded that high cocoa powder amounts reduces the speed of gas dissolution in different chocolate mixtures. The reason could be trapping of cocoa butter within the porous and rough cocoa particle structure and the 22wt% present within the cocoa powder particles themselves. This leads to a diffusion limitation of the gas inside the fat and a reducing speed of gas dissolution. Furthermore it seems that the viscosity of the chocolate itself does not significantly influence the carbon dioxide dissolution speed.

6.3.2 Effect of Chocolate Composition on the Foam Structure

The effect of chocolate composition on the gas solubility was described previously. In this chapter the influence of chocolate composition on the foam structure is discussed. Cocoa butter and Nestlé milk chocolate were therefore aerated with carbon dioxide at 70 bar and 40°C. The comparison of the micro CT pictures of equilibrium state samples are given in Figure 6-36.

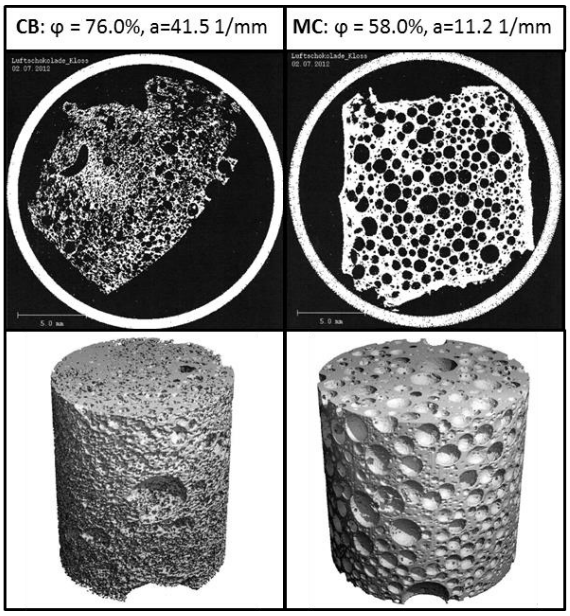

Figure 6-36: Comparison of the foam structure of CO_2 aerated cocoa butter (CB) and Nestlé milk chocolate (MS) at approximately 70bar, 40 °C and equilibrium (φ =porosity, a=specific surface)

The aerated cocoa butter foam has a different structure compared to the Nestlé milk chocolate foam. The cocoa butter foam is much more porous and has a higher specific surface area than the milk chocolate foam. Another visible difference is the shape of the gas cavities. In milk chocolate the bubbles are nearly spherical but the cocoa butter foam looks more like a sponge with a networked structure and no spherical bubbles. A reason for the strong structural differences could be related to the significant difference in viscosity. Because of the large number of particles in the continuous fat phase, the Nestlé milk chocolate has a much higher shear viscosity of 86.4 ± 16.4 Pas compared to pure cocoa butter with 0.064 ± 0.005 Pas at 40°C and a shear rate of 0.1 1/s. The high viscosity of the chocolate stabilizes the foam which leads to spherical bubbles. The low viscosity of the cocoa butter does not stabilize the foam so easily and this leads to a spongy ruptured structure through gas release. For a detailed comparison of the foam structure parameters of cocoa butter and Nestlé milk chocolate the lipids were aerated with carbon dioxide at different pressures and temperatures, the results are given in Figure 6-37.

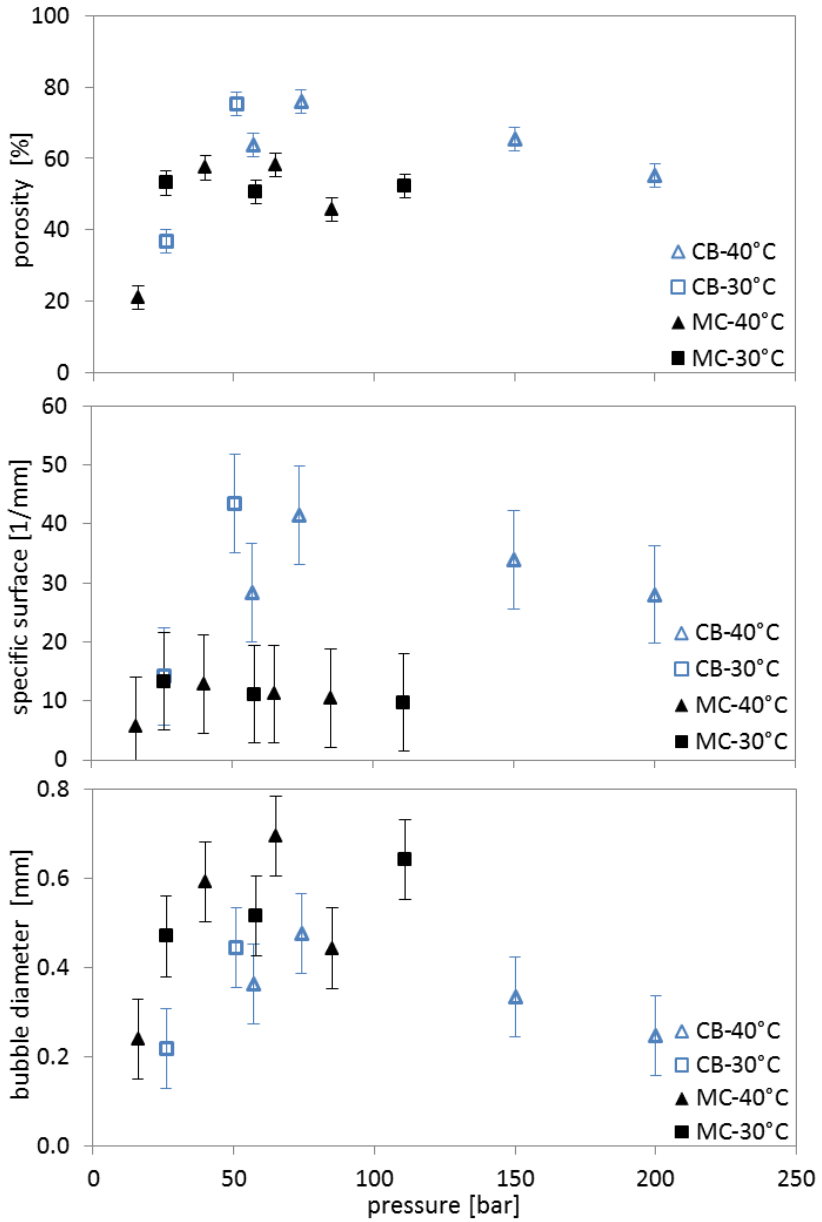

Figure 6-37: Influence of pressure on the porosity, the specific surface and the bubble diameter of CO_2 aerated cocoa butter and Nestlé milk chocolate at 30°C and 40 °C (□ cocoa butter 30°C, Δ cocoa butter 40°C, ▪ milk chocolate 30°C, ▲ milk chocolate 40°C)

These results show that higher pressures promote the solubility of gas in cocoa butter as well as in chocolate. At approximately 40-50 bar a maximum porosity value of 50% is reached, above which any further pressure increase does not change the porosity. These results are also discribed in chapter 6.2.1. Additionaly it can be said that cocoa butter foams have higher porosities than those produced from chocolate. For the Nestlé milk chocolate tested, the maximum porosity value achievable was 50-60% and for pure cocoa butter 60-75%. The reason could be the higher gas solubility in pure cocoa butter compared to chocolate and the different foam structures produced because of different stabilities. The specific surface area of the cocoa butter foam was higher than of milk chocolate because of the very porous spongy structure which leads to a higher surface compared to the spherical bubbles obtained in the chocolate. The calculated equivalent bubble diameter of the cocoa butter

foam cannot be considered as a meaningful indicator of the bubble size. This is because there are no spherical bubbles but instead a spongy highly porous structure for the cocoa butter foam. However Figure 6-37 shows a larger bubble diameter obtained in the milk chocolates compared to the cocoa butter as also illustrated in the micro-CT foam pictures (Figure 6-36).

After comparing the foam structure of aerated cocoa butter with aerated milk chocolate, the influence of each component present in the chocolate was investigated by using a statistical design of experiments (see chapter 5.1). The composition of 25 chocolate like mixtures (Table 4-5 in chapter 4.2.1) was calculated. As described before, the compositions consisted of cocoa butter, sugar, cocoa powder, milk powder and lecithin and were aerated using the high pressure process (see chapter 4.2) with carbon dioxide at constantly 55 bar and 30°C. The comparison of the resulting foam porosities of the 25 chocolate recipes compared to cocoa butter is given in Figure 6-38.

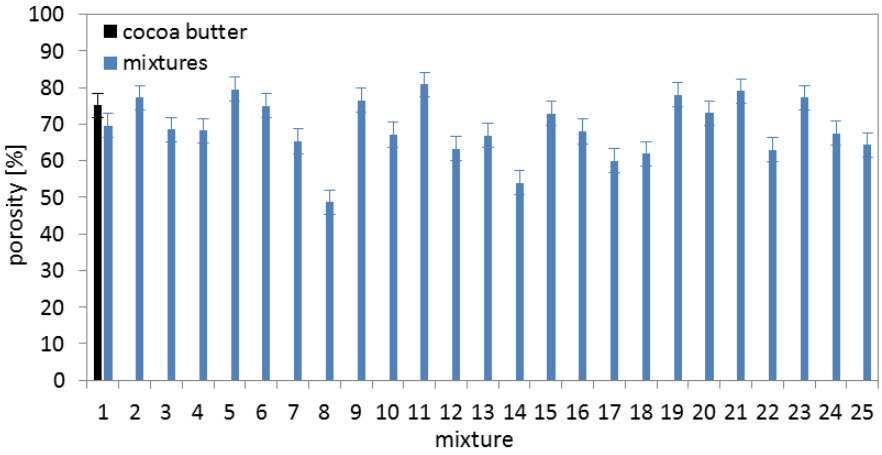

Figure 6-38: Comparison of cocoa butter foam porosity with 25 chocolate mixtures foam porosities, aerated with CO_2 at 55 bar and 30°C. (black bar = cocoa butter, blue bars = chocolate mixtures)

Figure 6-38 shows that the 25 investigated aerated chocolate mixtures have foam porosities ranging from 49% up to 81% depending on the composition. Pure cocoa butter (black bar) also has a porosity in the same range as the mixtures of around 75%. These results show that chocolate composition influences the aerated foam porosity. Figure 6-39 compares the bubble diameters of the 25 chocolate foams with those for cocoa butter.

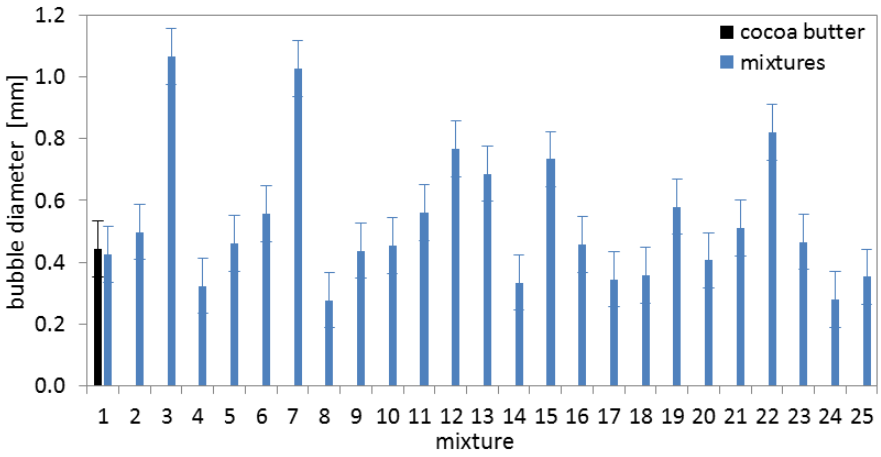

Figure 6-39: Comparison of the equivalent bubble diameter of CO_2 aerated cocoa butter and different chocolate mixtures at 55 bar and 30°C. (black bar = cocoa butter, blue bars = chocolate mixtures)

The equivalent bubble diameters of the 25 chocolate mixtures varies from 0.28mm up to 1.07mm depending on the composition. Pure cocoa butter has a bubble diameter in similar range to the mixtures of around 0.44mm. It is clear to see, that the composition of chocolates influences the bubble size of the aerated foams as well as the porosity. Due to this it can be concluded that also the specific foam surface is effected by the chocolate composition, as shown in Figure 6-40. The specific surface varies for the chocolate mixtures from 11 [1/mm] up to 62 [1/mm] and is 44 [1/mm] for the cocoa butter.

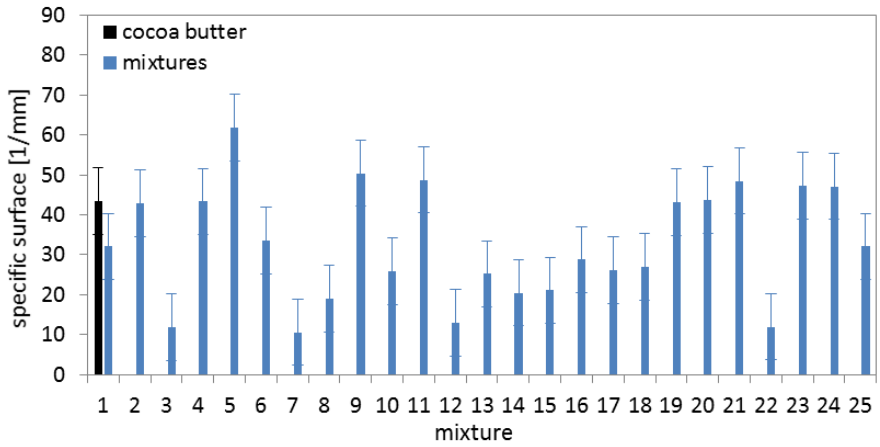

Figure 6-40: Comparrison of the specific foam surface of CO_2 aerated cocoa butter and different chocolate mixtures at 55 bar and 30°C. (black bar = cocoa butter, blue bars = chocolate mixtures)

In addition to the single foam parameters (porosity, equivalent bubble diameter and specific surface), the complete foam structure of the 25 aerated chocolate samples was compared. In order to do this, the foam structures were categorised into 8 different types as shown in Figure 6-41:

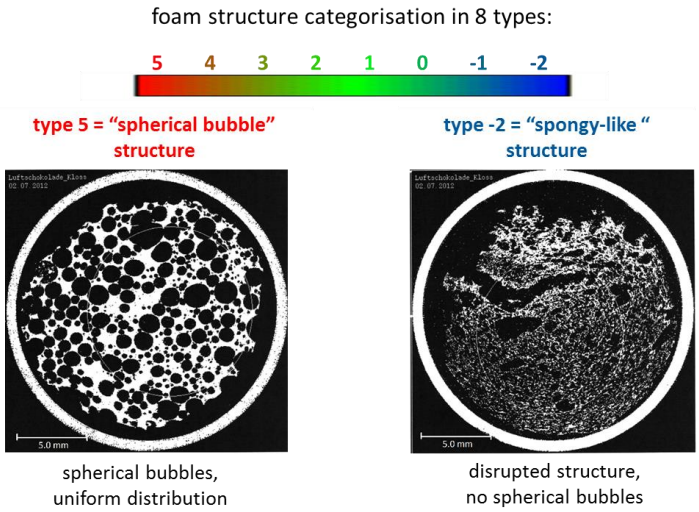

Figure 6-41: Categorisation of the 25 investigated chocolate mixture foams in 8 types

Foam type 5 was assigned to foams with spherical, uniform distributed bubbles, the lowest category -2 was assigned to foams with spongy-like, disrupted structures without any spherical bubbles. Figure 6-42 shows the dependency between the defined foam structure type and the specific surface of the foam:

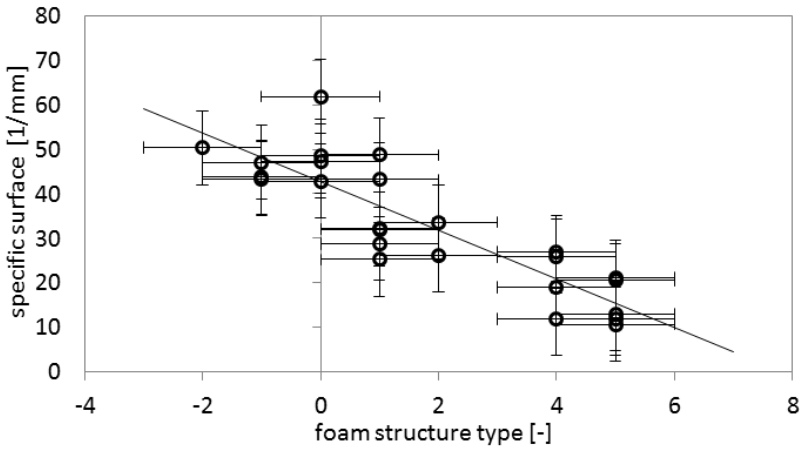

Figure 6-42: Influence of the foam structure type of the CO_2 aerated chocolate mixtures on the specific surface of the foam at 55 bar and 30°C

The results show a linear correlation between the measured specific foam surface and the defined foam structure category. In Figure 6-42 it is clear to see, that the specific surface decreases with increasing foam type. Due to this linear, inversely proportional correlation it is sufficient to evaluate only one of these two foam parameters.

The interactions between the components as well as the effects of each component on different foam parameter (porosity, bubble size, foam structre and viscosity) were calculated using a statistical design of experiments. The results were again plotted in three component diagrams in which two components must be kept constant. In Figure 6-43 the three component diagrams show the influence of the three

main particles in chocolate on foam porosity (A) and also the influence of cocoa butter, sugar and milk powder on the foam porosity (B).

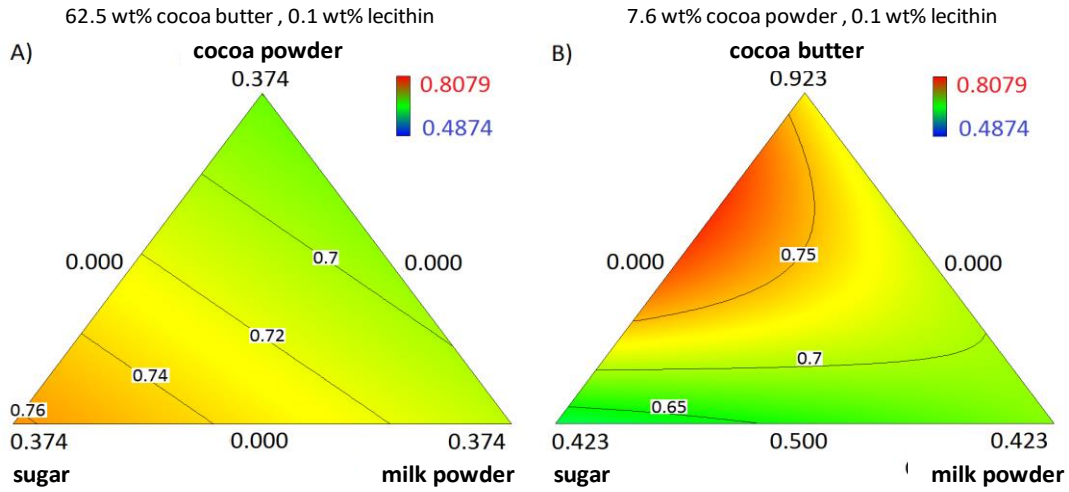

Figure 6-43: Influence of the chocolate components on the porosity of the 25 samples aerated at 50 bar, 30°C and equilibrium, A) relationship between the influence of cocoa powder, sugar and milk powder B) relationship between the influence of cocoa butter, sugar and milk powder; quadratical model

In Figure 6-43 B) it is clear to see, that the foam porosity decreases with increasing particle amounts in the mixture (sugar, milk powder or cocoa powder) and increases with increasing percentage of cocoa butter in the chocolate. This effect can be explained by the increasing gas solubility associated with increasing cocoa butter amount and thus increasing available gas volume which leads to higher porosities (see chapter 6.3.1). Additionally low interactions between cocoa butter and sugar which effected the porosity were identified. This is shown by the increasing porosity with increasing sugar content, simultaneous to increasing cocoa butter in the mixture. It is not possible to determine the effect of lecithin on the foam porosity from Figure 6-43 because in both plotted three component diagrams the lecithin amount was kept constant. The results of the quadratic model used show an increasing porosity effect with increasing lecithin amount in interaction with cocoa butter or cocoa powder. The porosity equation (6-1) of the quadratic model evaluated with statistical design of experiments shows the single ingredient effects as well as the interaction effects:

$$\begin{aligned} \text{porosity} = \; & + 0.708 \cdot \text{cocoa butter} \\ & - 0.596 \cdot \text{sugar} \\ & + 0.781 \cdot \text{milk powder} \\ & + 0.537 \cdot \text{cocoa powder} \\ & - 181.7 \cdot \text{lecithin} \\ & + 2.445 \cdot (\text{cocoa butter} \cdot \text{sugar}) \\ & + 229.9 \cdot (\text{cocoa butter} \cdot \text{lecithin}) \\ & + 231.2 \cdot (\text{cocoa powder} \cdot \text{lecethin}) \end{aligned} \qquad (6\text{-}1)$$

The three identified ingredient interaction effects have a very low influence on the porosity. Further taking into account that the model predictions are less accurate on the limits of the measurement range the interaction effects can be neglected.

In addition to porosity, the equivalent bubble diameter gives information about the influence of ingredient on foam structure. Figure 6-44 shows the influence of chocolate ingredients on the equivalent bubble diameter in three component diagrams evaluated with a linear model.

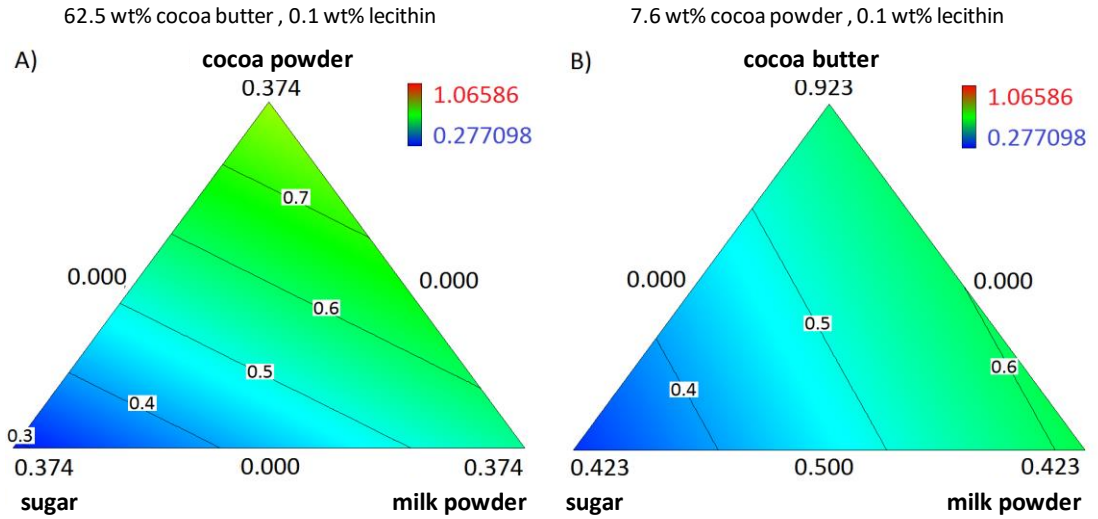

Figure 6-44: Influence of the chocolate components on the equivalent bubble diameter of the samples, aerated at 50 bar, 30°C and equilibrium, A) relationship between the influence of cocoa powder, sugar and milk powder B) relationship between the influence of cocoa butter, sugar and milk powder; linear model

It can be seen, that an increasing amount of cocoa powder leads to increasing bubbles diameters and an increasing amount of sugar to decreasing bubble sizes (Figure 6-44 A). Increasing lecithin amount also leads to decreasing equivalent bubble diameters. The enlarging effects of cocoa butter and milk powder on the equivalent bubble diameter are very low and can therefore be neglected. Increasing sugar amounts in the chocolate mixtures leads to decreasing bubble sizes due to the structure of sharp edged sugar particles which could break up bubbles keeping the bubble size low. Additionally sugar is lipophobic and will not well suspend in the lipid based chocolate and therefore a smooth cocoa butter layer does not accumulate on the sugar surface. This effect leads to a higher surface tension because more energy is required for a lipid molecule to adhereon the sugar surface compared to a lipophilic surface (for example cocoa powder). The Young-Laplace equation (see chapter 2.5.1, equation (2-34)) describes a decreasing bubble size with increasing surface tension at constant pressure. Cocoa powder, milk powder and lecithin are not as lipophobic as sugar and therefore leads to lower surface tensions and thus bigger bubbles compared to sugar. Lecithin in particular stabilises the bubble phase boundary due to its surface active character (see chapter 2.1.6) so that less coalescence occurs and overall the bubble size decreases with increasing lecithin amounts. It is assumed that cocoa powder does not exhibit surface active properties which prevent coalescence and therefore increasing amounts leads to a decreasing number of bubbles with increasing sizes.

The calculated equivalent bubble diameter is very descriptive for the bubble structure if the foam contains spherical bubbles of similar size (see chapter 4.4.4). For irregular foam structures with very different sized bubbles or even a spongy foam structure, the equivalent bubble diameter is a parameter for the ratio of gas volume to surface area. Due to this it is also important to look how the

chocolate ingredients influence the foam stucture. The defined foam structure is linear, inversely proportional to the specific foam surface and therefore it is sufficient to evaluate only one of both parameters as described before (Figure 6-42). Figure 6-45 shows the influence of chocolate ingredients on the foam structure type in three component diagrams evaluated with a linear model.

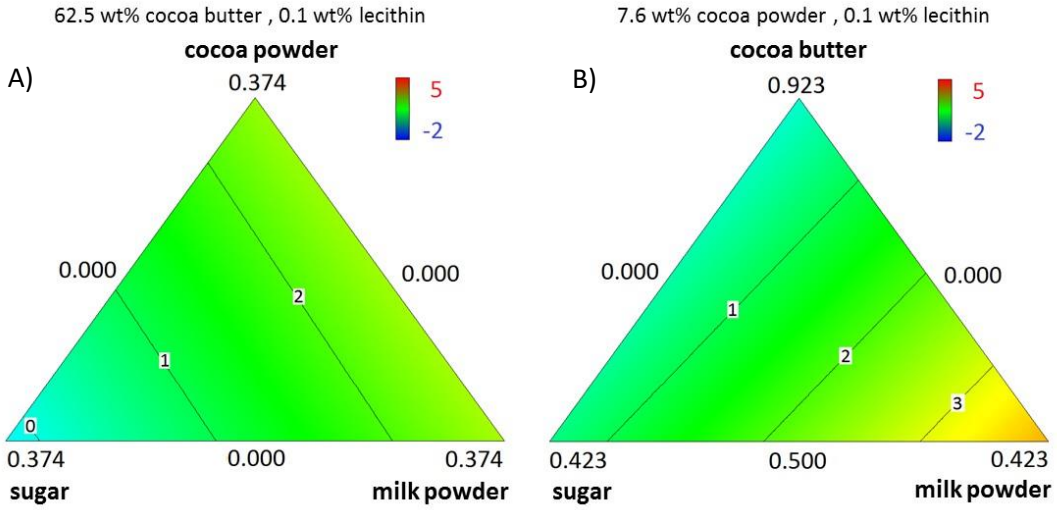

Figure 6-45: Influence of the chocolate components on the foam structure type of the samples, aerated at 50 bar, 30°C and equilibrium, A) relationship between the influence of cocoa powder, sugar and milk powder B) relationship between the influence of cocoa butter, sugar and milk powder; linear model

Figure 6-45 shows that an increasing amount of cocoa powder or milk powder leads to an increasing foam structure category (decreasing surface area) and thus to more spherical uniform distributed bubbles in the foam (see Figure 6-41). An increasing amount of cocoa butter or sugar leads in contrast to an decreasing foam structure category (increasing surface area) and thus to less spherical bubbles and more disrupted foam structures. An increasing amount of lecithin also leads to an increasing foam structure category.

Surface active substances like lecithin or caseins present in milk powder can stabilise the foam structure due to their effect on the phase boundary [26] (see chapter 2.1.6 and 2.1.5.). These surface active agents accumulate on phase boundaries reducing the surface tension, inhibiting drainage of the liquid [72] (see chapter 2.4.4) and leads to the formation of spherical bubbles. Cocoa powder also has this stabilising effect without containing any surface active substances. The reason could be the increasing viscosity with increasing cocoa powder amounts. The decreasing foam structure category with increasing cocoa butter amount can also be explained on the basis of mixture viscosity. Figure 6-46 shows the influence of cocoa butter amounts on the chocolate mixture viscosity considering the cocoa powder amounts:

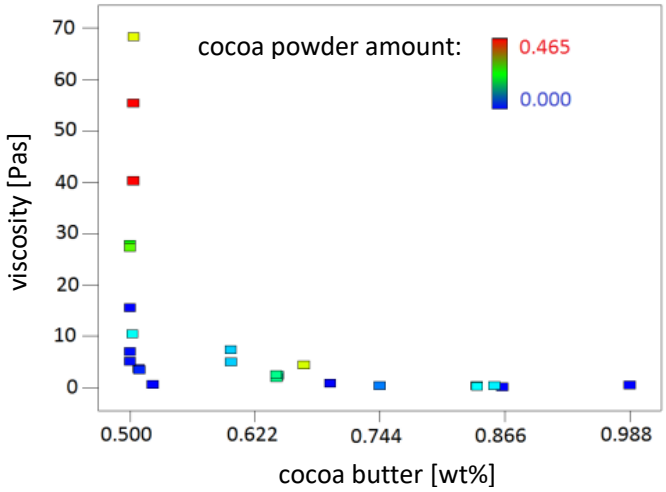

Figure 6-46: Influence of the cocoa butter amount in the chocolate mixtures on the viscosity at 40°C, atmospheric pressure and a shear rate of 0.1 1/s

In Figure 6-46 it is clear to see that the dynamic viscosity of the chocolate mixtures is high, when the cocoa butter amount is as low as possible and the cocoa powder amount as high as possible. It is apparent that the highest viscosities from around 30 Pas up to 70 Pas were measured for mixtures with the lowest cocoa butter amount of 50wt% but also in combination with high cocoa powder amounts of a minimum 25wt%. The effect of cocoa powder on the viscosity rapidly reduces with increasing cocoa butter amounts. From 75% cocoa butter in the mixture, the viscosity influencing effect of cocoa powder can be disregarded. In Figure 6-47 (A) the three component diagram shows the influence of the three particles types on viscosity for an exemplarily constant cocoa butter amount of 62.5wt%. In Figure 6-47 (B) the three component diagram shows the influence of cocoa butter, sugar and milk powder on the viscosity for an exemplarily constant cocoa powder amount of 7.6wt%.

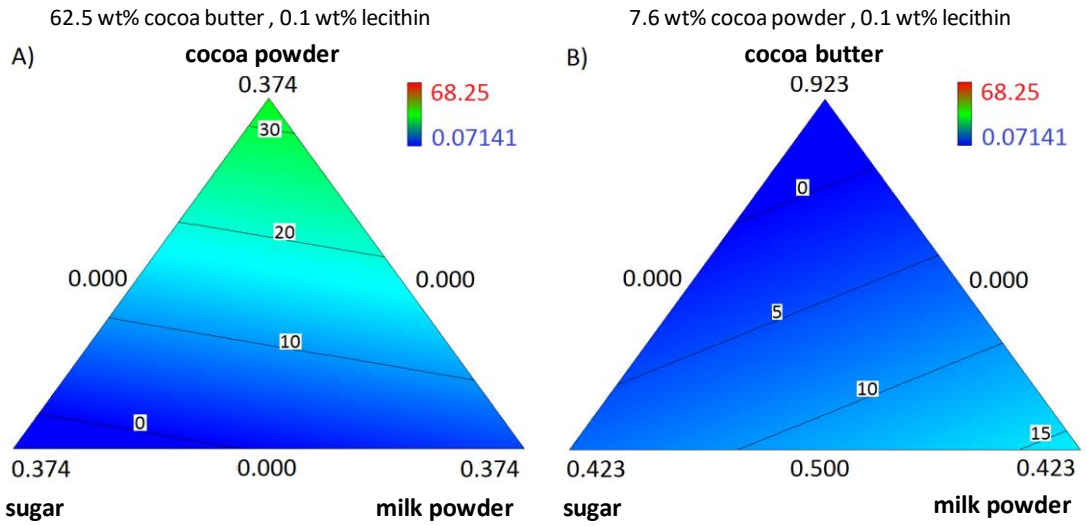

Figure 6-47: Influence of the chocolate components on the viscosity of the chocoalte mixtures at 40°C, atmospheric pressure and a shear rate of 0.1 1/s. A) relationship between the influence of cocoa powder, sugar and milk powder B) relationship between the influence of cocoa butter, sugar and milk powder, linear model

Also in Figure 6-47 (A) it is clear to see that an increasing cocoa powder amount leads to increasing viscosities for a constant cocoa butter amount of 62.5wt% in the chocolate mixture. Additionally it can be seen that increasing cocoa butter or cocoa powder amounts lead to increasing porosities as described before. High viscosities lead to lower bubble rising or rather slower outgassing and thus to higher gas volumes in the aerated chocolate foam. As a result of this, increasing cocoa powder amounts lead to an increase in foam structure category and thus to more spherical, stabilised bubbles in the foam with a low specific surface. Inversely an increasing amount of cocoa butter leads to a decreasing foam structure category and thus to less spherical bubbles and more disrupted foam structures with high specific surface.

For all experiments studying the influence of ingredients on the foam structure, only the equilibrium state in the aeration process was considered. The next step was to investigate the impact of chocolate ingredients on the foam structure, during the time until equilibrium was reached within the high pressure aeration process. The sugar, cocoa powder and milk powder were therefore each mixed with cocoa butter and aerated in the high pressure process with carbon dioxide at 55 bar and 40°C. In Figure 6-48 the porosity as well as the equivalent bubble diameter of the three different particle/cocoa butter foams are given for a time range up to 180 hours. The amount of particles in the cocoa butter is the maximum possible, whilst still maintaining a processable viscosity (including 0.3wt% lecithin).

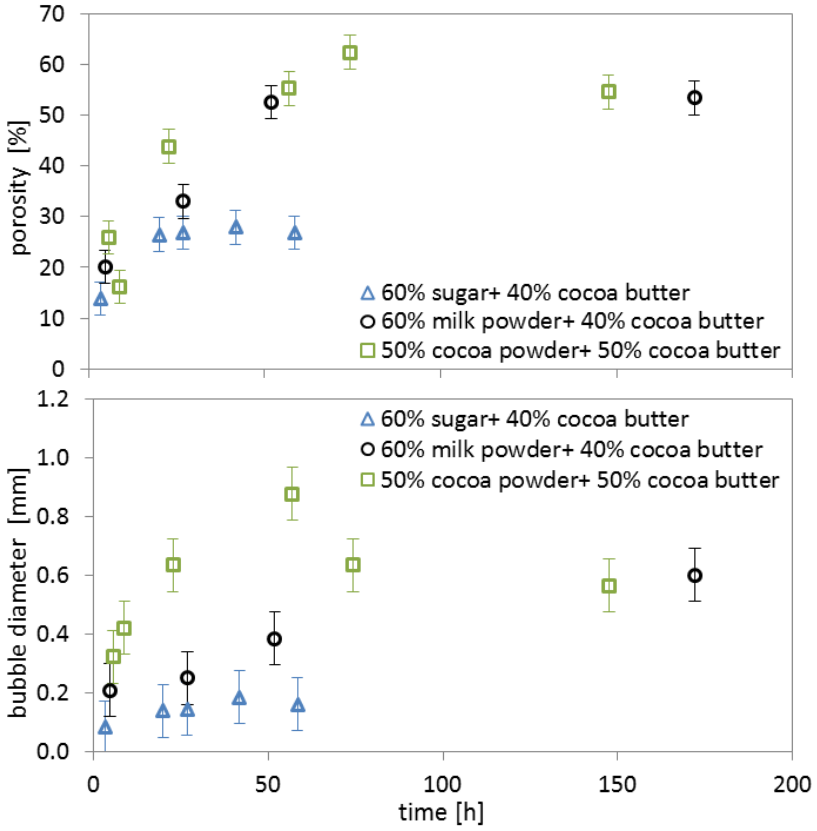

Figure 6-48: Influence of the single particles in cocoa butter on the porosity and the bubble diameter of CO_2 aerated mixtues at 55 bar and 40°C as function of the dissolution time (Δ 60wt% sugar powder + 40wt% cocoa butter, ○ 60wt% milk powder + 40wt% cocoa butter, □ 50wt% cocoa powder + 50wt% cocoa butter)

It can be seen that the porosities of all three investigated particle/cocoa butter foams firstly increase with aeration time and then reach an almost constant value, the “equilibrium porosity”. The porosities of the three single particle/cocoa butter mixtures increase approximately similarly in the first 20 hours of the aeration process. The equilibrium porosity of the sugar mixture is then reached after around 20 hours much earlier compared to the cocoa powder mixture and the milk powder mixture, taking around 50 hours. The further porosity increase of aerated cocoa powder and milk powder mixture from 20 hours up to around 50 hours leads to a higher equilibrium porosity of around 55% compared to the sugar mixture with around 25%. It has to be considered that the cocoa powder sample consists of 10wt% more cocoa butter and 10wt% less particles compared to both other mixtures due to the viscosity required for processing. A direct quantitative comparison of the porosities is therefore not possible due to the porosity increase with increasing cocoa butter amount as described before (Figure 6-43).

In Figure 6-48 it is clear to see that the equivalent bubble diameters of all three investigated particle/cocoa butter foams again increase with aeration time. In contrast to porosity the bubble diameter of the three single mixtures increases at different rates during the aeration process. The bubble diameter of the cocoa powder mixture increases the most and the bubble diameter of the sugar mixture increases the least. The bubble diameter of the sugar mixture foam reaches a relatively low constant value of around 0.2 mm during aeration. The milk powder and cocoa powder mixture has an approximately similar bubble diameter of 0.6 mm after around 100 aeration hours. This reducing effect of sugar and the increasing effect of cocoa powder (and milk powder in a low level) on bubble sizes was already described above (please see Figure 6-44). Figure 6-49 compares the foam structure micro CT pictures of the three aerated single particle/cocoa butter mixtures at equilibrium.

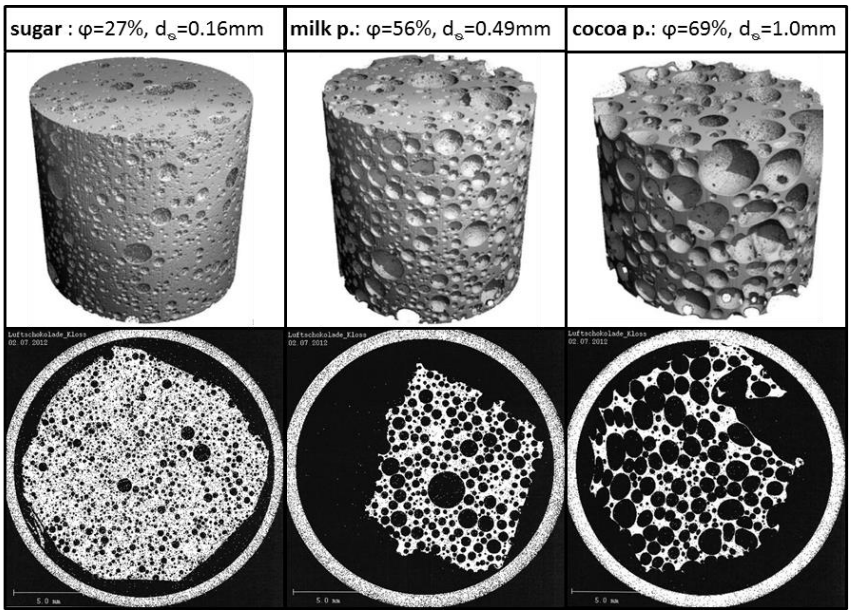

Figure 6-49: Comparisson of the foam structure of CO_2 aerated cocoa butter mixed with 60 wt% sugar, 60 wt% milk powder or 50 wt% cocoa powder at 55 bar, 40 °C and equilibrium (φ=porosity, $d_{⌀}$=equivalent bubble diameter)

In conclusion it can be said that sugar leads to very small bubbles. Milk powder generates medium sized bubbles and cocoa powder big bubbles. The foam porosities increase rapidly during the first aeration process hours until they reach a constant equilibrium porosity. Cocoa powder and milk powder has approximately similar effects on the foam porosity and leads to a high equilibrium porosity after around 50 hours of aeration. Sugar reduces the equilibrium porosity as well as the time till the equilibrium porosity is reached.

Additionally three real chocolate mixtures were aerated to investigate the interactive composition effect on the foam structure during the whole high pressure aeration process time. Therefore a milk chocolate, a dark chocolate and a white chocolate (for composition see Table 4-4) were aerated with carbon dioxide at 55 bar and 40°C. In Figure 6-50 the porosity as well as the equivalent bubble diameter of the three chocolate foams are given for a time range up to 190 hours.

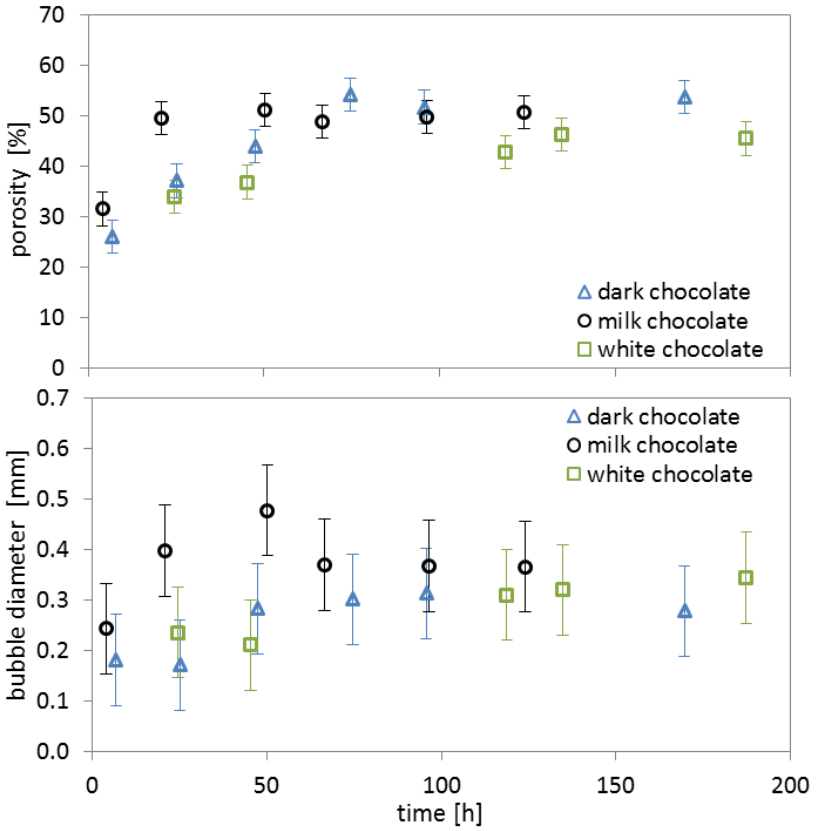

Figure 6-50: Influence of different chocolate compositions on the porosity and the bubble diameter of CO_2 aerated chocolates at 55 bar and 40°C as function of the dissolution time (Δ dark chocolate, ○ milk chocolate, □ white chocolate)

Figure 6-50 shows that the porosities of all three investigated aerated chocolate foams behave in a similar way during the aeration process, especially for the dark and white chocolate. Already all measured chocolate porosities after a few hours of aeration are very high with around 30% compared to the single particle/cocoa butter mixtures. After the porosity increase, the milk chocolate reaches a constant equilibrium porosity after around 20 hours and the milk and dark chocolate foams after around 75 hours. It can be seen, that the equilibrium porosities of all three investigated real chocolate

mixtures are in the range of 50%. It was shown above, that only sugar and cocoa butter amounts influence the foam porosity significantly. The three investigated chocolates have approximately similar cocoa butter, sugar and lecithin amounts. Only the amount of milk powder and cocoa powder vary significantly. Due to this the measured porosities of the different chocolate types show similar behaviours.

Figure 6-50 shows that the equivalent bubble diameter of the aerated dark and white chocolate foams behave in a similar way during the aeration process. The milk chocolate bubble diameter increases faster with aeration time compared to the other chocolate types. The constant equilibrium bubble diameter off all three chocolates is reached at the latest after 70 hours and is in the same range of approximately 0.3 mm. Milk chocolate has minimal bigger equivalent bubble diameters compared to dark and white chocolate during the whole aeration process but the deviations lie in the error margin. Milk chocolate exhibits slightly bigger bubbles, maybe because it contains cocoa powder and milk powder and not only milk powder like the white chocolate or cocoa powder like the dark chocolate This again leads to the assumption that similar sugar, cocoa butter and lecithin amounts in chocolates lead to approximately similar bubble sizes. Figure 6-51 compares the foam structure micro CT pictures of the three aerated chocolate types at equilibrium.

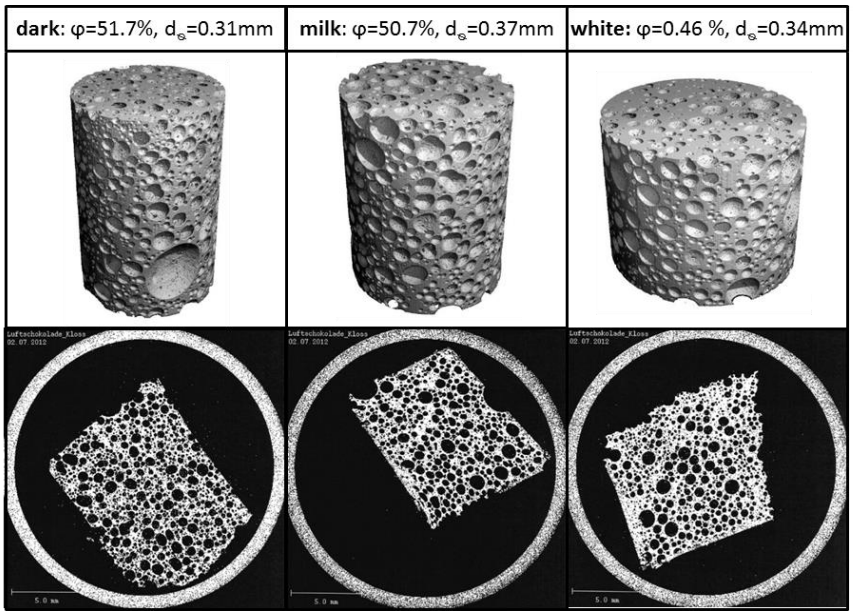

Figure 6-51: Comparisson of the foam structure of CO_2 aerated dark chocolate, milk chococlate and white chocolate at 55 bar, 40 °C and equilibrium (φ =porosity, $d_{⌀}$=equivalent bubble diameter)

Figure 6-51 confirms that dark, white and milk chocolate has approximately similar foam structures probably due to similar cocoa butter, sugar and lecithin amounts. Especially sugar was above identified to influence the foam structure of chocolate mixtures very strongly. Due to this it is important to take a further detailed look on the sugar influence.

6.3.3 Effect of Sugar

The effect of sugar on the chocolate foam structure was determined by investigating the influence of sugar amount, particle size and particle shape. Three milk chocolates with low (36wt%), medium (48wt%) and high (55wt%) sugar amount were aerated and compared to investigate the influence of sugar amount. Afterwards the influence of sugar particle size was investigated by comparing three aerated chocolates produced with icing sugar or air jet sieved sugar particle fractions with a diameter below 25 µm (d<25 µm) or between 25µm and 63µm (25 µm<d<63 µm). Finally the effect of sugar particle shape was investigated by comparing chocolates produced with spray dried round sugar particles or regular crystalline sugar (icing sugar).

Influence of the sugar amount. Three milk chocolates with different sugar amounts were produced and aerated with carbon dioxide at 40°C and 55 bar in the high pressure aeration process. The composition of the three chocolates with low (36wt%), medium (48wt%) and high (55wt%) sugar amount is given in Table 4-6 in chapter 4.2.1. In Figure 6-52 the scaled carbon dioxide dissolution, the foam porosity as well as the equivalent bubble diameter of the three chocolates with different sugar amounts are given for an aeration time range up to 175 hours.

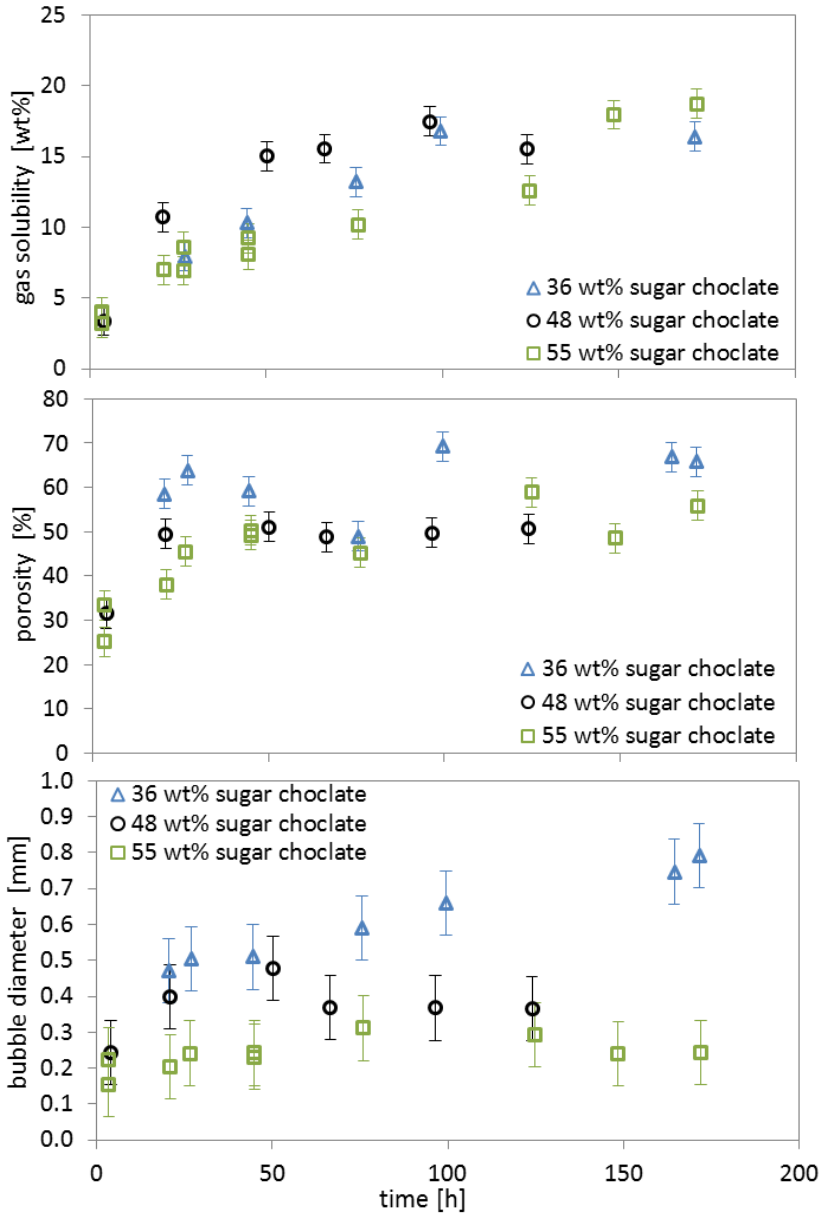

Figure 6-52: Influence of the sugar amount in milk chocolate on the CO_2 dissolution (scaled on 100wt% cocoa butter), the porosity and the bubble diameter of CO_2 aerated milk chocolate at 40 °C and 55 bar as function of the dissolution time (milk chocolate with Δ 36wt% sugar, ○ 48 wt% sugar, □ 55 wt% sugar)

Due to compositional differences of the three chocolates in terms of cocoa butter amount (26wt% - 31wt%), the gas solubility was scaled on 100wt% cocoa butter to allow a better comparison. It can be seen that the carbon dioxide dissolutions in the three chocolates do not differ significantly. Especially the equilibrium gas solubilities are approximately similar. It can be concluded that the sugar amount has no significant influence on the gas dissolution and equilibrium gas solubility, as already described in chapter 6.3.1.

The chocolate with a low sugar amount of 36wt% has higher porosities compared to the chocolates with more sugar. The porosities of the aerated chocolates with medium and high sugar amounts are approximately similar. The equilibrium porosity of the low sugar content chocolate foam is around 70% and the equilibrium porosities of the medium and high sugar amount chocolates foam are around 50%.

Above it was shown that the porosity is mainly influenced by the cocoa butter amount but this did not differ that much for the three investigated chocolates (26wt% - 31wt%, see Table 4-6 in chapter 4.2.1). This leads to the assumption that the foam porosity decreases with increasing sugar amount until a constant minimum porosity of 50% is reached. Table 6-9 shows the viscosities of the three chocolates with different sugar amounts.

Table 6-9: shear viscosity of chocolates with different sugar amounts at a shear rate of 0.1 1/s and 40 °C

	shear viscosity [Pa s]
36wt% sugar milk chocolate	53.7 ± 3.9
48wt% sugar milk chocolate	68.5 ± 3.6
55wt% sugar milk chocolate	25.8 ± 1.9

It is clear to see that the sugar amount and thus the total chocolate composition influences the viscosity. The composition of the three chocolates is given in Table 4-6 in chapter 4.2.1. Above it was already shown that cocoa butter reduces the viscosity and cocoa powder increases the viscosity (please see Figure 6-46, Figure 6-47 and Table 6-7). The 48wt% sugar milk chocolate has the lowest cocoa butter amount (26.3wt%) and therefore the highest viscosity. The 55wt% sugar milk chocolate has the lowest cocoa powder amount (4.0wt%) and therefore the lowest viscosity. The 36wt% sugar milk chocolate viscosity value lies between the both other viscosities due to a high cocoa butter (30.5wt%) and cocoa powder amount (9.2wt%).

Comparing Table 6-9 and Figure 6-52 , it is clear to see that the viscosities do not correspond to the measured porosity. The viscosities are influenced by the total chocolate composition and not only by the sugar amount. It can be concluded that chocolate viscosity is not the main influencing factor for porosity. The porosity differences must therefore be caused by the sugar particles themselves.

In Figure 6-52 it is also clear to see that the sugar amount influences the bubble diameter of the aerated chocolates. The low sugar amount chocolate has the highest equivalent bubble diameter with around 0.7mm in equilibrium and the high sugar amount chocolate has the lowest equivalent bubble diameter with around 0.25mm in equilibrium. The bubble equilibrium diameter of the medium sugar amount chocolate lies in between (around 0.3 mm). An increasing amount of sugar therefore leads to a decreasing bubble diameter in the chocolate foam. This effect of sugar particles was also described in the previous chapter. Figure 6-53 compares the foam structure micro CT pictures of the three aerated chocolates with different sugar amounts at equilibrium.

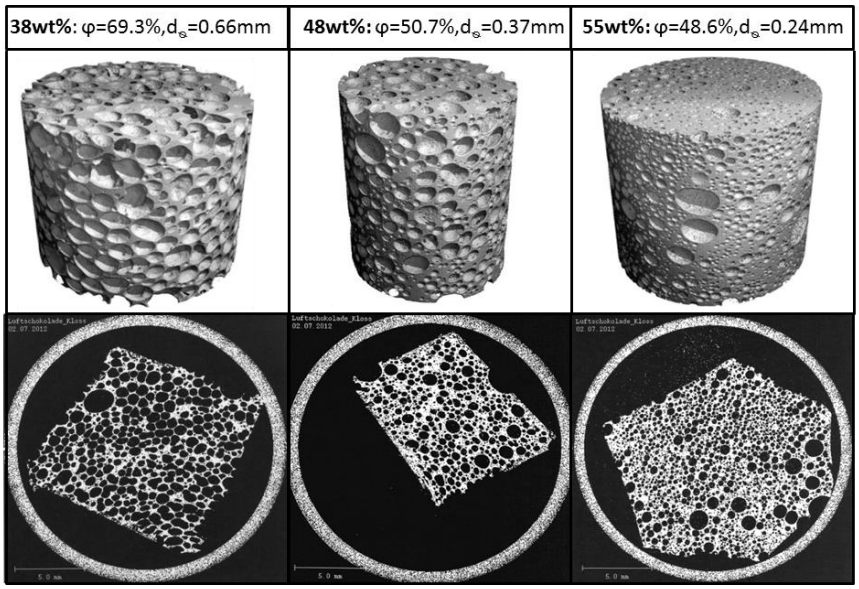

Figure 6-53: Comparisson of the foam structure of CO_2 aerated milk choclates with 38 wt% sugar, 48 wt% sugar and 55 wt% sugar at 55 bar, 40 °C and equilibrium (φ=porosity, $d_{ø}$=equivalent bubble diameter)

The micro-CT pictures of the aerated milk chocolates with different sugar amounts show clear differences in the foam structure. All the foams have uniformly distributed and spherical bubbles of a similar size. The 36wt% sugar milk chocolate has big bubbles, the 48% sugar chocolate has medium sized bubbles and the 55wt% sugar milk chocolate has small bubbles. It can be concluded that the sugar amount in aerated milk chocolates has a big influence on the foam structure. The bubble size in the foam decreases significantly for increasing sugar amounts and also the foam porosity is increased at the lowest sugar amount compared to the high and medium sugar amount chocolates. It was also explained above that increasing sugar amounts decreases the foam bubble size due to its sharp edged structure which could break up bubbles and keep the bubble size low. Additionally sugar is lipophobic and will not easily suspend in milk chocolate. This effect leads to a higher surface tension and therefore to a decreasing bubble size (Young-Laplace equation (2-34)).

Influence of the sugar particle size. In addition to the sugar amount, the influence of the sugar particle size on the foam structure was also investigated. This was important to identify if a higher sugar surface leads to the foam changing effects described above. Therefore three aerated regular milk chocolates (for composition see Table 4-4) were produced with icing sugar or air jet sieved sugar particle fractions with a diameter below 25 µm (d<25 µm) or between 25µm and 63µm (25 µm<d<63 µm) were compared. The gas solubility will not be further investigated because it was shown, that the gas solubility is equal for similar cocoa butter amounts. The separation efficiency of the air jet sieving and the achieved particle size distributions was already discussed in chapter 6.1.1 and chapter 6.1.2. It was noted, that the fractionation of icing sugar with air jet sieving was successful. In the following Table 6-10 the measured viscosities of the three milk chocolates of similar composition but with different sugar particle sizes are shown.

Table 6-10: shear viscosity of milk chocolates with different sugar particle sizes at a shear rate of 0.1 1/s and 40 °C

	shear viscosity [Pa s]
Icing sugar - milk chocolate	68.5 ± 3.6
d<25 µm sugar - milk chocolate	87.7 ± 4.7
25 µm<d<63 µm sugar - milk chocolate	58.5 ± 3.1

The milk chocolate with the smallest sugar particles and the smallest mean sugar diameter (d<25 fraction, $d_{Q3=50\%}$ = 15µm) has the highest viscosity and the milk chocolate with the biggest particles and the highest mean sugar diameter (25µm<d<63µm fraction, $d_{Q3=50\%}$ = 50µm) has the lowest viscosity. The icing sugar milk chocolate with small and bigger sugar particle sizes and a medium mean sugar diameter ($d_{Q3=50\%}$ = 27µm) has a viscosity in between the both other viscosities. The viscosity influencing effects of cocoa butter or cocoa powder amounts can be neglected in this case because of similar milk chocolate compositions used. This leads to the assumption that decreasing sugar particle sizes leads to increasing chocolate viscosities. A reason could be the higher sugar surface of smaller particles compared to bigger ones. For constant sugar amounts, the sugar surface area therefore increases with decreasing sugar particle size. For smaller sugar particles (higher surfaces area) more lecithin must accumulate on the sugar surface to suspend the hydrophilic particles in the lipid phase. This effect was also described by CHEVALLEY [27]. The lecithin amount in the three milk chocolates is 0.3wt%. For constant emulsifier amounts, it follows that the sugar surface covered with lecithin decreases with decreasing particle sizes and this also leads to an increase of viscosity. Figure 6-54 shows the foam structure micro CT pictures of the three aerated chocolates with different sugar sizes at equilibrium.

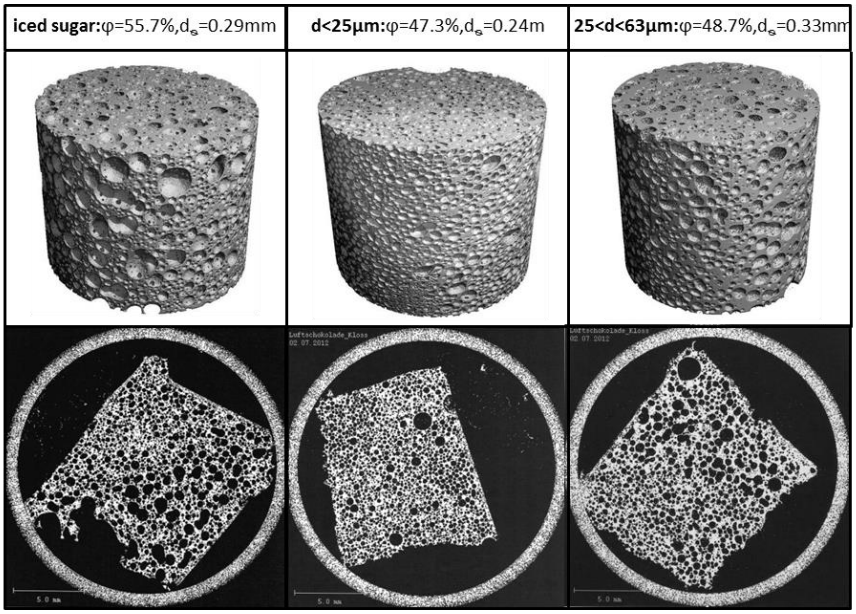

Figure 6-54: Influence of the sugar particle size in milk chocolate on the foam structure of CO_2 aerated milk chocolate at 40 °C and 55 bar and equilibrium (φ=porosity, d_s=equivalent bubble diameter)

The foam structures of the three aerated milk chocolates of similar compositions but with different sugar particle sizes show differences to each other. The milk chocolate with the smallest sugar particles (d<25µm fraction, $d_{Q3=50\%}$ = 15µm) has only very small bubbles while the chocolate with the biggest sugar particles (25µm<d<63µm fraction, $d_{Q3=50\%}$ = 50µm) has medium sized bubbles. The icing sugar milk chocolate with small and bigger sugar particle sizes and a medium mean sugar diameter ($d_{Q3=50\%}$ = 27µm) has both small and medium sized bubbles. This effect can be also seen by comparing the equivalent bubble diameters. The d<25µm sugar milk chocolate has a bubble diameter of $d_{\circlearrowleft}$= 0.24mm and the 25µm<d<63µm sugar milk chocolate of $d_{\circlearrowleft}$= 0.33mm. The equivalent bubble diameter of the icing sugar milk chocolate lies in between with $d_{\circlearrowleft}$= 0.29mm. It can be concluded that the bubble size decreases for increasing sugar surface due to increasing sugar particle sizes or increasing amounts with similar sugar size as shown above. The sugar surface covered with lecithin decreases with decreasing particle sizes and this leads to an increasing of viscosity of similar composed milk chocolates. Higher viscosities resulting from a greater sugar surface area could lead to a faster stabilisation of the aerated chocolate foam and therefore to less coalescence and smaller bubbles. Additionally sugar is lipophobic and will not easily suspend in milk chocolate. This effect leads to a higher surface tension and therefore to a decreasing bubble size with increasing sugar surface or amount (Young-Laplace equation (2-34)). Another reason could also be the sharp edged sugar structure which could break up bubbles and keep the bubble size low. This sharp surface increases with decreasing sugar particle size or sugar amount and leads to smaller bubbles. This effect was evaluated by investigating the influence of sugar particle shape.

Influence of the sugar particle shape. The influence of the sugar particle shape on the foam structure was investigated by comparing chocolates produced with regular crystalline sugar (icing sugar) or cocoa butter/crystalline sugar mixtures with cocoa butter/round sugar particles mixtures. Therefore sugar was spray dried (please see chapter 4.2.1) to achieve round spherical sugar particles. The electron microscope pictures of the particles used is given in chapter 6.1.2 (Figure 6-9). The spray dried sugar particle has a round smooth surface compared to the sharp edged structure of crystalline icing sugar. The particle size varies for both sugar samples but they are approximately similar. The sugar was spray dried by using a surface active whey protein which accumulates on the surface of the spray dried particles. In Figure 6-55 the scaled carbon dioxide dissolution, the foam porosity as well as the equivalent bubble diameter of the three mixtures are given for an aeration time range up to 165 hours.

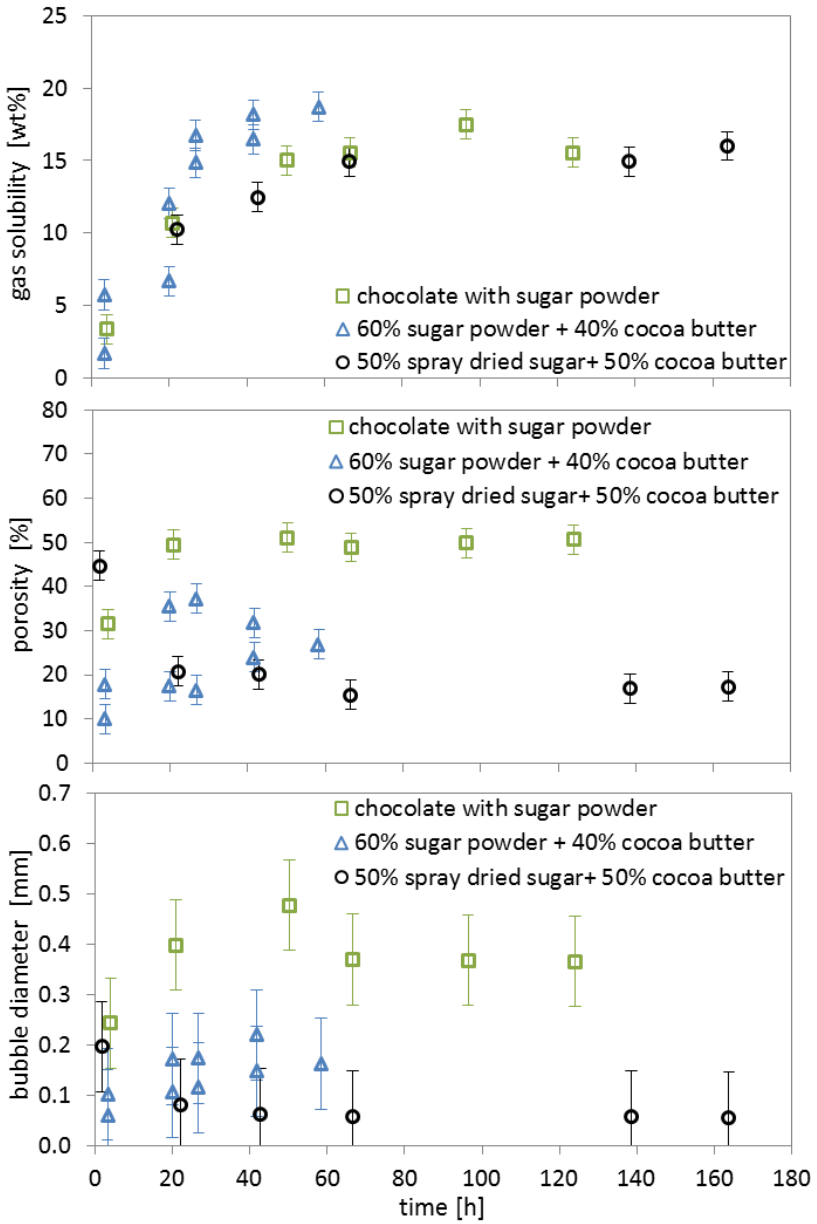

Figure 6-55: Influence of the sugar particle form in milk chocolate or cocoa butter on the CO_2 dissolution (scaled on 100wt% cocoa butter), the porosity and the bubble diameter at 40 °C and 55 bar as function of the dissolution time (□ milkchocolate with sugar powder Δ 60wt% sugar powder in 40wt% cocoa butter, ○ 50wt% spray dried sugar in 50wt% cocoa butter)

The gas dissolution in all mixtures is approximately similar and thus not influenced by the shape of the sugar particles. The porosity and bubble sizes of the aerated foams are highly influenced by the sugar particle shape as can be seen in Figure 6-55. The mixture with spray dried round sugar particles show a significantly lower porosity and bubble diameter compared to the mixtures with standard shaped sugar. Additionally a decreasing effect of porosity and bubble size with aeration time can be seen for the spherically shaped sugar mixture. The equilibrium porosity of these mixture is below 20% and the equilibrium bubble diameter around 0.05 mm and therefore much lower than for the mixtures with regular sugar shape. Figure 6-56 shows the foam structure micro CT pictures of the milk chocolate with regular sugar shape compared to the cocoa butter/spherical sugar mixture at equilibrium.

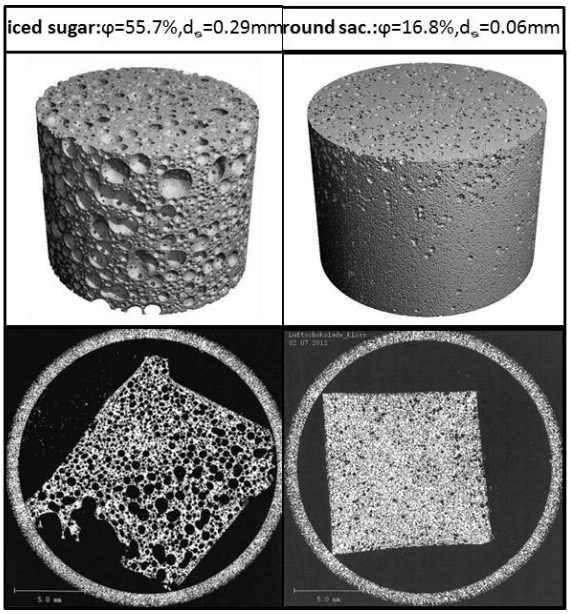

Figure 6-56: Influence of the sugar particle form in milk chocolate or cocoa butter on the foam structure of CO_2 aerated samples at 40 °C, 55 bar and equilibrium - 1. milk chocolate with crystalline saccharose (icing sugar), 2. 50wt% spray dried round saccharose + 50wt% CB (φ=porosity, d_{Θ}=equivalent bubble diameter)

The foam pictures also show the large differences in foam structure due to the sugar particle shape. The cocoa butter/spherical sugar mixtures has less very small bubbles inside and a dense foam structure with low porosity.

It can be concluded that the use of spherical sugar leads to foam with very low porosity and bubble sizes as well as less coalescence. A reason for this could be the round smooth surface compared to the sharp edged structure of crystalline icing sugar. Maybe the smooth surface of the spherical sugar is not so suitable for bubble nucleation. Another reason could be the covering of spay dried particles with surface active whey protein. These agglomerated components on the sugar surface increase the total emulsifier amount in the mixture and lead to an increase of viscosity. The reason for the significant differences in foam structure cannot be attributed to the shape of the sugar particles alone because of the surface active and foam structure influencing whey protein on the surface of the spray dried sugar particles. In order to clearly conclude how the sugar particle shape alone influences the foam characteristics, spherical sugar particles without any emulsifier present on the surface are required.

It was shown that sugar significantly influences the size of bubbles in aerated chocolates. The bubble size decreases with increasing surface area, due to increasing sugar particle sizes or increasing sugar amounts with a similar particle size.

6.3.4 Effect of Cocoa

In chapter 6.3.2 and chapter 6.3.1 it was shown that cocoa particles highly influence the foam structure and speed of gas dissolution in aerated cocoa butter and chocolate. An increase of cocoa powder leads to an increase of the bubble size and a decrease of gas dissolution speed in different chocolate mixtures compared to the other particulate ingredients used. The reason could be trapping of cocoa butter within the porous and rough cocoa particle structure, this leads to a diffusion limitation of the gas inside the fat and a reducing speed of gas dissolution. Furthermore it seems that the viscosity of the chocolate does not significantly influence the carbon dioxide dissolution speed. In this chapter the influence of different cocoa particle types, high de-oiled (10.66 wt% fat), low de-oiled (22 wt% fat) and cocoa mass (56.5 wt% fat) is investigated. Figure 6-57 shows the influence of the cocoa particle type in milk chocolate and cocoa butter on the scaled CO_2 dissolution with time.

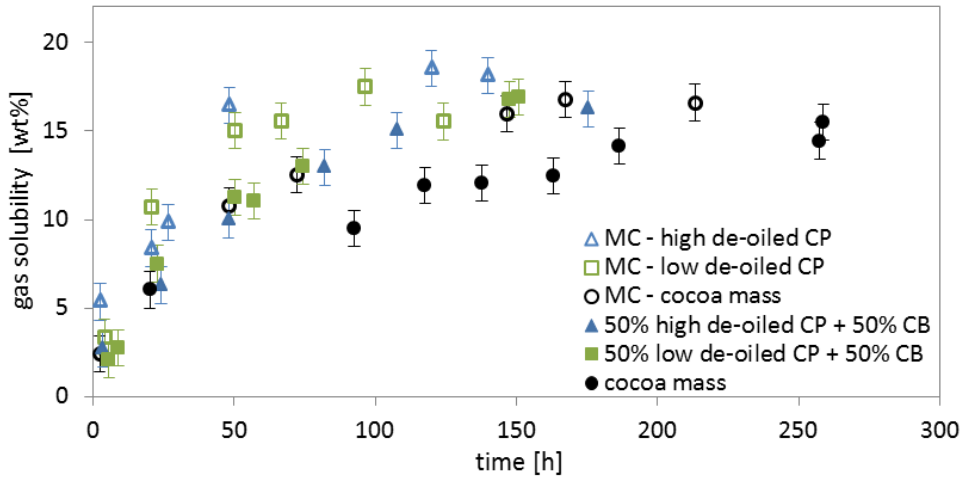

Figure 6-57: Influence of the cocoa particle type in milk chocolate (MC) or cocoa butter (CB) on the CO_2 dissolution (scaled on 100wt% cocoa butter) at 40 °C and 55 bar as function of the dissolution time (blanc symbols = milk chocolate, filled symbols = cocoa butter/cocoa powder mixtures, blue symbols = high de-oiled cocoa powder (CP), green symbols = low de-oiled cocoa powder, black symbols = cocoa mass)

The pure cocoa mass shows the slowest gas dissolution speed and thus the most diffusion limitation because of a high amount of cocoa particles and a high amount of trapped cocoa butter in the particle structure. The cocoa powder/cocoa butter mixtures show a medium gas dissolution speed and thus a medium diffusion limitation. This is because of a high amount of cocoa particles but only a smaller amount of trapped cocoa butter in the particle structure compared to the cocoa mass. In this mixture there seems to be more free available cocoa butter than in the pure cocoa mass. The fastest gas dissolution is observed in the milk chocolates with cocoa powder because there is only a low cocoa powder amount and thus less trapped cocoa butter and therefore less diffusion limitation. There is no significant difference in the gas dissolution speed in cocoa butter or chocolate with high or low de-oiled cocoa powder. The approximately 10 wt% more cocoa butter in the powder therefore makes no measurable difference in the gas dissolution speed. In contrast to this, the milk chocolate produced with cocoa mass exhibits a lower gas dissolution speed compared to the milk chocolates with cocoa powder. The gas dissolution speed is similar in cocoa powder/cocoa butter mixtures because the cocoa mass seems to have more trapped cocoa butter inside the cocoa particles and thus more of a diffusion

limitation. The equilibrium gas solubilities are similar for all investigated mixtures, however the equilibrium of pure cocoa mass with carbon dioxide is still not reached during the processing time of around 250 hours. In conclusion it can be said, that the amount of trapped cocoa butter in the cocoa particles influences the gas dissolution speed. An increase in trapped cocoa butter leads to a decrease of free available cocoa butter. This leads to a decrease in the gas dissolution speed due to a diffusion limitation because the diffusion of gas through the particles needs more time.

Figure 6-58 shows the influence of the cocoa particle type in milk chocolate and cocoa butter on the foam structure (porosity and bubble diameter) with time.

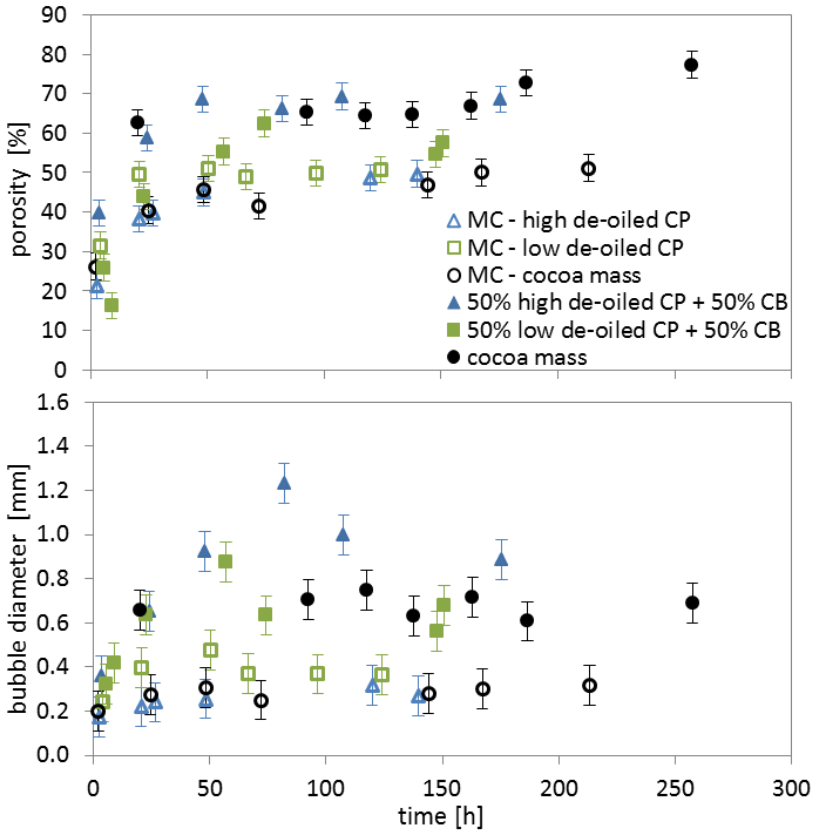

Figure 6-58: Influence of the cocoa particle type in milk chocolate (MC) or cocoa butter (CB) on the porosity and the bubble diameter at 40 °C and 55 bar as function of the dissolution time (blanc symbols = milk chocolate, filled symbols = cocoa butter/cocoa powder mixtures, blue symbols = high de-oiled cocoa powder (CP), green symbols = low de-oiled cocoa powder, black symbols = cocoa mass)

The porosities of all milk chocolates investigated with the same amount of cocoa butter are approximately similar. Both cocoa powder/cocoa butter mixtures and the cocoa mass show approximately similar porosities. The amount of trapped cocoa butter inside the cocoa particles seems to have no significant influence on the porosity. The bubble diameter seems to be similar especially for the chocolates. To take a closer look, Figure 6-59 and Figure 6-60 shows the micro CT pictures of the foam structure of all six investigated mixtures at equilibrium.

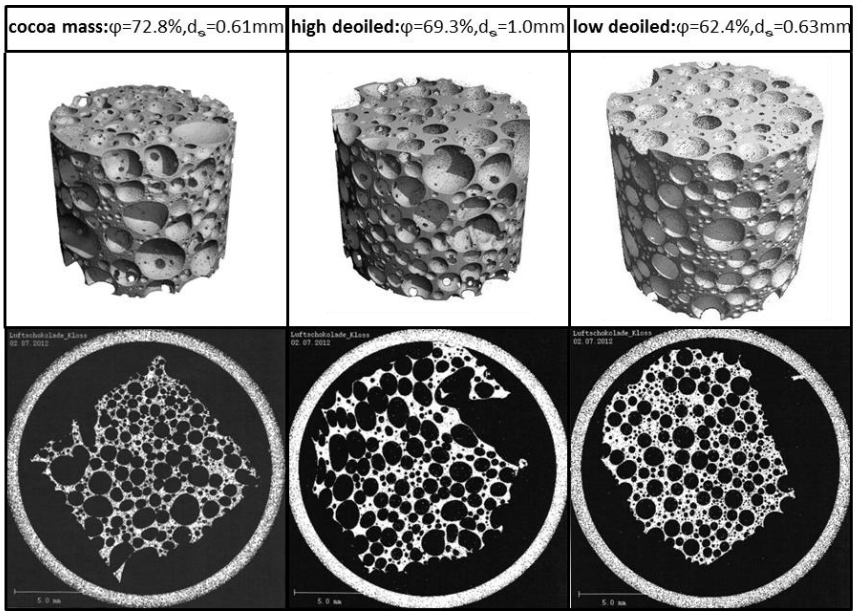

Figure 6-59: Comparisson of the foam structure of CO_2 aerated cocoa mass and 50 wt% cocoa butter mixed with high deoiled cocoa powder or low deoiled cocoa powder at 55 bar, 40 °C and equilibrium (φ=porosity, $d_{⌀}$=equivalent bubble diameter)

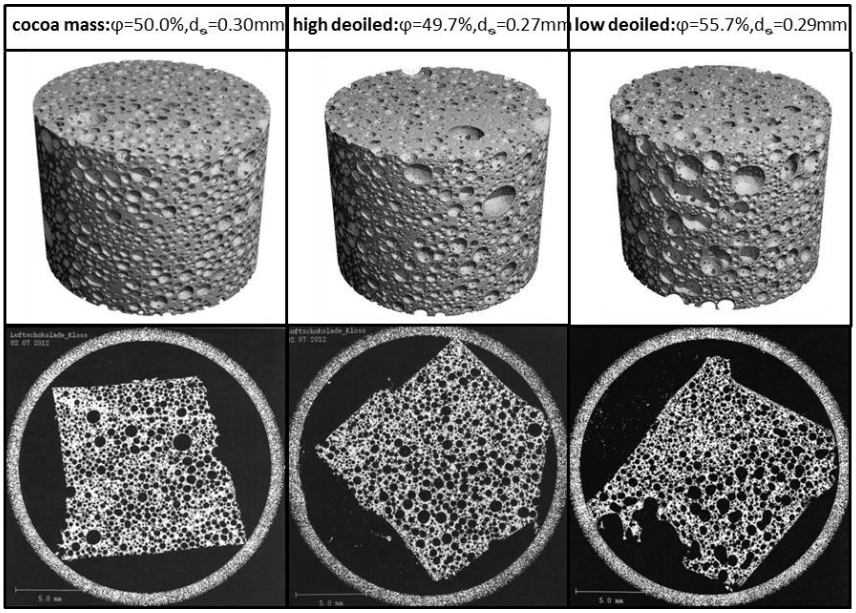

Figure 6-60: Comparisson of the foam structure of CO_2 aerated milk chocolates prepared with cocoa mass, high deoiled cocoa powder and low deoiled cocoa powder at 55 bar, 40 °C and equilibrium (φ=porosity, $d_{⌀}$=equivalent bubble diameter)

Both cocoa powder/cocoa butter mixtures and the cocoa mass show simultaneously very big and very small bubbles. This could be an indication for the diffusion limitation due to trapped cocoa butter inside the cocoa particles. The gas dissolved inside the freely available cocoa butter has enough time to coalescence during the depressurisation and crystallisation which results in big bubbles. The trapped gas inside the cocoa particles needs much more time to diffuse out of the particles. This leads to less time for coalescence during the depressurisation and crystallisation and therefore to small bubbles. The cocoa powder/cocoa butter mixtures and the cocoa mass show no drastic differences in foam

structure due to the different cocoa particle types used. It can perhaps be concluded that cocoa mass and the low de-oiled cocoa powder mixture show slightly more small bubbles compared to the high de-oiled mixture because of higher trapped cocoa butter amounts and thus more of a diffusion limitation.

The milk chocolates each have more similarly sized bubbles due to lower cocoa particle amounts and thus less trapped cocoa butter and less of a diffusion limitation. Additionally the three milk chocolates show no significant differences in terms of foam structure due to the different cocoa particle types used. It can therefore be said, that the diffusion limitation effect of cocoa particles on the foam structure of milk chocolates is insignificant.

6.4 Tempering of High Pressure Aerated Chocolate

It was shown that the dissolution of carbon dioxide in chocolate leads to a decrease in the melting point. The standard tempering method is therefore not suitable for high pressure aeration of chocolate because the formed stable crystal seeds melt during aeration. In this chapter an alternative method with intense cooling for the tempering of high pressure aerated chocolate is identified and investigated. At first the method (DSC) used for the assessment of temper quality is validated and then the effect of pressure, cooling temperature and cooling time on the crystal structure form of cocoa butter and milk chocolate is investigated. Finally the alternative tempering method is validated and compared with the standard method regarding energy consumption.

6.4.1 Validation - Effect of Heating Rate

The influence of heating rate on the melting range of cocoa butter and chocolate is described in this chapter for the validation of the DSC analytical method. The endothermic heat flow of the melting is plotted positively for a simple representation. The achieved peaks of the melting curves at different temperatures gives information about the crystal structure form of the sample. Peaks at higher temperatures correspond to more stable crystal forms compared to peaks at lower temperatures. The size of a heat flow peak illustrates the quantity of the crystal form.

At first cocoa butter, in the condition it was delivered, was melted in the DSC with different heating rates from 0.01 K/min up to 1 K/min (0.01, 0.05, 0.075, 0.1, 0.2, 0.35, 0.5, 0.1). Cocoa butter is delivered in tempered form [21] and therefore mostly consists of crystal form V. Due to the storage a transformation from form V to form VI partly occurs [12] so that both crystal forms are present. The measured heat flows with temperature are given in Figure 6-61 (A). The different measured maximal heat flows are scaled on one uniform value for better comparison because the sample weights differ slightly. The literature melting range of crystal form V and VI is marked with a blue and green bar (Table 2-3). Figure 6-61 (B) shows the influence of heating rate on the melting point (temperature on the maximum of the melting range curve).

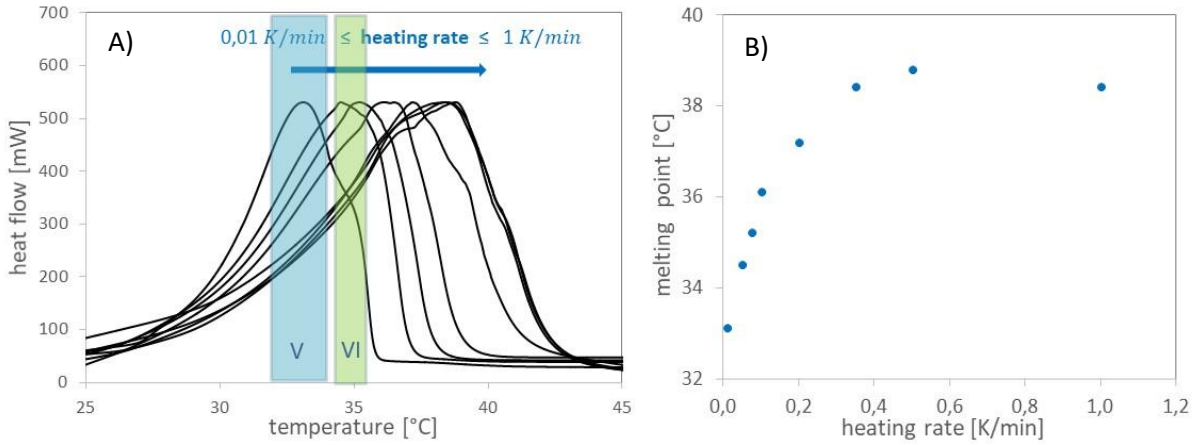

Figure 6-61: Influence of heating rate on the melting range of tempered cocoa butter (delivery condition); (A) heat flow with temperature for heating rate [K/min]: 0.01, 0.05, 0.075, 0.1, 0.2, 0.35, 0.5, 0.1 (blue bar: melting range of crystal form V, green bar: melting range of crystal form VI (Table 2-3), scaled heat flow) (B) Influence of heating rate on the melting point of tempered cocoa butter

It is clear to see, that the heating rate influences the melting range of the cocoa butter. The melting range increases to higher temperatures with increasing heating rate. This effect cannot be explained with the error of the DSC because this is only 2.5% but with the high sample volume of 7-15 g, which leads to a delayed heating and melting especially in the middle of the sample during fast heating. The result is a shifted melting range. In Figure 6-61 (B) it is shown, that a linear increase in heating rate does not lead to a linear increase of the melting point temperature. At low heating rates the melting point increases much faster and reaches a constant maximum at higher heating rates from 0.35 K/min on.

Duo to the explained effects the literature melting ranges of the different cocoa butter crystal forms (Table 2-3) cannot not be used for comparison. For an evaluation of the measured melting curves a method based melting range determination of crystal form V and VI has to be done for one defined heating rate. Therefore a medium heating rate of 0.1 K/min was used to ensure slow heating and at the same time a measuring time not too long. For the calibration, the melting curves of cocoa butter seeds consisting of pure crystal structure V was measured in the DSC and compared with cocoa butter (Figure 6-62). The two measured maximal heat flows are scaled on one value for better comparison.

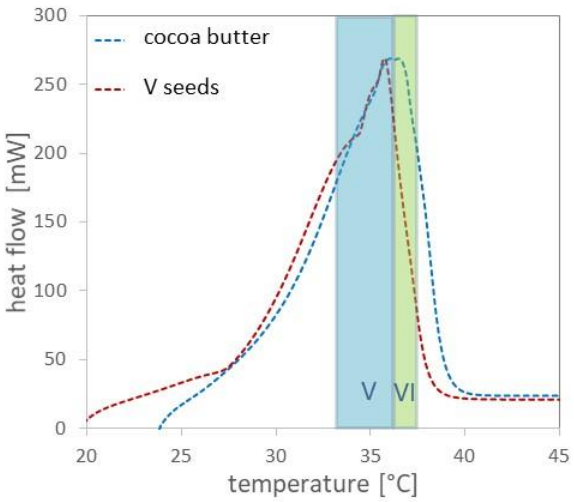

Figure 6-62: calibration of the melting ranges of crytsal form V and VI with cocoa butter seeds and cocoa butter (delivery conditions) at a heating rate of 0.1 K/min (blue bar: calibrated melting range of crystal form V, green bar: calibrated melting range of crystal form VI); scaled heat flow

The measured melting range of pure crystal form V (cocoa seeds) is also higher compared to literature values of 32°C up to 34°C (Table 2-3) at a heating rate of 0.1 K/min. For crystal form V a melting range of 34°C up to 36°C is determined with the melting curve of the seeds for the measuring method used and a heating rate of 0.1 K/min (blue bar in Figure 6-62). For crystal form VI a melting range of 36°C up to 37°C is determined with the difference in the cocoa butter and cocoa seeds melting curve (green bar in Figure 6-62).

In conclusion it can be said that the heating rate has an influence on the melting range of the cocoa butter measured with the DSC method used. The melting range of form V and VI crystals was therefore defined for a heating rate of 0.1 K/min, calibrated with cocoa butter seeds.

6.4.2 Effect of Pressure

The gas type and gas pressure is very important for the aeration of chocolate and has a big influence on the final product characteristics as shown in chapter 6.2.1. Because of this, the influence of gas type and pressure on the melting range of cocoa butter and chocolate is investigated in this chapter. Cocoa butter at delivery conditions and Nestlé milk chocolate was pressurised with carbon dioxide or nitrogen in the high pressure cell of the DSC. The melting range at elevated pressure was measured after a gas dissolution time of 1 hour to ensure the complete dissolution of gas in the sample. The melting curves of tempered cocoa butter (delivery conditions) saturated with carbon dioxide at different pressures (20, 55, 70 and 80 bar) are given in Figure 6-63. The measured maximal heat flows are scaled on one value for better comparison.

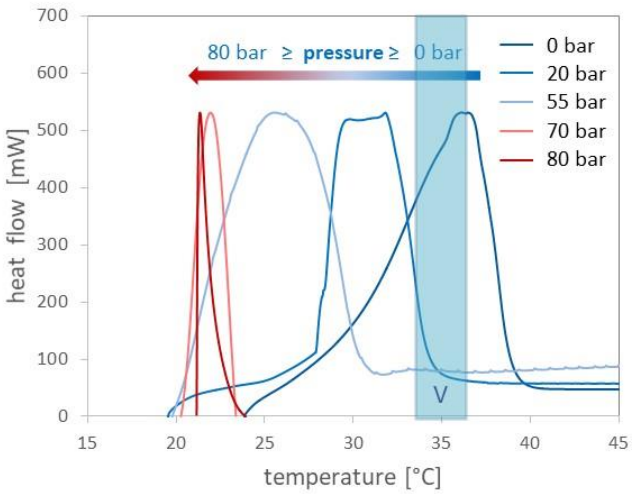

Figure 6-63: Influence of excess pressure on the melting range of tempered cocoa butter saturated with carbon dioxide at 0, 20, 55, 70 and 80 bar; heating rate: 0.1 K/min; scaled heat flow

It is clear to see, that the dissolution of carbon dioxide in the cocoa butter decreases the melting range to lower temperatures. The reason is that the carbon dioxide molecules disrupt the crystal structure of the cocoa butter and thus less energy is required for melting and the melting point decreases. The melting range decreases with increasing pressure up to around 70 bar. The melting ranges of cocoa butter at 70 bar and 80 bar are approximately similar which leads to the assumption, that pressures above 70 bar leads to no further decrease of the melting point. The reason is, that the gas solubility gradient is higher at low pressure ranges and much smaller at higher pressure ranges. Additionally two contrasting effects occur a decrease in the melting point with increasing dissolution of gas in the cocoa butter and a slight increase of the melting point with increasing hydrostatic pressure. This behaviour was also described by KOKOT, VENTER and KOLLER [11, 52, 57] (please see chapter 2.4.3).

Nestlé milk chocolate was also pressurised with carbon dioxide at pressures of 10, 20, 30 and 50 bar and measured in the high pressure cell of the DSC. The melting curves of milk chocolate saturated with carbon dioxide are given in Figure 6-63. The measured maximal heat flows are scaled on one value for better comparison.

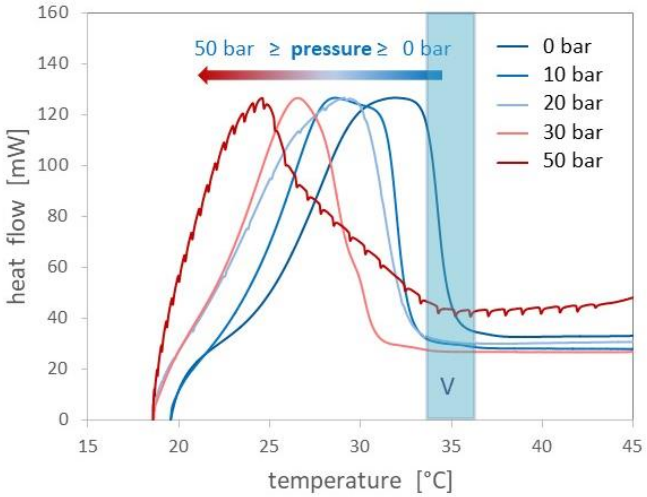

Figure 6-64: Influence of excess pressure on the melting range of milk chocolate saturated with carbon dioxide at 0, 10, 20, 30 and 50 bar; heating rate: 0.1 K/min; scaled heat flow

Milk chocolate exhibits similar behaviours to cocoa butter, a decrease in the melting temperature with increasing pressure and dissolved gas in the chocolate structure due to the crystal structure disruption. Evaluation of measurements above 50 bar could not be carried out because the melting curves of chocolate overlap with the phase transition curve of carbon dioxide to the supercritical state. In conclusion it can be said, that the melting range of cocoa butter and chocolate decreases with increasing pressure in the investigated pressure range. This makes regular tempering of carbon dioxide aerated chocolate not possible, because the solid crystal form V seeds achieved with tempering will be melted due to the melting range shift exhibited during the high pressure aeration.

The next step was the investigation of the effect of nitrogen at elevated pressures. Cocoa butter and milk chocolate were therefore aerated with nitrogen at pressures of 20 bar, 50 bar and 70 bar. The melting curves of cocoa butter and milk chocolate saturated with nitrogen at different pressures are given in Figure 6-65. The measured maximal heat flows are scaled on one value for better comparison.

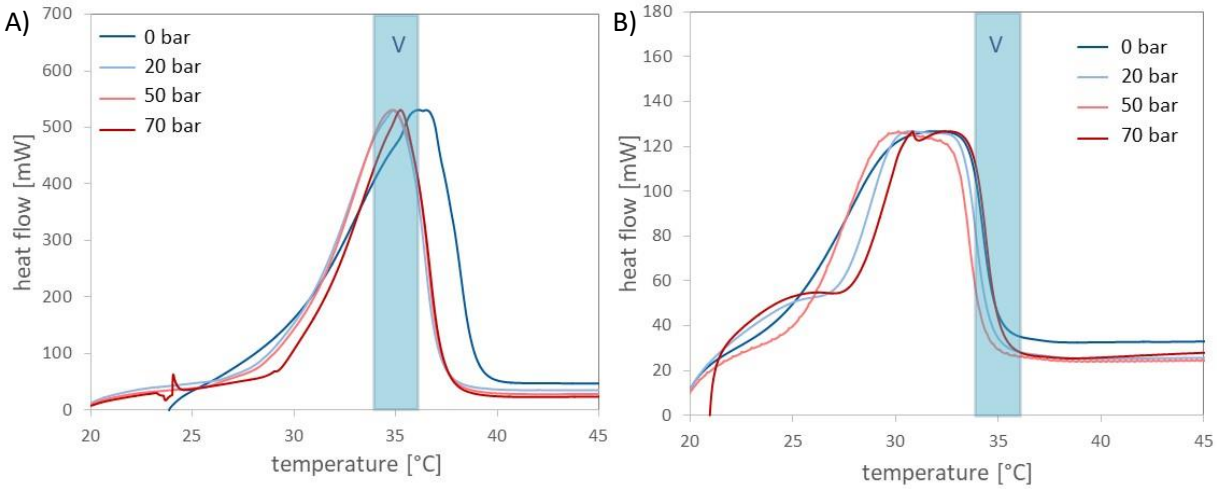

Figure 6-65: Influence of pressure on the melting range of cocoa butter (delivery conditions) (A) and milk chocolate (B) saturated with nitrogen at 0, 20, 50 and 70 bar; heating rate: 0.1 K/min; scaled heat flow

The dissolution of nitrogen at elevated pressures has no significant influence on the melting ranges of cocoa butter and milk chocolate. This behaviour was also shown by KOLLER [52]. Nitrogen has a very low solubility in cocoa butter and therefore no big influence on the crystal structure. This leads to the conclusion that tempering can be carried out in the conventional way for nitrogen aerated chocolate, when using a high-pressure process.

Figure 6-66 shows the melting points (temperature on the maximum of the melting range curve) of cocoa butter (A) and milk chocolate (B) saturated with carbon dioxide and nitrogen at different pressures. Figure 6-66 (A) compares the measured melting points of carbon dioxide saturated cocoa butter with literature values from KOKOT and VENTER [11, 57].

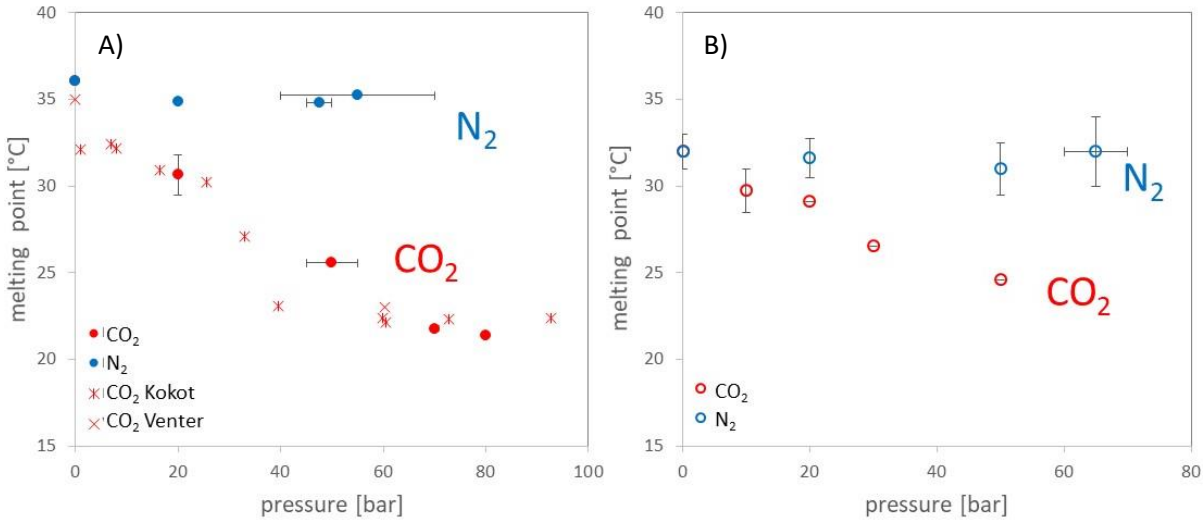

Figure 6-66: Influence of excess pressure on the melting point of cocoa butter (delivery conditions) (A) and milk chocolate (B) saturated with carbon dioxide and nitrogen ; heating rate: 0.1 K/min; measured melting points of cocoa butter compared with values from KOKOT and VENTER [11, 57]

The horizontal error bars mark the pressure drop during measurement of the DSC melting curve, so that only a pressure range and not a constant pressure can be identified. The vertical error bars show that the melting curve has a broader peak maximum and thus a melting range and not only a melting point can be identified. The error of the melting point measuring method was 1.1%, determined with dual measurement and therefore too small to mark it in Figure 6-66. In Figure 6-66 (A) it is clear to see, that the literature melting points of carbon dioxide saturated cocoa butter [11, 57] show a good agreement to the measured values. KOLLER also determined an approximately similar melting point of nitrogen saturated cocoa butter (≈ 37 °C) at different pressures up to 50 bar [52]. The melting point decrease of chocolate in the carbon dioxide system is smaller compared to that seen for cocoa butter. The milk chocolate also has a lower melting point than cocoa butter at ambient conditions (0 bar pressure) probably due to the included particles and foreign fats. These lead to a disruption of the crystal structure, less required melting energy and a lower melting point. Therefore, the effect of carbon dioxide dissolution in the cocoa butter is less pronounced. The melting point of cocoa butter and milk chocolate at higher pressures in the carbon dioxide environment is therefore approximately

similar. In the nitrogen environment, the milk chocolate melting point is lower over the whole pressure range because there is no significant gas effect but again the influence of the particles and foreign fats.

In conclusion it can be said, that the dissolution of gas in cocoa butter and milk chocolate decreases the melting point. Due to the different solubilities, carbon dioxide has a significant effect compared to nitrogen. With carbon dioxide the melting range decreases up to 70 bar and then stays nearly constant upon any further pressure increase. Milk chocolate at ambient conditions has a lower melting point compared to cocoa butter due to the particles and foreign fats present. For high pressure aeration of chocolate with carbon dioxide, regular tempering methods cannot be used but for aeration with nitrogen they can be. Therefore an alternative tempering method for the high pressure aeration with carbon dioxide has to be found. In the next chapter a method of tempering with cooling is investigated.

6.4.3 Effect of Cooling Temperature and Time

It was observed during this work that chocolate can be well tempered with cooling and that the temperature difference between the cocoa butter or chocolate and the cooling temperature influences the tempering quality. At first approximately 10 g liquid cocoa butter at 80°C without any seed crystals, was crystallised at different temperatures between -78.5°C and 6 °C for 3-4 hours. Afterwards the samples were analysed with the DSC. The achieved melting curves for different crystallisation temperatures are given in Figure 6-67. The heat flow was scaled on a sample weight of 10 g.

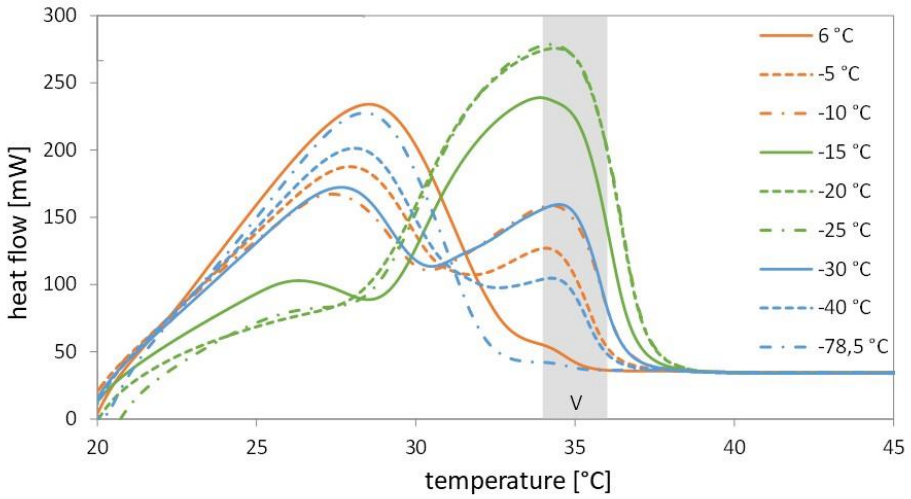

Figure 6-67: Influence of crystallisation temperature on the melting range of cocoa butter; cooling time: 3-4 hours; heating rate: 0.1 K/min; scaled heat flow

In Figure 6-67 it is clear to see that the measured cocoa butter sample show two different melting peaks with a peak maximum at approximately 28 °C and 35°C. The melting peak at 28°C represents the unstable crystal forms of cocoa butter (I – IV) and the melting peak at 35°C represents the stable crystal form V. The crystallisation of cocoa butter at -20°C and -25°C leads to the desired stable crystal form V and a negligible quantity of unstable crystal forms. Chocolate treated with these conditions is therefore well tempered. At the lowest crystallisation temperature of -78.5°C and the highest

temperature of 6°C a negligible quantity of crystal form V and mainly only unstable crystal forms are observed. Due to this no tempering of the cocoa butter at 6°C and -78.5°C takes place. The crystallisation of cocoa butter at -5°C, -10°C, -15°C, -30°C and -40°C leads to unstable and stable crystal forms in different compositions and thus only a partial tempering. Therefore a reduction of the crystallisation temperature up to -20°C/-25°C leads to an increasing amount of crystal form V in the cocoa butter. A further decrease of crystallisation temperature leads again to a decreasing amount of crystal form V.

At very low temperatures (-78.5°C) the crystallisation takes place very fast due to the high temperature difference and thus no transformation of unstable to stable crystal forms can happen. The crystallisation is driven by diffusion (please see chapter 2.3.4) and the diffusion coefficient decreases with decreasing temperature. This leads to a slowdown of transformation to crystal form V at very low crystallisation temperatures. At high crystallisation temperature (6°C) the temperature difference is not big enough to ensure a fast transformation to crystal form V. The best tempering result, with mainly form V crystals, is achieved with a crystallisation temperature of -20°C and -25°C. An optimal crystallisation temperature of -20°C was selected for further investigation because of the reduced energy requirement compared to -25 °C.

Furthermore the influence of cooling time on the tempering result of cocoa butter was investigated. Approximately 10 g of liquid cocoa butter at a starting temperature of 80°C was crystallised at -20 °C for different times between 0.5 and 4 hours. Afterwards the samples were analysed with the DSC. The achieved melting curves are given in Figure 6-67. The heat flows are scaled on a sample weight of 10g.

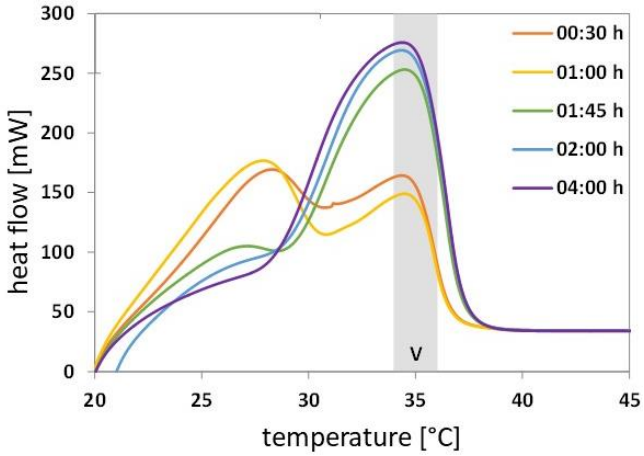

Figure 6-68: Influence of cooling time on the melting range of cocoa butter; crystallisation temperature: -20°C; heating rate: 0.1 K/min; scaled heat flow

Figure 6-67 shows with increasing cooling time, more transformation of unstable crystal forms to stable crystal form V. After approximately 2 hours of cooling it can be assumed that the cocoa butter is well tempered. The melting curves of cocoa butter cooled for 0.5 and 1 hour are nearly similar due to the bigger errors of the cooling method at low cooling times (max. 10%) compared to higher cooling times. The measuring error of the DSC was very small at only 2.5%. Nestlé milk chocolate was also cooled for different periods of time and afterwards measured with the DSC to determine the quality

of tempering. The chocolate was therefore melted for 2 hours at 60°C to destroy all crystals and then cooled for 0.5, 1, 2, 4 or 23.5 hours at -20°C. The results with a scaled heat flow on a sample weight of 15 g are given in Figure 6-69.

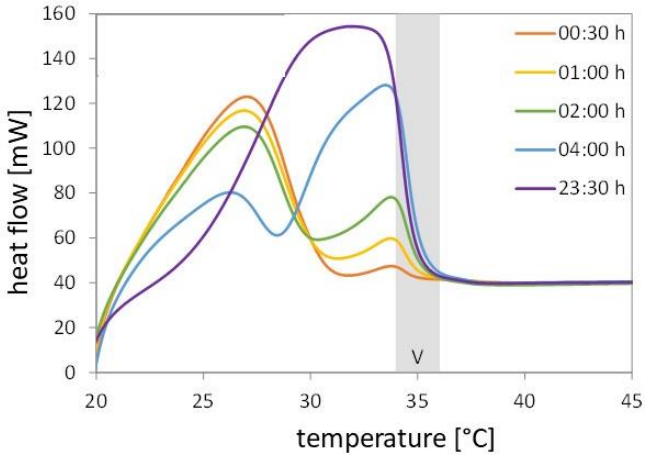

Figure 6-69: Influence of cooling time on the melting range of milk chocolate; crystallisation temperature: -20°C; heating rate: 0.1 K/min; scaled heat flow

Again it is clear to see, that increasing cooling times leads to increasing amounts of the stable crystal form V. Milk chocolate needs much longer for the transformation process of unstable to stable crystal forms compared to cocoa butter. After 2 hours of cooling, cocoa butter has nearly no unstable crystals present and milk chocolate has more unstable crystal forms than stable ones. After 4 hours milk chocolate still has unstable crystal forms and only after around 24 hours of cooling are the most of the unstable forms transformed to stable crystal forms. The reason for the slower transformation could be again the high quantity of particles in chocolate. The particles disrupt the crystal structure and hinder the diffusion driven transformation to stable crystal forms.

It was shown that a longer cooling time leads to a better tempering result. To exclude, that this is only due the heat transfer between sample and environment, the heat transfer during cooling was investigated. The heat transfer is important for the tempering of chocolate with cooling because a slower cooling of the sample leads to slower crystallisation and transformation to crystal form V. Therefore the temperature in the centre of the sample cell filled with cocoa butter (Figure 6-70 (A)) or milk chocolate (Figure 6-70 (B)) was measured for cooling temperatures of 4.5°C, -21.5°C and -38 °C.

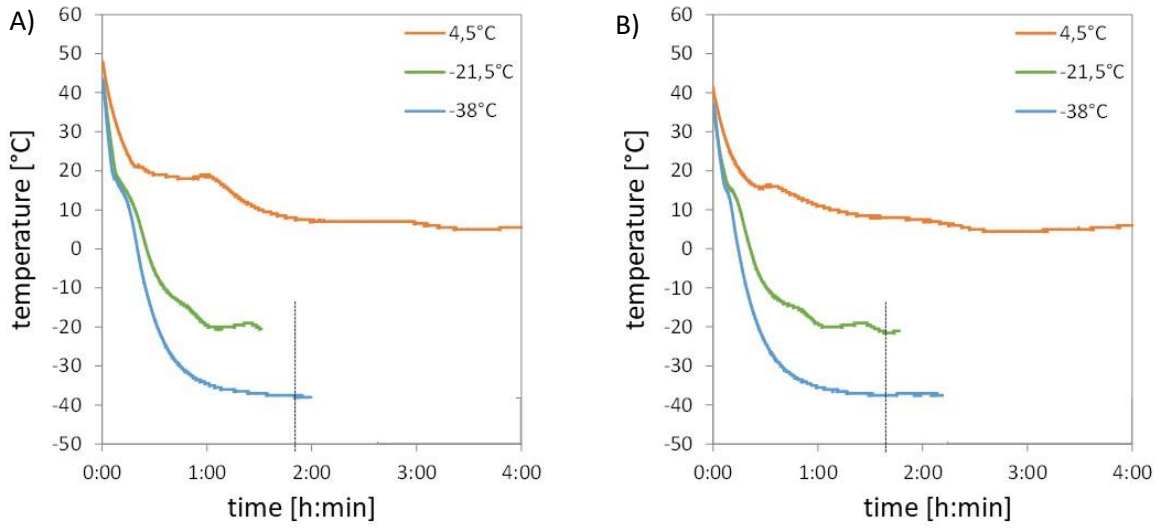

Figure 6-70: Heat transfer between the enviroment and cocoa butter (A) and milk chocolate (B) during cooling; temperature measured in the centre of the sample cell.

In Figure 6-70 it is clear to see, that the centre of the cocoa butter sample as well as the centre of the milk chocolate sample reaches the environmental cooling temperature after approximately 3 hours at a cooling temperature of 4.5°C. At adjusted temperatures of -21.5°C and -38 °C the cooling temperature was reached after around 1.5 to 2 hours in the centre of cocoa butter and milk chocolate. However it was shown that the tempering of cocoa butter is complete only after 3-4 hours, longer than the 2 hours needed for the complete cooling of the cocoa butter to environmental conditions. This leads to the assumption that the time needed for tempering is not influenced by heat transfer alone. The time needed for the heat transfer with milk chocolate is similar to cocoa butter although the tempering of milk chocolate needs much longer. This verifies the assumption that the long tempering time needed for chocolate is due to the particles present, which disrupt the crystal structure and lead to a small diffusion coefficient and thus a slower transformation of the crystals. Figure 6-70 shows that the temperature of the samples decreases linearly until approximately 20°C for cocoa butter and 15°C for chocolate at all adjusted cooling temperatures. It can be assumed that crystallisation starts from this point on, which leads to a release of heat. The crystallisation heat is also obvious in Figure 6-70 and is marked with a small peak at 20°C (cocoa butter) or 15°C (milk chocolate). Further decrease of the centre temperature is therefore much slower and not linear anymore for all cooling temperatures. At a cooling temperature of 4.5°C the heat does not dissipate as well as at lower temperatures which results in a low amount of stable crystal forms as shown before. In conclusion it can be said, that heat transfer is not the main influencing factor for tempering. It must only be ensured that the chocolate bulk achieves the adjusted crystallisation temperature, which mainly influences the types of crystals which are formed and thus the quality of tempering.

In conclusion it can be said, that a decrease of crystallisation temperature firstly leads to an increasing amount of crystal form V. A further temperature decrease leads then to a decrease of the crystal form V amount. A crystallisation temperature optimum was found at -20°C, where complete tempering of cocoa butter takes place. It was shown that the amount of form V crystals in cocoa butter and

chocolate increases with increasing cooling time and that the tempering of milk chocolate needs more time then tempering of cocoa butter due to the presence of particles.

6.4.4 Validation of the Tempering by Cooling

It was shown that dissolution of carbon dioxide in chocolate decreases the melting point. Due to this standard tempering is not possible for the high pressure aeration of chocolate because the formed stable crystal seeds melt during the process. An alternatively tempering method with intense cooling was identified. In this chapter the cooling tempering method is investigated with respect to well-tempered high pressure aerated chocolate. Milk chocolate aerated at 20 bar and 130 bar (Table 4-6) was afterwards tempered using the cooling method at -20°C for 24 hours and then analysed with the DSC to determine the crystal forms present. The results compared to non-aerated Nestlé milk chocolate are given in Figure 8-1.

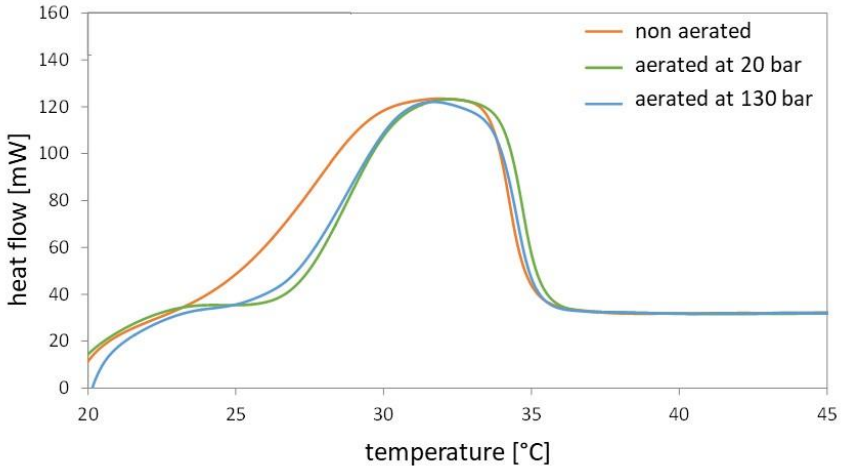

Figure 6-71: Melting curves of Nestlé milk chocolate and aerated milk chocolates (20 bar and 130 bar) tempered with the cooling method (T=-20°C) after high pressure aeration; scaled heat flow

The melting curves of all three investigated chocolates are similar. The melting curves show that the Nestlé milk chocolate and both aerated chocolates are well tempered after 24 hours of cooling at -20 °C. The non-aerated Nestlé milk chocolate has a slightly lower melting range compared to the aerated one which may be due to the fact other fats are present (Table 4-2). The aerated chocolate was produced with cocoa butter only.

It can be concluded that the tempering of high pressure aerated chocolate can be realised by using a cooling method suggested in this work. The problem of the melting point shifting due to carbon dioxide dissolution can therefore be overcome with this method.

6.4.5 Comparison of Tempering by Cooling and Standard Tempering

In this chapter the standard tempering method is compared with the alternative cooling tempering method regarding energy consumption and costs. Therefore the energy needed to be supplied or removed is compared for regular tempering and the cooling method at -20°C by using equation (2-5).

For the calculation, the specific heat capacity of cocoa butter and milk chocolate is necessary. They were determined using the DSC in a temperature range from 0°C up to 60°C. The heat capacity can be only measured for the solid and liquid state because the melting curves overlap the measurement. Due to this, a linear function for the heat capacity of cocoa butter (equation (6-2(6-3)) and milk chocolate (equation (6-3)) are used to determine the heat capacity for all temperatures.

$$c_{p,CB} = 0.0017 \cdot T + 1.9554 \qquad (R^2 = 0.7106) \tag{6-2}$$

$$c_{p,MC} = 0.0054 \cdot T + 1.3204 \qquad (R^2 = 0.9030) \tag{6-3}$$

The specific heat capacities of cocoa butter and milk chocolate increase with increasing temperatures. The heat capacities of solid and liquid state was directly measured and the heat capacities at temperatures in the melting range are interpolated using equation (6-2(6-3) for cocoa butter and (equation (6-3) for milk chocolate. Only the heat capacity at -20°C was extrapolated with the equations, which can lead to eventually higher errors. The measured, interpolated and extrapolated specific heat capacities of cocoa butter and milk chocolate for different temperatures are given in Table 6-11.

Table 6-11: measured, extrapolated and interpolated specific heat capacities of cocoa butter (CB) and milk chocolate (MC) at different temperatures and phase states.

temperature	$c_{p,CB}$ [kJ/(kg K)]	$c_{p,MC}$ [kJ/(kg K)]	determination
-20	1.92	1.21	extrapolated
3	-	1.22	measured
9	1.98	-	measured
14	-	1.40	interpolated
16	1.94	-	measured
27	-	1.47	interpolated
29	2.00	1.48	Interpolated
31	2.01	-	Interpolated
32	-	1.49	Interpolated
35	2.01	-	interpolated
50	2.05	1.60	measured

The specific heat capacities of milk chocolate are slightly more influenced by temperature than the heat capacities of cocoa butter. The maximal measurement error was only 3% and determined with measurements done in duplicate for milk chocolate. The error of the calculated values could be much higher, especially the extrapolated value at -20°C.

The determined specific heat capacities of cocoa butter and milk chocolate are approximately in the same range as the literature values given in Table 2-11 and Table 2-12 in chapter 2.3.2. [45–47]. The literature referred heat capacities of liquid cocoa butter (2.0 – 2.1 kJ/(kgK) [45, 47]) and chocolate (1.55 kJ/(kgK) [45]) are similar to the own measured values in the same temperature range. The literature referred specific heat capacities of solid cocoa butter are slightly higher compared to the own measured values (cocoa butter 2.2 – 2.4 kJ/(kgK) [45]; milk chocolate 1.5 -1.7 kJ/(kgK) [45]). The heat

capacities measured by DEUERLING [46] are much higher compared to the other literature referred values and the results in this work and therefore not used for comparison.

The temperatures used in the standard tempering process for Nestlé are given in Table 2-9 and for the alternative cooling tempering method a temperature of -20°C was identified to be optimal. For the calculation of heat consumption during the different tempering methods the following temperature stages are therefore necessary:

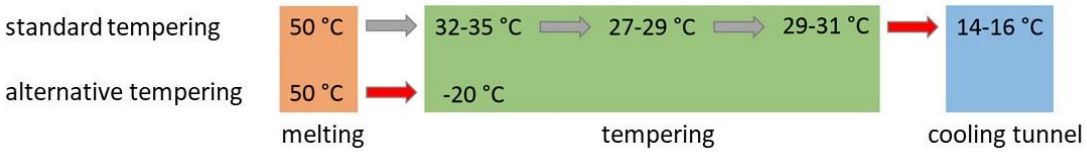

Figure 6-72: Temperature profiles of standard tempering used by Nestlé and the alternative cooling tempering method (red arrows represent the aeration step of the chocolate)

The lower given temperatures are used for calculation with milk chocolate and the higher temperatures for cocoa butter. The red arrows show at which intermediate step the aeration of the product takes place. For the standard process, tempering is done before the aeration and for the alternative method the aeration is done before the tempering. The calculation of heat needed to be supplied or removed in the standard tempering can be done in three steps: cooling from 50 to 27-29°C, heating again up to 29-31°C and subsequent cooling in the tunnel to 14-16°C. The calculation of the heat of these three steps are given exemplarily for cocoa butter in equation (6-4),(6-5) and (6-6):

$$Q_{standard,CB,1} = m \cdot (c_{p,CB,50} \cdot 323.15K - c_{p,CB,29} \cdot 302.15K) \quad (6\text{-}4)$$

$$Q_{standard,CB,2} = m \cdot (c_{p,CB,29} \cdot 302.15K - c_{p,CB,31} \cdot 304.15K) \quad (6\text{-}5)$$

$$Q_{standard,CB,3} = m \cdot (c_{p,CB,31} \cdot 304.15K + \Delta h_s - c_{p,CB,16} \cdot 289.15K) \quad (6\text{-}6)$$

For the calculation the specific heat capacities are taken from Table 6-11. The total heat consumption with the standard tempering method is the sum of all three single heat amounts. The specific melting enthalpies of cocoa butter and milk chocolate used for the calculation are given in Table 2-13. The melting enthalpy is added in the third step because the main part of crystallisation takes place there.

The same procedure was done for the alternative cooling tempering method. Therefore only one step is necessary given in equation (6-7):

$$Q_{cooling} = m \cdot \left(c_{p,50} \cdot 323{,}15\mathrm{K} + \Delta h_S - c_{p,-20} \cdot 253{,}15\mathrm{K}\right) \quad (6\text{-}7)$$

The calculated energy consumption of the standard tempering method and the alternative tempering method are given exemplarily for 1 kg cocoa butter and milk chocolate in Table 6-12:

Table 6-12: calculated energy consumption of the standard and alternative tempering method with 1kg cocoa butter and milk chocolate.

product	tempering method	Q [kJ]
cocoa butter	standard	273
	alternative	333
milk chocolate	standard	171
	alternative	255

The energy consumption of cocoa butter with the standard tempering method is approximately 20% lower compared to the alternative cooling tempering method. For milk chocolate around 30% less energy is required with the standard method. The energy consumption of cocoa butter is in general higher compared to milk chocolate because of the lower melting enthalpy. For the alternative tempering method one process step is no longer necessary because tempering can be done in the cooling tunnel. Therefore one production plant can be saved with the alternative cooling tempering method.

The comparison of the standard tempering with alternative cooling tempering showed that the standard tempering needs slightly less energy, for example 30% less for milk chocolate.

It was shown that the dissolution of carbon dioxide in chocolate leads to a decreasing of the melting point. The standard tempering method is therefore not suitable for the high pressure aeration of chocolate because the formed stable crystal seeds melt during the process. In this work an alternative method with intense cooling for the tempering of high pressure aerated chocolate was identified. It was shown that a decrease of crystallisation temperature firstly leads to an increase and then to a decrease of the quantity of form V crystals. A crystallisation temperature optimum was found at -20°C, where complete tempering of cocoa butter takes place. Additionally it was shown that the crystal structure V amount in cocoa butter and chocolate increases for increasing cooling time and that the tempering of milk chocolate needs more time then tempering of cocoa butter due to its particles present. It can be concluded that the tempering of high pressure aerated chocolate can be realised with the subsequent cooling method and that the problem of melting point shifting due to carbon dioxide dissolution can be overcome with this method. Finally it was shown, that the standard tempering of milk chocolate needs 30% less energy compared to the alternative tempering method with intense cooling.

6.5 Modelling of Foam Formation

In this chapter the results of the MATLAB Model developed for the prediction of bubble formation and bubble growth during depressurisation will be discussed for carbon dioxide high pressure aerated cocoa butter. This model considers the spatial bubble formation, the coalescence, bubbles rising and the change of material properties during the process. Detailed description of the developed model are given in chapter 5.2. The prediction was done for four coalescence calculation methods: bubble pressure as in the case of bubble formation, implementation of a growth rate, bubble pressure equal to environmental pressure or assumption of a constant volume with the additional option of a maximum bubble radius (please see chapter 5.2.5). A sensitivity analysis regarding pressure and simulation time change and a detailed comparison with experimental results was carried out for the model variation with the closest alignment to real behaviour.

A depressurisation from 58 bar down to 1 bar during 2 seconds was at first chosen as standard for all prediction variations. Fife key parameter describing the foam were calculated for each time step during the depressurisation: number of bubbles in the foam $n_{bubbles}$, porosity of the foam φ , average radius of the bubbles $\bar{r}$, average concentration of carbon dioxide in cocoa butter $\bar{c}$ and the bubble nucleation rate *J*.

6.5.1 Effect of Starting Conditions and Parameters

In this chapter the prediction results using four different coalescence calculation methods are considered and evaluated.

Method 1: Bubble pressure as in the case of bubble formation

In this method the bubble pressure of the newly formed bubble due to coalescence was calculated using Henry's law (equation (5-10)). Figure 6-73 shows the key simulation parameters with simulation time and the final 3D result of the foam simulation (red bubbles mark the bubbles formed due to coalescence).

A)

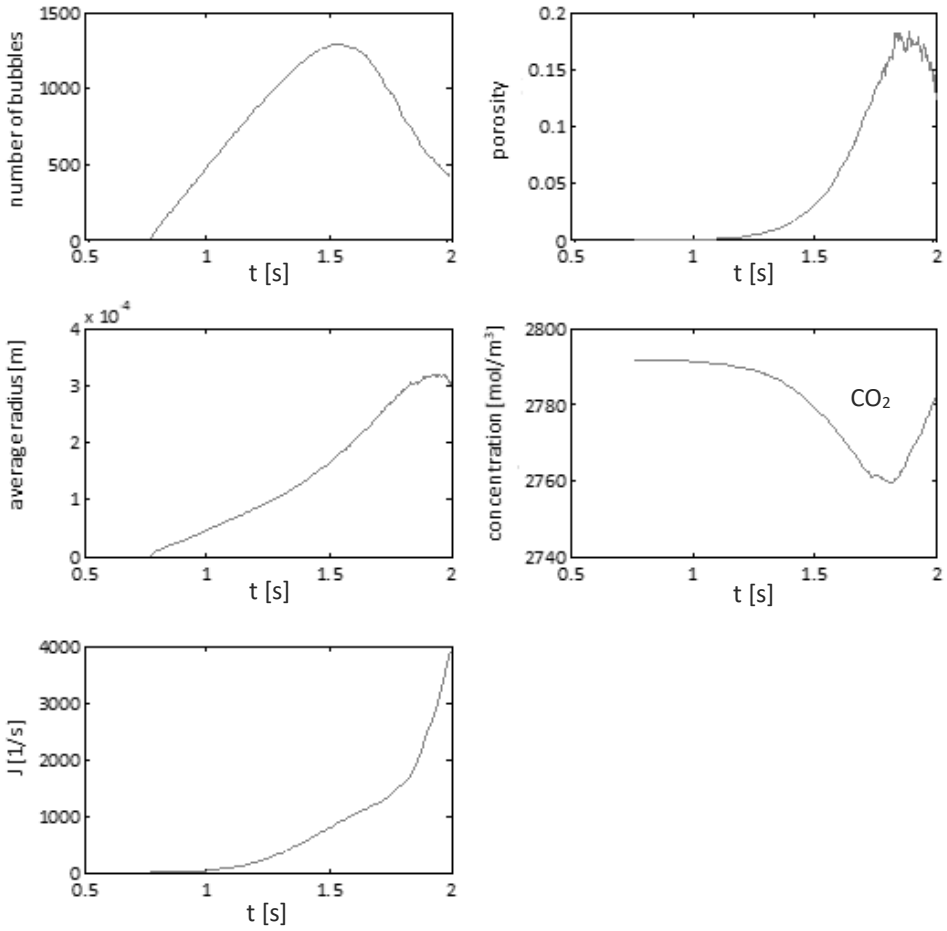

B)

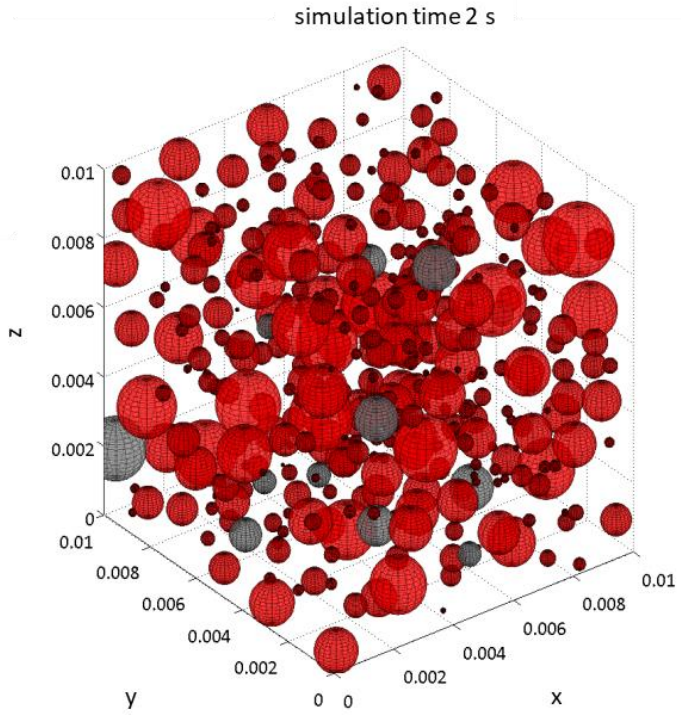

Figure 6-73: Foam model prediction of depressurisation from 58 bar in 2 s using the coalescence method 1: (A) number of bubbles in the foam, foam porosity φ, average bubbles radius $\bar{r}$, average carbon dioxide concentration in cocoa butter $\bar{c}$ and bubble nucleation rate *J* with time, (B) final 3D foam picture of the 1 cm^3 simulation area (red bubbles mark the bubbles formed due to coalescence)

The bubble formation starts from 0.765 seconds onwards because before the bubble nucleation rate *J* was lower than the threshold of $J_{threshold} = 0.01\ \mathrm{s}^{-1}$. The number of bubbles then increases up to 1.5 seconds and decreases afterwards again but the porosity and the average radius still increase further and decrease slightly only towards the end of the simulation. It is therefore obvious that a lot of coalescence take place from 1.5 seconds onwards, which leads to a decreasing number of bubbles and an increasing porosity and bubble radius at the same time.

Two coalescing bubbles form a new bubble with a much smaller volume compared to the two existing bubbles using this model method 1. In the next time step, the growth of the new formed bubble shows a sharp increase and decreases than continuously in the following time steps. This first increasing and then decreasing radius of the bubbles formed due to coalescence leads to small fluctuations of porosity. CHEN also described that a new bubble is initially not in equilibria with the environment and its radius will oscillate until the equilibria is reached [74]. However, in the model using method 1, no bubble growth is observed again. Overall the bubbles are slightly smaller and this leads to a dense bubble structure and slow rising of bubbles. This in turn leads to a frequent coalescence which leads to a decrease in porosity and average bubble diameter at the end of the simulation. The decreases seen in new bubbles also leads to an increase of the carbon dioxide concentration in the cocoa butter and the bubble nucleation rate. It can be noted, that the final foam porosity of 12 % is much too low compared to experimental results (50 - 80%). This fact, as well as the low amount of gas in the bubbles (0.4%) and the shrinking of the newly formed bubbles leads to the assumption this these coalescence model method is not suitable for a realistic prediction of foam formation.

Method 2: Implementation of a growth rate

In this coalescence model method the growth per time step of both coalescing bubbles was determined and rated by the gas mole content. The starting parameter of the newly formed bubble due to coalescence are calculated using method 2 with these growth rates. Figure 6-74 shows changing of the key simulation parameters during simulation time and the final 3D result of the foam simulation (bubbles formed due to coalescence are marked red).

A)

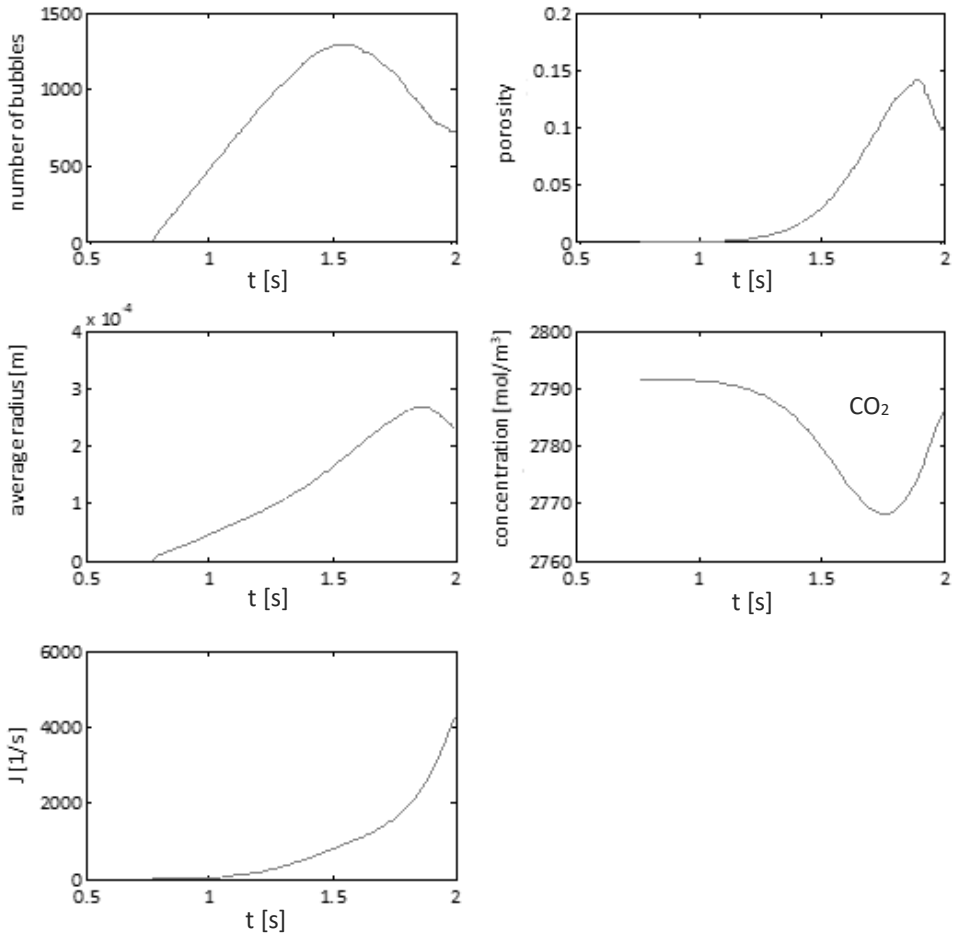

B)

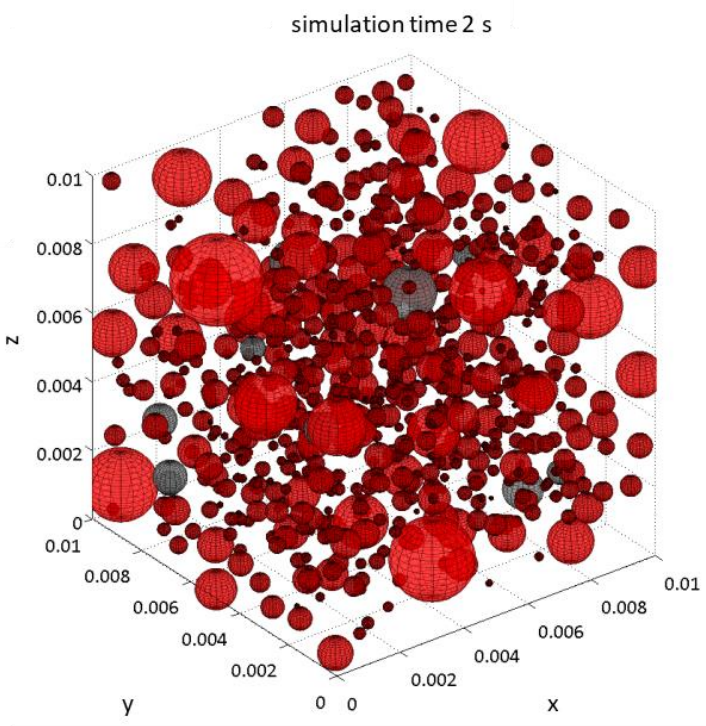

Figure 6-74: Foam model prediction of depressurisation from 58 bar in 2 s using the coalescence method 2 :(A) number of bubbles in the foam, foam porosity φ, average bubbles radius $\bar{r}$, average carbon dioxide concentration in cocoa butter $\bar{c}$ and bubble nucleation rate *J* with time, (B) final 3D foam picture of the 1 cm^3 simulation area (red bubbles mark the bubbles formed due to coalescence)

The curves of key parameters with simulation time are approximately similar to the curves resulting from method 1. The number of bubbles first increases up to 1.5 seconds and decreases afterwards due to coalescence. The calculated gas volume of the new bubble is bigger than the sum of the volume of both coalesced bubbles. A shrinking of the new bubble can be seen again because the bubble is not in equilibria with the environment. This also leads to a decrease of porosity and the average bubble radius in the end of the simulation and an increase of the carbon dioxide concentration in the cocoa butter similar to method 1. Using coalescence method 2, more bubbles are formed compared to method 1. These bubbles have a comparatively small radius and therefore still a low porosity. It can be noted, that the final foam porosity of 8 % is much too low compared to experimental results (50 - 80%) and also lower than the results achieved with method 1. This facts leads to the conclusion that these coalescence models are not suitable for a realistic prediction of foam formation.

Method 3: Bubble pressure equal to environmental pressure

In this coalescence calculation method the pressure of the newly formed bubble was assumed to be the same as atmospheric pressure p_c to calculate the starting parameter of the newly formed bubble. Figure 6-75 shows the impact of changing the key simulation parameters during simulation time and the final 3D result of the foam simulation (bubbles formed due to coalescence are marked red).

A high increase of the number of bubbles and a low increase of the porosity can be seen up to 1.5 s. The porosity increases approximately exponentially after a further decrease of the number of bubbles due to coalescence. The calculated starting parameter of the newly formed bubbles due to coalescence are not in equilibria with the environment which leads to a sharp increase of the bubble volume using method 3 for prediction. The greatly enlarged bubbles rise very fast and coalesce more often with other bubbles on their way. A coalescence of two bubbles also formed due to coalescence leads to very big bubbles with radii up to 5 mm, which occupy a large amount of the 1 cm^3 simulation area. The large bubbles with a high gas volume, in turn lead to a high porosity with maximum calculated porosity of approximately 50%. The escape of the big bubbles from the simulation lead to a sharp decrease of the porosity at approximately 1.8 s. The remaining simulation time is not sufficient to form again a large number of new bubbles although only 10% of the dissolved gas amount was outgassed. The final number of bubbles achieved is much lower and the final porosity and average radius higher compared to both methods shown before. The final radius of approximately 0.5 mm has good agreement with experimental results of this work. The calculated final porosity of 27% is however, again too low compared with experimental results. The bubbles formed due to coalescence are much too big due to the sharp volume increase but this method has better results with bubble growth instead of shrinkage as described for both methods described previously.

A)

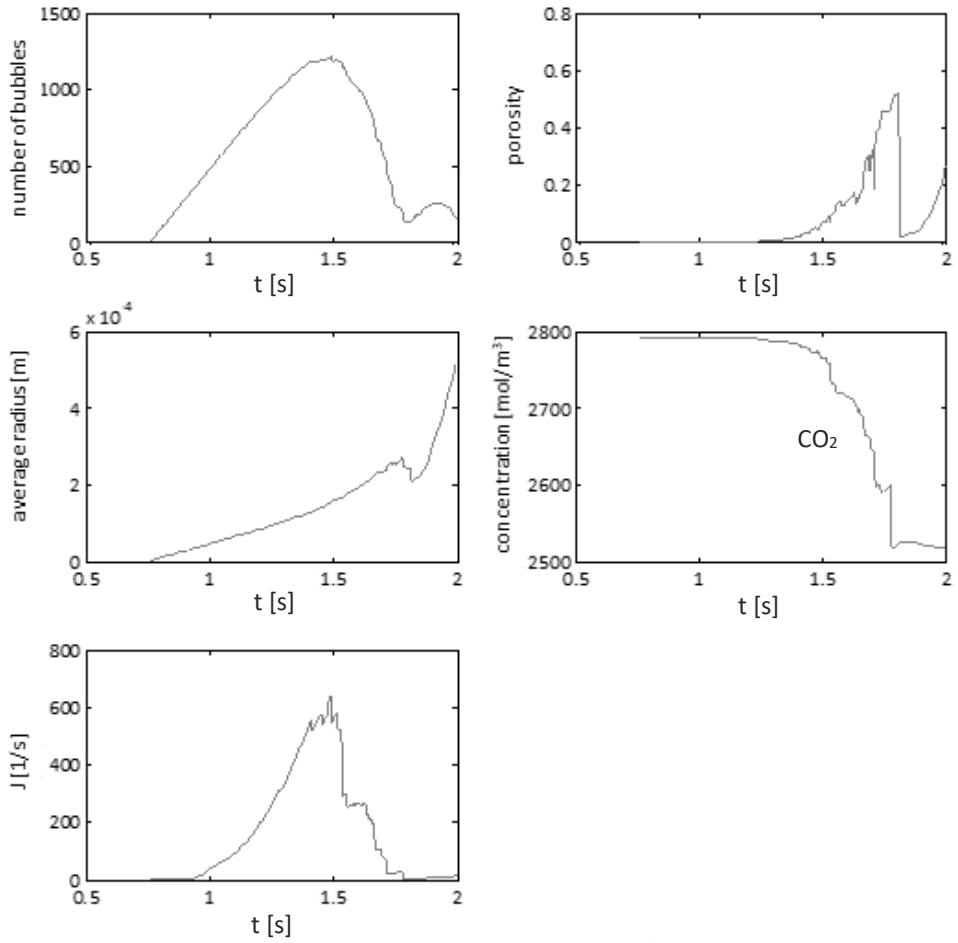

B)

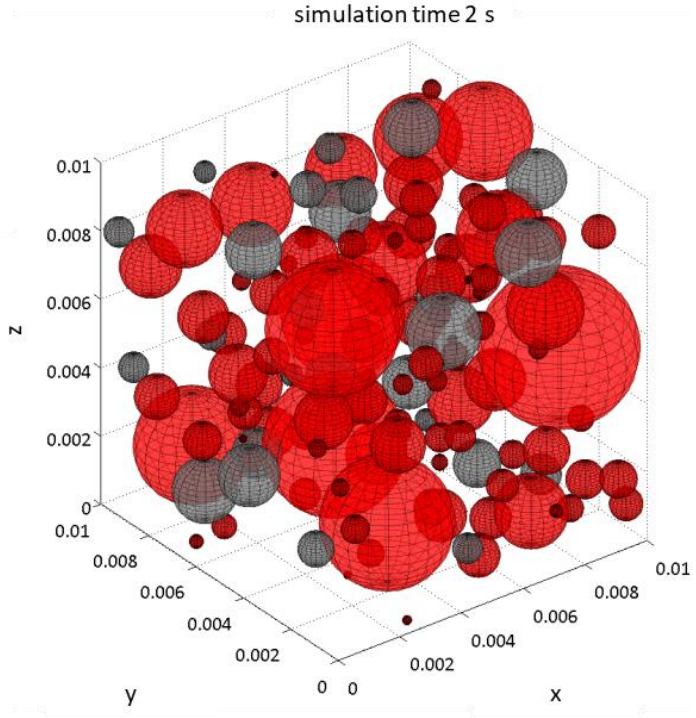

Figure 6-75: Foam model prediction of depressurisation from 58 bar in 2 s using the coalescence method 3 :(A) number of bubbles in the foam, foam porosity φ, average bubbles radius $\bar{r}$, average carbon dioxide concentration in cocoa butter $\bar{c}$ and bubble nucleation rate *J* with time, (B) final 3D foam picture of the 1 cm^3 simulation area (red bubbles mark the bubbles formed due to coalescence)

Method 4: Assumption of a constant volume

The starting parameters of the new bubbles formed due to coalescence were calculated with the assumption of a constant gas volume during coalescence using method 4. The changing of the key simulation parameters during simulation time and the final 3D result of the foam simulation (bubbles formed due to coalescence are marked red) are given in Figure 6-76.

The number of bubbles increases up to 1.5 s and decreases afterwards due to coalescence as also shown in all other methods before. The porosity increases exponentially from 1.4 s on but shows simultaneously strong fluctuations. The average bubble radius increases over the total simulation time. Coalescence and additionally bubble growth is similar to method 3. After the coalescence, bubbles grow rapidly. Coalescence of two bubbles also formed due to coalescence leads to very enlarged bubbles which rise very fast and coalesces frequently with other bubbles on their way. The outgassing of these big bubbles leads to a more temporary, sharp decrease in the porosity. The remaining simulation time is not sufficient to form a lot of new bubbles although only 4% of the soluted gas amount was outgassed. This finally results in a low porosity of 11% and a small number of bubbles. The porosity is as low as for method 1 and 2 but the average radius of 0.5 mm shows a good agreement with experimental results similar to method 3. The final foam porosity is much too low but this method has better results with bubble growth instead of shrinkage as described for methods 1 and 2.

A)

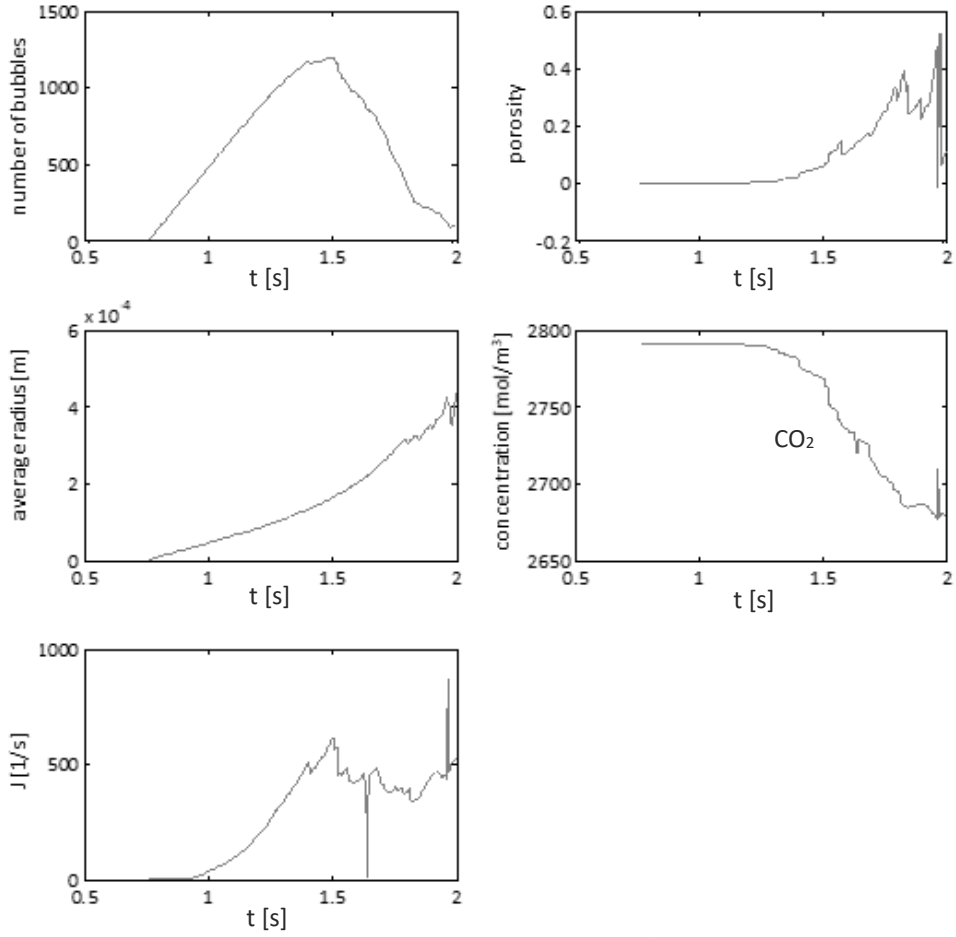

B)

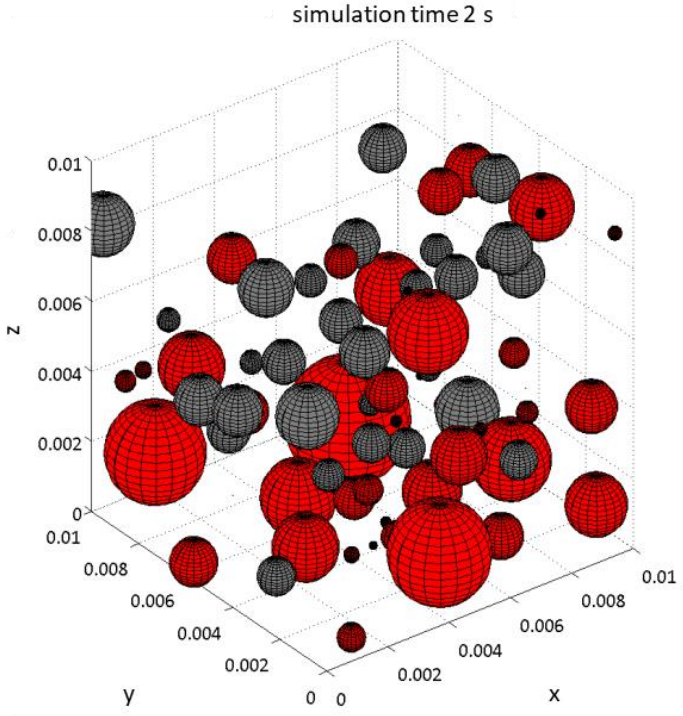

Figure 6-76: Foam model prediction of depressurisation from 58 bar in 2 s using the coalescence method 4: (A) number of bubbles in the foam, foam porosity φ, average bubbles radius $\bar{r}$, average carbon dioxide concentration in cocoa butter $\bar{c}$ and bubble nucleation rate *J* with time, (B) final 3D foam picture of the 1 cm^3 simulation area (red bubbles mark the bubbles formed due to coalescence)

A comparison of the final key parameter results calculated with all four coalescence methods are given in Table 6-13.

Table 6-13: Comparison of the final key parameter results of foam model prediction (depressurisation from 58 bar in 2 s) using four different coalescence calculation methods.

	final results			
parameter	**method 1**	**method 2**	**method 3**	**method 4**
number of bubbles	414	682	145	92
foam porosity [%]	12	8	27	11
average radius [mm]	0.3	0.2	0.5	0.4
average CO_2 concentration [mol/m^3]	2782	2787	2518	2680
amount of gas in bubbles [%]	0.4	0.2	10	4
bubble nucleation rate [1/s]	3911	4351	12.7	529
bubble behaviour after coalescence	shrinkage	shrinkage	growth	growth

The final number of bubbles varies very strongly for all the coalescence models used from 92 up to 682 bubbles in the 1 cm^3 simulation area. The calculated final porosities are much too low compared with experimental results (50-80%) but using method 3 leads to the highest final porosity of 27%. The final radius calculated with methods 3 and 4 shows the best agreement with experimental results of approximately 0.5 mm, while the radii calculated with methods 1 and 2 are much too small. All four, calculated, final, average concentrations of carbon dioxide in the cocoa butter and all four amounts of outgassed carbon dioxide do not differ so much or are not the critical factors. Important is the point, that using method 1 or 2 leads to a shrinkage of bubbles formed due to coalescence and using method 3 or 4 leads to a growth of these bubbles. Bubble growth was observed experimentally during this work and the shrinkage was not. In conclusion, it can be said that coalescence methods 3 and 4 are much more suitable for the prediction of foam formation during depressurisation compared to methods 1 and 2. Coalescence method 3 assumes that the new bubble pressure is equal to the environmental pressure and method 4 assumes a constant volume. Both assumptions provide good conditions for the prediction and lead to bubble growth after coalescence and an average bubble radius with good agreement to experimental results. The assumptions of a constant volume during coalescence are also described by ORCUTT AND CARPENTER [73] and therefore used for further simulations.

Additional option: Maximum bubble radius

To avoid the prediction of very big unrealistic bubbles due to repeated coalescence, an additional fitting parameter of a maximum bubble radius r_{max} is implemented to the foam model using method 4. These bubbles up to radii of 5 mm occupy a large volume of the simulation area of 1 cm^3. The bubble growth is therefore stopped and the ability of a bubble to coalesce is eliminated, if these bubbles have a similar or bigger bubble radius than the adjusted maximum radius r_{max}. Four different maximal radii of 0.2 mm, 0.3 mm, 0.5 mm and 1 mm were tested to achieve realistic foam predictions. The final results of the key parameters of these simulations are given in Table 6-14.

Table 6-14: Comparison of the final key parameter results of foam model prediction (depressurisation from 58 bar in 2 s) using coalescence calculation methods 4 without and with four different maximum radii of 0.2 ; 0.3 ; 0.5 and 1 mm.

	final results	**final results using r_{max}=**			
parameter	**∞**	**0.2 mm**	**0.3 mm**	**0.5 mm**	**1 mm**
number of bubbles	92	1152	1685	702	359
foam porosity [%]	11	66	20	54	45
average radius [mm]	0.4	0.4	0.3	0.5	0.5
average CO_2 concentration [mol/m^3]	2680	2716	2748	2715	2709
amount of gas in bubbles [%]	4	2.7	1.6	2.8	3.0
Bubble nucleation rate [1/s]	529	1090	2061	1066	946

The implementation of the additional parameter r_{max} leads to a significant improvement of the foam simulation results, this is especially true for the porosity and the number of bubbles. The number of bubbles in the simulated foam decreases with increasing maximum radius due to more enabled coalescence. The average carbon dioxide concentration, the amount of outgassed gas as well as the bubble nucleation rate are not influenced so significantly by the implementation of the maximum radii and its exact value. The calculated final average radius is higher that the adjusted maximum radius at r_{max} of 0.2 mm. At r_{max} of 0.3 mm and 0.5 mm, the average radius is similar to the maximum radius. Only the setting of r_{max} = 1 mm leads to an average radius lower than the adjusted maximal radius. It can be assumed that with a r_{max} of 1 mm the average radius is not strongly inhibited by the maximum radius. A maximum radius of 1 mm was therefore chosen as the fitting parameter for the foam prediction and evaluated as follows. The changing of the key simulation parameters during simulation time using method 4 with a r_{max} of 1 mm is given in Figure 6-77.

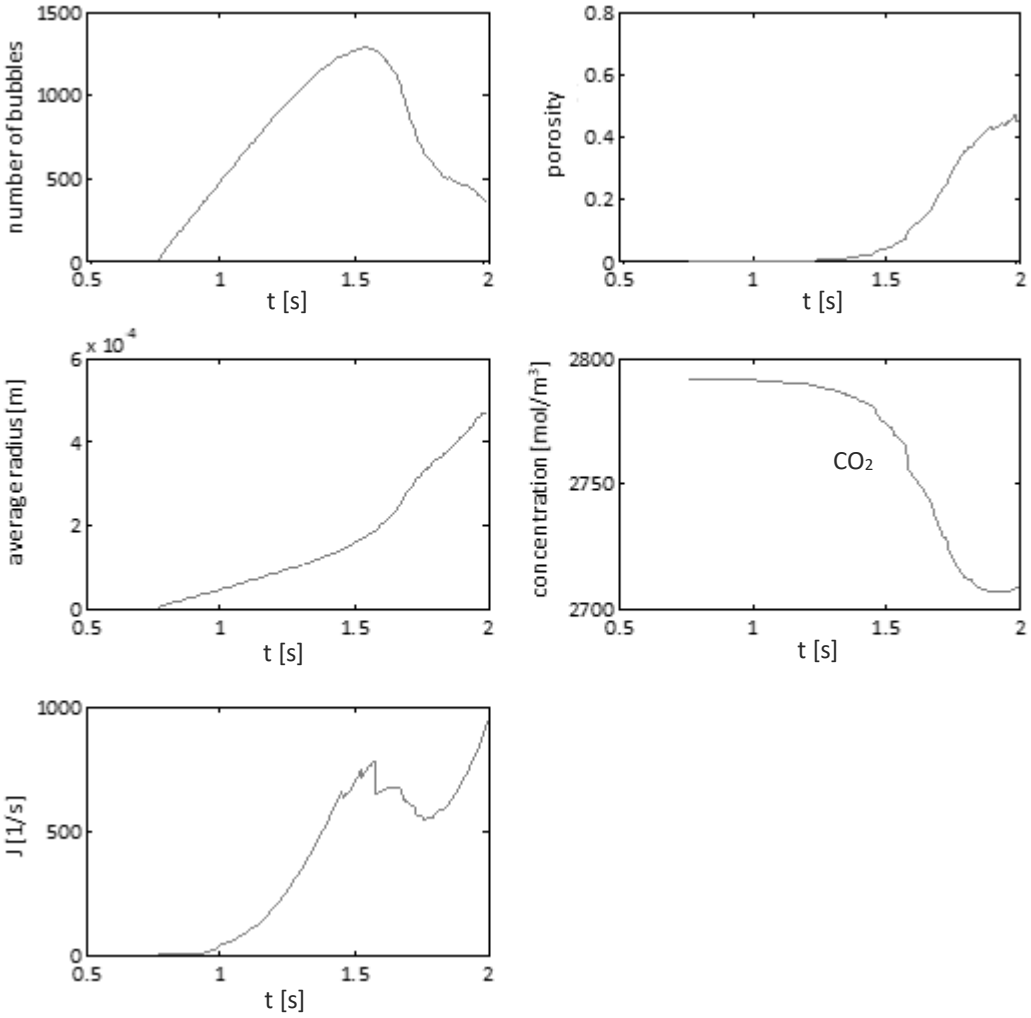

Figure 6-77: Foam model prediction of depressurisation from 58 bar in 2 s using the coalescence method 4 with an additional maximum radius of 1 mm: number of bubbles in the foam, foam porosity φ, average bubbles radius $\bar{r}$, average carbon dioxide concentration in cocoa butter $\bar{c}$ and bubble nucleation rate *J* with time

The number of bubbles increases up to 1.5 s and decreases afterwards due to coalescence as also shown in all other simulations before. The porosity as well as the average bubble radius increases with time without showing fluctuations or decreasing in the end of the simulation like in the simulation without maximum radius before. The porosity during the simulation as well as the final porosity of 45 % is much higher compared to the prediction without maximum radius. The porosity therefore has a better agreement with experimental results (porosities of 50-80%). The calculated final average bubble radius of 0.5 mm has also a good agreement with experimental values. The final 3D foam picture of the simulation (bubbles formed due to coalescence are marked red) as well as the bar diagram for final bubble size distribution is given in Figure 6-78.

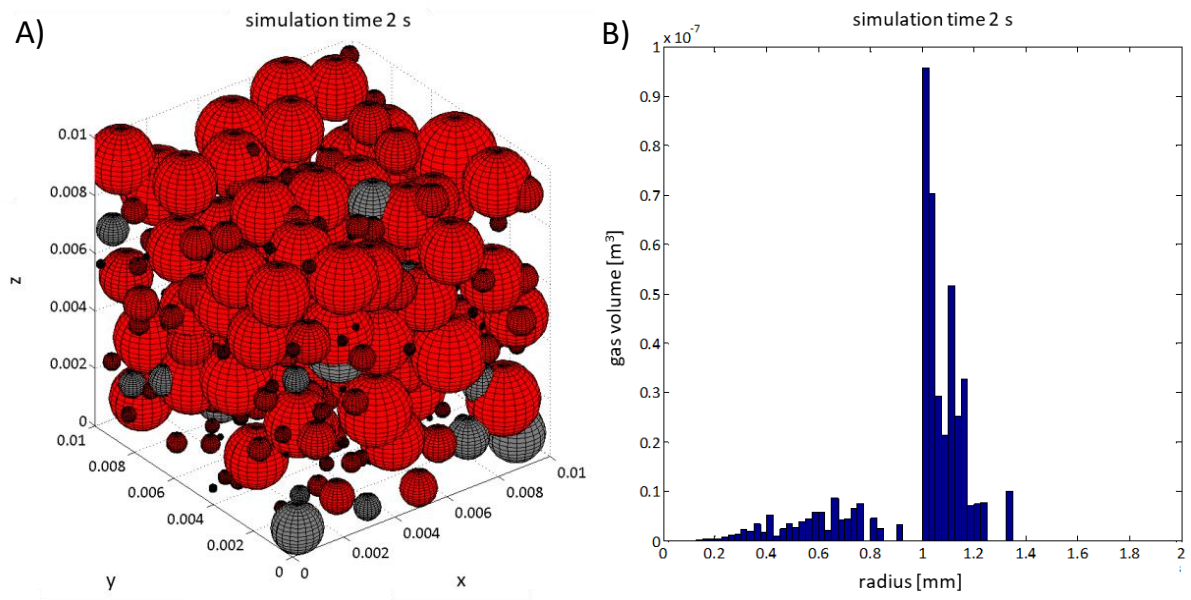

Figure 6-78: Final results of the foam model prediction of depressurisation from 58 bar in 2 s using the coalescence method 4 with an additional maximum radius of 1 mm: A) final 3D foam picture of the 1 cm^3 simulation area, bubbles formed due to coalescence are marked red; B) bar diagram for final bubble size distribution

Using a maximum radius of 1 mm in combination with the assumption of a constant volume during coalescence (method 4) leads to a homogenous bubble distribution within the simulation area. This is in good agreement with experimental results, there was also observed an approximately homogeneous bubble distribution. It is obvious that at the end of the simulation, most bubbles are formed due to coalescence. In the bar diagram for final bubble size distribution it is clear to see that the bubbles with a radius of 1 mm represent the greatest proportion of gas volume. Smaller bubbles have only a low bubble volume not only due to their small size but also due to frequent coalescence. Although maximum bubble radius was adjusted to 1 mm, bigger bubbles with a radius up to approximately 1.35 mm also occur.

In this work a spatial model for the prediction of bubble formation, growth, rising and coalescence during depressurisation of cocoa butter aerated with high pressure carbon dioxide was successfully developed. Four different methods for the calculation of the starting conditions of a bubble formed due to coalescence were observed. Simulations with the assumption of bubble pressure as in the case of bubble formation, as well as the implementation of a growth rate leads to unsatisfactory results like shrinking bubbles and low porosities. Simulations with the assumption of bubble pressures equal to atmospheric pressure as well as of a constant volume, leads to a growing of the bubbles formed to coalescence. Some very large bubbles also form due to repeated coalescence, which rise very fast and lead again to low final porosities. The method with assumption of a constant volume was chosen for further simulation because this method was also referred to in literature. An addition of a maximum bubble radius was further implemented as a fitting parameter, to avoid the formation of unrealistically large bubbles due to repeated coalescence. The bubble growth is stopped and the ability of a bubble to coalesce is eliminated, if these bubble has a similar or bigger bubble radius than the adjusted

maximum radius. A maximum radius of 1 mm was identified to be optimal for the prediction of a realistic homogenous foam without strong inhibition of the average radius. The assumptions of a constant volume during coalescence and a maximum bubble radius of 1 mm was chosen for further calculations. With this setting a final porosity of 45% and a final average bubble radius 0.5mm was achieved. This is in good agreement with the experimental results of this work. In conclusion it can be said that the developed bubble model can successfully predict the foam formation during depressurisation. A detailed sensitivity analysis and validation of the model is done in chapter 6.5.2.

6.5.2 Sensitivity and Validation of the Model

In this chapter the sensitivity of the developed model is determined regarding the depressurisation time and the starting pressure. Additionally the predictions were repeated to determine the error of the simulation.

The depressurisation starting at 58 bar to atmospheric conditions was calculated for six different depressurisation times (1s, 2s, 4s, 8s, 15s and 20s) to determine the influence of the depressurisation rate on the predicted results. The calculation with simulation times of 1s and 2s was done in triplicate to determine the simulation error. The maximum error of each parameter was transferred on the other results done in single calculations (4s, 8s, 15s and 20s). The influence of depressurisation time on the predicted final key parameter results for constant starting pressure of 58 bar are given in Figure 6-79. The results predicted with a simulation time of 2 s are chosen as standard values for the calculation of the percentage change of the parameters.

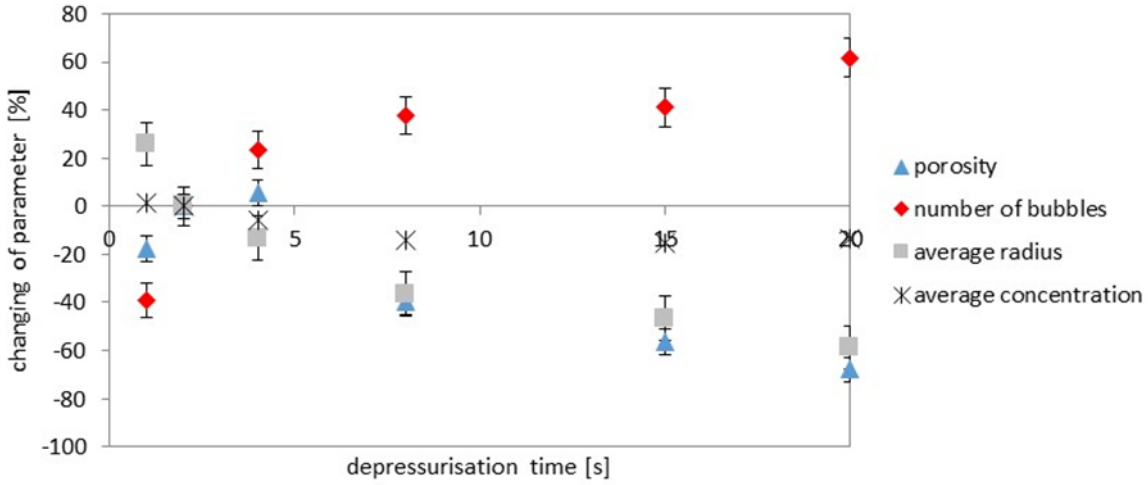

Figure 6-79: Influence of the depressurisation time (simulation time) on the predicted final number of bubbles in the foam, foam porosity φ, average bubbles radius $\bar{r}$ and average carbon dioxide concentration in cocoa butter $\bar{c}$; results at 2 s are chosen as standard values; depressurisation from 58 bar to atmospheric conditions

In Figure 6-79 it is clear to see, that an increase of the depressurisation time (simulation time) with a constant starting pressure leads to decrease in the predicted final average bubble radius and an increase in the final number of bubbles. A slower decrease of pressure therefore leads to more

constant formed bubbles and a slower predicted bubble growth. The “older” bigger bubbles in the system have enough time to rise and outgas. The final average carbon dioxide concentration in the cocoa butter decreases with increasing depressurisation time, due to steady bubble formation and the increasing amount of bubbles in the system. The final predicted porosity is mainly influenced by the increasing number of bubbles and the decreasing average bubble radius with simulation time. This leads to two overlaying effects and therefore firstly to an increase of the porosity up to a depressurisation time of 4s and then to a decrease in the porosity with further increase of the depressurisation time. Up to 4s, the increase in the number of bubbles is greater than the decrease in average bubble radius, due to the fast pressure drop at short depressurisation times. This leads to many newly formed bubbles with faster growth compared to longer depressurisation times. For simulation times above 4 seconds, the decrease of the porosity with increasing depressurisation time can be explained with the outgassing of the old big bubbles and the decreasing average bubble radius. The experimental results also show a decrease of the porosity with increasing depressurisation time but the depressurisation time does not significant influence the mean bubble diameter of the experimental aerated milk chocolate (please see chapter 6.2.4). The reason is that experimentally, a higher pressure gradient and thus a faster depressurisation leads to a quicker temperature decrease due to the Joule-Thomson effect. This leads to a faster crystallisation of the foam with a higher trapped gas amount up to a maximum porosity level.

In addition to the influence of the depressurisation time, the influence of the starting pressure on the predicted results was evaluated. Six different starting pressures between 50 bar and 70 bar (50 bar, 55 bar, 58 bar, 60 bar, 65 bar, 70 bar) are calculated in triplicate. A starting pressure above 50 bar was used for the prediction because no bubbles are formed below this pressure due to a bubble nucleation rate smaller than the threshold of 0.1 1/s. Starting pressures above 70 bar weren’t used because they lead to problems with the solving of the differential equation for the bubble growth. For this setup the amount of outgassed carbon dioxide was calculated for a better evaluation because the average carbon dioxide concentration is influenced by the varying starting pressure. The influence of the starting pressure on the predicted final key parameter results for constant simulation time of 2s are given in Figure 6-80. The results predicted with a starting pressure of 58 bar are chosen as standard values for the calculation of the percentage change of the parameters.

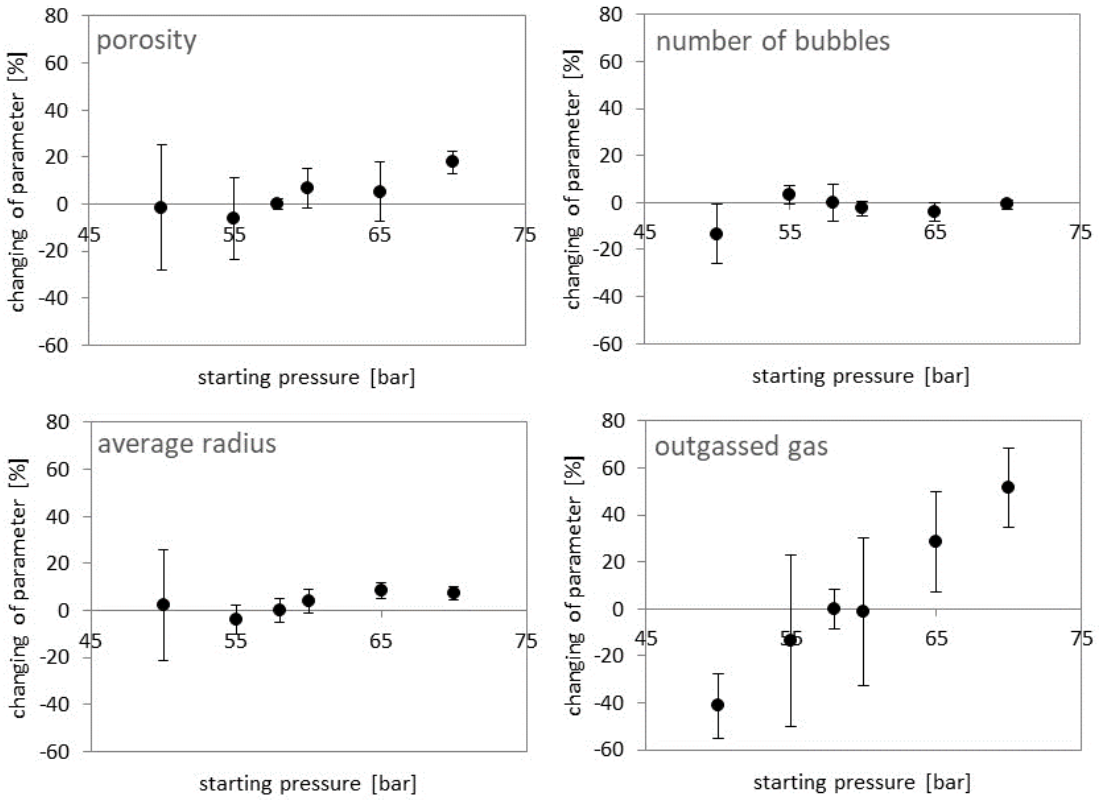

Figure 6-80: Influence of the starting pressure on the predicted final number of bubbles in the foam, foam porosity φ, average bubbles radius $\bar{r}$ and outgassed carbon dioxide amount; results at 58 s are chosen as standard values; depressurisation in 2 s to atmospheric conditions

The results show no strong influence of the starting pressure on the foam porosity, the number of bubbles and the average radius. Only the amount of outgassed carbon dioxide increases with increasing starting pressure. The reason for the low impact is the small range of the investigated depressurisation rate. Table 6-15 shows the corresponding depressurisation rates of the simulations done with varying simulation time and starting pressure.

Table 6-15: Comparison of the adjusted prediction starting pressure and depressurisation time and the resulting depressurization rates

Starting pressure [bar]	**Depressurisation time [s]**	**Depressurisation rate [bar/s]**
58	1	58
58	2	29
58	4	14.5
58	8	7.3
58	15	3.9
58	20	2.9
50	2	25
55	2	27.5
58	2	29
60	2	30
65	2	32.5
70	2	35

In the first setting with varying simulation time (1-20 s), the depressurisation rate changes from 3 to 58 bar/s. In the setting with varying starting pressure (50-70 bar) the depressurisation rate varies between 25 and 35 bar/s. This fact leads, in the second case, to smaller changes in the resulting key parameters like porosity or average bubble diameter. The foam structure is strongly influenced by the depressurisation rate, less so by the starting pressure and depressurisation time. Figure 6-81 shows the influence of the depressurisation rate on the simulated foam porosity, number of bubbles and average radius. Both setting results (varying simulation time and varying starting pressure) are therefore combined.

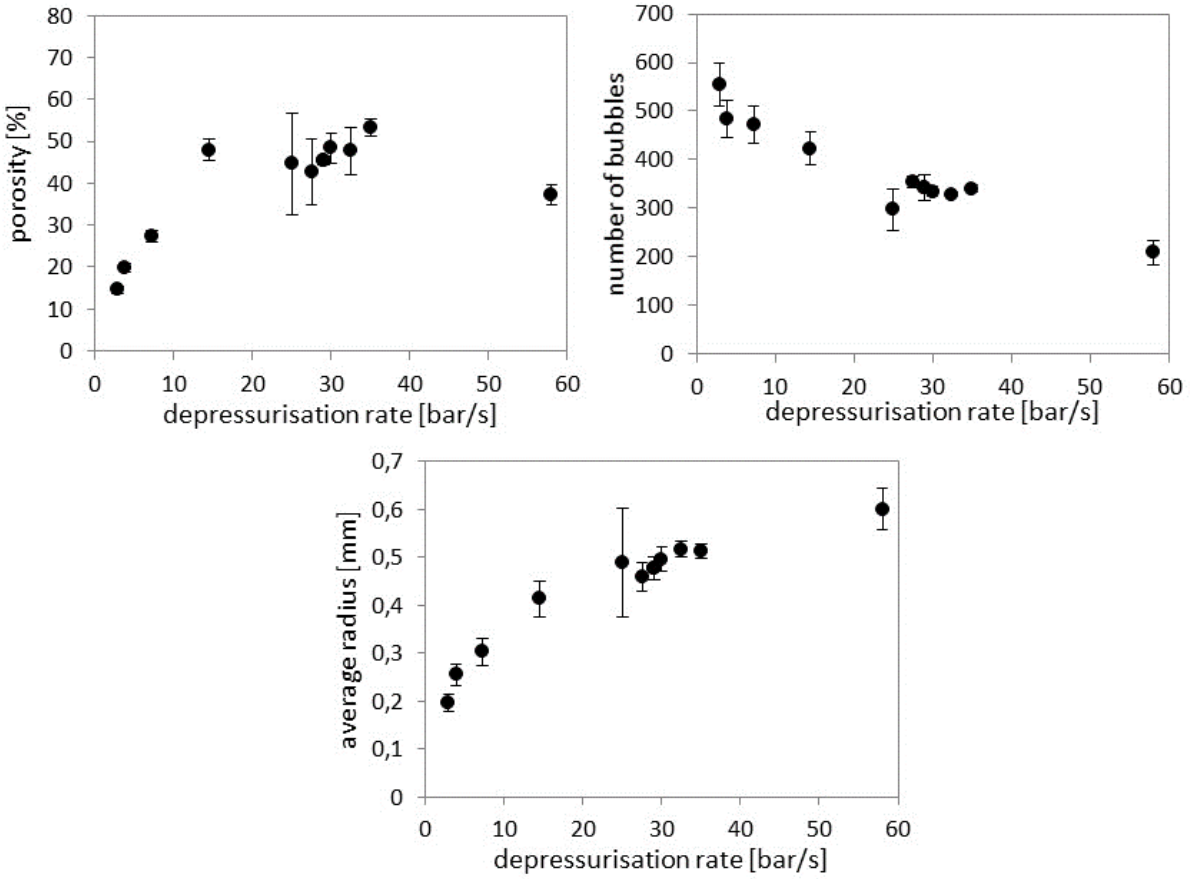

Figure 6-81: Influence of the depressurisation rate on the predicted final number of bubbles in the foam, foam porosity φ and average bubbles radius $\bar{r}$ calculated with the foam model

In Figure 6-81 it is clear to see, that an increase of the depressurisation rate leads to an increase in the predicted final average bubble radius and a decrease in the final number of bubbles. An increase of depressurisation rate therefore leads to less formed bubbles and a faster predicted bubble growth. The older bigger bubbles in the system have enough time to rise and outgas. The final foam porosity increases with increasing depressurisation rate up to 20-30 bar/s and stays then approximately similar. The predicted porosity is influenced by the decreasing number of bubbles and the increasing average bubble radius with increasing depressurisation rate. This leads to two overlaying effects and therefore firstly to an increase of the porosity and then to an approximately constant porosity level with increase of the depressurisation rate. Firstly the number of bubbles reduces by half and the average bubble

radius increases from 0.2 mm (average bubble volume = 0.034 mm^3) up to 0.5 mm (average bubble volume = 0.524 mm^3) during increasing the depressurisation rate up to approximately 30 bar/s. The average bubble volume increases by a factor of 15.4 and is therefore much higher than the bubble number which reduces by a factor of 2. This leads to a significant increase in the porosity with increasing depressurisation time up to approximately 30 bar/s. Afterwards the average bubble radius further increases only up to 0.6 mm (average bubble volume = 0.905 mm^3) and the number of bubbles reduces by one third. The average bubble volume therefore increase by a factor of 1.7 and the number of bubbles reduces by a factor of 0.87. These changes are small and cancel each other out, leading to an approximately constant porosity for depressurisation rates above 30 bar/s.

The influence of the depressurisation rate on the foam structure of CO_2 and N_2 aerated milk chocolate was also investigated experimentally in this work using the autoclave high pressure aeration process and the high pressure viewing cell, described in chapter 6.2.4. Using the autoclave it was shown that the depressurisation rate influences the porosity of the milk chocolate and the number of bubbles in the foam. A faster depressurisation leads to a more quickly temperature decrease due to the Joule-Thomson effect. This leads to an increase of porosity and number of bubbles with increasing depressurisation rate because of the faster crystallisation (higher trapped gas amount) and the reason that due to this less coalescence take place. In the experiments it was also shown, that the depressurisation rate does not influence the mean bubble diameter of the foam. Still, a reason could be the big error of the measurement method. Experiments in the viewing cell also show, that the porosity increases with increasing depressurisation speed up to a maximum porosity level and that the depressurisation rate do also not significantly influence the mean bubble diameter. In the viewing cell experiments the porosity firstly increases fast up to around 80% with increasing depressurisation rate. From a depressurisation rate of around 1 bar/s the chocolate porosity remains almost constant. The achieved porosities are not strictly comparable with the porosities of regular autoclave aerated milk chocolate in this work or the industrially produced chocolate because of process differences. In the viewing cell, a very low sample amount was taken and the depressurisation takes place directly in the viewing cell. However the developed model can successfully predict the influence of depressurisation rate on the foam porosity. The influence of the depressurisation rate on the model predicted number and size of bubble is different to the experimental results of this work. KOLLER also carried out high pressure chocolate aeration experiments and described that a higher bubble number density and faster coalescence were observed at higher depressurisation rate and that the main formation of small bubbles took place when ambient pressure was just reached [52]. TAKI et al. [115] described that an increased depressurisation rate lead to an increase in bubble nucleation and growth rate for carbon dioxide saturated polymers [115]. PARK et al. [116] described that faster pressure drop leads to a higher nucleation rate by investigating the influence of nozzle geometries and depressurization rates on bubble nucleation [116]. All these findings described in literature [52, 115, 116] confirm the experimental and model prediction results of this work suggesting that porosity increases with increasing depressurisation speed. Additionally this literature experiments [52, 115, 116] show that the nucleation rate, growth rate and the coalescence increase with increasing depressurisation rate.

This could lead to an increasing bubble size with increasing depressurisation rate like also predicted with the developed foam model. The reason is that in the model prediction the bubbles grow faster and the big bubbles has less time for outgassing with increasing depressurisation rate. The increase of nucleation rate with increasing depressurisation rate shown in the literature [52, 115, 116] was not predicted with the foam model. The predicted number of bubbles decreases with increasing depressurisation rate due to the decreasing number of intervals for the bubble nucleation. KOLLER described that in the experiment the main formation of small bubbles took place when ambient pressure was just reached [52]. This could be an explanation for the differences between the predicted and experimental number of bubble results because the model prediction stops when ambient pressure is reached. In experiments it was therefore shown that the bubble nucleation, growth and coalescence goes further (after ambient pressure is reached) until the total solidification of the foam take place[52]. It can be said, that the formation and growth of bubbles during the aeration as well as the coalescence are very complex processes which are highly dependent on the explicit process conditions.

Table 6-16 shows the comparison of the predicted results at standard parameters with the results of one example experiment with chocolate in the viewing cell (at constant porosity conditions).

Table 6-16: Comparison of the experimental and predicted process parameters and achieved foam parameter

	foam model	**experimental**
material	cocoa butter	chocolate
pressure	58 bar	51 bar
temperature	40 °C	40 °C
depressurisation rate	28.5 bar/s	4.6 bar/s
number of bubbles/ cm³	359	1528
porosity	45 %	80 %
average radius	0.5 mm	0.5 mm

The predicted results for cocoa butter show a good agreement with the results determined experimentally for chocolate under approximately similar process conditions. The predicted average radius of 0.5 mm is similar to the experimentally determined average radius. The predicted foam porosity in the viewing cell is lower than the experimentally determined chocolate porosity but on the same scale. The chocolate porosities achieved with autoclave aeration also have a porosity of approximately 50%. Additionally it can be seen that the predicted final number of bubble is also slightly lower but on the same scale and that new bubbles are formed continuously during the whole simulation time likely in experiments.

The bubbles in the developed foam model are arranged in a spatial area and the model includes calculations of complex realistic processes like coalescence, bubble rising and bubble growth. It was shown that the model can predict the influence of depressurisation rate on the foam structure. An increase in depressurisation rate leads to less formed bubbles and a faster predicted bubble growth. The porosity is influenced by both factors. This leads to two overlaying effects and therefore firstly to

an increase in the calculated final porosity and then to an approximately constant final foam porosity level with further increase in the depressurisation rate. In experiments done in this work and literature it was also shown that the depressurisation rate influences the porosity in the same way as was predicted. Literature experiments [52, 115, 116] show that the nucleation rate, growth rate and the coalescence increase with increasing depressurisation rate. This could lead to an increasing bubble size with increasing depressurisation rate like also predicted with the developed foam model. The reason is that in the model prediction the bubbles grow faster and the big bubbles has less time for outgassing with increasing depressurisation rate. The effect of depressurisation rate on the number of bubbles in experiments differ from the predicted results. A reason could be that in experiments the main formation of small bubbles took place when ambient pressure was just reached [52] but the model prediction already stops when ambient pressure is reached. The developed model can however successfully predict the influence of depressurisation rate on the foam formation especially the foam porosity. In conclusion it can be said, that the developed model is suitable for the description of high pressure aerated chocolate.

7 Conclusion

Aerated chocolate is one important product for the confectionary industry and its texture is a key driver for consumer preference. The need for differentiation through texture will gain even more importance in the future. The current state of the art is much too incomplete to allow a full understanding of the chocolate aeration process and due to this the control and prediction of the aeration process is difficult. This work should fill this gap. The aim was to understand the physical processes underlying gas solubility and bubble formation, as well as to determine the process conditions leading to optimal bubble formation during aeration of chocolate masses and to find the most suitable process control for various dimensions of consumer preference. Therefore the high pressure aeration of chocolate was experimentally investigated with the aim to develop a kinetic model of bubble formation and coalescence. The influence of different process parameters and chocolate composition on the gas solubility and the final product foam structure was experimentally determined for the high pressure aeration process. Additionally an alternative method for the tempering of high pressure aerated chocolate was identified and evaluated. Finally a MATLAB Model for the prediction of bubble formation and bubble growth for the high pressure aeration process was successfully developed and evaluated.

It was found, that the foam structure of aerated milk chocolate can be controlled through the gas composition used as the aerating agent. An increasing amount of carbon dioxide in the gas leads to bigger bubbles and higher porosities (with nitrogen the opposite behaviour is observed). Higher pressures promote the gas solubility and the chocolate foam porosity (until reaching a maximum porosity value of approximately 50 %). It was also shown that the foam porosity increases with increasing depressurisation rate and that temperature (process temperature and temperature reduction during depressuristion) and therefore the viscosity of the chocolate influences the foam structure. This results in the formation of foams with higher porosity and smaller bubbles at lower aeration temperatures.

A statistical design of experiments was used to investigate the influence of every chocolate component (cocoa butter, sugar, cocoa powder, milk powder and lecithin) on the gas solubility, dissolution time and foam structure. In conclusion it can be said that carbon dioxide is dissolved only in the cocoa butter and that no significant adsorption of the gas molecules on the particles takes places. Because of this, the gas solubility in the mixtures increases linearly with the amount of cocoa butter.

It was found out that high cocoa powder amounts reduce the speed of gas dissolution due to trapping of cocoa butter within the porous and rough cocoa particle structure and that this leads to a diffusion limitation of the gas inside the fat. The amount of trapped cocoa butter in the cocoa particles also influences the gas dissolution speed. An increase in trapped cocoa butter amount leads to a decrease

in freely available cocoa butter. These lead to a decrease in the gas dissolution speed due to a diffusion limitation because the diffusion of gas through the particles needs more time. Additionally it was found out, that the diffusion limitation effect of cocoa particles on the foam structure of aerated milk chocolates is insignificant. It was also shown that cocoa particles highly influence the foam structure in aerated cocoa butter and chocolate. An increase in cocoa powder leads to an increase in the bubble size in different chocolate mixtures compared to the other particulate ingredients.

It was shown that sugar leads to the generation of very small bubbles, milk powder generates medium sized bubbles and cocoa powder big bubbles. The foam porosities increase rapidly during the first aeration process hours until they reach a constant equilibrium porosity. Cocoa and milk powders have approximately similar effects on the foam porosity and lead to a high equilibrium porosity after around 50 hours of aeration. Sugar reduces the equilibrium porosity as well as the time until the equilibrium porosity is reached. Aerated dark, white and milk chocolate has approximately similar foam structures probably due to similar cocoa butter, sugar and lecithin amounts. Because of the strong influence of sugar on the foam structure, the detailed influence of sugar amount, particle size and particle shape was investigated. It was shown that the size of bubbles in aerated chocolates decreases with increasing sugar surface area, resulting from either increasing sugar particle sizes or increasing amounts with similar sugar size.

It was shown that the dissolution of carbon dioxide in chocolate leads to a decrease in the melting point. Standard tempering methods are therefore not suitable for a high pressure aeration process of chocolate because the stable seeds crystals melt during aeration. In this work an alternative method with intense cooling for the tempering of high pressure aerated chocolate was identified. It was shown that the crystallisation temperature and time influences the crystal structure form of cocoa butter and milk chocolate. It can be concluded that the tempering of high pressure aerated chocolate can be realised with the subsequent cooling method at -20°C, where complete tempering of the cocoa butter takes place. The challenge of the melting point shifting due to carbon dioxide dissolution can therefore be overcome with this method.

In this work a MATLAB model for the prediction of bubble formation and bubble growth during depressurisation of carbon dioxide high pressure aerated cocoa butter was successfully developed. This model considers the spatial bubble formation, the coalescence, bubbles rising and the change of material properties during the process. The assumption of a constant volume during coalescence and the addition of a maximum bubble radius of 1 mm was identified to be optimal for the prediction of a realistic, homogenous foam. With these parameters, a final porosity and a final average bubble radius in good agreement with the experimental results of this work was achieved. It was shown that the depressurisation rate also influences the foam structure especially the predicted porosity in the same way as it was shown in the experiments of this work and in literature. In conclusion it can be said, that the bubble model developed can successfully predict the foam formation of aerated cocoa butter/chocolate during depressurisation.

In conclusion it can be said, that in this work the effect of different process parameters and chocolate composition on the gas solubility and foam structure of aerated chocolate mixtures was successfully determined for the high pressure aeration process. For the first time a MATLAB Model for the successfully prediction of three-dimensional foam formation during depressurisation was developed and evaluated. This allows a deep understanding of the physical processes underlying gas solubility and bubble formation. It was shown that the differentiation through product texture can be realised by varying the chocolate composition or the process parameters. These findings could further enable a better control of the chocolate aeration process to obtain the production of various aerated chocolate products with different texture and foam characteristic.

8 Appendix

8.1 Appendix – Experimental Results

8.1.1 High Pressure Aeration

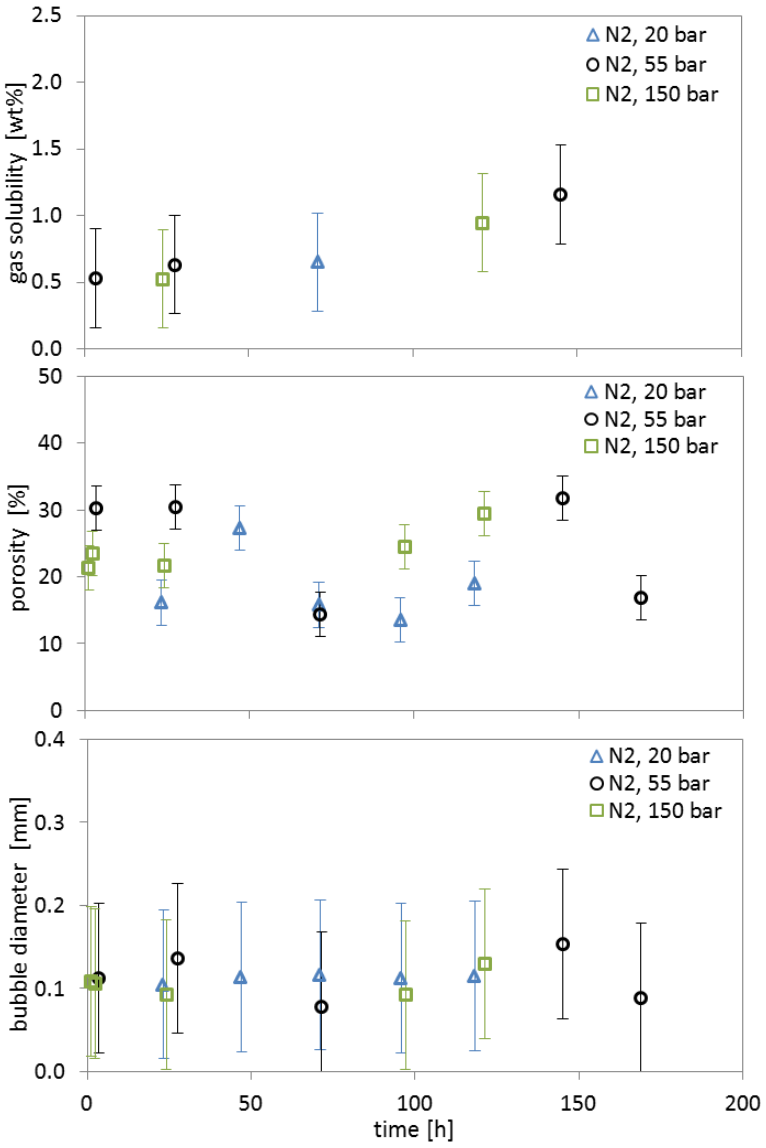

Figure 8-1: Influence of the pressure on the N_2 solubility, the porosity and the bubble diameter of N_2 aerated milk chocolate at 40 °C as function of the dissolution time (Δ 20 bar, ○ 55 bar, □ 150 bar)

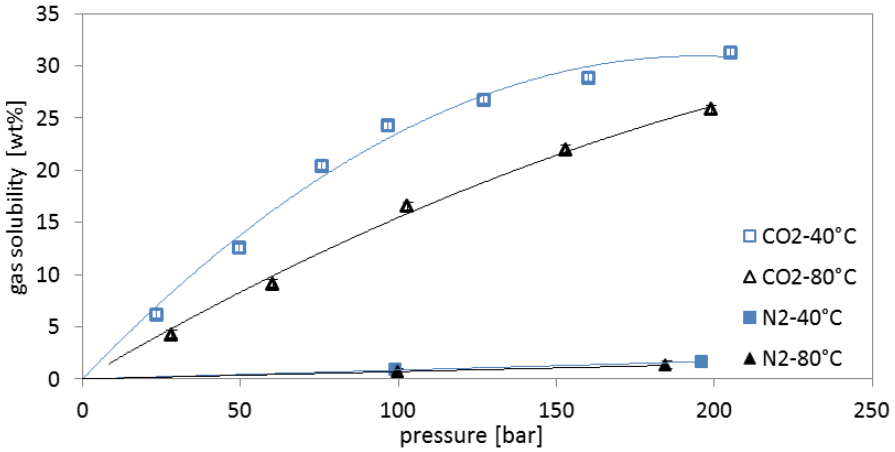

Figure 8-2: Influence of the pressure on the CO_2 and N_2 solubility in aerated cocoa butter at 40 °C and 80°C (□ CO2-40°C, Δ CO_2-80°C, ▪ N_2-40°C, ▲N_2-80°C)

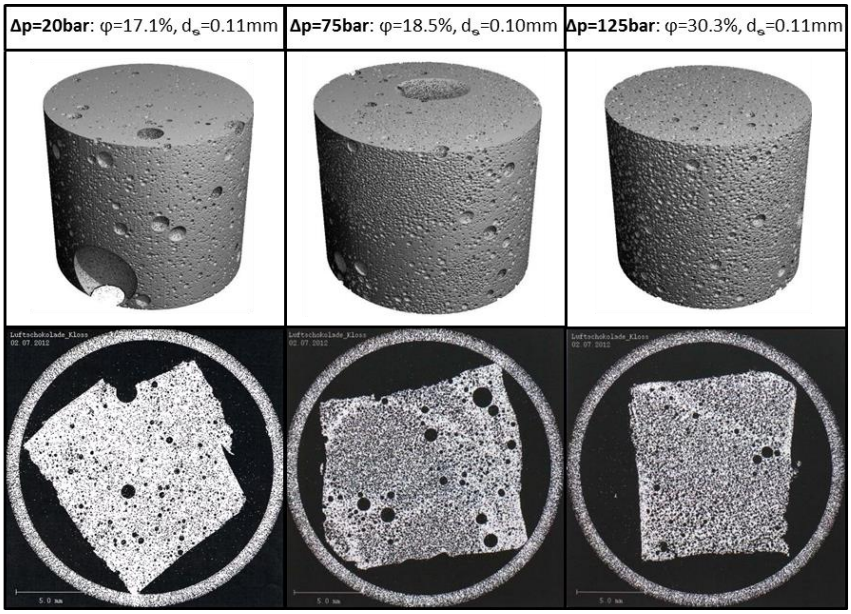

Figure 8-3: Influence of the depressurisation rate (Δp = 20bar, 75bar, 125bar) on the foam structure of N_2 aerated milk chocolate at 20 bar, 40°C and equilibrium (ϕ=porosity, d_ω=equivalent bubble diameter)

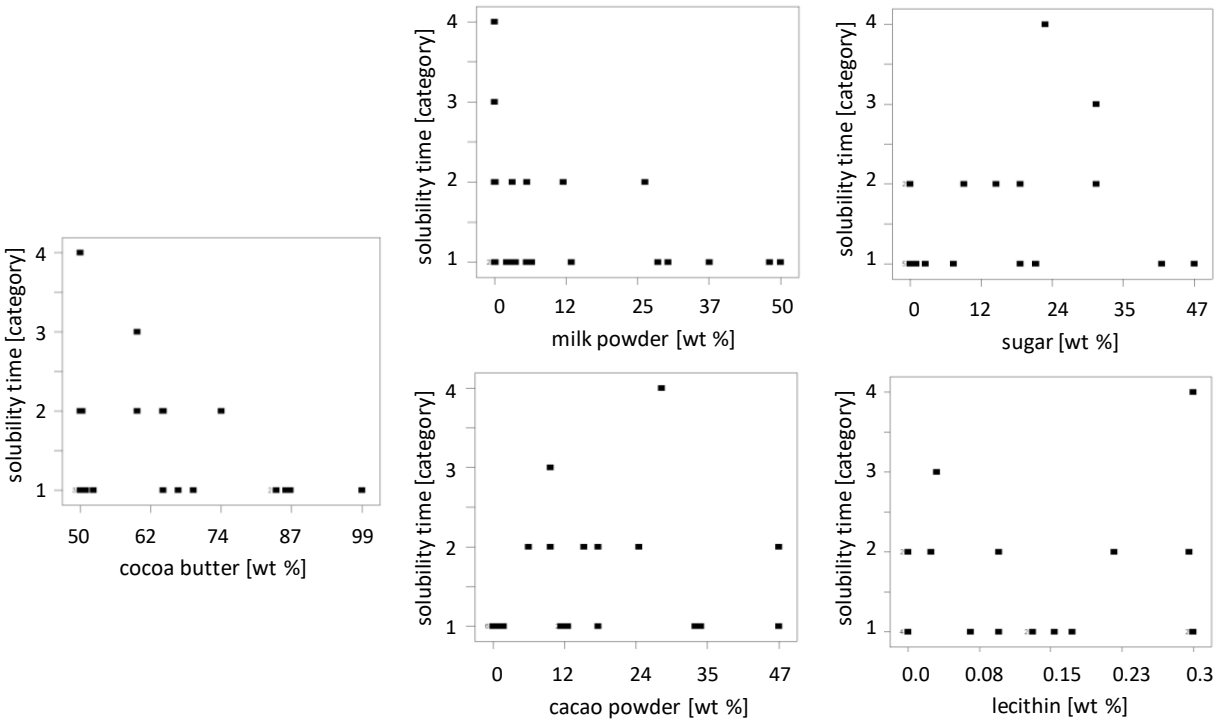

Figure 8-4: Influence of the single chocolate component amounts in the chocolate mixtures on the CO_2 dissolution time at 50 bar, 30°C and equilibrium

8.1.2 Effect of Dissolution Time on the Foam Structure

In Figure 8-5 the micro-CT foam pictures of high pressure aerated milk chocolate at 55 bar and 40°C are shown for different dissolution times using nitrogen, carbon dioxide or a 50% Nitrogen/50% carbon dioxide mixture as foaming agent.

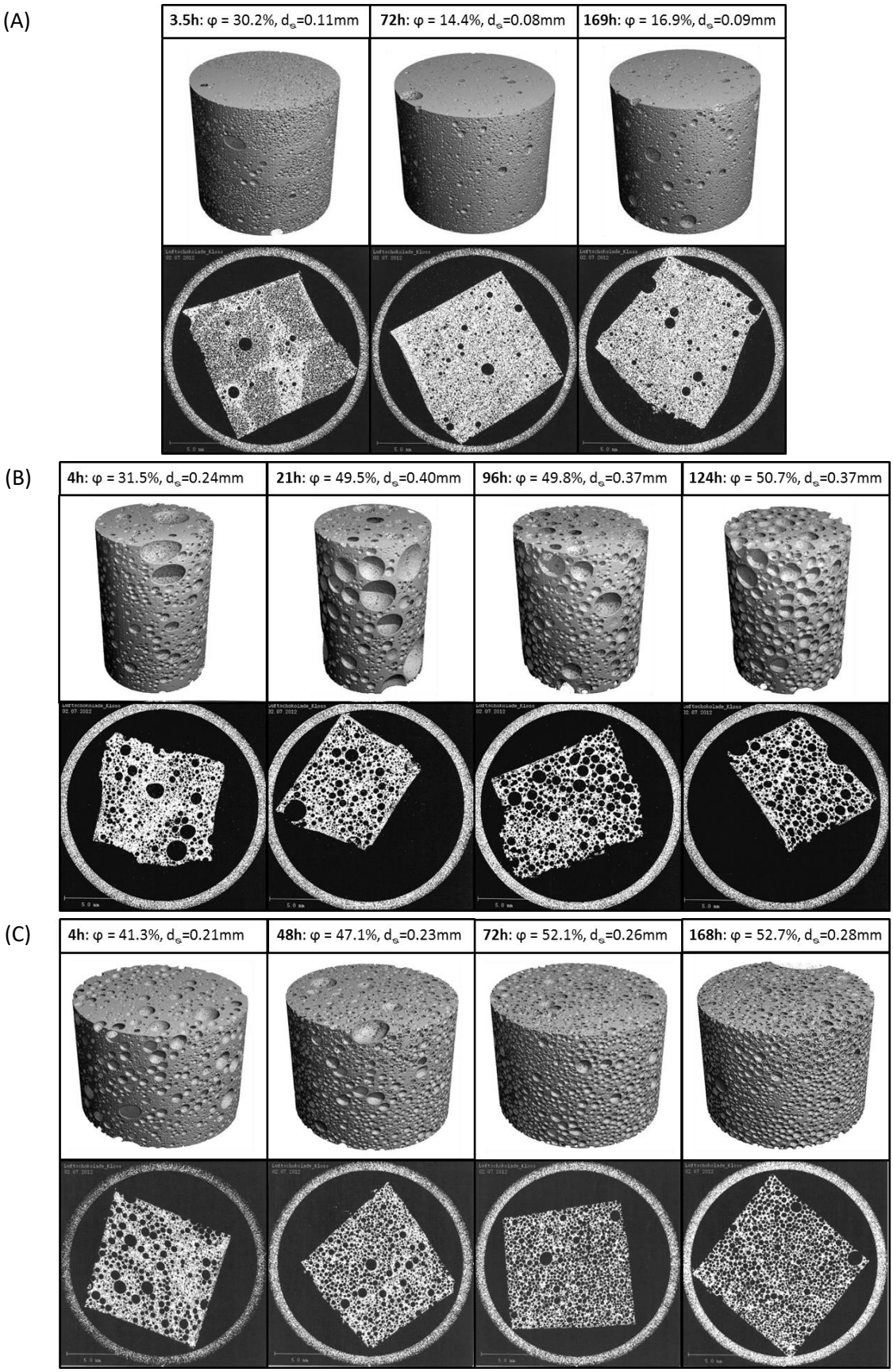

Figure 8-5: Influence of the gas phase on the foam structure of aerated milk chocolate at 55 bar and 40°C for different dissolution times. (A) N_2 (B) CO_2 (C) 50% CO_2 + 50% N_2 (ϕ = porosity, $d_⌀$ = equivalent bubble diameter)

8.2 Appendix – Modelling

8.2.1 Signal Flow Diagram

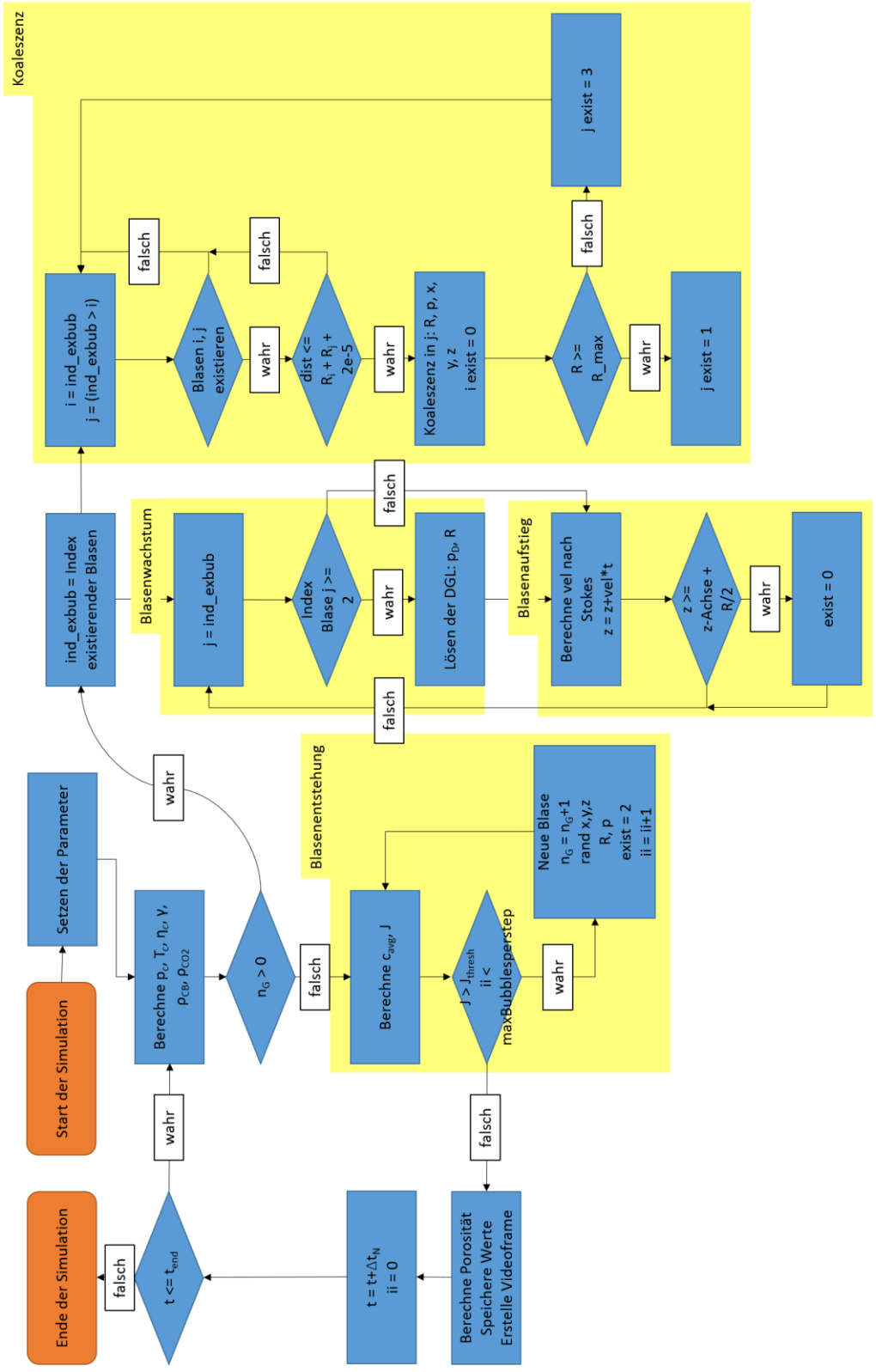

Figure 8-6: signal flow diagram of the developed foam model

8.2.2 MATLAB source code

```
clc
clear all
close all
rng('shuffle');
%% Programm nach Taki_2008
global j t t_end delta_t_N p_C p_0 p_end n_G V_L0 c_0 c_average J
global J_threshold f_0 M_W N_A F k_B D k_H R_g g
global eta_0 eta_end eta_C T_0 T_end T_C gamma rho_CB rho_CO2
global boxsize_x boxsize_y boxsize_z l l_stop
global n_real V_G phi epsilon
global bubbles mol_out R_max
global counter plots delta_R R_Vektor V_r max_R Filmchen
%% Eingabewerte
t = 0;                    %Laufende Zeit, hier Startzeit in s
t_end = 2;                %Endzeit in s
delta_t_N = 0.005;        %Schrittweite in s
maxBubblesperstep=10;     %Maximale Anzahl an Blasen pro Zeitschritt
p_0 = 5800000;            %Anfangsdruck außen in Pa
p_end = 100000;           %Enddruck außen in Pa
T_0 = 313.15;             %Anfangstemperatur in Kelvin, 40°C
T_end = 268.15;           %Endtemperatur in Kelvin, -5°C
eta_end = 0.4;            %Viskosität 13°C und 1bar (Dhorsi 2006)
J_threshold = 0.01;       %Grenz-Keimbildungsrate in 1/s
f_0 = 3.5e-25;            %Korrektur(fitting)-Faktor des Zeldovich Faktors
M_W = 0.044;              %Molekulargewicht des CO2 in kg/mol
F = 0.5*0.014085;         %Korrektur(fitting)-Faktor für die freie
                          %Energiebarriere
l_stop = 3000;            %Wann soll ode15s abgebrochen werden?
%% Kantenlängen des Kakaobutter-Würfels und Volumen (Startwerte)
boxsize_x = 1e-2;                       %Kantenlänge x der Kakaobutter 1cm
boxsize_y = 1e-2;                       %Kantenlänge y der Kakaobutter 1cm
boxsize_z = 1e-2;                       %Kantenlänge z der Kakaobutter 1cm
V_L0 = boxsize_x*boxsize_y*boxsize_z;   %Anfangsvolumen in m^3
R_max = 1.0e-3;                         %maximaler Blasenradius
max_R = 2e-3;                           %maximaler Blasenradius der
                                        %Balkendiagrammsdarstellung: 2mm
delta_R = 2.5e-5;                       %Schrittweite Balkendiagramm 0,025mm
%% Konstanten
k_B = 1.3806488e-23;      %Boltzmann Konstante in J/K
N_A = 6.0221412927e23;    %Avogadrozahl in 1/mol
D = 0.000000001;          %Diffusionskoeffizient in m^2/s,
                          %Diffusionskoeffizient von CO2 in Rapsöl
k_H = 0.0005091;          %Henrykoeffizient in mol Gas/m^3/Pa nach HEITZ
                          %(bei 40°C)
R_g = 8.3144621;          %molare (allgemeine) Gaskonstante
g = 9.81;                 %Erdbeschleunigung m/s^2
%% Startwerte
c_0 = startconc(p_0, M_W);      %Anfangskonzentration CO2 in KB
eta_0 = starteta(p_0);              %Anfangsviskosität der KB
n_G = 0;                            %Anfangszahl Blasen
mol_out = 0;                        %Mol des nicht in Blasen ausgelösten
                                    %Gases
l=1;                                %Zähler
counter = 1;                        %Zähler
Filmchen = struct('cdata',{},'colormap',{});
R_Vektor = (0+delta_R/2):delta_R:(max_R-delta_R/2);
%Vektor mit allen Mittelpunkten für Balkendiagramm V(r)
%% Hauptschleife
startTime=tic;                      %Zeitmessung der Berechnung
```

```
while t <= t_end
    p_C=presentPc(p_0,p_end,t,t_end);           %Außendrucksdrucks in Pa
    T_C=presentTc(T_0,T_end,t,t_end);           %Außentemperatur in K
    eta_C=presentEtaC(eta_0,eta_end,t,t_end);   %Viskosität in Pas
    rho_CB=presentCB(p_C);                      %Dichte von KB in kg/m^3
    rho_CO2=presentCO2(p_C);                    %Dichte von CO2 in kg/m^3
                                                %(bis 90bar)
    gamma=surfacetension(p_C);                  %Oberflächenspannung in N/m
    if n_G>0
        ind_exbub = find(arrayfun(@(bub) bub.exist >= 1-1e-14 , bubbles));
        %Indizes aller existierenden Blasen von 'bubbles'
        for j=ind_exbub
            %% Blasenwachstum
            if bubbles(j).exist >= 2-1e-14
            %Blasenwert 'exist' sagt: Blase darf noch wachsen
                bubbles = growth(j,bubbles);
            end
            %% Blasenaufstieg
            [bubbles,mol_out] = rising(j,bubbles,mol_out);
        end
        %% Koaleszenz
        bubbles = coalescence(bubbles);
    end
    c_average=averageconc(V_L0,c_0,R_g,T_0,n_G,mol_out);
    %Berechnung der mittleren Konzentration in mol/m^3
    J=nucleationrate(f_0,gamma,M_W,N_A,F,k_B,T_C,c_average,k_H,p_C);
    %Berechnung der Keimbildungsrate in 1/s
    ii=0;
    %% Blasenentstehung
    while J>J_threshold && ii < maxBubblesperstep
        bubbles = bubble_nucl();
        ii = ii+1;
    end
    %% Durchschnittlicher Blasenradius / Plot 3D / Vorbereitung Plot V(r)
    V_G = 0;
    sum_radius = 0;
    if n_G > 0
        ind_exbub = find(arrayfun(@(bub) bub.exist >= 1-1e-14 , bubbles));
        %Indizes aller existierenden Blasen von 'bubbles'
        V_r = zeros(1,length(R_Vektor));
        %Volumen-Vektor für Balkendiagramm
        for n = ind_exbub
            sum_radius=sum_radius+bubbles(n).R; %Aufsummierung Radien
            V_i = real(4/3*pi*bubbles(n).R^3);  %Gasvolumen Blase i
            V_G = V_G + V_i;                    %Volumen aller Blasen
            zaehler=ceil(real(bubbles(n).R)/delta_R);
            V_r(zaehler)=V_r(zaehler)+V_i;
            %% Plotten der Blasen in 3D
            plot_3D(n);
        end
        n_real = length(ind_exbub);         %Anzahl existierender Blasen
        average_radius=sum_radius/n_real;   %durchschnittlicher Radius
        %% Berechnung der Volumenanteile
        epsilon = real((V_L0-V_G)/V_L0);    %Volumenanteil Flüssigkeit
        phi = real(V_G/V_L0);               %Volumenanteil Gas
        %% Plotten des Balkendiagramms: V über r
        plot_V_r();
        %% Datensammlung für spätere Grafiken
        plots = getData(plots, average_radius);
        %% Video aufnehmen
        set(gcf,'Renderer','zbuffer');      %zum Video erstellen unter Win7
```

```
        Filmchen(counter)=getframe(gcf);    %Aufnahme des Frames
        counter=counter+1;
    end
    hold off
    t=t+delta_t_N;
    fprintf('\n\nCurrent time: %6.3f \n',t);
end
endTime=toc(startTime);
save Variablen_2s_58bar.mat     %speichern der Variablen
movie2avi(Filmchen,'Video-bennene-mich.avi','compression','none','fps',5)
%speichern des Videos als .avi


function [ c_0 ] = startconc( p_0 , M_W)
% Berechnung der Anfangskonzentration c_0
% von CO2 in Kakaobutter bei 40°C in Abhängigkeit vom Druck
p_bar = p_0*1e-5;
c_0 = (-1.0437*1e-4*p_bar^3-0.6011*p_bar^2+246.994*p_bar)/(100*M_W);
end


function [ eta_0 ] = starteta( p_0 )
%Berechnung der Viskosität zu Simulationsbeginn
%   in Abhängigkeit von p_0 für Drücke bis 70bar
eta_0 = -0.0005*p_0*1e-5+0.0412;
end


function [ p_C ] = presentPc(p_0,p_end,t,t_end)
% Druckfunktion
%   Annahme: Druckabfall hauptsächlich bis 1/2 der Zeit
t_percentage = 0.5;
t_p = t_percentage*t_end;
p_tp = p_0 - 0.67 * p_0;
if t <= t_p
    p_C = p_0-((p_0-p_tp)/t_p)*t;
elseif t > t_p
    p_C = p_tp-((p_tp-p_end)/(t_end-t_p))*(t-t_p);
end
end


function [ T_C ] = presentTc(T_0,T_end,t,t_end)
%Berechnung der Temperatur - linearer Verlauf über der Zeit
T_C = T_0-((T_0-T_end)/t_end)*t;
end


function [ eta_C ] = presentEtaC(eta_0,eta_end,t,t_end)
%Berechnung der Temperatur - linearer Verlauf über der Zeit
eta_C = (eta_end-eta_0)/t_end * t + eta_0;
end


function [ rho_CB ] = presentCB( p_C )
%Berechnung der Dichte des Kakaobutter-CO2 Gemischs in Abhängigkeit vom
%Druck
rho_CB = 0.1491*(p_C*10^-5)+916.15;
```

```
end


function [ rho_CO2 ] = presentCO2( p_C )
%Berechnung der Dichte von CO2 in Abhängigkeit vom Druck
%gültig für Drücke <= 90 bar
global p_bar
p_bar = p_C*10^-5;
rho_CO2 = 2*10^-8*p_bar^6-3*10^-6*p_bar^5+0.0003*p_bar^4-0.0107*p_bar^3 ...
    +0.193*p_bar^2+0.5*p_bar+1.5413;
end


function [ gamma ] = surfacetension( p_C )
%Berechnung der Oberflächenspannung in Abhängigkeit vom Druck
gamma = -2.693*1e-9*p_C + 2.854*1e-2;
end


function [ bubbles ] = growth( j,bubbles )
% Berechnung des Blasenwachstums, Aufruf ode15s
global l l_stop delta_t_N
bubbles(j).R_old = bubbles(j).R;
R=real(bubbles(j).R);
%Abschneiden des mögl. Imaginärteils vom Blasenradius (in m)
p_D=real(bubbles(j).p_D);
%Abschneiden des mögl. Imaginärteils vom Blasendruck (in Pa)
l=1;
options = odeset('Events',@Abbruch, 'RelTol', 1e-4,...
    'AbsTol', [1e-12 1e-6], 'NonNegative', [1 2]);
    %Setzen der Toleranzen und Abbruchfunktion für das Lösen der ODE
[do_not_care, Y, ~, YE, ~] = ode15s(@Radius_8_Han_vS,[0 delta_t_N],...
    [R+1e-15 p_D], options);
    %Aufruf Funktion [t_0 t_end],[Anfangsradius Anfangsdruck in der Blase]
%% Auslesen der Daten aus entstandenem Vektor Y
if l>=l_stop
    bubbles(j).R=YE(end,1);
    bubbles(j).p_D=YE(end,2);
else
    bubbles(j).R=Y(end,1);
    bubbles(j).p_D=Y(end,2);
end
end


function [ value, isterminal, direction ] = Abbruch( t, y)
%Abbruchbedingung für ode15s
global l l_stop
value = l-l_stop; %bricht ab, wenn l=l_stop, also nach l_stop
Anpassungsschritten
isterminal = 1;
direction = 0;
end


function dydt = Radius_8_Han_vS(t,y)
%ODE zur Berechnung von y(1)= R und y(2)= p (der Blase)
global j p_C c_average bubbles
global eta_C gamma D k_H R_g T_0 l
```

```
dydt = zeros(2,1);
dydt(1) = y(1)*y(2)*1/(4*eta_C)-y(1)*p_C/(4*eta_C)-2*(gamma)/(4*eta_C);
dydt(2) = 6*D*R_g*T_0*(c_average-k_H*y(2))/(-y(1)^2+(y(1)^4+2*y(1)/...
    (R_g*T_0)*((y(2)*y(1)^3-(bubbles(j).p_D_0)*(bubbles(j).R_0)^3)/...
    (c_average-k_H*y(2))))^(1/2))-3*y(2)/y(1)*dydt(1);
l = l+1;
end


function [ bubbles ] = coalescence(bubbles)
% Abfrage und Durchführung von Koaleszenz
%   Vergleich der Blasen i,j paarweise: Abstand => Koaleszenz?!
%   Koaleszenz findet in der Blase j statt
global R_g T_0 eta_C rho_CB rho_CO2 t g %grad p_C gamma delta_t_N
ind_exbub = find(arrayfun(@(bub) bub.exist >= 2-1e-14 , bubbles));
%Indizes aller existierenden Blasen von 'bubbles'
for i=ind_exbub
    for j=ind_exbub(ind_exbub>i)     %j>i
        if bubbles(i).exist >=2 && bubbles(j).exist >=2
        %nur Blasen mit exist >= 2 dürfen koaleszieren
            dist_ij = (bubbles(i).x-bubbles(j).x)^2 +...
                (bubbles(i).y-bubbles(j).y)^2 +...
                (bubbles(i).z-bubbles(j).z)^2;      %quadrierter Abstand
            if dist_ij < (bubbles(i).R + bubbles(j).R + 2e-5)^2
            %Koaleszenz, wenn Abstand < Summe der Radien + Überlappung
                n_i = real((4/3*pi*(bubbles(i).R)^3*bubbles(i).p_D)/...
                    (R_g*T_0));     %Mole der Blase i
                n_j = real((4/3*pi*(bubbles(j).R)^3*bubbles(j).p_D)/...
                    (R_g*T_0));     %Mole Blase j
                n_i_j = n_i + n_j;  %Summe der Mole Blase i + Blase j
                %% Variante 1: Druck wie bei Neubildung einer Blase; R(p)
%                 bubbles(j).p_D_0 = c_average/k_H;
%                 bubbles(j).R_0 = ((bubbles(i).p_D*bubbles(i).R^3+...
%                   bubbles(j).p_D*bubbles(j).R^3)/bubbles(j).p_D_0)^(1/3);
%                 bubbles(j).p_D = bubbles(j).p_D_0;
%                 bubbles(j).R = bubbles(j).R_0;                          1
                %% Variante 2: Bildung einer Wachstumsrate
%                 grad = abs((bubbles(i).R-bubbles(i).R_old)/delta_t_N*...
%                   n_i/n_i_j + (bubbles(j).R-bubbles(j).R_old)/...
%                   delta_t_N*n_j/n_i_j);
%                 bubbles(j).p_D_0 = grad*4*eta_C+p_C+2*gamma;
%                 bubbles(j).R_0 = ((bubbles(i).p_D*bubbles(i).R^3+...
%                   bubbles(j).p_D*bubbles(j).R^3)/bubbles(j).p_D_0)^(1/3);
%                 bubbles(j).p_D = bubbles(j).p_D_0;
%                 bubbles(j).R = bubbles(j).R_0;                          2
                %% Variante 3: Druck gleich Umgebungsdruck
%                 bubbles(j).p_D_0 = p_C;
%                 bubbles(j).R_0 = ((bubbles(i).p_D*bubbles(i).R^3+...
%                   bubbles(j).p_D*bubbles(j).R^3)/bubbles(j).p_D_0)^(1/3);
%                 bubbles(j).p_D = bubbles(j).p_D_0;
%                 bubbles(j).R = bubbles(j).R_0;                          3
                %% Variante 4: Annahme eines konstante Volumens
                bubbles(j).R_0 = (bubbles(i).R^3 + bubbles(j).R^3)^(1/3);
                bubbles(j).p_D_0 = (bubbles(i).R^3*bubbles(i).p_D+...
                    bubbles(j).R^3*bubbles(j).p_D)/(bubbles(j).R_0^3);
                bubbles(j).p_D = bubbles(j).p_D_0;
                bubbles(j).R = bubbles(j).R_0;                          4
                %% für alle Varianten:
                bubbles(j).R_old = bubbles(j).R_0;
                bubbles(j).x = bubbles(i).x*n_i/n_i_j+...
                    bubbles(j).x*n_j/n_i_j;
```

```
                bubbles(j).y = bubbles(i).y*n_i/n_i_j+...
                    bubbles(j).y*n_j/n_i_j;
                bubbles(j).z = bubbles(i).z*n_i/n_i_j+...
                    bubbles(j).z*n_j/n_i_j;
                %gewichtete Koordinaten x, y, z
                bubbles(j).vel = real((2*(bubbles(j).R)^2*g*...
                    (rho_CB - rho_CO2))/(9*eta_C));
                    %Geschwindigkeit der Blase
                bubbles(j).t_nucleation = t;
                %Entstehungszeit der koaleszierten Blasen
                bubbles(i).t_death = t;     %Todeszeitpunkt der Blase i
                bubbles(i).exist = 0;       %Blase i existiert nicht mehr
                if (bubbles(j).z+bubbles(j).R/2) > boxsize_z    %Ausgasen?
                    bubbles(j).t_death = t; %Todeszeitpunkt der Blase
                    bubbles(j).exist = 0;   %Blase existiert nicht mehr
                    mol_out=mol_out+...
                        (4/3*pi*(bubbles(j).R)^3*bubbles(j).p_D)/(R_g*T_0);
                        %Mole, die ausgegast sind
                elseif bubbles(j).R > R_max
                %wenn Blase nicht ausgegast ist und R größer als R_max ist
                    bubbles(j).exist = 1;   %Exist=1:
                                            %Blase darf nicht mehr wachsen
                else
                %wenn Blase weder ausgegast, noch zu groß ist
                    bubbles(j).exist = 3;   %Exist=3: koaleszierte Blase
                end
                break
            end
        end
    end
end
end
```

Additional option

```
function [ c_average ] = averageconc(V_L0, c_0, R_g, T_0, n_G, mol_out)
%Berechnung der mittlere Konzentration in der Flüssigkeit
global bubbles sum_mol
sum_mol=mol_out;    %Startwert: ausgelöste Blasen
for i = 1:n_G       %Aufsummieren des Blasenanteils in mol
    if bubbles(i).exist>=1
        sum_mol=sum_mol+(4/3*pi*(bubbles(i).R)^3*bubbles(i).p_D)/(R_g*T_0);
        %ideales Gasgesetz: n= (p*V)/(R*T)
    end
end
c_average=c_0-sum_mol/V_L0;
end
```

```
function [ J ] = nucleationrate( f_0, gamma, M_W, N_A, F, k_B, T_C,...
    c_average, k_H, p_C )
% Keimbildungsrate, übernommen aus Taki 2008 Gleichung (15)
J=f_0*(2*gamma/(pi*M_W/N_A))^(1/2)*exp(-16*pi*gamma^3*F/...
    (3*k_B*T_C*(c_average/k_H-p_C)^2))*N_A*c_average;
end
```

```
function [ bubbles ] = bubble_nucl()
% Entstehung neuer Blasen für J > J_threshold
% maximale Anzahl: maxBubblesperstep
global J n_G t gamma c_average k_H p_C rho_CB rho_CO2 eta_C g bubbles
```

```
global boxsize_x boxsize_y boxsize_z
global V_L0 c_0 R_g T_0 mol_out %Variablen für function averageconc
global f_0 M_W N_A F k_B T_C    %Variablen für function nucleationrate
n_G=n_G+1;
bubbles(n_G).t_nucleation = t;
bubbles(n_G).x = rand*boxsize_x;
bubbles(n_G).y = rand*boxsize_y;
bubbles(n_G).z = rand*boxsize_z;
bubbles(n_G).R = 2*gamma*1.5/(c_average/k_H-p_C);
bubbles(n_G).R_old = 2*gamma*1.5/(c_average/k_H-p_C);
bubbles(n_G).R_0 = 2*gamma*1.5/(c_average/k_H-p_C);
bubbles(n_G).p_D = c_average/k_H;
bubbles(n_G).p_D_0 = c_average/k_H;
bubbles(n_G).t_death = []; %Blase noch nicht gestorben
bubbles(n_G).vel = real((2*(bubbles(n_G).R)^2*g*(rho_CB -
rho_CO2))/(9*eta_C)); %Aufstiegsgeschwindigkeit
bubbles(n_G).exist = 2;
%% Neuberechnung von c_average und J
c_average=averageconc(V_L0, c_0, R_g, T_0, n_G, mol_out);
J=nucleationrate(f_0,gamma,M_W,N_A,F,k_B,T_C,c_average,k_H,p_C);
end


function [ ] = plot_3D( n )
%3D-Plot der Blasen
global x y z bubbles t boxsize_x boxsize_y boxsize_z
[x,y,z]=sphere;
colormap([1 0 0 ; 0.5 0.5 0.5 ; 1 0 0])
M=[real(bubbles(n).x) real(bubbles(n).y) real(bubbles(n).z)];
r=real(bubbles(n).R);
x=x*r+M(1);
y=y*r+M(2);
z=z*r+M(3);
C = ones(size(z))*bubbles(n).exist;
%zum Setzen der Blasenfarbe in Abhängigkeit des exist-Wertes
subplot(2,3,[1,2,4,5])
surf(x,y,z,C,'EdgeAlpha', 0.5,'CDataMapping','direct')
alpha(0.5)
axis([0 boxsize_x 0 boxsize_y 0 boxsize_z])
axis vis3d
xlabel('Koordinate x'), ylabel('Koordinate y'), zlabel('Koordinate z')
str=sprintf('Zeit %.3f s',t);
title(str)
hold on
end


function [  ] = plot_V_r( )
%Plot des Balkendiagramms V(r)
global R_Vektor V_r t
subplot(2,3,[3,6])
bar(R_Vektor,V_r,1)
axis([0 2e-3 0 1e-7])
xlabel('r in m'), ylabel('Gasvolumen in m^3')
str=sprintf('Zeit %.3f s',t);
title(str)
hold on
end
```

8.2.3 Variables

Table 8-1: MATLAB model variables

Matlab	Text	Value or calculation equation	Definition
delta_t_N	Δt_N	0.005 s	Time step
p_end	p_{end}	1 bar	End pressure
T_0	T_0	40 °C	Initial saturation temperature
T_end	T_{end}	-5 °C	End temperature
eta_0	η_0	0.0105 Pa·s	Initial viscosity
eta_end	η_{end}	0.4 Pa·s	End viscosity
D	D	$10^{-9}\mathrm{m}^2 \cdot \mathrm{s}^{-1}$	Diffusion coefficient
k_B	k_B	$1.3806488 \cdot 10^{-23} J \cdot K^{-1}$	Boltzmann constant
k_H	$H_{1,2}$	$0.0005091\ \mathrm{mol} \cdot \mathrm{Pa}^{-1}\mathrm{m}^{-3}$	Henry coefficient
N_A		$6.0221412927 \cdot 10^{23}\mathrm{mol}^{-1}$	Avogadro constant
R_G	R_G	$8.3144621\ \mathrm{J} \cdot \mathrm{mol}^{-1}\mathrm{K}^{-1}$	Universal gas constant
g	g	$9.81\ \mathrm{m} \cdot \mathrm{s}^{-2}$	gravity
J_threshold	J_{thresh}	$0.01\ \mathrm{s}^{-1}$	Threshold nucleation rate
f_0	f_0	$3.5 \cdot 10^{-25}$	Fitting parameter
F	F	0.5·0,014085	Fitting parameter
maxBubblesperstep		10	Maximum number of formed bubbles per time step
R_max	R_{max}	1 mm	Maximum Bubble radius
p_C	p_C	-	Present environmental pressure
T_C	T_C	Equation (5-7)	Present temperature
eta_C	η_C	Equation (5-9)	Present viscosity
rho_CB	$\rho_{KB,CO2}$	Equation (5-2)	Density of CO_2 saturated cocoa butter
rho_CO2	ρ_{CO2}	Equation (5-3)	Density of CO_2
gamma	σ	Equation (5-6)	Surface tension
c_average	$\bar{c}$	Equation (2-36)	Average concentration
J	J	Equation (2-35)	Nucleation rate

Literature

[1] J. Haedelt, An investigation into bubble inclusion into liquid chocolate, *Dissertation*, The University of Reading **2005**.

[2] B. W. Minifie, *Chocolate, cocoa, and confectionery: Science and technology*, 3rd ed., An AVI book, Van Nostrand Reinhold, New York **1989**.

[3] W. Frede, *Taschenbuch für Lebensmittelchemiker: Lebensmittel - Bedarfsgegenstände - Kosmetika - Futtermittel*, 2nd ed., Springer, Berlin **2006**.

[4] Bundesministerium für Verbraucherschutz, Ernährung und Landwirtschaft, *Verordnung über Kakao- und Schokoladenerzeugnisse (Kakaoverordnung): KakaoV 2003* **2008**.

[5] K. Jackson, in *Moderne Schokoladentechnologie: Rohstoffe, Verfahrenstechnik, Qualitätskontrolle, Marketing* (Eds: S. T. Beckett), Behr. Hamburg **1990**.

[6] G. Ziegleder, in *Lebensmitteltechnologie: Biotechnologische, chemische, mechanische und thermische Verfahren der Lebensmittelverarbeitung* (Eds: R. Heiss), Springer. Berlin **2004**.

[7] O. Sticher, E. Steinegger, *Pharmakognosie - Phytopharmazie*, 9th ed., Springer-Lehrbuch, Springer-Verlag Berlin Heidelberg, Berlin, Heidelberg **2010**.

[8] S. T. Beckett, *The science of chocolate*, 2nd ed., Royal Society of Chemistry, Cambridge **2009**.

[9] G. Talbot, in *Industrial chocolate manufacture and use* (Eds: S. T. Beckett), Wiley-Blackwell. Chichester, UK, Ames, Iowa, Hoboken, NJ **2009**.

[10] S. Chaiseri, P. S. Dimick, *J Am Oil Chem Soc* **1989**, *66 (12)*, 1771 – 1776. DOI: 10.1007/BF02660745.

[11] M. J. Venter, P. Willems, S. Kareth, E. Weidner, Kuipers, N. J. M., de Haan, A. B., *The Journal of Supercritical Fluids* **2007**, *41 (2)*, 195 – 203. DOI: 10.1016/j.supflu.2006.10.010.

[12] R. L. Wille, E. S. Lutton, *J Am Oil Chem Soc* **1966**, *43 (8)*, 491 – 496. DOI: 10.1007/BF02641273.

[13] K. Larsson, S. J. Cyvin, L. Rymo, J. H. Bowie, D. H. Williams, E. Bunnenberg, C. Djerassi, R. Records, *Acta Chem. Scand.* **1966**, *20*, 2255 – 2260. DOI: 10.3891/acta.chem.scand.20-2255.

[14] B. Calvignac, E. Rodier, J.-J. Letourneau, Almeida dos Santos, Pedro Miguel, J. Fages, *International Journal of Chemical Reactor Engineering* **2010**, *8 (1)*. DOI: 10.2202/1542-6580.2191.

[15] L. Hernquist, in *Moderne Schokoladentechnologie: Rohstoffe, Verfahrenstechnik, Qualitätskontrolle, Marketing* (Eds: S. T. Beckett), Behr. Hamburg **1990**.

[16] Y. E. Mehrle, Solidification and contraction of confectionery systems in rapid cooling processing, ETH Zürich **2007**.

[17] Uni Kiel, *Kristall = Gitter + Basis*, http://www.tf.uni-kiel.de/matwis/amat/mw1_ge/kap_3/backbone/r3_1_2.html **2014**.

[18] H.-A. Kurzhals, *Lexikon Lebensmitteltechnik*, Behr, Hamburg **2003**.

[19] J. Kleinert, in *Moderne Schokoladentechnologie: Rohstoffe, Verfahrenstechnik, Qualitätskontrolle, Marketing* (Eds: S. T. Beckett), Behr. Hamburg **1990**.

[20] H. J. Kamphius, in *Industrial chocolate manufacture and use* (Eds: S. T. Beckett), Wiley-Blackwell. Oxford **2009**.

[21] *Alkaloidhaltige Genussmittel, Gewürze, Kochsalz*, Handbuch der Lebensmittelchemie, Vol. 6 (Eds: H. Beitter et al.), Springer Berlin Heidelberg, Berlin, Heidelberg **1970**.

[22] C. Krüger, in *Moderne Schokoladentechnologie: Rohstoffe, Verfahrenstechnik, Qualitätskontrolle, Marketing* (Eds: S. T. Beckett), Behr. Hamburg **1990**.

[23] P. Margaretha, *Chemie für Mediziner*, Springer-Lehrbuch, Springer, Berlin **2002**.

[24] *Industrial chocolate manufacture and use*, 4th ed. (Eds: S. T. Beckett), Wiley-Blackwell, Chichester, UK, Ames, Iowa, Hoboken, NJ **2009**.

[25] C. Krüger, in *Industrial chocolate manufacture and use* (Eds: S. T. Beckett), Wiley-Blackwell. Chichester, UK, Ames, Iowa, Hoboken, NJ **2009**.

[26] E. H. Reimerdes, Mehrens H.-A., in *Moderne Schokoladentechnologie: Rohstoffe, Verfahrenstechnik, Qualitätskontrolle, Marketing* (Eds: S. T. Beckett), Behr. Hamburg **1990**.

[27] J. Chevalley, in *Moderne Schokoladentechnologie: Rohstoffe, Verfahrenstechnik, Qualitätskontrolle, Marketing* (Eds: S. T. Beckett), Behr. Hamburg **1990**.

[28] G. Kretschmann, *Margarine - mehr als ein Brotaufstrich*, http://chids.online.uni-marburg.de/dachs/expvortr/639/magarine.htm.

[29] *Moderne Schokoladentechnologie: Rohstoffe, Verfahrenstechnik, Qualitätskontrolle, Marketing* (Eds: S. T. Beckett), Behr, Hamburg **1990**.

[30] B.L. Hancock, in *Moderne Schokoladentechnologie: Rohstoffe, Verfahrenstechnik, Qualitätskontrolle, Marketing* (Eds: S. T. Beckett), Behr. Hamburg **1990**.

[31] A. Prins, *Chemie in unserer Zeit* **2005**, *39 (6)*, 373.

[32] J.C. Hoskin, P.S. Dimick, in *Moderne Schokoladentechnologie: Rohstoffe, Verfahrenstechnik, Qualitätskontrolle, Marketing* (Eds: S. T. Beckett), Behr. Hamburg **1990**.

[33] E. O. Afoakwa, *Chocolate science and technology*, Wiley-Blackwell, Chichester, U.K, Ames, Iowa **2010**.

[34] Ed: R. Macrae, R.K. Robinson, M.J. Sadler, *Encyclopaedia of food science, food technology and nutrition* **1993**.

[35] D. Ley, in *Moderne Schokoladentechnologie: Rohstoffe, Verfahrenstechnik, Qualitätskontrolle, Marketing* (Eds: S. T. Beckett), Behr. Hamburg **1990**.

[36] E. J. Windhab, in *Industrial chocolate manufacture and use* (Eds: S. T. Beckett), Wiley-Blackwell. Chichester, UK, Ames, Iowa, Hoboken, NJ **2009**.

[37] R. B. Nelson, in *Moderne Schokoladentechnologie: Rohstoffe, Verfahrenstechnik, Qualitätskontrolle, Marketing* (Eds: S. T. Beckett), Behr. Hamburg **1990**.

[38] *Lieferumfang Turbotemper®*, http://www.google.de/url?sa=t&rct=j&q=&esrc=s&source=web&cd=2&cad=rja&uact=8&ved=0CCkQFjAB&url=ftp%3A%2F%2Ftrabant.tr.fh-hannover.de%2FSchwarzes_Brett%2FSchwermer%2FVertiefung_TR_6Sem%2FSollich-Doku_alt%2FD_0795_Mini_B%2BRTouch_A__FHH.DOC&ei=OH1HVJyMN8XUOsSigPgP&usg=AFQjCNEUsu__eGik7BgjVOdZ2QnWAIq-EQ&bvm=bv.77880786,d.ZWU.

[39] Sollich North America, *Sollich tempering machine Turbotemper Top Type TT and TTD*, http://www.sollichna.com/products/product-lines-by-sollich/chocolate-tempering/turbotemper-top-tt-ttd.

[40] Nestlé Product Technology Centre York, *Tempering and cooling profile*, *E-Mail*, 17.10.2014.

[41] W. Asche, *CLB Chemie in Labor und Biotechnik* **1998**, *49 (2)*, 63 – 64.

[42] W. J. Bartz, *Viskosität und Fließverhalten: Glossary*, Handbuch der Tribologie und Schmierungstechnik, Vol. 7, expert-Verl, Renningen-Malmsheim **1994**.

[43] G. Ziegleder, C. Moser, J. Geier-Greguska, *Fett/Lipid* **1996**, *98 (7-8)*, 253 – 256. DOI: 10.1002/lipi.19960980706.

[44] H. Herwig, *Wärmeübertragung A - Z: Systematische und ausführliche Erläuterungen wichtiger Größen und Konzepte*, VDI-Buch, Springer, Berlin **2000**.

[45] J. Engmann, M. R. Mackley, *Food and Bioproducts Processing* **2006**, *84 (2)*, 95 – 101. DOI: 10.1205/fbp.05104.

[46] A. Deuerling, T. Wilhelm, *Mathematische und Naturwissenschaftliche Unterricht* **2011**, *64 (7)*, 408.

[47] N. A. Morad, A. A. M. Kamal, F. Panau, T. W. Yew, *Journal of the American Oil Chemists' Society* **2000**, *77 (9)*, 1001 – 1005. DOI: 10.1007/s11746-000-0158-6.

[48] G. M. Chapman, E. E. Akehurst, W. B. Wright, *J Am Oil Chem Soc* **1971**, *48 (12)*, 824 – 830. DOI: 10.1007/BF02609292.

[49] *Industrial High Pressure Applications* (Eds: R. Eggers), Wiley-VCH Verlag GmbH & Co. KGaA, Weinheim, Germany **2012**.

[50] S. Su-Jia, C. Dong, X. Shi-Chao, *Journal of Food Process Engineering* **2013**, *36 (4)*, 544 – 547. DOI: 10.1111/jfpe.12017.

[51] V. R. Ciccone, *US2784096 A*, **1953**.

[52] C. Koller, High-Pressure Micro-Foaming of Fat-Continuous Confectionery Systems, *Dissertation*, ETH Zurich **2015**.

[53] J. Gmehling, B. Kolbe, *Thermodynamik*, Lehrbuchreihe Chemieingenieurwesen, Verfahrenstechnik, Thieme, Stuttgart **1988**.

[54] H. D. Baehr, S. Kabelac, *Thermodynamik*, Springer Berlin Heidelberg, Berlin, Heidelberg **2009**.

[55] W. P. W. J. Moore, *Grundlagen der Physikalischen Chemie*, Bod Third Party Titles **1990**.

[56] A. Mersmann et al., *Thermische Verfahrenstechnik: Grundlagen und Methoden*, 2nd ed., Springer **2005**.

[57] K. Kokot, Z. Knez, D. Bauman, *Acta Alimentaria* **1999**, *28 (2)*, 197 – 208. DOI: 10.1556/AAlim.28.1999.2.8.

[58] P. M. A. dos Santos, Characterization of Cocoa butter saturated with supercritical CO2: Experimental set-up and Modelling, *Dissertation* **2008**.

[59] H. Kuchling, *Taschenbuch der Physik: Mit Tabellen*, 20th ed., Fachbuchverl. Leipzig im Carl Hanser Verl, München **2011**.

[60] P. W. Atkins, *Physical Chemistry*, 3rd ed., Oxford University Press **1986**.

[61] H. Oertel, *Prandtl - Führer durch die Strömungslehre*, Springer Fachmedien Wiesbaden, Wiesbaden **2012**.

[62] C. A. Lockemann, Flüssigseitiger Stofftransport in Hochdrucksystemen mit einer überkritischen und einer flüssigen Phase, Univ **1994**.

[63] K. Taki, *Chemical Engineering Science* **2008**, *63 (14)*, 3643 – 3653. DOI: 10.1016/j.ces.2008.04.037.

[64] M. A. Shafi, J. G. Lee, R. W. Flumerfelt, *Polym. Eng. Sci.* **1996**, *36 (14)*, 1950 – 1959. DOI: 10.1002/pen.10591.

[65] M. Blander, J. L. Katz, *AIChE J.* **1975**, *21 (5)*, 833 – 848. DOI: 10.1002/aic.690210502.

[66] M. Thies, Lattice Boltzmann Modeling with Free Surfaces Applied to Formation of Metal Foams, *Dissertation*, Universität Erlangen-Nürnberg **2005**.

[67] P. Walstra, in *Foams: Physics, chemistry and structure*, Springer series in applied biology (Eds: A. J. Wilson), Springer. London **1989**.

[68] R. K. Prud'homme, *Foams: Theory, measurements, and applications*, Surfactant science series, Vol. 57, Dekker, New York **1996**.

[69] M. Schlüter, *Vorlesung: Strömungsmechanik 2* **2012**.

[70] H. Schade, E. Kunz, F. Kameier, C. O. Paschereit, *Strömungslehre*, 4th ed., De Gruyter Studium, de Gruyter **2013**.

[71] A. Colin, in *Foam Engineering* (Eds: P. Stevenson), John Wiley & Sons, Ltd. Chichester, UK **2012**.

[72] *Foams: Physics, chemistry and structure*, Springer series in applied biology (Eds: A. J. Wilson), Springer, London **1989**.

[73] J. C. Orcutt, B. H. Carpenter, *Chemical Engineering Science* **1971**, *26 (7)*, 1049 – 1064. DOI: 10.1016/0009-2509(71)80019-2.

[74] R. H. Chen, W. X. Tian, G. H. Su, S. Z. Qiu, Y. Ishiwatari, Y. Oka, *Chemical Engineering Science* **2011**, *66 (21)*, 5055 – 5063. DOI: 10.1016/j.ces.2011.06.058.

[75] E. L. Cussler, *Diffusion - Mass Transfer in Fluid Systems*, Cambridge University Press, Cambridge/New York **1997**.

[76] M. A. Shafi, R. W. Flumerfelt, *Chemical Engineering Science* **1997**, *52 (4)*, 627 – 633. DOI: 10.1016/S0009-2509(96)00434-4.

[77] E. J. Barlow, W. E. Langlois, *IBM Journal of Research and Development* **1962**, *6 (3)*, 329 – 337. DOI: 10.1147/rd.63.0329.

[78] C. D. Han, H. J. Yoo, *Polym. Eng. Sci.* **1981**, *21 (9)*, 518 – 533. DOI: 10.1002/pen.760210903.

[79] J. Barclay, D. S. Riley, Sparks, R. S. J., *Bull Volcanol* **1995**, *57 (6)*, 422 – 431. DOI: 10.1007/BF00300986.

[80] J. P. Dias, Barbosa Jr., Jader R., A. T. Prata, *J. Braz. Soc. Mech. Sci. & Eng.* **2012**, *34 (2)*, 155 – 166. DOI: 10.1590/S1678-58782012000200007.

[81] A. R. Paschedag, *CFD in der Verfahrenstechnik: Allgemeine Grundlagen und mehrphasige Anwendungen*, Wiley-VCH, Weinheim **2004**.

[82] L. D. Landau, E. M. Lifšic, *Fluid Mechanics*, 2nd ed., Vol. 6, Pergamon Press, Oxford **1989**.

[83] K. Brakke, *Experimental Mathematics* **1992**, 141 – 165.

[84] J. P. Kermode, D. Weaire, *Computer Physics Communications* **1990**, *60 (1)*, 75 – 109. DOI: 10.1016/0010-4655(90)90080-K.

[85] G. Verbist, D. Weaire, A. M. Kraynik, *J. Phys.: Condens. Matter* **1996**, *8 (21)*, 3715 – 3731. DOI: 10.1088/0953-8984/8/21/002.

[86] F. Bolton, D. Weaire, *Philosophical Magazine Part B* **1991**, *63 (4)*, 795 – 809. DOI: 10.1080/13642819108205538.

[87] D. J. Durian, *Phys. Rev. E* **1997**, *55 (2)*, 1739 – 1751. DOI: 10.1103/PhysRevE.55.1739.

[88] A. Bhakta, E. Ruckenstein, *Advances in Colloid and Interface Science* **1997**, *70*, 1 – 124. DOI: 10.1016/S0001-8686(97)00031-6.

[89] D. F. Baldwin, C. B. Park, N. P. Suh, *Polym. Eng. Sci.* **1998**, *38 (4)*, 674 – 688. DOI: 10.1002/pen.10232.

[90] K. Zähringer, J.-P. Martin, J.-P. Petit, *Journal of Materials Science* **2001**, *36 (11)*, 2691 – 2705. DOI: 10.1023/A:1017960729550.

[91] L. W. Schwartz, R. V. Roy, *Journal of Colloid and Interface Science* **2003**, *264 (1)*, 237 – 249. DOI: 10.1016/S0021-9797(03)00425-9.

[92] Institut für Arbeitsschutz der Deutschen Gesetzlichen Unfallversicherung, *GESTIS-Stoffdatenbank*, http://gestis.itrust.de/.

[93] Gesellschaft Verfahrenstechnik und Chemieingenieurwesen, *VDI-Wärmeatlas: Mit 320 Tabellen*, 11th ed., VDI-Buch, Springer Vieweg, Berlin **2013**.

[94] M. Stiess, *Mechanische Verfahrenstechnik: Partikeltechnologie*, 3rd ed., Springer-Lehrbuch, Berlin, Heidelberg **2009**.

[95] K. Siebertz, D. van Bebber, T. Hochkirchen, *Statistische Versuchsplanung: Design of Experiments (DoE)*, VDI-Buch, Springer, Heidelberg **2010**.

[96] Retsch Technology GmbH, *Camsizer Characteristics* **2009**.

[97] Deutsches Institut für Normung e.V., *Partikelgrößenanalyse – Formelzeichen, Einheiten* **2010** *(66161)*, http://shan02.tib.uni-hannover.de/han/PerinormTUHH/https/secure.beuth.de/cmd%3Bjsessionid=FKM1ZDP53BYE0CEGOM5KJG6D.2?workflowname=instantdownload&customerid=328165&docname=1715673&contextid=eeas&servicerefname=eeas&LoginName=bvollbrecht1 (13.11.2013).

[98] W. Fresenius, H. Günzler, W. Huber, I. Lüderwald, G. Tölg, *Analytiker-Taschenbuch*, Vol. 4, Springer, Berlin **1984**.

[99] R. Androsch, Reversibles Schmelzen und Kristallisieren von Polymeren, *Kumulative Habilitationsschrift*, Martin-Luther-Universität Halle-Wittenberg **2005**.

[100] Deutsches Institut für Normung e.V., *Kunststoffe - Dynamische Differenz-Thermoanalyse (DSC) - Teil 4: Bestimmung der spezifischen Wärmekapazität* **2013**, *83.080.01 (11357-3)* (30.10.2014).

[101] Deutsches Institut für Normung e.V., *Kunststoffe - Dynamische Differenz-Thermoanalyse (DSC) - Teil 3: Bestimmung der Schmelz- und Kristallisationstemperatur und der Schmelz- und Kristallisationsenthalpie* **2013**, *83.080.01 (11357-3)* (30.10.2014).

[102] Deutsches Institut für Normung e.V., *Kunststoffe - Dynamische Differenz-Thermoanalyse (DSC) - Teil 1: Allgemeine Grundlagen* **2010**, *83.080.01 (11357-1)* (30.10.2014).

[103] Deutsches Institut für Normung e.V., *Thermische Analyse (TA); Differenzthermoanalyse (DTA); Grundlagen* **1994**, *71.040.40 (51007)* (30.10.2014).

[104] SETARAM Instrumentation, *Calorimetry - BT 2.15*, http://www.setaram.com/BT-2.15.htm.

[105] M. E. Brown, P. K. Gallagher, R. B. Kemp, *Handbook of Thermal Analysis and Calorimetry*, Elsevier Science, Amsterdam Netherlands, New York **1998**.

[106] Laboratory for Thermophysical Properties, *Caloric Properties*, http://www.ltp-oldenburg.de/index.php/caloric-properties.html.

[107] Lehrstuhl für Technische Chemie, *Mikrokalorimetrie zur Bestimmung von Adsorptionswärmen*, http://www.techem.ruhr-uni-bochum.de/index2.php?section=techem&ordner=research&group=group&sub=muhler&lang=de&page=micro_calorimetry_for_regulation_of_heats_of_adsorpion.html.

[108] SETARAM Instrumentation, *Benefits of "3D Sensor Inside" Technology*, http://www.setaram.com/3dsensor.php.

[109] M. Betz, Encapsulation-related Characterisation and Applications of Thermal Whey Protein Hydrogels, *Dissertation*, Technische Universität München **2013**.

[110] Stat-Ease, *Design Expert* **2010**.

[111] Ž. R. Lazić, *Design of experiments in chemical engineering: A practical guide*, Wiley-VCH, Weinheim **2004**.

[112] C. Koller, E. J. Windhab, *Messungen der Druckabhängigkeit von physikalischen Eigenschaften für das System CO_2-Kakaobutter*, Eidgenössische Technische Hochschule Zürich, IFNH Food Process Engineering Group **2013**.

[113] D. Dhonsi, Stapley, A. G. F., *Journal of Food Engineering* **2006**, *77 (4)*, 936 – 942. DOI: 10.1016/j.jfoodeng.2005.08.022.

[114] M. Müller und R. Eggers, *Chemie Ingenieur Technik* **2013** *(Bd. 85 Nr. 12)*, pp. 1-9.

[115] Taki ,K. ,T.Nakayama ,T. Yatsuzuka ,and M. Ohshima, .*Journal of Cellular Plastics* **2003**, *39 (2)*, 155 – 169.

[116] C. B. Park, D. F. Baldwin, N. P Suh, *Polymer Engineering & Science* **1995**, *35 (5)*, 432 – 440.

Im Zuge dieser Arbeit wurden folgende studentische Arbeiten betreut:

Student	**Arbeit**	**Titel**	**Jahr**
Nina Maria Heitz	Bachelorarbeit	Vergleich von unter Hochdruck begaster Kakaobutter und Milchschokolade: Experimentelle Untersuchung der Gaslöslichkeit von CO2 sowie der Struktur des auskristallisierten Schaums	2013
Ilka Selmer	Masterarbeit	Einfluss der Schokoladenkomponenten auf die Charakteristik der unter Hochdruck begasten Schokolade: Experimentelle Untersuchungen und Modellentwicklung	2013
Jannik Sellin	Projektarbeit	Einfluss der Einlösezeit von Kohlenstoffdioxid auf die Charakteristik begaster Schokoladenmischungen	2014
Tobias Becke	Projektarbeit	Einfluss der Entspannung auf die Blasenstruktur in Hochdruck begaster Schokolade: experimentelle Untersuchungen und Modellierung	2014
Clarissa Lechtenberg	Masterarbeit	Betrachtung von unter Hochdruck begaster Schokolade: Schmelzverhalten und Blasenwachstum	2014
Jannik Sellin	Masterarbeit	Untersuchung der Einflüsse von Prozessparametern und Schokoladenbestandteilen auf die Charakteristik unter Hochdruck begaster Schokoladen	2015